Engineered Microneedles for Transcutaneous Vaccine Delivery

By

PETER C. DeMUTH

Bachelor of Science, Chemical and Biomolecular Engineering
University of Maryland, College Park, 2008

Bachelor of Science, Biochemistry
University of Maryland, College Park, 2008

SUBMITTED TO THE DEPARTMENT OF BIOLOGICAL ENGINEERING IN PARTIAL FULFILLMENT OF THE REQUIREMENTS FOR THE DEGREE OF

DOCTOR OF PHILOSOPHY

AT THE

MASSACHUSETTS INSTITUTE OF TECHNOLOGY

MARCH 2013

© Massachusetts Institute of Technology, 2013. All rights reserved.

ARCHIVES

MASSACHUSETTS INSTITUTE OF TECHNOLOGY

JUN 27 2013

LIBRARIES

Signature of Author: _____

Department of Biological Engineering
March 12, 2013

Certified by: _____

Darrell J. Irvine
Professor of Materials Science and Engineering and Biological Engineering
Thesis Supervisor

Certified by: _____

Paula T. Hammond
Professor of Chemical Engineering
Thesis Supervisor

Accepted by: _____

Forest M. White
Associate Professor of Biological Engineering
Chairman, Graduate Program Committee for Biological Engineering

Members of Thesis Committee:

Darrell J. Irvine
Professor of Materials Science and Engineering and Biological Engineering
Massachusetts Institute of Technology
Thesis Supervisor

Paula T. Hammond
Professor of Chemical Engineering
Massachusetts Institute of Technology
Thesis Supervisor

K. Dane Wittrup
Professor of Chemical Engineering and Biological Engineering
Massachusetts Institute of Technology
Committee Chair

Michael F. Rubner
Professor of Chemical Engineering
Massachusetts Institute of Technology

Engineered Microneedles for Transcutaneous Vaccine Delivery

By

PETER C. DeMUTH

Submitted to the Department of Biological Engineering
On March 12th, 2013 in partial fulfillment of the requirements for the degree of
Doctor of Philosophy in Biological Engineering at the Massachusetts Institute of Technology

ABSTRACT

Immunization is a powerful approach for the prevention and control of infectious disease, however despite the successes of modern vaccine development, there remain several notable obstacles for the advancement of vaccine-mediated improvements in global healthcare. Many of the current limitations in vaccine availability and administration are the result of obligate needle-based delivery, which in addition to contributing to reduced speed, ease, and compliance in administration, has been shown to contribute to reduced overall safety due to needle re-use and needle-based injuries. Needle-based vaccine delivery to immunologically passive tissues such as muscle may limit efficacy, thus motivating the targeting of more inherently potent immune-competent sites. These inherent limitations of needle-based vaccination on global health have led to a strong impetus to develop needle-free vaccination strategies which have the potential to improve vaccine efficacy and availability, enhance the ease, speed, and safety of vaccine administration, and reduce vaccination-associated costs world-wide.

Here we present the design and preclinical testing of several parallel materials strategies for the non-invasive delivery of subunit vaccines to the skin. We have utilized laser ablative micro-molding of poly(dimethylsiloxane) to generate bioresorbable poly(lactide-co-glycolide) micro-structured skin patches bearing ~100 micron-scale needles arrayed across their surface. Upon topical application, these 'microneedle arrays' are able to safely, and painlessly insert into the immune-competent epidermal skin layers to generate microscopic conduits through which otherwise impermeant vaccines and therapeutics are able to passage into the body.

We have leveraged this approach in combination with layer-by-layer (LbL) directed assembly to generate vaccine-loaded conformal coatings on the surface of these microneedle arrays, which are then delivered into the skin through topical patch application. The construction of coatings containing antigen-expressing plasmid DNA (pDNA), together with immune-stimulatory RNA, and degradable cationic polymers provided tunable control over vaccine dosage, rapid and effective vaccine delivery in murine and primate skin models, and potent immunogenicity against a model HIV antigen in mice. In this case, DNA vaccine delivery was able to elicit strong functional $CD8^+$ T cell and humoral responses matching or exceeding the potency of *in vivo* electroporation, currently the most promising approach for clinical DNA delivery in humans. Further efforts have explored the use of LbL for encapsulation and delivery of soluble and particulate protein subunit vaccines, giving enhanced generation of diverse and potent humoral responses in mice.

In other work, we have developed an approach enabling rapid delivery of micron-scale degradable polymer matrices or hydrogel depots using dissolvable composite microneedle structures for the delivery of vaccines with programmable kinetics. These efforts have demonstrated the potential of persistent vaccine release on tuning immune potency following non-invasive microneedle delivery, including induction of potent effector and memory $CD8^+$ T cell responses and more powerful and diverse antigen-specific humoral responses.

Finally, we have developed an approach for simple loading and delivery of clinically advanced recombinant adenoviral vaccine vectors from sugar-glass coatings on bioresorbable microneedles. Formulation in microneedle coatings improved vaccine stability at room temperature and preclinical testing of these vaccine patches in mice and nonhuman primates demonstrated equivalent immunogenicity compared to parenteral injection, eliciting strong systemic and disseminated mucosal $CD8^+$ and $CD4^+$ T cell responses to a model HIV antigen. These cellular responses were correlated with a similarly potent systemic and mucosal humoral response, together suggesting the utility of this approach for non-invasive adenoviral immunization in a model close to humans.

Together these results strongly demonstrate the potential of materials engineering strategies for the effective formulation, delivery, and release of recombinant vaccines by microneedle patches targeting the skin. In addition to the significant practical advantages enabled by microneedle delivery including improved safety, convenience, and storage, we have shown that advanced formulation strategies paired with controlled release are able to initiate humoral and cellular adaptive immunity more potently than possible through parenteral injection. Comprehensive tests in both mice and primates have suggested that these principles may be broadly applied to enhance various recombinant vaccination strategies potentially targeting numerous disease targets. Finally, initial tests performed in nonhuman primates have indicated the promise of engineered microneedle approaches for successful translation to humans. Overall, these findings provide a strong basis for the continued development of similar vaccination strategies for the comprehensive transformation of conventional vaccination enabling significant vaccine-mediated improvements in global health.

Thesis Supervisor: Darrell J. Irvine
Title: Professor of Biological Engineering and Materials Science and Engineering

Thesis Supervisor: Paula T. Hammond
Title: David H Koch Professor of Chemical Engineering

Table of Contents

Acknowledgements

This dissertation would not have been possible without the help of so many people. It is hard to express what the support, encouragement, and help of so many people has meant to me. I would like to extend my heartfelt appreciation to the following people.

To my thesis advisors: Prof. Darrell Irvine – for your mentorship, constant encouragement and support; for your significant investment of time and effort mentoring me over the last 5 years; for encouraging me to push through the most difficult technical challenges when I didn't believe I could; perhaps most of all, for your inspiration, and for pushing me to think differently. Your example of dedication as a scientist and mentor is something that I will always aspire to. Prof. Paula Hammond – for your mentorship, kindness, and support; for your constant excitement, passion, and enthusiasm for science and mentoring; for convincing me that polymer science can do anything. I will always admire your commitment to multi-disciplinary work – thank you for instilling in me a belief in the power of collaboration.

To my thesis committee: Prof. Dane Wittrup – for your encouragement in classes and research; for your careful guidance as my committee chair. Thank you for your insights, encouragement, and your example that a chemical engineer can do great things in biology. Prof. Michael Rubner – for your help and encouragement throughout this project; and for your valuable perspectives and technical expertise.

To my labmates: For encouragement, discussions, and support; for walking with me through every day with a smile; for inspiring me with your abilities, knowledge, and dedication; for making science exciting, amazing, and fun. Younjin – for your creativity and drive and for your help throughout this project. James – for your insight, perseverance, and technical help. Byeong-Su, Xingfang, and Jinkee – for your careful help and patience in the beginning when I didn't know anything. Mark and Bonnie – for mentoring me as a rotation student and for help throughout this project. Chris, Adrienne, Melissa, Greg, Erin, Mila, Mathias, Heikyung, Wuhbet, Anna, Maria, Chyan-ying, Kavya, Sharon, Haipeng, Yiran, Prahbani, Sabrina, Anasuya, Brandon, Dan, and Stephen, – for helpful discussions, answering questions, and fun times.

To my Rotation Students/UROPs: For providing new ways of thinking and fresh perspectives. Your excitement, and thoughtfulness were a great inspiration to me. Wilfredo – for your incredible creativity and energy; for pushing me to think hard about materials science and walking with me to solve many of the early issues we faced together. Michelle – for your hard work and eagerness to learn; you inspired me to continue working to overcome obstacles, to understand, and solve many of the technical issues we encountered together. Zach – for your perseverance, and bravery in accepting every challenge I gave you. Kwadwo – for your amazing work ethic, and constant drive to learn and apply new ideas.

To my collaborators and people who contributed to this project:

Mike Nguyen – for working with me to optimize the initial microneedle fabrication process; Peter Abbink – for help with adenoviral vector studies in mice and primates; Dan Barouch – for

incredible support and help with adenoviral vector studies; for being willing to take a chance on an unproven vaccination technology; Joshua Kramer and Andrew Miller – for providing assistance with primate tissues and husbandry; Jordi Mata-Fink – for help with gp120 protein vaccination; The veterinarians and staff at the MIT Division of Comparative Medicine – for animal handling training.

To my internship mentors at Novartis Vaccines: Dr. Peter Mason, Dr. Clayton Beard, Cole Jones, Dr. Antu Dey, and everyone else; For your patient mentoring and training; For your encouragement and support in teaching me virology, and welcoming me into your research community.

Technical assistance at shared core facilities: Scott Malstrom (*in vivo* imaging), Glenn Paradis and Mike Jennings (flow cytometry), Yong Zhang (SEM), Bill DiNatale (SEM and AFM), Weijia Zhang (histology)

To my wife, Debbie: Thank you for believing in me; for sharing every success and every challenge; for listening to me, and reminding me that I am loved no matter what. Everything that I've done would not have been possible without you, nor would it have meant anything without you to share it with. You make me realize how truly blessed I am.

To my parents: For loving me and teaching me to believe in myself. Thank you for every sacrifice. Thank you for teaching me the value of hard work in every part of life. Your commitment to each other, our family, your work, and the people around you will always inspire me.

To my brother, Scott: For walking with me through life; for encouragement and understanding that only a brother can give.

To my in-laws: For your support and gracious care for Debbie and I.

To my friends: For making us feel like Boston is home; for being a family to us.

List of Figures

1. BACKGROUND

1.1. The Need for, and Challenge of Developing New Generation Vaccines: HIV-1 as a Case Study

There are a reported 3 million new cases of HIV infection worldwide every year and despite the success of combinatorial anti-retroviral therapies, greater than 2 million people die annually from HIV-related causes.[1] In addition, although anti-retroviral therapies have found success in preventing the progression of HIV in infected individuals, these therapies are not curative, and because these drugs are prohibitively expensive they are not readily available in the developing world. The WHO reports that the developing world continues to bear a disproportionate share of the global burden of HIV infection, with greater than 35% of new infections and 38% of HIV-related deaths occurring in sub-Saharan Africa during 2007.[1] Furthermore, recent statistics demonstrate a rapid increase in new HIV-infections across the Indian subcontinent and Southeast Asia. The devastating individual and societal consequences of this infection, together with the deficiencies of current treatment options, specifically for those most acutely effected, makes the development of an effective vaccine against HIV of critical importance.

However, despite decades of scientific effort in pursuit of this objective, there remain significant scientific challenges facing current vaccine development efforts. Among these are considerations originating from the unique transmission and replication mechanisms of HIV-1, such as the need to generate both protective mucosal and systemic immunity, as well as effective cellular and humoral immune responses.[2] In addition, the molecular mechanisms of HIV-1 replication are inherently inaccurate and this results in extraordinary diversity among viral isolates.[2,3] Therefore, any potential strategy for an effective vaccine against HIV-1 must have the flexibility to successfully address this inherent antigenic diversity. To date, traditional approaches for generating effective antiviral immunity such as administration of live attenuated virus, have either proven unsuccessful in immunizing against HIV-1, or are too dangerous given the high rate of viral mutation. Alternative vaccination strategies such as the delivery of recombinant peptide antigen or plasmid DNA constructs have met with limited success, partially due to their relatively lower immunogenicity in humans.[4,5] The combination of these approaches for antigen delivery with administration of immuno-stimulants such as cytokines or adjuvants, has demonstrated their potential to increase vaccine-elicited immune responses.[6] Therefore, it seems likely that future improvements to this paradigm may lead to more effective protection conferred by immunization. Specifically, approaches that increase plasmid transfection efficiency or improve immunogenicity of protein subunit or plasmid DNA constructs,[7-9] as well as the development of new non-viral vectors should drastically improve the magnitude and duration of vaccine-elicited immune responses.

1.2. Potential Advantages of Needle-free Vaccination

Vaccines currently represent a significant strategy for the control of infectious disease on a global level. However, despite the successes of modern vaccine development, there remain several notable obstacles for the advancement of vaccine-mediated improvements in global healthcare. Among these are factors which limit vaccine availability, such as cost and the need

for cold storage,[10-12] or vaccine efficacy and compliance, such as the ease and speed of vaccine delivery.[13] Many of the current limitations in vaccine availability and administration are the result of obligate needle-based delivery, which in addition to contributing to reduced speed, ease, and compliance in administration, has been shown to contribute to reduced overall safety due to needle re-use and needle-based injuries.[14-17] The inherent limitations of needle-based vaccination on global health, together with emerging concern over global pandemic disease, has led to a strong impetus to develop materials platforms supporting needle-free vaccination strategies which have the potential to improve vaccine availability, enhance the ease, speed, and safety of vaccine administration, and reduce vaccination-associated costs world-wide.[13,18]

1.3. Transcutaneous Vaccine Delivery as a New Paradigm for Immunization

1.3.1. The Skin is Inherently Immuno-competent

Given the inherent drawbacks of needle-based vaccination, one promising alternative is immunization through transcutaneous delivery of antigen/adjuvant, thereby inducing protective immunity.[19-23] The skin is the primary interface between the body and the environment and, as such, is inherently endowed with natural immune competencies for the purpose of serving as the first defense against microbial pathogens. For example, the anatomical structure and cellular composition of the skin is in many ways ideal for immuno-surveillance and the initiation and orientation of the adaptive immune response. On a cellular level, the skin represents a rich immunological environment containing resident epidermal and dermal dendritic cells (DCs), macrophages, T and B lymphocytes, and NK cells (**Figure 1-1,** reviewed in [24]). In addition, epidermal keratinocytes, the major cellular component of the skin, are active in detecting invading pathogens through expression of germ-line encoded pattern recognition receptors (PRRs) such as Toll-like receptors (TLRs).[25,26] Keratinocytes also constitutively or inductively secrete many inflammatory cytokines that allow them to serve as instigators of inflammation.[27,28] Skin-resident DCs have been shown to serve in a variety of immune-sentinel roles including antigen uptake[29,30] and migration to draining lymph nodes,[31] antigen presentation,[32] and mediation of inflammatory state through cytokine and chemokine secretion.[33-35] Together with skin-resident macrophages, keratinocytes and DCs represent a sensitive network for detection of inflammatory signals, and transmission and processing of those signals to interface with and orient the adaptive immune response.

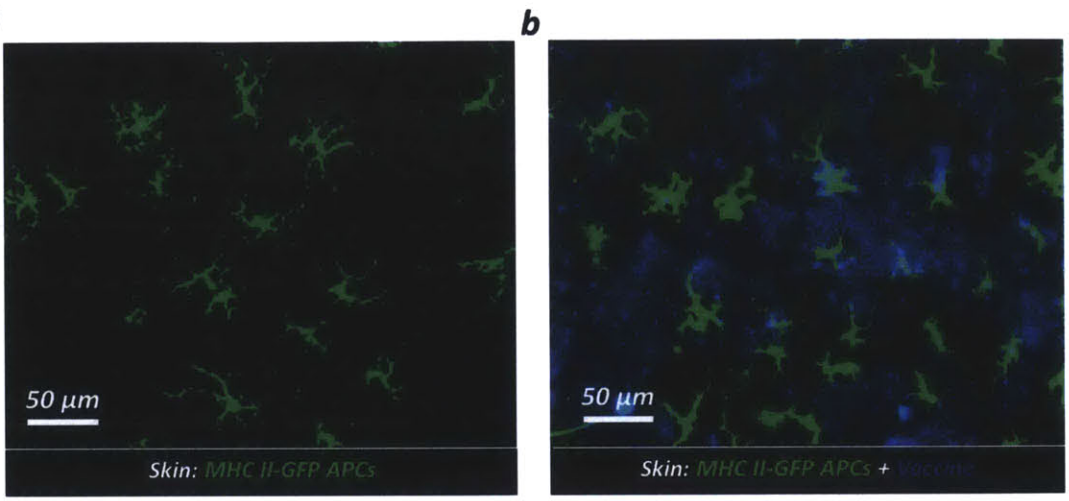

Figure 1-1. Resident antigen presenting cells form an immune-sentinel network in the skin.

(a-b) *Confocal micrographs of dissected murine skin showing the sentinel network of MHC-II-GFP-expressing antigen presenting cells (green).* ***(a)****MHC-II-GFP cells reside in the epidermal and dermal tissue dispersed in a dense network and* ***(b)*** *are able to colocalize with vaccine delivered into the skin (blue).*

1.3.2. Transcutaneous Immunization Indicates the Potential of Cutaneous Vaccine Delivery

The transcutaneous delivery of antigen and adjuvant has been recently explored for the purpose of immunization with great success (reviewed in [36]). For example, many instances of co-administration of antigen with cholera toxin or heat-labile toxin from *Escherichia coli* have produced potent cellular and humoral immune responses to both peptide[37,38] and genetic[39,40] vaccine formulations. In addition, transcutaneous application of antigen with adjuvant has been shown to induce both IgG and IgA antibodies[41,42] as well as cellular responses[43] in mucosal secretions in mice and more recently in human clinical trials.[20] These effects were amplified in cases where potent adjuvants were co-administered with either peptide or DNA vaccines[44,45] resulting in protective immunity in several cases of pathogenic challenge.[39] These studies, although serving as a strong proof of principle for the potential efficacy of skin-based immunization, are dependent upon the use of separate mechanical disruption of the stratum corneum, as well as strong adjuvants that present significant associated safety concerns in the context of translation to human clinical application. Therefore, although transcutaneous immunization represents a significant opportunity for improving vaccine efficacy, further progress is needed to ensure safe, convenient, consistent, and cost-effective methods for delivery.

1.4. Microneedles are a Promising Platform for Cutaneous Delivery

Recent work in the area of microneedle fabrication (arrays of needles less than a millimeter in length) has demonstrated the utility of these materials for safe, efficient, and pain-free disruption of the stratum corneum, promoting transcutaneous delivery of a variety of therapeutics and other

bio-active materials (**Figure 1-2**).[46-49] To date, various fabrication strategies have been employed to create solid microneedles from silicon, metal, and various polymers[50,51] and these have been applied for cutaneous delivery primarily through ***(i)*** application of liquid formulations to pretreated skin,[52,53] through ***(ii)*** the transfer of dried, surface-coated materials from microneedles upon application,[48,54,55] or more recently, through ***(iii)*** the application of rapidly dissolving microneedles encapsulating materials for delivery to the skin.[56-59] Although these approaches have combined to provide a convincing proof of concept for the application of microneedle arrays in cutaneous delivery, there are several issues, which must be considered to allow microneedle-based delivery to address a more broad range of clinical applications. One significant issue is the fact that current microneedle delivery approaches are deficient in providing control over the kinetics of materials delivery. Delivery through the transfer of dried surface-based coatings, as well as application of liquid formulations to microneedle treated skin, provides therapeutics in a single bolus. Microneedles designed to rapidly dissolve upon application effectively accomplish the same kinetic timeline for materials delivery. Therefore, these approaches cannot begin to address clinical situations in which extended or controlled release is important for improving therapeutic effect. In addition, although rapidly dissolving microneedles begin to address the need for solid state stabilization of biologically sensitive materials, thereby avoiding the cost of reliance upon the cold-chain and improving global availability, there is still a need to combine this with more rigorous methods of materials encapsulation that will allow for methodical design of materials formulation for delivery. This is specifically true in the case of vaccination, where the recent push towards strategies utilizing combinations of recombinant antigen and adjuvant requires a more modular approach to allow for the necessary flexibility and control needed for rational design of vaccines.

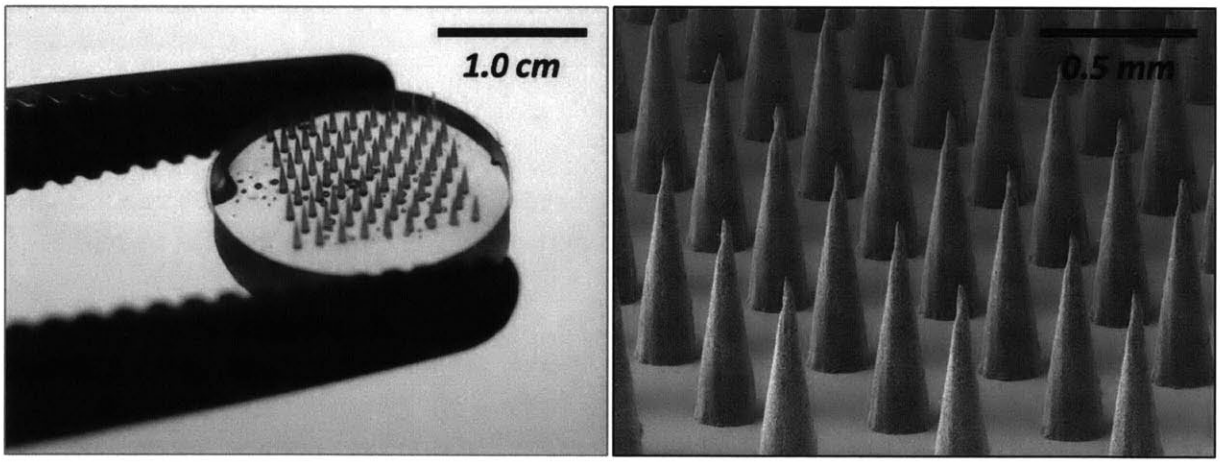

Figure 1-2. PLGA microneedle patches for transcutaneous delivery

Photograph of a microneedle array fabricated from poly-lactide-co-glycolide (PLGA), a biodegradable FDA-approved plastic (left). Upon application to the skin, these microneedle-arrays can safely and painlessly create microscopic channels for vaccine delivery into the body. A scanning electron microscope image of a similar microneedle array (right) shows the presence

of uniform needles only 0.5mm in length. This prevents access to blood vessels and nerves deeper within the skin upon topical microneedle treatment.

1.5. Polyelectrolyte Multilayers (PEMs) Provide Robust Control over Surface-based Delivery

1.5.1. PEMs are a Robust and Flexible Approach to Surface Modification

To address the technological insufficiencies of current strategies for formulating vaccines for delivery by microneedles, we have pursued layer-by-layer (LbL) nano-layer construction, a film fabrication approach capable of nano-scale control over coating composition and modular tunable incorporation of multiple constituents important for vaccine efficacy, delivery, and storage. The surface-based directed-assembly of complimentary polymers through LbL adsorption is a well-established method for the deposition of multi-component polymer thin films. This approach takes advantage of complimentary functionality, such as electrostatic charge or hydrogen bond status, in constituent materials to allow for deposition of thin films onto surfaces in which film growth is achieved through iterative exposure to materials of alternating character (**Figure 1-3**).

Extensive work in the area of polyelectrolyte multilayer (PEM) directed-assembly has demonstrated the potential for simple and versatile materials encapsulation into conformal thin films providing robust control over materials release, solid-state stabilization of environmentally-sensitive encapsulated materials, and nanometer-scale control over film structure and composition.[60-64] Control over film structure and composition is generally achieved through the selection of polyelectrolyte materials, the specific conditions of directed-assembly, and the number of bi-layers deposited. As film structure and composition are inherent determinants of film behavior, these factors also provide a robust handle for controlling materials encapsulation and release. In addition, because the entire process is aqueous-based, the LbL technique is readily extensible to a variety of diverse natural and synthetic materials, specifically potentially sensitive biologically active materials. Finally, this approach is ideally suited for application to substrates of complex geometry, enabling the formation of conformal composite films on irregular surfaces. Together these factors make the LbL technique an attractive and versatile platform for rational assembly of functional multi-layered films with broad utility in a variety of biological and medical applications.

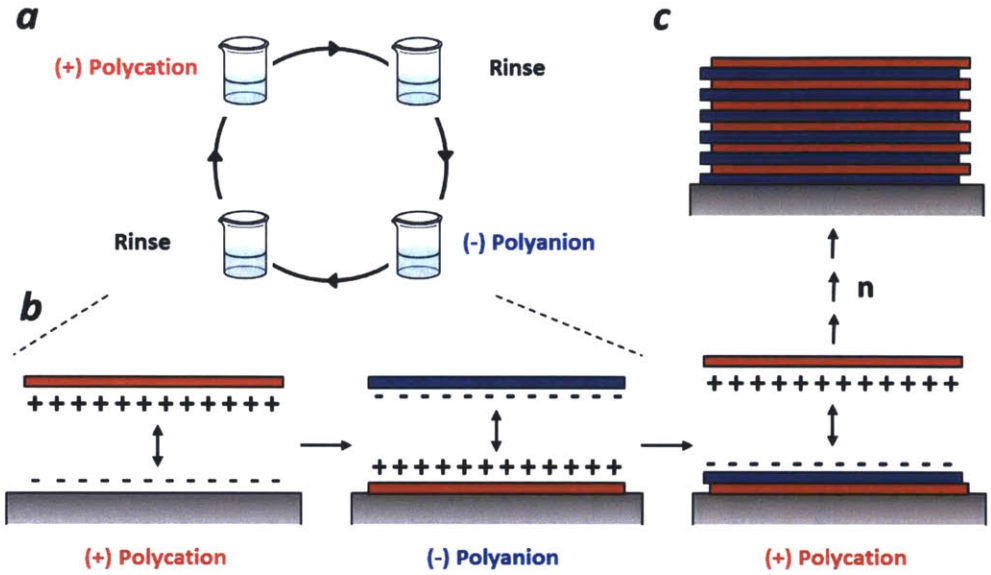

Figure 1-3. LbL is simple, bio-friendly, and scalable

(a) *Schematic of electrostatic LbL directed-assembly for generation of polymer surface films through iterative exposure to materials of complimentary charge.* ***(b)*** *Surface films are created through sequential adsorption of charged polymers through electrostatic attraction with concomitant reversal of surface charge yielding* ***(c)*** *surface films of defined nano-scale polymer composition and structure.*

1.5.2. Poly-β-amino Esters Allow for Controlled Release from Hydrolytically Degradable PEMs

Past efforts to design PEM systems capable of controlled release of biological materials has led to the development of PEM film architectures utilizing a family of hydrolytically degradable poly-cations known as poly-β-amino esters (PBAEs). First developed by Lynn and Langer in an effort to create an improved vector for non-viral gene delivery, PBAEs have previously been shown to be biocompatible, degradable over a time-scale of hours to days, are capable of mediating efficient transfection of cells *in vitro*, and have adjuvant activity when co-delivered with DNA vaccines.[7,65-69] In addition to their straightforward synthesis, PBAEs are readily degradable by hydrolysis of the ester bonds in their backbone to yield bio-compatible by-products, all of which have been observed to have no detrimental effect on cell growth or metabolism *in vitro*. In all cases, PBAEs show differential degradation kinetics depending on pH conditions. Specifically, degradation is observed to occur with a much lower half-life at pH 7.4 than at pH 5.1, with the half-life of polymer-1, a representative PBAE, being approximately one hour or eight hours at pH 7.4 and 5.1 respectively. Finally, PBAEs have been shown to effectively complex with plasmid DNA through electrostatic interactions at physiologically relevant conditions, and this has led to improved transfection *in vitro*.

These characteristics have led to the extensive use of PBAEs for self-assembly into degradable PEMs. PBAEs have been shown to readily self-assemble with a variety of poly-anions, and to deconstruct in aqueous conditions *via* parallel disassembly and degradation of the constituent polymers, giving gradual top-down erosion, the kinetics of which can be robustly tuned through the combinatorial selection of constituent PBAE and poly-anion pairs. In particular, polymer-1, has been used recently by Irvine and Hammond to fabricate LbL films with controlled erosion and tunable drug release,[64] and by others to fabricate PEM films promoting the controlled release of plasmid DNA from surfaces for potential gene delivery applications.[67,70,71]

1.5.3. DNA PEM Self-Assembly is a Promising Approach for Surface-based Gene Delivery

The localized and controlled delivery of plasmid DNA from surfaces has been the objective of recent research efforts focused on improving gene delivery for both *in vitro* and *in vivo* applications, including tissue engineering[72] and cell culture,[67,73,74] as well as delivery from implantable devices such as intravascular stents.[70] Progress in the area of delivery from DNA-containing PEMs has been especially promising given the ability for controlled deposition of DNA together with various polymers into conformal thin films on geometrically complicated surfaces. The ability provided by LbL deposition for robust control over nano-scale thin film composition, and the inherent rigorous control over self-assembly and release that this capacity allows, makes this approach of significant interest as more complicated systems are engineered. Prior results in this area have demonstrated that DNA can be deposited by LbL self-assembly together with a variety of natural and synthetic poly-cations (reviewed in [71]). Because DNA is incorporated directly into these films as a poly-anionic constituent, the LbL approach provides not only an inherent ability to easily and finely control dosage through variation of deposition cycle number, but also creates significant opportunities for designing films that efficiently modulate release and promote efficient transfection through the careful selection of alternative cationic polymers. For example, the self-assembly of plasmid DNA with various members of the aforementioned PBAEs serves as an illustrative example. Studies of plasmid self-assembly with PBAEs demonstrate simple dosage control as film growth and DNA encapsulation are both linearly correlated with bilayer number.[75] In addition, the self-assembly of DNA with PBAEs (or other degradable cationic polymers) with differing kinetics of hydrolysis has been shown to allow for rational tuning of the kinetics of DNA release.[75,76] Finally, PBAEs have been observed to improve pDNA transfection efficiency relative to naked pDNA and to enhanced immune response when co-delivered with antigen-encoding plasmid DNA.[7] Therefore, the selection of these polymers for self-assembly with plasmid DNA may confer these same advantages in an LbL-based genetic vaccine delivery approach.

1.5.4. Nano-carrier PEM Self-Assembly Enhances PEM Flexibility and Modularity

Despite the success of hydrolytically degradable multi-layer thin films for surface-based controlled release, this general paradigm for delivery is inherently limited. For example, although LbL self-assembly has been shown to be generally applicable and extensible to encapsulation and release of a variety of diverse materials within a broad range of film

compositions,[62,75] this approach does not provide the generality to apply a single film architecture to obtain equivalent delivery of chemically diverse species. Instead, independent design and optimization must be carried out to engineer films capable of encapsulating chemically or physically distinct materials. Further effort must then be expended in characterization and control of materials release. This requirement for independent accommodation of material cargos of interest is a significant obstacle in the development of multi-layer films capable of delivering multiple materials in combination, an objective of particular interest in biological and medical applications. Recent approaches have begun to improve upon this paradigm through incorporation of nano-carriers within multi-layer films (**Figure 1-4**). Through the incorporation of cargo-encapsulating micelles,[60,77] liposomes,[78] and nanoparticles[79] not only can single film architectures provide the flexibility to encapsulate various diverse materials, but control over release behavior can be achieved independent of chemical and physical properties of the desired therapeutic cargos. Among these approaches, nanoparticle-based PEMs are especially promising given that nanoparticle surface functionality can be easily manipulated independent of cargo, that degradation kinetics can be tuned based on the choice of degradable polymer, and that structural integrity can be maintained under various processing conditions. Together, these factors also provide the opportunity for an enhanced ability for combinatorial encapsulation and delivery of diverse materials with robust and independent control over release kinetics necessary to address various complex applications.

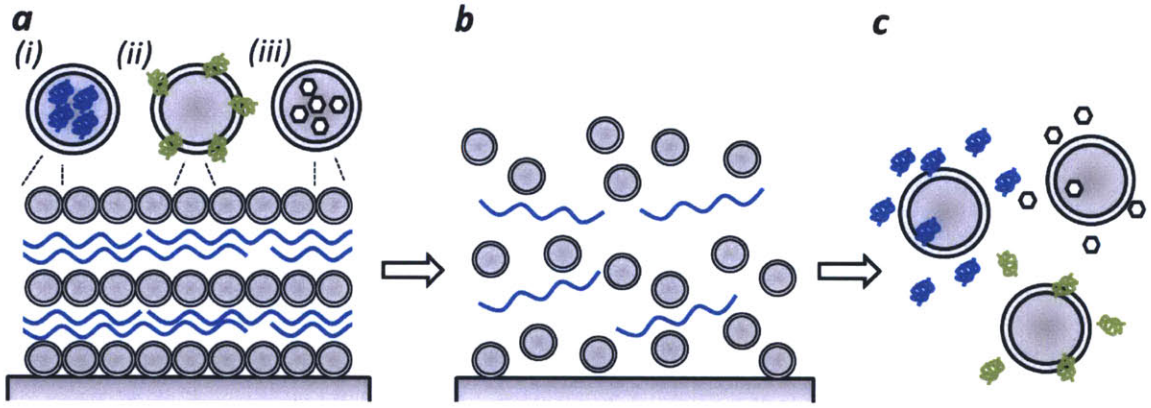

Figure 1-4. Nano-carrier PEMs provide additional flexibility and modularity

LbL films encapsulating loaded nano-carriers allow for greater flexibility and control, as diverse materials (i-iii) can be ***(a)*** *first loaded into particles, and then into films. Thus identical films can encapsulate various and multiple materials where 'two-stage' loading and* ***(b-c)*** *release are controlled by the particle and film design.*

1.6. Toll-like Receptor (TLR) Agonists are Effective Vaccine Adjuvants

In order to improve the immunogenicity of peptide or genetic subunit vaccine formulations, defined molecular adjuvants are frequently co-delivered to provide the necessary innate immune

stimulus to initiate adaptive immunity. Agonists that stimulate TLRs have been extensively used for this purpose due to their potency and defined cellular and molecular mechanisms. TLRs comprise a group of evolutionarily conserved cell-surface and endosomal receptors, which serve an important role in the regulation of the innate immune response and its interface with adaptive immunity. Specifically, these receptors recognize compounds conserved among microorganisms and subsequently activate many diverse cell populations involved in the innate immune response.[50] Following TLR activation, downstream signaling is mediated by the activation of the nuclear factor-κB (NFκB) transcription factor[80] to induce transcription of inflammatory cytokines such as IL-12, IL-6, IFN-α, and TNF-α.[81] Activation events induced by these cytokines activate both the innate and adaptive pro-inflammatory immune response. Rapid progress in the understanding of TLR function in the detection of pathogens by the innate immune system has indicated the significant promise of TLR agonists for enhancing vaccine efficacy. For example, certain TLR agonists have been shown to promote DC maturation and antigen presentation,[82-84] leading to more effective T cell activation in response to both protein[85] and DNA-based[86] vaccines. As development of non-traditional vaccination strategies continues to progress, the controlled co-delivery of TLR agonists as vaccine adjuvants should improve immunogenicity in recombinant vaccines and allow for more rational design of vaccine formulations.

1.7. Scope and Outline of Thesis

This thesis describes the design, development, and application of several strategies for improved cutaneous delivery using microneedles as a flexible materials platform. Compared to parenteral injection, microneedle delivery offers many practical advantages including improved safety, convenience, patient compliance, and cost-effective storage/distribution. Delivery of vaccines to the skin also provides the ability to more directly target critical immune cell populations which are densely distributed within the epidermal and dermal tissues and provide pivotal functionality in the development of effective immunity. Thus, cutaneous vaccination through microneedle delivery can potentially yield protective immunity that is functionally more potent, and phenotypically superior to responses elicited by traditional administration. We have explored several broad hypotheses as a part of this work: *(i)* that microneedle delivery of recombinant subunit vaccines should provide additional immunogenicity relative to parenteral administration, *(ii)* that greater control over formulation of recombinant multi-component vaccines should improve microneedle-elicited immunity, *(iii)* that sustained release of vaccines following microneedle delivery should allow for additional control over the strength and character of resulting immune responses, and *(iv)* that these strategies for engineered vaccines should be flexible to accommodate various diverse recombinant vaccine platforms (protein, pDNA, virus, RNA, etc.) with reliable performance in both murine and primate animal models of disease. Therefore, the broad goal of these studies was the development of new microneedle approaches for cutaneous vaccination by microneedle delivery of recombinant subunit vaccines and to evaluate them for preclinical correlates of efficacy.

Chapter 2 describes the development of a flexible approach for generating a microneedle delivery platform using LbL directed-assembly. Fabrication of microneedle arrays was accomplished using FDA-approved thermoplastics, to ensure safe, cost-effective, and scalable production for use in humans. Controlled formulation of both pDNA and therapeutic nano-particles on microneedle patches was achieved through deposition of dried surface coatings using LbL directed-assembly. These microneedle patches were then shown to be effective in delivering film-loaded cargos, and in the case of pDNA to produce tunable gene delivery and expression in mice. These studies serve as a strong proof-of-principle for our directed-assembly approach, demonstrating the effective control over multiple therapeutic components, effective transfer into the skin upon microneedle treatment, and controlled release of bio-active delivered materials in the skin.

Chapter 3 expands upon the results shown in Chapter 2, specifically the design and evaluation of a materials approach for rapid implantation of controlled-release vaccine films upon microneedle skin treatment. Here we employed a pH-sensitive polymer to mediate dissolution-based cutaneous delivery of multilayer films from the surfaces of degradable microneedles upon skin insertion. We explored the ability of this platform to effectively implant multilayer films, and control the release of encapsulated vaccine components over time *in vivo*. These studies culminated in the demonstration of this approach for eliciting potent cellular and humoral immunity against a model HIV antigen comparable to the most effective pDNA vaccination strategies currently in clinical use. Finally, we completed a series of tests in non-human primate tissues to confirm the ability of microneedle-based cutaneous delivery to mediate successful pDNA delivery in a model tissue similar to humans. These studies, together with those described in Chapter 2, serve as a strong indicator of the potential for multilayer delivery to improve subunit vaccination through microneedle administration, controlled multi-component vaccine formulation, and sustained release of vaccines.

Chapter 4 continues to explore these concepts for multilayer vaccine formulation and microneedle delivery within the context of particulate-formulated whole protein vaccines. The design of pathogen-mimicking synthetic particle-based vaccines has recently shown promise for enhancing immunity without the potential safety concerns of live or attenuated vaccine vectors. Building on the success of multilayer delivery described in Chapters 2 and 3, we next designed an approach for encapsulating lipid nano-capsules into degradable vaccine films on microneedle surfaces to evaluate the potentially synergistic effects of microneedle delivery, sustained vaccine release, and particulate vaccine presentation to the immune system. In this case, we observed the potential for multilayer deposition to generate robust degradable vaccine nano-capsule loaded films on the surface of microneedles for rapid delivery and sustained release *in vivo*. In parallel comparisons to injected particulate vaccines, or microneedle delivered soluble vaccines, microneedle delivery of vaccine particles gave significantly improved humoral immunity. The enhanced potency and breadth of the generated antibody repertoire measured here suggests that cutaneous microneedle delivery, sustained vaccine release from degradable multilayers, and

particulate vaccine formulation combine synergistically to improve humoral immune responses *in vivo*.

Chapters 5 and 6 describe the design and testing of an alternative microneedle delivery approach utilizing composite structures intended to provide rapid dissolution-based disintegration of skin-inserted microneedles to implant controlled-release polymer or hydrogel depots within the skin. Here we continue to explore the effect of sustained vaccine release for enhancing immunity following microneedle immunization. Composite microneedles were able to rapidly implant cutaneous polymer or hydrogel depots which persisted in the tissue to sustain vaccine release for days to weeks. Deployment of this system for the delivery of soluble protein vaccines demonstrated improved immunity compared to parenteral bolus injection of dose-matched vaccine formulations again indicating the potential of sustained vaccine exposure to boost functional immunity *in vivo*. Further, the ability of these systems to provide varied and sustained kinetics of antigen and adjuvant exposure was critical for maximizing the potency of elicited immune responses.

Finally, Chapter 7 describes studies meant to evaluate the clinical potential of microneedles for cutaneous vaccination through preclinical testing in non-human primates. Although microneedle vaccination has proven effective in many preclinical rodent models of disease, the potential of any vaccine system must be established in primate models which more accurately represent human physiology, immunology, and the human disease state. Here we vaccinated mice and Rhesus macaques with microneedles bearing vaccine-loaded sugar coatings intended to stabilize vaccines at room temperature, and rapidly deliver loaded vaccines upon sugar dissolution in treated skin. The results of these studies indicated that microneedle vaccination induced potent cellular and humoral immunity in both systemic circulation and mucosal tissues of mice and primates comparable to those elicited through parenteral injection, indicating the potential of this approach for effective translation to human clinical trials.

2. NANO-LAYERED MICRONEEDLES FOR TRANSCUTANEOUS DELIVERY OF POLYMER NANOPARTICLES AND PLASMID DNA

2.1. Introduction

Current vaccine and therapeutic delivery is largely needle-based,[13] but a number of inherent risks and disadvantages to needle-based delivery have been recognized, such as the need for cold storage of liquid formulations,[11,13] the requirement of trained personnel for administration, and reduced safety due to needle re-use and needle-based injuries.[14] To address these limitations, vaccination and therapeutics administration through the skin represents a promising alternative strategy,[20,22,23] and technologies promoting efficient transcutaneous delivery of a variety of drugs and vaccines has become a significant focus of recent research (reviewed in [87]). Recent work in this area has demonstrated the utility of microneedle arrays for efficient and pain-free disruption of the stratum corneum (SC), promoting transcutaneous delivery of a variety of bio-active materials.[46,48] Microneedle delivery is often achieved by coating dried water-soluble drug formulations directly on the surfaces of solid microneedles. Parallel studies in the area of polyelectrolyte multilayer (PEM) engineering have demonstrated the potential for simple and versatile materials encapsulation into conformal thin films, providing robust control over materials release, solid-state stabilization of environmentally-sensitive encapsulated materials, and nanometer-scale control over film structure and composition.[60,61,63,64,88-90] Prior studies in the Hammond and Irvine laboratories reported the construction of PEM films loaded with vaccine components prepared on flexible substrates for transcutaneous vaccine delivery.[60] However, these planar multilayer patches required prior SC disruption to permit entry of released cargos from the PEM films into the epidermis. We hypothesized that combining the flexible and highly tunable nature of PEM thin film coatings with microneedle substrates enabling direct entry of films into the viable epidermis could provide a versatile platform for single-step transcutaneous delivery of a broad range of drugs and drug carriers that is effective, generally applicable, inherently safe and pain-free, and potentially cost effective.

In vitro delivery of plasmid DNA from PEMs has been demonstrated using multilayers that deconstruct in aqueous conditions *via* parallel disassembly and degradation of the constituent polymers.[67,75] We show here that microneedle arrays coated with DNA-carrying PEMs allows this concept to be translated to *in vivo* transfection in murine skin, an approach of great interest for DNA vaccine delivery. Similarly, we show that biodegradable poly(lactide-*co*-glycolide) (PLGA) nanoparticles (NPs), ubiquitous in drug delivery, can be embedded within microneedle PEM coatings, and subsequently deposited in the epidermis following a brief application of microneedles to unmanipulated skin. Finally, we show that multilayers combining these two diverse types of therapeutic cargos can be prepared for co-delivery into skin. To our knowledge, this is the first report of functional coating deposition onto microneedle arrays through the use of layer-by-layer (LbL) PEM self-assembly. Furthermore, although transcutaneous plasmid DNA delivery has been demonstrated by topical application to barrier disrupted skin[91,92] and recently through application of microneedles coated with dried formulations,[93] this is the first reported

demonstration of *in situ* DNA delivery from PEM films or PEM-coated microneedles to mediate *in vivo* gene delivery and expression.

2.2. Materials and Methods

2.2.1. PLGA Microneedle Fabrication.

PDMS molds (Sylgard 184, Dow Corning) were fabricated by laser ablation using a Clark-MXR, CPA-2010 micromachining system. PLGA pellets (50:50wt lactide: glycolide, 46 kDa, Lakeshore Biomaterials) were melted over the molds under vacuum (-25 in. Hg) at 145°C for 40 minutes, and then cooled at -20°C before separating the cast microneedle arrays. Arrays were characterized using a JEOL 6700F FEG-SEM.

2.2.2. PLGA Nanoparticle Preparation

PLGA nanoparticles were prepared as previously described.[80] Briefly, PLGA (30mg), DOPC/DOPG lipids (4:1 mol ratio, 5mg, Avanti Polar Lipids), and DiI or DiD (6.4ng, Invitrogen) were co-dissolved in 1 mL dichloromethane. PBS (200 μL) was added, the emulsion was sonicated (7W, 1 min) using a Microson cell disruptor, added to 4mL of Milli-Q (MQ) water, and sonicated again (12W, 5 min), followed by incubation for 12 hrs at 25°C. The resulting particles were purified on a sucrose gradient and analyzed using a BIC 90+ light scattering instrument (Brookhaven Instruments Corp).

2.2.3. Polymer Multilayer Film Preparation

All LbL films were assembled using a Carl Ziess HMS DS50 slide stainer. Films were constructed on silicon wafers, quartz slides, and PLGA microneedle arrays following treatment with O_2 plasma. To build (PS/SPS) baselayers, substrates were dipped alternatively into PS (2mg/mL, 100M NaOAc, Sigma-Aldrich) and SPS (5mM, 20mM NaCl, Sigma-Aldrich) solutions for 10 min separated by two sequential 1 minute rinses in MQ water.[94] (Poly-1/pLUC) multilayers were deposited similarly, alternating 5 min dips in Poly-1 (2mg/mL in 100mM NaOAc, synthesized according to previous literature [65,69]) and pLUC (1mg/mL, 100mM NaOAc, a gift from Dr. Daniel Barouch, Beth Israel Deaconess Medical Center) solutions separated by two sequential rinsing steps in 100mM NaOAc, pH 5.0. Fluorescent pLUC was prepared using Cy3 Label-IT reagent (Mirus Bio Corporation). All solutions (except pLUC) were adjusted to pH 5.0 and filtered (0.2μm) prior to dipping.

2.2.4. Particle Multilayer Film Preparation

Films were assembled using a previously described spray LbL technique.[81] Briefly, microneedle arrays were coated with atomized spray solutions using modified air-brushes. Poly-1 (2mg/mL, 100mM NaOAc) and PLGA NP (20mg/mL in MQ water) solutions were sprayed alternatively for 3 seconds (0.2mL/s, 15 cm range) separated by 6 second rinses with 100mM NaOAc. Film thickness was measured using a Tencor P-16 surface profilometer. Film delivery was characterized through CLSM imaging of microneedle arrays using a Zeiss LSM 510 and data analysis using Image J.[95]

2.2.5. *In Vivo Transcutaneous Delivery*

Animals were cared for in the USDA-inspected MIT Animal Facility under federal, state, local, and NIH guidelines for animal care. Microneedle application experiments were performed on anesthetized C57BL/6 mice (Jackson Laboratories) and MHC II-GFP transgenic mice (a gift from Prof. Hidde Ploegh).[96] Ears were rinsed briefly with PBS on the dorsal side and dried before application of microneedle arrays by gentle pressure. Microneedles were then removed or secured in place using Nexcare medical tape (3M). Mice were sacrificed and excised ears were stained with trypan blue before imaging for needle penetration. Ears collected from mice treated with Cy3-pLUC- and/or DiI-PLGA-NP-coated microneedle arrays were mounted on glass slides and imaged by CLSM. Transfection in mice treated with pLUC-coated arrays was measured using an IVIS Spectrum 200 (Caliper Lifesciences) to detect bioluminescence, following IP injection of luciferin.

2.3. ***Results and Discussion***

2.3.1. *PLGA Microneedle Fabrication*

We first used laser micromachining to prepare poly(dimethylsiloxane) (PDMS) slabs with arrays of tapered pyramidal or conical microscale cavities across their surface, to serve as molds for polymer microneedle fabrication. Similar to prior reports,[50] PLGA pellets placed over the molds were melted under vacuum, cooled, and separated from the PDMS (**Supplementary Figure S2-1**) to obtain arrays of microneedles each 250μm in diameter at their base and 900μm in height (**Figure 2-1a, Supplementary Figure S2-2**). Microneedles of similar dimensions have been shown to produce negligible pain sensations in humans, while maintaining adequate structural integrity to efficiently penetrate the SC.[97]

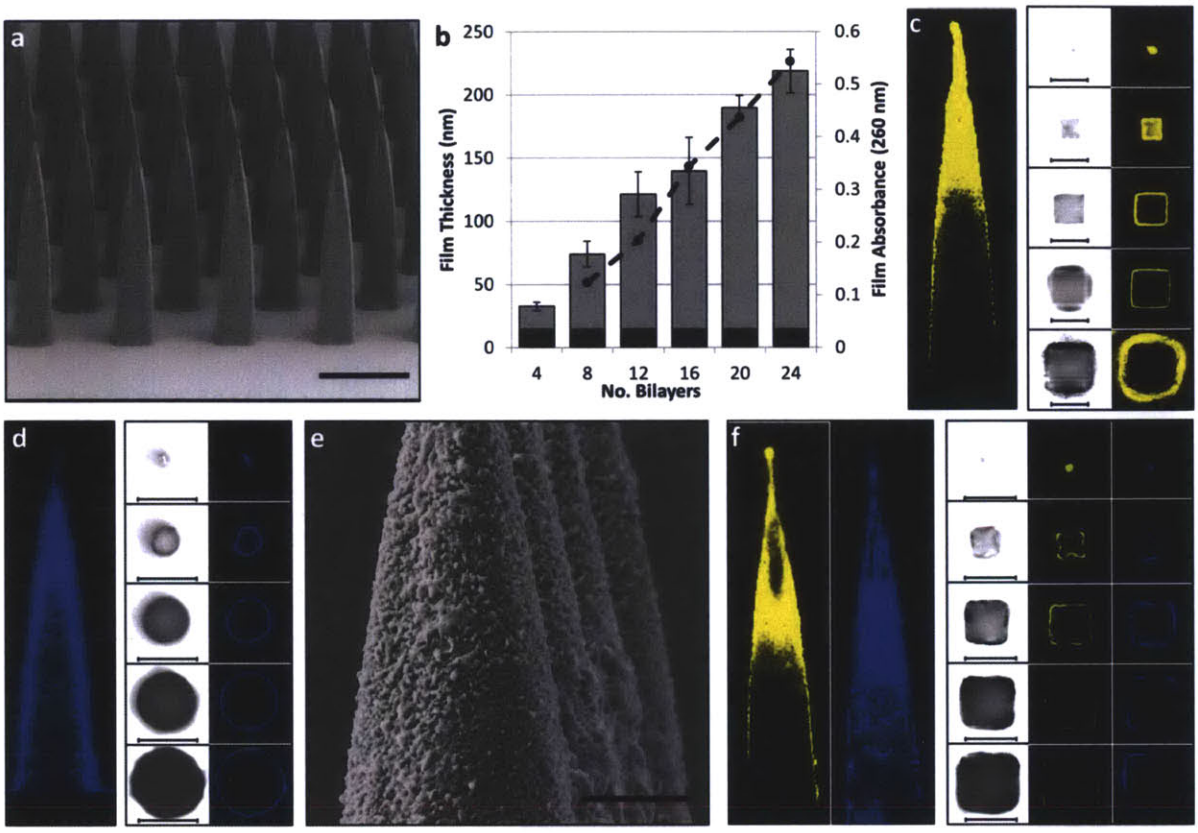

Figure 2-1: PLGA microneedle fabrication and LbL coating

(a) *SEM micrograph of uncoated PLGA microneedle arrays of pyramidal geometry (scale - 500μm).* ***(b)*** *Film growth (left axis) and absorbance (right axis) for (Poly-1/pLUC)$_n$ multilayers assembled on silicon/quartz substrates bearing a (PS/SPS)$_{20}$ initiating layer (black bar - (PS/SPS)$_{20}$, grey bar - (Poly-1/pLUC)$_n$, dashed line – Ab-260 nm).* ***(c, d)*** *Representative confocal micrographs showing a* ***(c)*** *(PS/SPS)$_{20}$-(Poly-1/Cy3-pLUC)$_{24}$ coated microneedle and a* ***(d)*** *(PS/SPS)$_{20}$-(Poly-1/DiI-PLGA NP)$_4$ coated microneedle (left – transverse section, right – lateral sections, 200μm intervals, scale - 200 μm).* ***(e)*** *SEM micrograph showing a (PS/SPS)$_{20}$-(Poly-1/PLGA NP)$_4$ coated microneedle array (scale - 50μm).* ***(f)*** *Representative confocal micrographs showing a (PS/SPS)$_{20}$-(Poly-1/Cy3-pLUC)$_{24}$-(Poly-1/DiD-PLGA NP)$_4$ co-coated microneedle (transverse and lateral sections, left – Cy3-pLUC, right – DiD-PLGA NP, scale - 200 μm).*

2.3.2. *Polymer Multilayer Deposition*

To fabricate a biodegradable PEM coating capable of controlled DNA release *in vivo*, we employed a hydrolytically degradable poly(β-amino ester) (PBAE), designated polymer-1 (poly-1, **Supplementary Figure S2-3**).[69] PBAEs have been previously shown to be biocompatible and degradable, to build multilayers with DNA that transfect cells *in vitro*, and to have adjuvant

activity when co-delivered with DNA vaccines.[7,65,67] Poly-1 in particular has been used recently by our group to fabricate LbL films with controlled erosion and tunable drug release,[64,98,99] and by others to fabricate DNA-releasing PEM films for potential gene delivery applications.[71,91] To provide a uniform initial surface charge density for PEM film growth on the PLGA microneedles, we first deposited twenty bilayers of poly(4-styrene sulfonate) (SPS), a synthetic polyanion, and protamine sulfate (PS), a mixture of four related biocompatible, highly cationic polypeptides of approximately 30 amino acids (**Supplementary Figure S2-1**).[100,101] Onto this base film, PEMs were built through the alternating adsorption of poly-1 and plasmid DNA (encoding firefly luciferase, pLUC). Surface profilometry and UV absorbance indicated linear growth of poly-1/plasmid DNA multilayers (~0.5 ± 0.1 μg pDNA/cm^2/bilayer) when deposited onto the (PS/SPS) base-layer (**Figure 2-1b**). Confocal laser scanning microscopy (CLSM) was used to qualitatively examine microneedles coated with Cy3-labeled pDNA PEMs. Microneedle arrays coated in this way showed surface-localized fluorescence conformally coating each microneedle (**Figure 2-1c and Supplementary Figure S2-4a**), while control uncoated needles showed no background fluorescence (data not shown).

We next tested whether a similar approach could be used to incorporate biodegradable polymer NPs into microneedle coatings. Lipid-coated PLGA NPs (244 nm in diameter, PDI 0.15) bearing a phospholipid surface layer composed of the zwitterionic lipid DOPC, the anionic lipid DOPG, and containing a lipophilic tracer dye (DiI or DiD) were prepared using an emulsion/solvent evaporation process we recently described.[80] Microneedles were primed with a (PS/SPS) base layer as before, and then alternating layers of poly-1 and PLGA NPs were deposited onto the arrays *via* spray LbL multilayer self-assembly (**Supplementary Figure S2-1**).[81] CLSM (**Figure 2-1d and Supplementary Figure S2-4b**) and SEM (**Figure 2-1e**) imaging of the nanoparticle PEM-coated arrays revealed conformal coatings on the microneedles, similar to the results seen with poly-1/DNA films. Four (poly-1/NP) bilayers produced a coating approximately 2 μm thick as measured by profilometry. In addition, serial deposition of (poly-1/pLUC) followed by (poly-1/NP) bilayers on the same microneedle array permitted the creation of films carrying both functional components (**Figure 2-1f and S2-4c**). Thus, PEM-coated microneedles have the potential to act as multifunctional delivery platforms, carrying cargos with diverse physical properties.

2.3.3. *Microneedle Insertion and Delivery In Vivo*

We next analyzed the penetration of microneedle arrays into the dorsal ear skin of C57Bl/6 mice or C57Bl/6-MHC II-GFP mice, transgenic animals expressing green fluorescent protein (GFP) fused to all class II major histocompatibility complex (MHC) molecules.[96] The MHC II-GFP fusion protein provided an *in situ* fluorescence marker for the viable epidermis in skin samples from these mice, as fluorescent epidermal MHC II$^+$ Langerhans cells (LCs) are readily detected by CLSM in mouse auricular skin.[64] Prior reports have demonstrated that microneedles prepared from biodegradable polymers with suitable elastic moduli and needle geometries can penetrate human cadaver skin.[97] To confirm that our PLGA arrays could similarly penetrate murine skin,

uncoated microneedles were applied to dorsal ear skin. Trypan blue staining revealed efficient and consistent penetration of PLGA microneedle arrays through the SC;[48] light microscopic inspection of arrays before/after application showed some buckling/bending but little breakage of the needle tips (**Figure 2-2a and Supplementary Figure S2-5**). CLSM imaging of ear skin from MHC II-GFP transgenic mice showed that microneedles readily penetrated into the viable epidermis where LCs were colocalized within the same z-plane (**Supplementary Figure S2-6**). To determine if PEM-coated microneedle arrays could deliver pDNA and/or NP cargos into the skin, we prepared PEM-coated microneedles carrying Cy3-labeled pLUC DNA (Cy3-pLUC) or DiI-labeled PLGA NPs (DiI-PLGA NPs). These PEM-coated arrays were applied to the ears of live anesthetized MHC II-GFP mice for 1 min, 5 min or 24 hrs, and then both the freshly explanted ear skin and the applied microneedles were examined by CLSM. Interestingly, the cargo delivery properties of these two types of microneedle coatings were quite distinct. Microneedles carrying (poly-1/pDNA) films examined before and after application to skin showed very little loss of DNA from the needle surfaces after applications of 1 or 5 min (**Figure 2-2b and Supplementary Figures S2-7a, b, d, and data not shown**), and little detectable transferred DNA in the epidermis (**Figure 2-2d and Supplementary Figure S2-8a**), but arrays applied to skin for 24 hours led to nearly complete loss of pDNA from the microneedles (**Figure 2-2b and Supplementary Figure S2-7c, d**) with a corresponding pronounced accumulation of DNA in the skin at depths colocalizing with LCs (**Figure 2-2e and Supplementary Figure S2-8b**). In contrast, microneedles carrying 4 bilayers of spray-deposited (poly-1/PLGA NP) films showed immediate transfer of NPs into the epidermis and coincident loss of NP signal from the microneedles themselves following even a 5 minute application on the skin (**Figure 2-2c, 2-2f, and Supplementary Figures S2-9, S2-10**). These disparate results suggest that plasmid DNA-containing PEM thin films remained intact upon microneedle penetration and subsequently release DNA over a period of 24 hours, while PLGA NP-containing PEM thin films are likely deposited in the skin concomitantly with microneedle insertion. It is anticipated that pDNA undergoes some degree of interpenetration during incorporation in PEMs, consistent with other polyion species. This would lead to molecular entanglements that would not be present in the nanoparticle thin films and could account for the relative ease of removal of these films once inserted into the skin. Thus both PEM multilayer architecture and the nature of the encapsulated components are parameters controlling the delivery properties of PEM-coated microneedles. Notably, arrays coated first with (poly-1/pLUC) followed by 4 bilayers of spray-deposited (poly-1/PLGA NPs) co-delivered DNA and PLGA NPs to the skin of live mice after a 24-hr application (**Figures 2-2g and Supplementary Figure S2-11**).

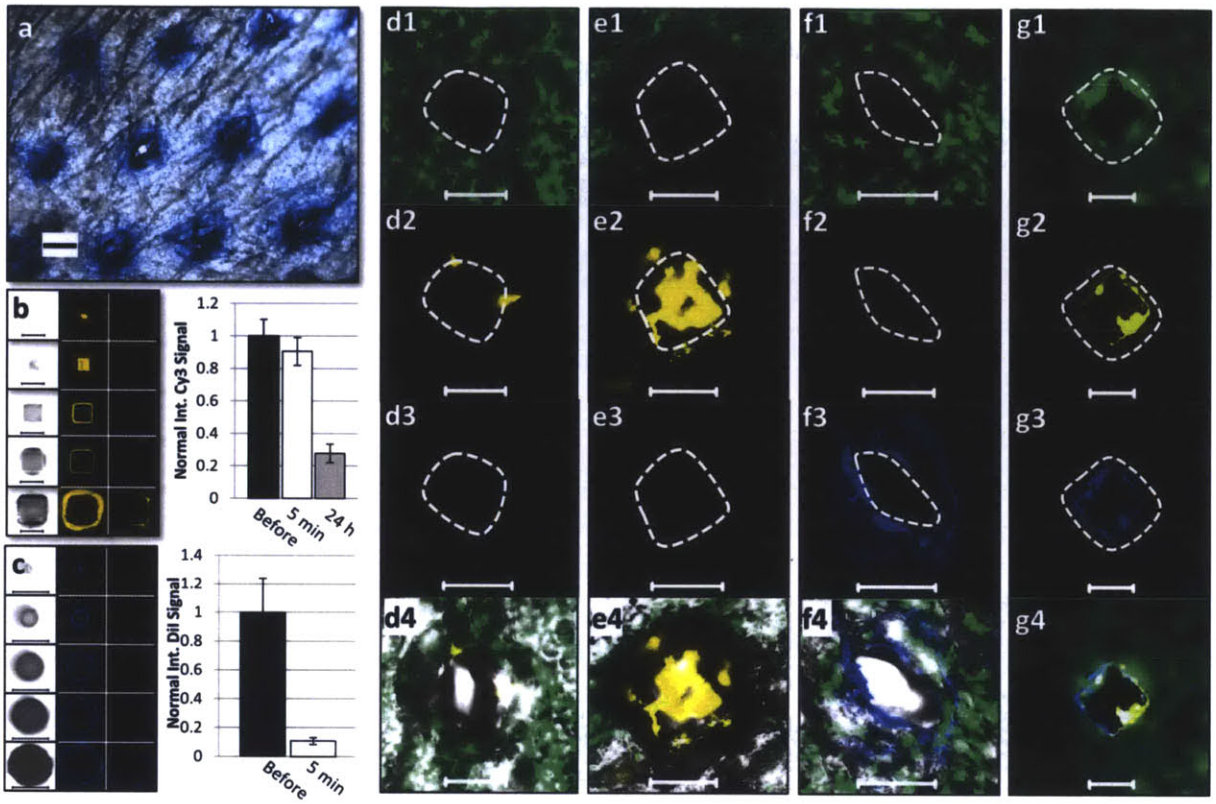

Figure 2-2. Microneedle delivery of polymer nanoparticles and plasmid DNA

(a) *Optical micrograph of ear skin showing microneedle penetration pattern stained using trypan blue (scale – 100μm).* ***(b)*** *Representative confocal z-stacks and quantification (n = 6) of $(PS/SPS)_{20}$-$(Poly\text{-}1/Cy3\text{-}pLUC)_{24}$-coated microneedle arrays (left – brightfield, middle – before application, right – after 24 hour application, 200μm interval, scale - 200μm).* ***(c)*** *Representative confocal z-stacks and quantification (n = 6) of $(PS/SPS)_{20}$-$(Poly\text{-}1/DiI\text{-}PLGA\text{-}NP)_4$ coated microneedle arrays (left – brightfield, middle – before application, right – after 5 minute application, 200μm interval, scale – 200μm). Representative confocal micrographs (1 – MHC-GFP II, 2 – Cy3-pLUC, 3 – DiI/D-PLGA NP, 4 – overlay, scale – 200μm) showing dorsal ear skin following* ***(d)*** *5 minute and* ***(e)*** *24 hour application of a $(PS/SPS)_{20}$-$(Poly\text{-}1/Cy3\text{-}pLUC)_{24}$ coated microneedle array,* ***(f)*** *5 minute $(PS/SPS)_{20}$-$(Poly\text{-}1/DiI\text{-}PLGA\text{-}NP)_4$ coated microneedle application, and* ***(g)*** *24 hour $(PS/SPS)_{20}$-$(Poly\text{-}1/Cy3\text{-}pLUC)_{24}$-$(Poly\text{-}1/DiD\text{-}PLGA\ NP)_4$ coated microneedle application.*

Although murine and human skin exhibit a number of structural differences, preclinical mouse studies of transcutaneous vaccine delivery have been remarkably predictive of clinical trial results.[20] In addition, the mouse model permits a detailed functional analysis of biological responses to delivered pDNA or NPs. In order to further evaluate the potential of PEM-coated microneedle arrays for transcutaneous DNA delivery, we assessed the ability of (poly-1/pLUC)-coated PLGA microneedles to transfect cells *in vivo*. PEM-coated microneedles were applied to

the dorsal ear skin of C57BL/6 mice, and *in vivo* transfection was quantified over time using whole animal bioluminescence imaging to detect luciferase expression. Mice were treated by application of a 24 bilayer (poly-1/pLUC)-coated microneedle array to ear skin for 5 minutes (**Figure 2-3a**), or a 1- (**Figure 2-3b**), 5- (**Figure 2-3c**) or 24-bilayer (**Figure 2-3d**) array for 24 hrs. Bioluminescence was then monitored *in vivo* for 7 days. Successful *in vivo* transfection and expression of firefly luciferase in the ear skin was detected for both 5 minute and 24 hr application times, despite the low level of pDNA detected in skin for the former (**Figure 2-3e**). In both cases, luciferase expression was detected for over a week, though pLUC-coated microneedles applied for 24 hours resulted in an increase in the intensity of luciferase expression, as expected from the CLSM results described above. Additionally, the iterative nature of LbL film construction is amenable to robust dosage control. Application of microneedle arrays coated with 1, 5, or 24 bilayers of (poly-1/pLUC) for 24 hrs gave luciferase expression levels spanning an order of magnitude (**Figure 2-3f**).

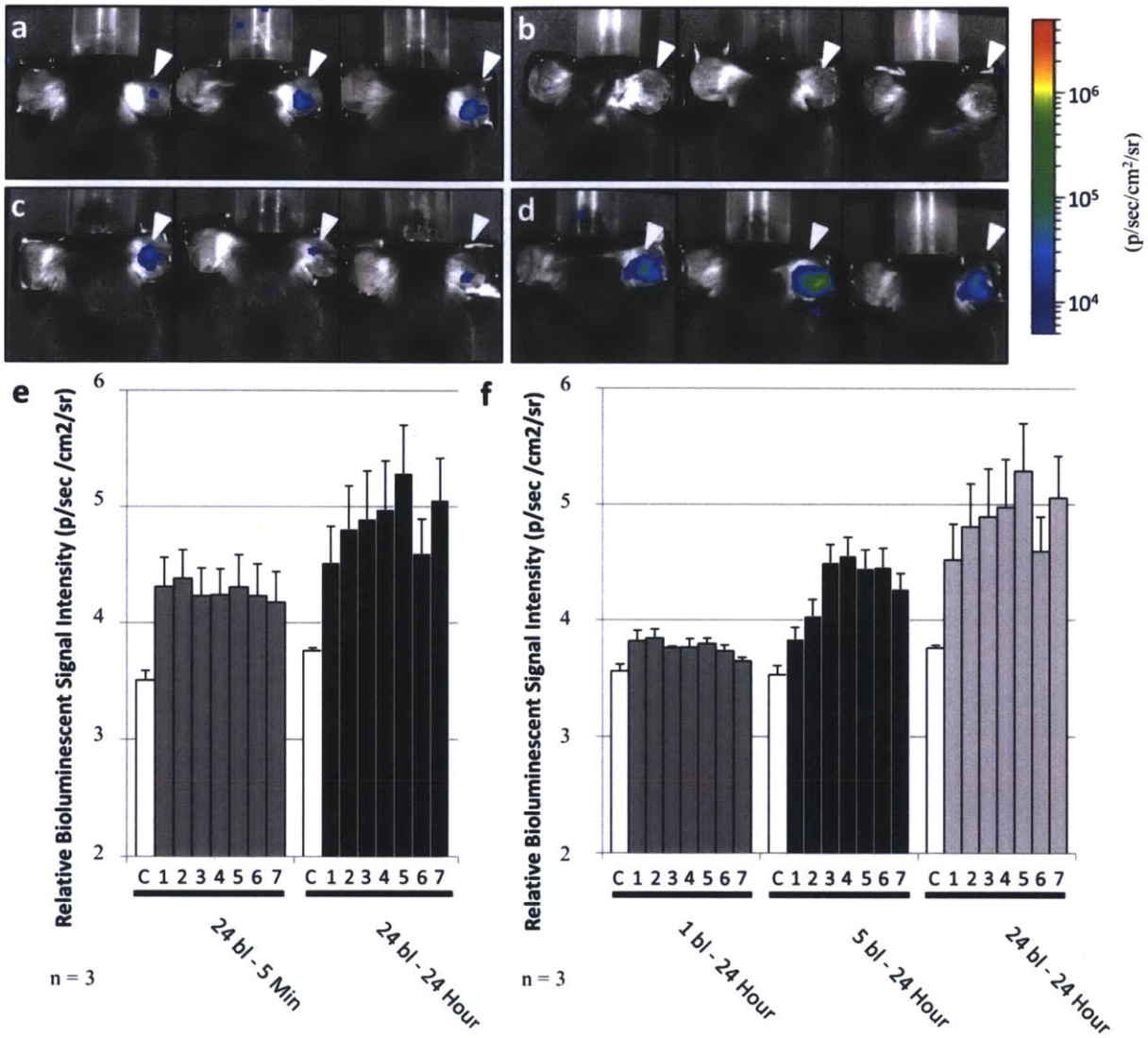

Figure 2-3. *In vivo* delivery and transfection of plasmid DNA

In vivo bioluminescent signal observed in C57BL/6 mice (n = 3) following treatment with a $(PS/SPS)_{20}$-$(Poly\text{-}1/pLUC)_n$ – coated microneedle array to the right ear: ***(a)*** *24 bilayers for 5 minutes,* ***(b)*** *1 bilayer for 24 hours,* ***(c)*** *5 bilayers for 24 hours, and* ***(d)*** *24 bilayers for 24 hours. The bioluminescent results following treatment are summarize in* ***(e, f)*** *for 7 days together with the negative control signal (denoted C) collected from the untreated ear, with* ***(e)*** *demonstrating the effect of application time and* ***(f)*** *showing the result of increasing pLUC dosage.*

2.4. Conclusions

In conclusion, as a first step towards the design of a general materials platform for transcutaneous DNA and therapeutic NP delivery, we have demonstrated for the first time the application of LbL directed-assembly for the deposition of functional coatings on microneedle

arrays. We have shown the versatility of this approach, engineering PEM films containing pDNA and/or degradable polymer NPs, and demonstrating their utility for delivery into the viable epidermis through microneedle application. Finally, we have shown for the first time to our knowledge, successful *in vivo* transfection *via* DNA released from microneedle-supported PEM films. These findings suggest the potential utility of these materials for DNA vaccine delivery and gene therapy, as well as the possibility of co-delivery of therapeutic-loaded degradable polymer NPs for sustained and controlled release of encapsulated materials *in vivo*.

3. POLYMER MULTILAYER TATTOOING FOR ENHANCED DNA VACCINATION

3.1. Introduction

In Chapter 2 we described the design and testing of an approach for therapeutic formulation and delivery from multilayer films deposited on microneedle surfaces. Despite the success of this system for effective delivery *in vivo* important limitations remained unresolved. Prolonged application times were required *in vivo* to mediate effective delivery through film degradation, thus limiting the practicality of administration and limiting the potential use of polymers with longer degradation kinetics. In Chapter 3, we present the design and testing of an improved system intended to provide rapid administration and enable the use of slower degrading polymers for more sustained vaccine release *in vivo*.

DNA vaccines have been intensively studied due to potential advantages such as ease of GMP production, lack of anti-vector immunity, and capability to promote both cellular and humoral immune responses.[4,102] However, plasmid DNA (pDNA) immunization has shown poor efficacy in non-human primates and human trials,[4,5] and the most promising methods for increasing the potency of these vaccines have employed involved methods such as *in vivo* electroporation that are not attractive for widespread prophylactic vaccination.[103] Parallel to the technical challenges of DNA vaccination, traditional needle-based administration of vaccines has a number of disadvantages: liquid vaccine formulations typically require refrigeration that raises the cost and complexity of global distribution (the "cold chain"),[12] administration requires trained personnel, and safety is hampered by needle re-use and needle-based injuries.[14] These issues become particularly acute for vaccine distribution in the developing world.[13-15]

We hypothesized that DNA vaccine delivery would be substantially enhanced by an approach that could simultaneously *(i)* target DNA to tissues rich in immune-response-governing dendritic cells, *(ii)* promote sustained transfection without toxicity, *(iii)* and provide supporting inflammatory cues to enhance the induction of a potent immune response. In addition, vaccines have been shown to vary widely in potency depending on the kinetics of both antigen and adjuvant exposure, with optimal immunity often stimulated by persistence of antigen and inflammatory signals for up to one week.[104-107] To meet these design goals, we developed a strategy using microneedles to rapidly implant into the skin biodegradable polymer films, which continuously release DNA polyplexes and adjuvant molecules in this immunologically-competent tissue over a tunable and sustained period of time. We show that skin-implanted vaccine multilayers allow control over the physical and functional persistence of inflammatory adjuvants and pDNA, efficiently transfecting cells in murine skin and eliciting cellular and humoral immune responses comparable to or exceeding *in vivo* electroporation of pDNA, one of the most promising current technologies for DNA vaccine delivery.[103] We have termed this approach of implanting persistent polymer films into the skin 'multilayer tattooing', by analogy to conventional tattooing where persisting inks are deposited in the skin. These multilayer vaccine formulations allow for dry-state storage of coated microneedle patches at room

temperature for weeks without loss of activity, an important advantage for decreasing costs and improving vaccine availability in remote areas. Further, when applied to viable macaque skin *ex vivo*, multilayer tattooing elicited 140-fold greater gene expression compared to naked DNA injection. Thus, this polymer film tattooing approach may offer a route to efficacious DNA vaccines *via* a pain-free and self-administrable dry skin-patch platform.

3.2. Materials and Methods

3.2.1. Materials

(b)PNMP (31:59:10 oNBMA:MMA:PEGMA by mol, 17 kDa), poly-1 (15 kDa), and poly-2 (20 kDa) were synthesized as previously reported.[69,108] AL-11/H-2K^b-peptide-MHC II tetramers were provided by the NIH tetramer core facility.

3.2.2. PLLA Microneedle Fabrication

PDMS molds (Sylgard 184, Dow-Corning, Midland, Michigan) were prepared using a Clark-MXR-CPA-2010 (VaxDesign Inc., Orlando, Florida). PLLA (IV 1.9 dL g^{-1}, Lakeshore Biomaterials) was melted over the molds under vacuum (-25 in. Hg, 200°C, 40 min), and then cooled to -20°C before removal and crystallization at 140°C for 4 hr for solvent resistance.

3.2.3. PNMP Release Layer Deposition

On Si substrates, 3 wt% PNMP in 1,4-dioxane was deposited using a Specialty Coating Systems P6700 (Indianapolis, Indiana). On PLLA microneedles, 0.25 wt% (b)PNMP was spray deposited as previously described (0.2 mL s^{-1}, 15 cm range, 10s).[81] Films were dried under vacuum at 25°C for 12 hr. bPNMP release-layers were labeled with Alexafluor-488-conjugated-SAv (10 μg mL^{-1} in PBS pH 6.0, Sigma-Aldrich, St. Louis, Missouri).

3.2.4. Polymer Multilayer Film Preparation

LbL films were assembled using a Carl Ziess HMS-DS50 stainer. Films were constructed on Si wafers and PLLA microneedles following deposition of (b)PNMP and photoswitching *via* UV-irradiation (254 nm, 2.25 mW cm^{-2}) for 15 min. (PS/SPS) base layers were deposited through alternative immersion into PS (2 mg mL^{-1}, Sigma-Aldrich) and SPS (5 mM, Sigma-Aldrich) for 10 min, separated by two 1 min PBS rinses. (PBAE/nucleic acid) multilayers were deposited similarly, alternating 5 min dips in poly-1/2 (2 mg mL^{-1}) and either pLUC, pGag, or poly(I:C) (Invivogen, San Diego, California) solutions (1 mg mL^{-1}) separated by two 30 sec PBS rinses. Fluorescent pLUC and poly(I:C) were prepared using Cy5 and tetramethyl-rhodamine (TMR) Label-IT reagent (Mirus Bio Corporation, Madison, Wisconsin). All solutions were in PBS, adjusted to pH 5.0. Films were characterized using a Veeco Dektak profilometer and a Zeiss LSM510. Data analysis was performed using Image J. Film loading was determined using a SpectraMax 250 following elution of films in PBS, pH 7.4, 2M NaCl for 24 hours.

3.2.5. In Vitro/In Vivo Delivery

For *in vitro* release experiments, $(PS/SPS)_{20}(PBAE/nucleic\ acid)_{35}$ films were incubated in PBS at 37°C and aliquots were assayed for pLUC or poly(I:C) using picogreen or ribogreen assay kits (Invitrogen). For *in vitro* delivery, coated microneedles were incubated in PBS, pH 7.4 and imaged by confocal microscopy. *In vivo* delivery experiments were performed on anesthetized C57BL/6 mice (Jackson Laboratories, Bar Harbor, Maine) and MHC II-GFP transgenic mice (a gift from Prof. Hidde Ploegh).[96] Ears were rinsed with PBS on the dorsal side and dried before application of microneedle arrays by gentle pressure. Applied microneedles were imaged by confocal. Treated skin was excised and stained with trypan blue for needle penetration. Ears treated with Cy5-pLUC- or TMR-poly(I:C)-coated microneedles (±UV-treatment) were mounted and imaged by confocal. Clearance of fluorescent poly(I:C) and transfection in mice treated with pLUC-coated arrays (±UV-treatment) was measured using an IVIS Spectrum 200 (Caliper Lifesciences, Hopkinton, Massachusetts). For luminescent measurements of pLUC expression, mice were imaged following IP administration of D-luciferin (150mg kg^{-1}). For luminescent imaging of MPO-dependent oxidative burst, luminol sodium salt (Santa Cruz Biotech, Santa Cruz, California) was administered IP (250mg kg^{-1}) before imaging as previously described.[109] Fluorescence/bioluminescence data was processed using region of interest (ROI) analysis with background subtraction and internal control ROI comparison to untreated skin using the Living Image 4.0 software package (Caliper).

3.2.6. *Vaccinations*

Animal studies were approved by the MIT IUCAC and animals were cared for in the USDA-inspected MIT Animal Facility under federal, state, local, and NIH guidelines for animal care. Groups of 4 C57Bl/6 mice were immunized with 20 μg pGag and 10 μg poly(I:C) by intramuscular injection (15 μl, quadriceps) with or without *in vivo* electroporation (Harvard Apparatus ECM830, 2x60ms pulses, 200V cm^{-1}), intradermal injection (15 μl, dorsal ear skin, poly(I:C) mixed with free DNA or DNA/poly-1 polyplexes), or by microneedle array (15 min application of $(PS/SPS)_{20}(poly\text{-}1/poly(I:C))_{35}(poly\text{-}1/pGag)_{35}$ on *uv*-PNMP and native-PNMP coated PLLA arrays). To form poly-1/pDNA polyplexes, pDNA was mixed as previously described with PBAE (1:1 ratio by mass) in deionized water and vortexed briefly prior to injection.[65] All animals received the same delivered doses of pGag and poly(I:C); microneedle-delivered dosages were determined by comparison of total eluted pDNA from coated arrays before and after treatment. Frequencies of Gag-specific $CD8^+$ T-cells and their phenotypes were determined by flow cytometry analysis of peripheral blood mononuclear cells following staining with DAPI (live/dead), anti-CD8α, anti-CD44, anti-CD62L, and AL-11/H-$2K^b$-peptide-MHC tetramers. Anti-Gag IgG titers, defined as the dilution of sera at which OD reading was 0.25, were determined by ELISA using SIV-mac251 (My Biosource, San Diego, California) coated plates, and UV-Vis detection of peroxidase conversion of tetramethybenzydine (KPL, Gaithersburg, Maryland) using HRP-conjugated anti-IgG (Jackson Immunoresearch, West Grove, Pennsylvania). To assess recall responses, microneedle-treated animals were challenged with 50 μg intramuscular pGag in the quadriceps and cytokine expression was measured by flow

cytometry in peripheral blood mononuclear cells following stimulation with AL11 peptide, treatment with brefeldin A, and staining with DAPI, anti-CD8 α, and anti-IFN γ, anti-TNF α.

3.2.7. *Ex Vivo Macaque Skin Culture and Microneedle Testing*

Macaque studies were approved by the Harvard Medical School IACUC. Outbred Rhesus monkeys were housed at New England Primate Research Center. Fresh skin was obtained from the quadriceps of euthanized Rhesus macaques. Skin was mounted on slides and microneedles were applied by gentle pressure. Skin was stained using trypan blue for needle insertion, formaldehyde fixed, and embedded in paraffin for histological sectioning, hemotoxylin and eosin staining, and optical imaging. To assay *ex vivo* transfection, pLUC was injected intradermally (20 μg in 10 μl PBS) or delivered by microneedle in $(PS/SPS)_{20}(poly\text{-}1/pLUC)_{35}$ multilayers overlying native or *uv*-PNMP. Skin was cultured as previously described[110] and imaged using an IVIS Spectrum after addition of 300 μg luciferin to the culture media. Data analysis was performed as before using the Living Image Software package.

3.2.8. *Statistical Analysis*

Statistical analysis was performed with Graphpad Prism (La Jolla, California) using two-way analysis of variance or t-test. Values are reported as mean ± s.e.m.

3.3. ***Results and Discussion***

3.3.1. *PLLA Microneedle Fabrication and Multilayer Coating*

We first set out to create implantable vaccine coatings using polyelectrolyte multilayers (PEMs, **Figure 3-1a**),[111,112] nanostructured films formed by iterative adsorption of alternately-charged polymers, which embed large weight-fractions of biologic cargos (e.g., DNA, up to 40% of total film mass),[62] stabilize embedded molecules in the dried state,[113,114] and exhibit release kinetics predetermined by the film architecture/composition. We hypothesized that rapid multilayer transfer from coated microneedles into the epidermis could be achieved *via* an underlying polymer film designed to instantly dissolve when microneedles are applied to the skin (**Figure 3-1b**), allowing the kinetics of DNA/adjuvant release in the tissue to be tailored separately from the time required for a microneedle patch to be kept on the skin. To create such releasable vaccine coatings, we employed a photo-sensitive and pH-responsive polymer, Poly(o-Nitro-benzyl-methacrylate-*co*-Methyl-methacrylate-*co*-Poly(ethylene-glycol)-methacrylate) (PNMP), for the release-layer. PNMP is initially organic-soluble, but on brief exposure to UV, cleavage of the o-nitrobenzyl groups converts the polymer to a weak polyelectrolyte (*uv*-PNMP) soluble in water above pH ~6.5.[108] As shown below, this photo-switchable solubility provided the means to prove that PEM film implantation depended on PNMP release-layer dissolution.

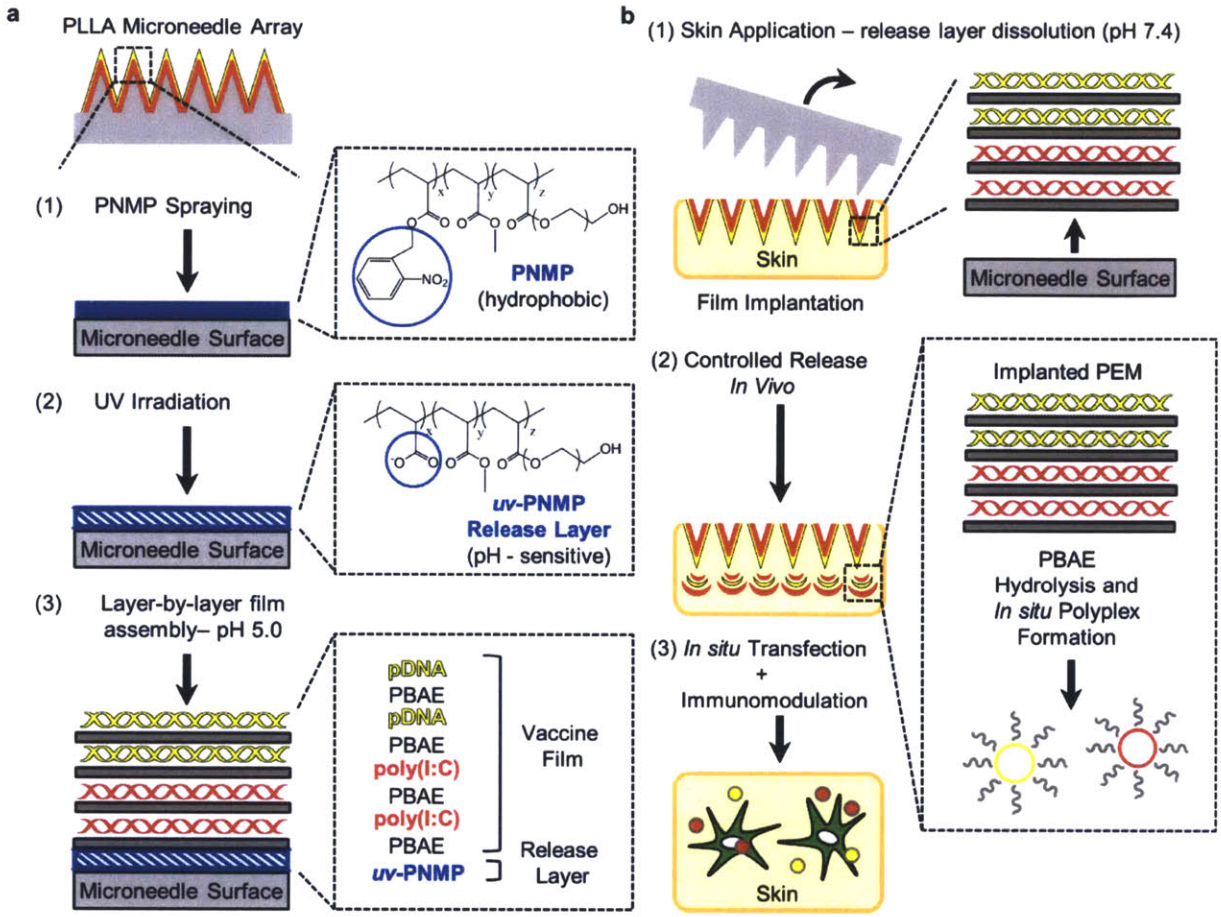

Figure 3-1. Design of quick-release vaccine loaded microneedle coatings

(a) *Schematic view of release-layer-mediated multilayer tattooing strategy using coated microneedles: (1) PLLA microneedles are coated with PNMP release-layer films through spray deposition; (2) UV-irradiation imparts pH-sensitive aqueous solubility to the PNMP film, forming a uv-PNMP 'release-layer'; (3) Overlying multilayer films containing nucleic acids are constructed using LbL deposition at pH 5.0.* ***(b)*** *Mechanism of action for multilayer tattooing: (1) Microneedle application to skin and exposure to interstitial fluid gives rapid release-layer dissolution, mediating overlying film delamination and retention in skin following microneedle removal; (2) Implanted films provide sustained release of nucleic acids through hydrolytic PBAE degradation and release of in situ-formed PBAE/nucleic acid polyplexes; (3) released polyplexes mediate local transfection and immune modulation in the tissue.*

Skin patches were fabricated by melt-molding poly(L-lactide) (PLLA) on poly(dimethyl-siloxane) (PDMS) molds to obtain arrays of microneedles each 250 μm in diameter at their base and 650 μm in height (Supplementary **Figure S3-1**).[115] Biotinylated-PNMP (bPNMP, **Supplementary Figure S3-2a**) films were coated on microneedles by spray deposition[81] from 1,4-dioxane solutions, UV-exposed to trigger the photochemical transition in the film, and then

stained with fluorescent streptavidin (SAv) to permit visualization of the release-layer by microscopy. Next, LbL deposition was used to construct an overlying PEM film composed of Cy5-labeled pDNA encoding luciferase (Cy5-pLUC) and the transfection agent poly-1, a biodegradable poly(β-amino-ester) (PBAE, **Supplementary Figure S3-2b**).[67,115] PEM films were initiated by depositing 20 bilayers of protamine-sulfate (PS) and poly(4-styrene-sulfonate) (SPS) to provide a uniform charge density, followed by iterative adsorption of poly-1 and Cy5-pLUC (**Figure 3-2a**). Profilometry measurements performed on PEMs constructed in parallel on Si substrates showed linear multilayer growth with increasing deposition cycles as previously reported for (PBAE/pDNA) films (**Figure 3-2b**).[67,115] Confocal imaging of microneedles coated with composite (*uv*-bPNMP)$(PS/SPS)_{20}$(poly-1/Cy5-pLUC)$_{35}$ PEM films showed conformal co-localized fluorescence from SAv-labeled *uv*-bPNMP and Cy5-pLUC over the surface of each PLLA microneedle (**Figure 3-2c**). (Individual *uv*-bPNMP and PEM films were too thin to resolve as distinct layers). When analyzed at sequential stages of PEM film deposition, the mean total SAv-bPNMP fluorescence signal from single microneedles was stable but Cy5-pLUC fluorescence linearly increased with increasing rounds of bilayer deposition, confirming linear film growth on microneedles (**Figure 3-2d**). Measurement of DNA recovered from microneedle coatings disrupted by treatment with sodium chloride showed ~4.2μg DNA deposited per bilayer per cm^2 of the microneedle array (**Figure 3-2d**). Sequential assembly of PEM films comprising layers of (poly-1/poly(I:C)) followed by layers of (poly-1/pLUC) generated microneedles coated with complete vaccine multilayers containing pDNA, a transfection agent, and a strong adjuvant (**Figure 3-2e**). These composite films showed conformal coating of both vaccine components (**Figure 3-2f**) and linear growth of pLUC layers over poly(I:C) layers with increasing number of deposition cycles (**Figure 3-2g, h**). Key to this process is that the DNA-containing PEM is never exposed to UV-irradiation, thus avoiding any potential damage due to UV exposure.

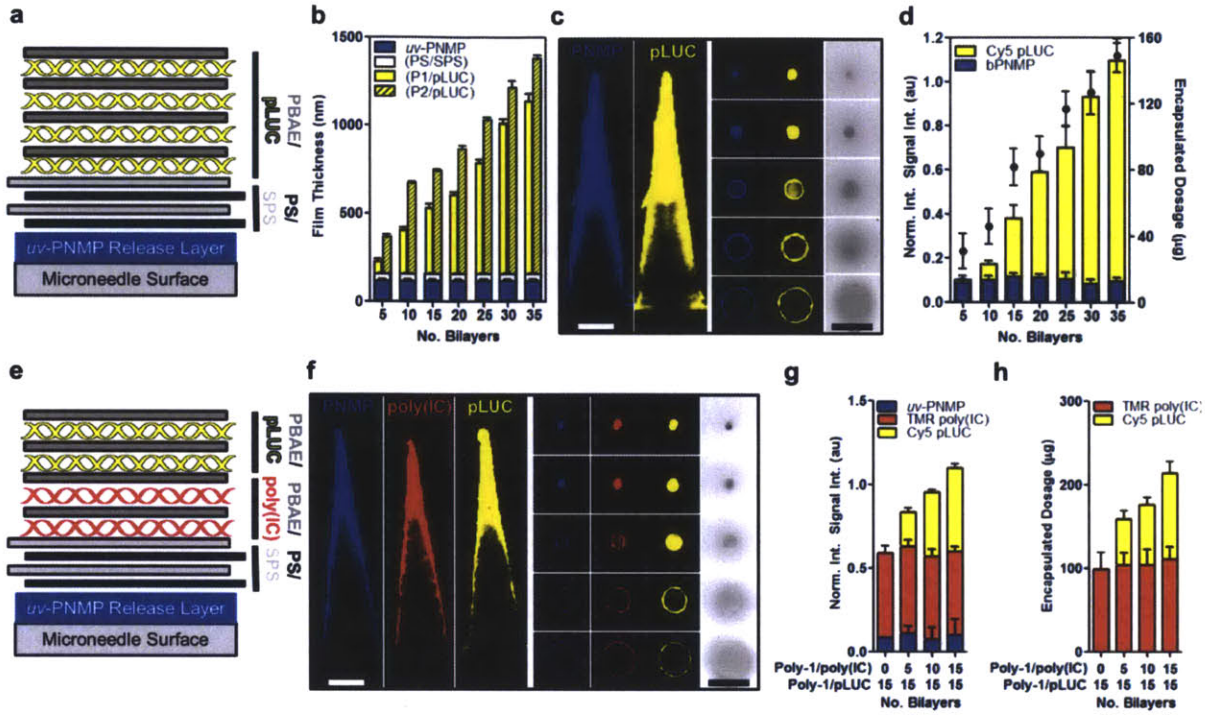

Figure 3-2. LbL assembly of microneedle coatings carrying DNA, immunostimulatory RNA, and transfection agents

*(**a**) Film architecture for (uv-PNMP)(PS/SPS)$_n$(PBAE/pLUC)$_n$ multilayers.(**b**) Growth of (poly-1/pLUC)$_n$ and (poly-2/pLUC)$_n$ multilayers assembled onto (uv-PNMP)(PS/SPS)$_{20}$ films on silicon substrates as a function of the number of deposited (PBAE/pLUC) bilayers as measured by surface profilometry. Data represent the mean±s.e.m, n = 8. (**c**) Representative confocal images of PLLA microneedles coated with (SAv488-bPNMP)(PS/SPS)$_{20}$(poly-1/Cy5-pLUC)$_{35}$ films (left – transverse optical sections, right – lateral sections, 100µm z-intervals, scale bars 200 µm, blue – Sav488-uv-bPNMP, yellow – Cy5-pLUC). (**d**) Quantification of Cy5-pLUC and Sav488-bPNMP incorporated into (SAv488-bPNMP)(PS/SPS)$_{20}$(poly-1/Cy5-pLUC)$_n$ films on microneedles through confocal fluorescence intensity analysis (left axis, n = 15) and measurement of total DNA recovered from dissolved films (right axis, n = 3). Data represent the mean±s.e.m. (**e**) Film architecture for (uv-PNMP)(PS/SPS)$_{20}$(poly-1/pLUC)$_n$(poly-1/poly(I:C))$_n$ multilayers. (**f**) Representative confocal images of microneedles coated with (SAv488-uv-bPNMP)(PS/SPS)$_{20}$(poly-1/TMR-poly(I:C))$_{15}$(poly-1/Cy5-pLUC)$_{15}$ films (left – transverse sections, right – lateral sections, 100µm z-intervals, scale 200 µm, blue – Sav488-uv-bPNMP, yellow – Cy5-pLUC, red – TMR-poly(I:C)). (**g, h**) Quantification of Cy5-pLUC, TMR-poly(I:C), and SAv488-bPNMP incorporated into (SAv488-bPNMP)(PS/SPS)$_{20}$(poly-1/TMR-poly(I:C))$_n$(poly-1/Cy5-pLUC)$_n$ films on microneedles through confocal fluorescence intensity analysis (**g**, n = 15) and measurement of total nucleic acids recovered from dissolved films (**h**, n = 3). Data represent the mean±s.e.m,*

Lack of toxicity/biocompatibility is critical for materials used in prophylactic vaccines, and the components of the microneedle system were chosen with biocompatibility in mind: polylactide used as the microneedle base is a bioresorbable polymer with a long history of clinical use in resorbable sutures and drug delivery devices. Although we chose to use (PS/SPS) 'base-layer' films for convenience in lab-scale studies, simplified film architectures composed of only PNMP and (PBAE/nucleic acids) could be deposited with linear growth per deposition cycle for 20 or more bilayers (data not shown). Previous studies have demonstrated the biocompatibility of both PNMP *in vitro*[108,116] and poly-1 and poly-2 polymers *in vitro* and *in vivo*.[66,69,117] Consistent with these data, we observed no apparent local toxicity in any of the mice treated throughout these studies.

3.3.2. *In Vitro/In Vivo Multilayer Delivery*

To test PEM film release from microneedle arrays, dried composite (SAv-labeled *uv*-bPNMP)(PS/SPS)$_{20}$(poly-1/Cy5-pLUC)$_{35}$ coatings (referred to henceforth as PNMP/PEM films) on microneedles were immersed in pH 7.4 PBS for varying times *in vitro* and imaged by confocal microscopy to quantitate *uv*-bPNMP and Cy5-pLUC fluorescence remaining on the microneedle surfaces. After 15 minutes incubation in PBS, we observed a significant loss of both bPNMP and Cy5-pLUC fluorescence from microneedle arrays (**Supplementary Figure S3-3**). By contrast, no film release was observed if PEMs were assembled onto PNMP coatings that had not been irradiated to photo-switch the release-layer's solubility. To determine whether microneedles coated with releasable films would permit rapid multilayer implantation *in vivo*, we applied dry (PNMP/PEM)-coated microneedles to the auricular skin of C57Bl/6-MHC II-GFP mice.[96] Trypan blue staining of treated skin in this case showed consistent microneedle insertion (**Figure 3-3a**). Mirroring our *in vitro* observations, confocal imaging of microneedles after 15 minutes application to murine skin showed that both *uv*-bPNMP and Cy5-pLUC fluorescence was rapidly lost from coated microneedles, but only if PNMP films were irradiated before multilayer assembly to prime for rapid dissolution of the release-layer (**Figure 3-3b, c**). Confocal imaging of skin samples following application of (PNMP/PEM)-coated microneedles for 15 minutes showed significant transfer of Cy5-pLUC in the epidermis co-localized with MHC II-GFP$^+$ Langerhans cells (LCs) (**Figure 3-3d**) and up to 400 μm deep into the skin (**Figure 3-3e**), but only when the PNMP layer was UV-primed. Similarly, microneedles carrying poly(I:C)-loaded PEM films deposited fluorescently-labeled poly(I:C) into the skin, colocalizing in the same z-plane with MHC II-GFP-expressing cell populations (**Figures 3-3f**). Twenty-four hours after implantation of (poly-1/nucleic acid) multilayers, the degrading films were observed dispersed into the tissue around the needle insertion site and showed apparent uptake in colocalized LCs (**Figure 3-3g**). Thus, the *uv*-PNMP release-layer promotes rapid transfer of DNA- or RNA-loaded films from microneedles into the skin.

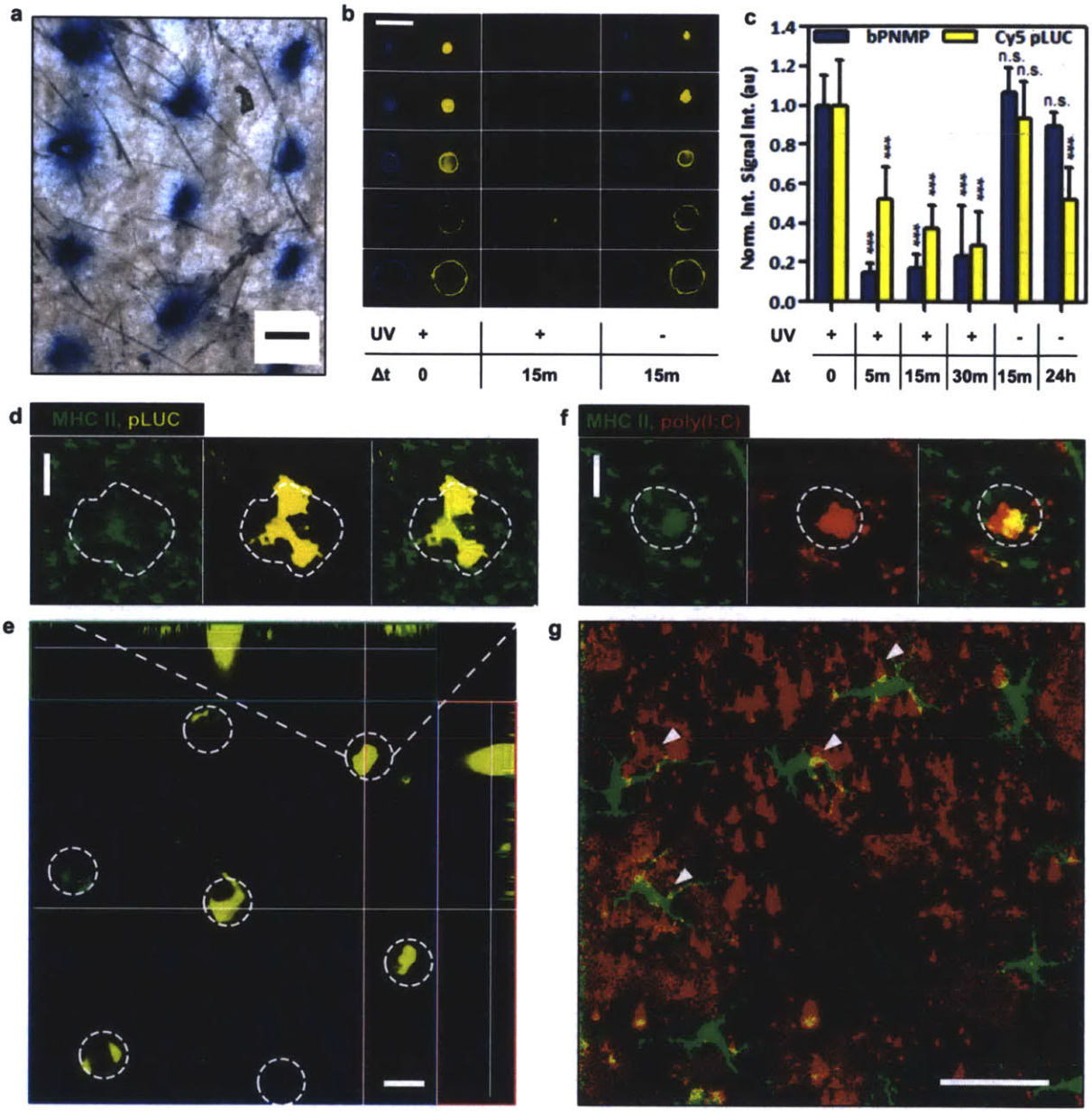

Figure 3-3. PNMP release-layers promote rapid implantation of multilayer films at microneedle penetration sites *in vivo*

(a) *Optical micrograph of ear skin stained with trypan blue to reveal epidermal penetration following PLLA microneedle application (scale bar, 500μm).* ***(b)*** *Representative confocal images of (SAv488-bPNMP)(PS/SPS)$_{20}$(poly-1/Cy5-pLUC)$_{35}$-coated PLLA microneedles with or without UV sensitization of the PNMP layer (blue - Sav488-bPNMP; yellow - Cy5-pLUC), before application, or after 15 min application to murine ear skin (lateral sections, 100 μm z-intervals, scale bar 200 μm).* ***(c)*** *Quantitation of confocal fluorescence intensities (n = 15) showing loss of Sav488-uv-bPNMP and Cy5-pLUC films from coated microneedles upon application to skin,*

*dependent on UV-induced photo-switching of the PNMP layer solubility. Data represent the mean±s.e.m, ***, p< 0.0001, analyzed by unpaired t-test.* ***(d)*** *Representative confocal image of treated murine skin showing film implantation after 15 min (green - MHC II-GFP; yellow - Cy5-pLUC; penetration site outlined, scale bar 100μm).* ***(e)*** *x-y/x-z/y-z confocal images showing depth of Cy5-pLUC film deposition after 15 minute microneedle application (green - MHC II-GFP; yellow - Cy5-pLUC; penetration sites outlined, scale bar 200μm).* ***(f)*** *Representative confocal image of treated murine skin showing TMR-poly(I:C) film implantation after 15 min microneedle application (green - MHC II-GFP; red - TMR-poly(I:C); penetration site outlined, scale bar 100 μm).* ***(g)*** *Colocalization and uptake of TMR-poly(I:C) by MHC II-GFP$^+$ LCs at microneedle insertion site 24 hrs following film implantation (green - MHC II-GFP; red - TMR-poly(I:C); yellow - overlay, scale bar 50 μm).*

3.3.3. Multilayer Control Over Vaccine Release In Vivo

We next tested whether the *in vivo* kinetics of nucleic acid release into the surrounding tissue could be controlled *via* the composition of multilayers implanted in the skin. Past studies have demonstrated the ability of multilayers composed of pDNA assembled with the PBAEs poly-1 or poly-2 to mediate release with varying kinetics.[70,118] Consistent with this prior work, $(PS/SPS)_{20}$(poly-1/poly(I:C))$_{35}$ and $(PS/SPS)_{20}$(poly-1/pLUC)$_{35}$ multilayers constructed on Si substrates exhibited rapid release at 37°C of ~80% pLUC or poly(I:C) within 24 hours, while analogous films constructed with poly-2 showed a slower release lasting ~1 week (**Supplementary Figure S3-4**). To determine whether the composition of PBAE multilayers implanted *via* microneedle delivery could mediate similar tunable release of nucleic acid therapeutics *in vivo*, we constructed (PBAE/Cy5-poly(I:C)) PEM films on *uv*-PNMP-coated microneedles using poly-1 or poly-2 as the PBAE component. Following application of coated microneedles to the skin of C57Bl/6 mice for 15 min, we monitored the fluorescence signal of implanted Cy5-poly(I:C) over time using whole-animal fluorescence imaging. Similar to the *in vitro* trend, films encapsulating poly(I:C) with poly-1 were quickly cleared from the application site, while (poly-2/poly(I:C)) films persisted for 10 days following application (**Figure 3-4a**). To quantify the functional impact of sustained polyI:C adjuvant release *in vivo*, we applied microneedles carrying (poly-2/poly(I:C)) multilayers to the auricular skin of mice or injected equivalent doses of free poly(I:C) intradermally at the same site, and administered the chemiluminescent probe luminol to trace local inflammation over time. Systemically-injected luminol emits photons when catabolized by myeloperoxidase (MPO) produced by activated innate immune cells at sites of inflammation.[109,119] As shown in **Figure 3-4b**, bolus poly(I:C) injection elicited a transient burst of inflammation that resolved by 48 hr, while multilayer implantation resulted in 2-fold higher peak MPO activity at 24 hr that decayed slowly to baseline over ~1 week. Importantly, poly(I:C)-triggered inflammation was highly localized to the application site, as no elevation of systemic cytokines was observed following multilayer implantation (data not shown). Thus, the composition of implanted PEM films can directly control the kinetics of release and local inflammatory response in the skin.

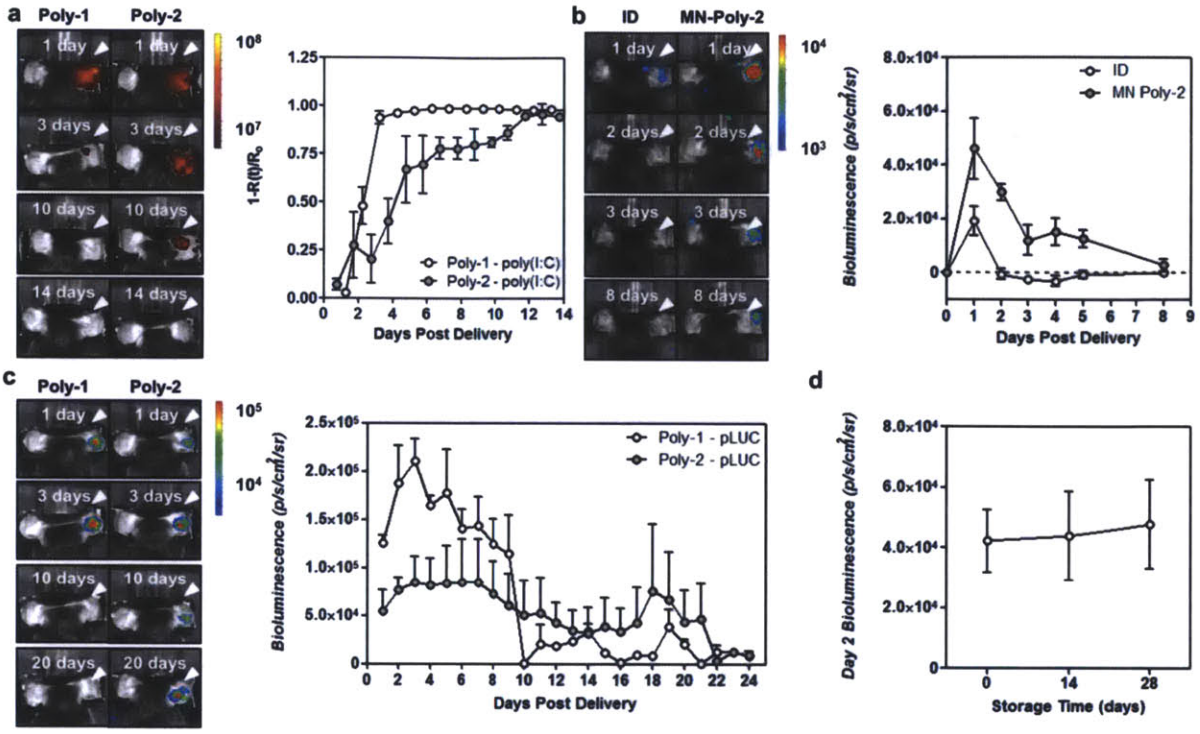

Figure 3-4. Implanted films control the physical and functional persistence of pDNA and polyI:C *in vivo*

(a) *Representative whole-animal fluorescence images showing TMR-poly(I:C) retention at the application site and quantitative analysis of normalized total fluorescence R(t) relative to initial fluorescence R_o from groups of animals (n = 3) over time following 15 min application of PLLA microneedles coated with (uv-PNMP)(PS/SPS)$_{20}$(PBAE/TMR-poly(I:C))$_{35}$ multilayers containing poly-1 or poly-2 as the PBAE component. Data represent the mean±s.e.m.* ***(b)*** *Representative whole-animal luminescent images and quantitative analysis of luminol signal from MPO-dependent oxidative burst in activated phagocytes at the treatment site over time following intradermal injection of 10 μg poly(I:C) or 15 min application of PLLA microneedles coated with (uv-PNMP)(PS/SPS)$_{20}$(poly-2/poly(I:C))$_{35}$ multilayers. Data represent the mean±s.e.m., n = 4.* ***(c)*** *Representative whole animal bioluminescence images of pLUC expression at the application site and mean bioluminescence intensity over time following 15 minute application of microneedles coated with (uv-PNMP)(PS/SPS)$_{20}$(PBAE/pLUC)$_{35}$ multilayers containing poly-1 or poly-2 as the PBAE component. Data represent the mean±s.e.m., n = 4* ***(d)*** *Mean bioluminescent intensity on day 2 following 15 min application of microneedles coated with (uv-PNMP)(PS/SPS)$_{20}$(Poly-1/pLUC)$_{35}$ multilayers stored dry at 25°C for 0, 14, or 28 days. Data represent the mean±s.e.m., n = 4.*

The selection of poly-1 and poly-2 as biodegradable polycation components of these PEM coatings was motivated not only by their ability to regulate nucleic acid release, but also to

directly promote transfection by forming pDNA polyplexes *in situ* during film degradation.[67,120] Dynamic light scattering analysis of supernatants collected from these eroded films *in vitro* revealed large aggregates (50-300nm, data not shown), consistent with previous evidence of *in situ* polyplex formation/release from degrading (PBAE/pDNA) multilayers.[70,120] To determine whether controlled polyplex release from implanted films would allow gene expression kinetics to be regulated *in vivo*, we used bioluminescence imaging to monitor expression of luciferase-encoding DNA longitudinally in live animals. Although *in vivo* optical imaging analysis of bioluminescent signals is limited by variable photon penetration from different tissue depths and locations, it is useful for accurate comparison of relative signal from identical tissue sites and for longitudinal analysis of the duration of expression. Microneedles were prepared with (PNMP/PEM) coatings containing pLUC as before, with or without UV-priming of the PNMP release-layer. We verified that pDNA released from multilayers *in vitro* retained bioactivity over the entire course of film degradation comparable to fresh PBAE/DNA polyplexes (**Supplementary Figure S3-5**). *In vivo*, control microneedles (where the release-layer was not UV-primed) applied to the skin of mice for 15 min led to no detectable expression of pLUC by bioluminescence imaging (**Supplementary Figure S3-6**), consistent with the lack of detectable film transfer into skin under this condition. By contrast, mice treated with microneedles coated with (*uv*-PNMP/PEM) films showed significant levels of bioluminescence one day after application, demonstrating transfection of cells *in situ* (**Figure 3-4c**). Further, the kinetics of pLUC expression varied greatly depending on the PBAE used: delivery of (poly-1/pLUC) multilayers led to luciferase expression that peaked after 3 days and declined to background levels after 10 days, while implantation of slower-degrading (poly-2/pLUC) films showed prolonged bioluminescence, peaking on day 3 then slowly decreasing to background levels by day 22 (**Figure 3-4c**). Together this data shows that, multilayer tattooing can be used to tailor the duration of both inflammatory signals and antigen-encoding DNA expression *in vivo*, *via* selection of constituent polymers with varying degradation rates.

3.3.4. Stabilization of Vaccines in Multilayer Coatings

Embedding bioactive molecules in multilayer films has previously been shown to enhance their stability for dry-state storage at room temperature,[113,114] an attractive feature for vaccines given the costs and availability limitations imposed by the need for refrigeration of liquid vaccine formulations. To test whether (PBAE/pDNA) multilayer films coated on microneedles stabilize their DNA cargo for dry storage, we fabricated microneedle arrays coated with (*uv*-PNMP/PEM) films and stored them dry at 25°C for 0, 14, or 28 days before application to the skin of mice as before. Bioluminescence imaging of these animals after treatment revealed no significant decrease in transfection resulting from storage, indicating the maintenance of pDNA bioactivity in multilayers for extended durations (**Figure 3-4d**). These results suggest that microneedles coated with vaccine-containing multilayers could be easily packaged for inexpensive dry-state storage and transportation to remote areas of the world, bypassing the 'cold-chain' requirements of conventional vaccines.

3.3.5. *Enhanced Vaccination Through Multilayer Tattooing*

Previous work has demonstrated DNA uptake in both keratinocytes and local APCs following delivery to the skin in both humans and mice, both of which can contribute to induction of immune responses in DNA vaccination (reviewed in [121]). To test the ability of multilayer tattooing with vaccine-loaded polymer films to enhance DNA immunization, we coated microneedles with (*uv*-PNMP)(PS/SPS)$_{20}$(poly-1/poly(I:C))$_{35}$(poly-1/pGag)$_{35}$ composite releasable multilayers containing the adjuvant poly(I:C) and pGag, a plasmid encoding the model HIV antigen SIV-*gag* (**Figure 3-5a**). We compared multilayer tattooing to several control immunizations using the same delivered dose of pGag and poly(I:C): injection of "naked" pDNA, the most common experimental strategy for DNA immunization in mice and humans; and *in vivo* electroporation, where DNA is administered in the presence of an electric field to promote DNA uptake.[103,122] To confirm the importance of the pH-responsive release-layer, we also tested microneedles where the PNMP layer was not UV-treated, and hence unable to dissolve upon skin insertion. Finally, we also compared immune responses in mice receiving intradermal injections of poly-1/pGag polyplexes, to determine the importance of the sustained-release multilayer film architecture for generating immunity. In all cases we immunized groups of animals on days 0 and 28 with 20 μg pGag and 10 μg poly(I:C). Multilayer tattooing was performed with microneedles (MN ± UV) applied to the dorsal ear skin for 15 min. Control mice were injected intradermally (ID and ID Polyplex) in the ear skin, or intramuscularly with or without *in vivo* electroporation (IM ± EP). Peptide-MHC tetramer staining of peripheral blood mononuclear cells showed that IM and ID ± Polyplex administration produced only weak antigen-specific $CD8^+$ T cell responses (**Figure 3-5b-d**). By contrast, microneedle-treated groups showed robust expansion of Gag-reactive T-cells exceeding 5% of the circulating $CD8^+$ population two weeks following the boost, a response that was quantitatively similar to frequencies observed for IM + EP immunized mice (**Figure 3-5b-d**). Notably, the response to MN vaccination was ablated if the PNMP release-layer was not UV-treated (and was therefore unable to dissolve on application). Additionally, compared to all of the other vaccination regimens, microneedle administration generated substantially greater frequencies of $CD44^+CD62L^+$ central memory T-cells, a population thought to be important for recall immunity and long-term protection (**Figure 3-5e-f**).[123] Following injection of naked pDNA 3.5 months after the prime to test recall responses, large frequencies of IFN-γ-producing $CD8^+$ T-cells were elicited (**Figure 3-5g**), suggesting the establishment of robust T-cell memory. Finally, two weeks following the boost, we measured total Gag-specific IgG titers in sera and observed a 10-fold increase in microneedle treated mice over those given any other immunization regimen ($P < 0.01$, **Figure 3-5h**). Thus, DNA vaccination *via* multilayer tattooing shows the potential to match (or exceed) the potency of *in vivo* electroporation, using a skin patch that can be stored in a dry state, is painlessly applied with no extraneous apparatus, and could be self-applied in minutes.

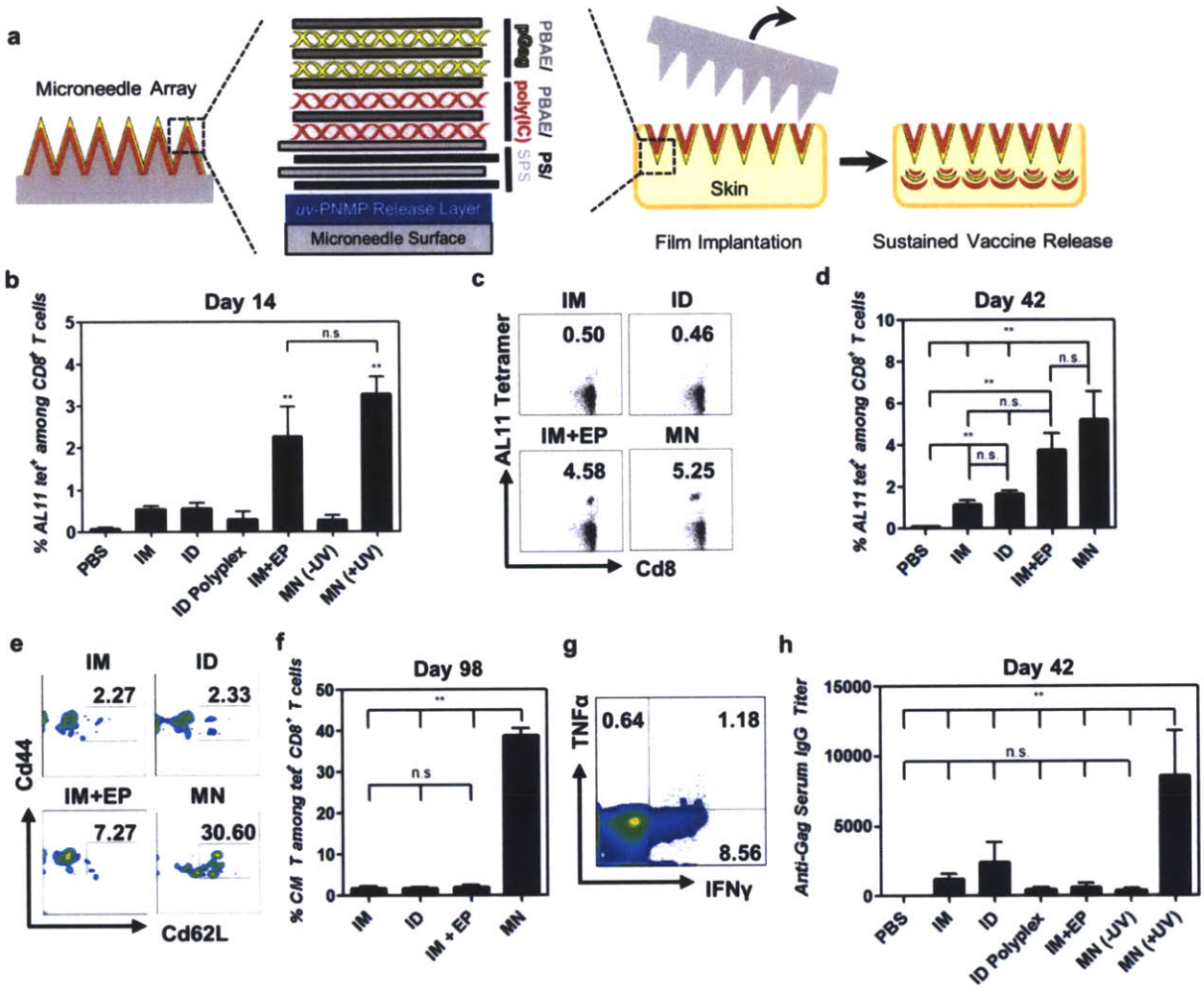

Figure 3-5. Microneedle tattooing with multilayer films carrying pDNA and polyI:C generates potent cellular and humoral immunity against a model HIV antigen

(a) *C57Bl/6 mice (n = 4 mice/group) were immunized with 20 μg pGag and 10 μg poly(I:C) on days 0 and 28 intramuscularly (with or without electroporation (EP)) in the quadriceps, intradermally in the dorsal ear skin (with free pGag or pGag/poly-1 polyplexes, ID ± Polyplex), or by 15 minute application of* $(PNMP)(PS/SPS)_{20}(poly\text{-}1/poly(I:C))_{35}(poly\text{-}1/pLUC)_{35}$*–coated microneedles without or without UV priming of the PNMP release-layer (MN ± UV) to the dorsal ear skin.* ***(b-d)*** *Frequency of Gag-specific* $CD8^+$ *T-cells in peripheral blood assessed by flow cytometry analysis of* $tetramer^+$ $CD8^+$ *T-cells. Shown are mean±s.e.m.* $tetramer^+$ *values from* ***(b)*** *day 14 and* ***(c)*** *representative cytometry plots from individual mice and* ***(d)*** *mean±s.e.m.* $tetramer^+$ *values from day 42.* ***(e-f)*** *Analysis of T-cell effector/central memory phenotypes in peripheral blood by CD44/CD62L expression of* $tetramer^+$ *cells from peripheral blood. Shown are* ***e,*** *representative cytometry plots from individual mice at day 49 and* ***f,*** *mean±s.e.m. percentages of* $tetramer^+CD44^+CD62L^+$ *among* $CD8^+$ *T cells at day 98.* ***(g)*** *Mice immunized with microneedles were recalled on day 105 by IM injection of 50 μg pGag, and assessed for*

cytokine production on ex vivo restimulation with AL11 peptide on day 112. Shown is representative flow cytometry analysis of IFN-γ/TNF-α-producing $CD8^+$ T-cells. ***(h)*** *Enzyme-linked-immunosorbent assay analysis of total Gag-specific IgG in sera at day 42. Data represent the mean±s.e.m., **, $p < 0.005$, analyzed by two-way ANOVA.*

3.3.6. Multilayer Tattooing in Non-human Primate Skin

While naked DNA injections stimulate immune responses in small animals, responses observed in non-human primates and humans have been much weaker.[4,5,102] To determine whether multilayer tattooing could also enhance the efficacy of DNA delivery in non-human primates, we tested the ability of PNMP-coated microneedles to deliver (poly-1/pLUC) multilayers into fresh explanted skin from Rhesus macaques *ex vivo*. Trypan blue staining and histological sectioning of macaque skin treated with uncoated PLLA microneedles showed uniform patterns of microneedle insertion into the superficial layers of the skin without disruption of underlying dermal layers or capillary vessels (**Figure 3-6a, b**). We tested the ability of microneedles coated with (*uv*-PNMP/PEM) films to transfect *ex vivo* cultured macaque skin explants compared to intradermal injections of equivalent doses of naked pDNA. Microneedles coated with (PNMP/PEM) multilayers effectively transfected macaque skin explants following a 15 min application period, but as in mice, transfection only occurred if the PNMP release-layer was UV-primed for dissolution (**Figure 3-6c**). Bioluminescence imaging of the treated skin samples showed that microneedle delivery generated consistent expression of luciferase at 140-fold greater levels compared to intradermally-injected naked DNA controls for several days ($P < 0.01$, **Figure 3-6d**). Previous results in mice have indicated that the magnitude of gene expression following DNA vaccination correlates with the strength of T-cell responses *in vivo*.[7] Thus, although the limitations of *ex vivo* skin explant culture prevent measurement of the long-term duration of gene expression, these results indicate that microneedle delivery promotes strong initial DNA expression in non-human primate skin, where naked DNA injection elicits very weak transfection only a few fold above background. Although the magnitude of gene expression is only one parameter determining the ultimate strength of immune responses following DNA vaccination, the ability to improve expression levels in primates is a significant result given that poor transfection efficiency is an acknowledged obstacle for improving DNA immunogenicity in large animal models and humans.[122,124]

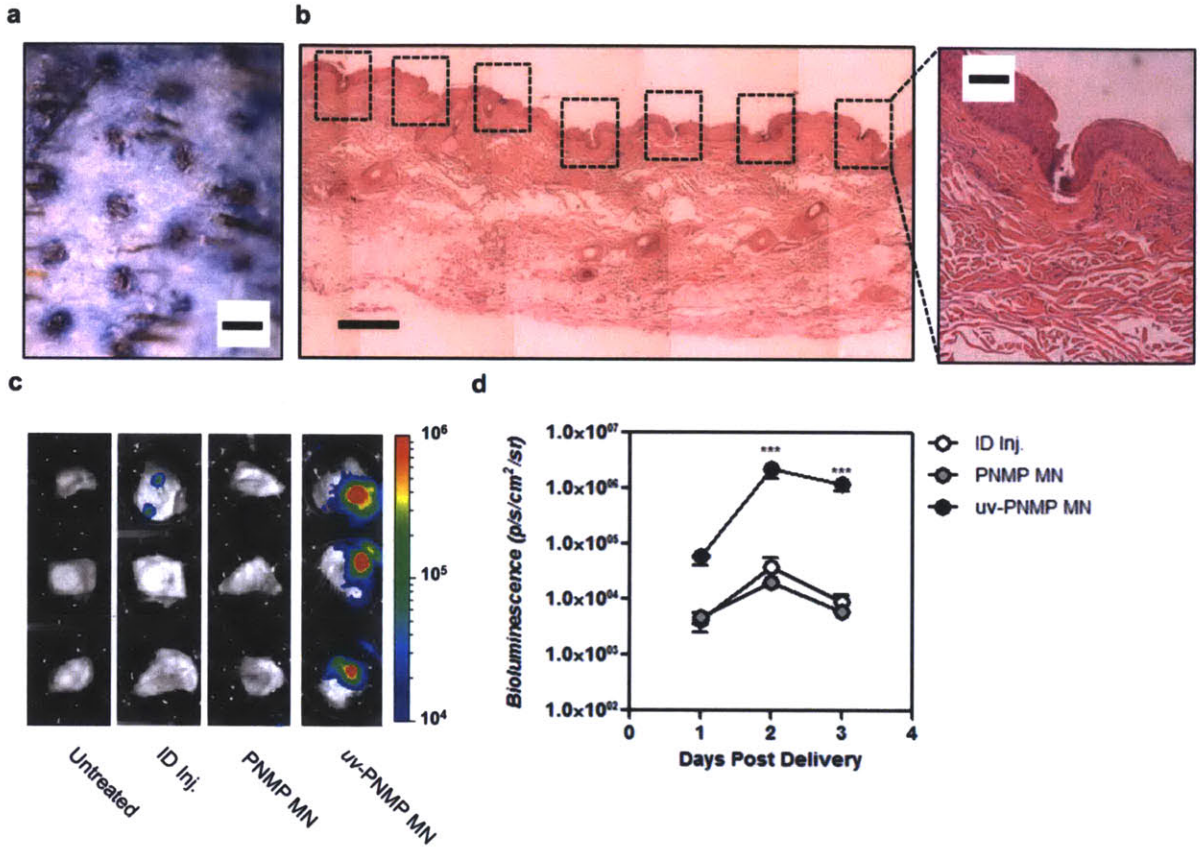

Figure 3-6. Multilayer tattooing enhances transfection in non-human primate skin

(a) *Optical micrograph of macaque quadriceps skin showing microneedle penetration pattern stained using trypan blue (scale bar 500μm).* ***(b)*** *Histological section of microneedle-treated macaque skin showing epidermal disruption at microneedle insertion sites (boxed, left, scale bar 500μm; right, scale bar 100μm).* ***(c)*** *Bioluminescence images of luciferase expression 2 days following pLUC delivery by ID injection or microneedle tattooing with* $(PS/SPS)_{20}(poly\text{-}1/pLUC)_{35}$ *films from either uv-PNMP- or non-irradiated PNMP-coated microneedles following a 15 minute application.* ***(d)*** *Quantification of total bioluminescent signal in cultured skin tissue explants 1, 2, and 3 days following treatment. Data represent the mean±s.e.m., n = 3. ***, p< 0.0001, analyzed by unpaired t-test.*

3.4. Conclusions

Microneedles have recently shown substantial promise in vaccine delivery,[125] and several reports have begun to explore the use of metal microneedles to deliver DNA into the skin.[92,93,126,127] These studies have demonstrated the ability of naked DNA delivery by microneedles to provide enhanced immune responses compared to intramuscular injection, but only one study compared microneedle administration to alternative approaches designed to elicit improved transfection; in that test microneedles elicited T-cell responses comparable to gene gun delivery of DNA if twice

the DNA dose was given by the microneedle array.[93] Here we have demonstrated a new approach for DNA vaccination *via* multilayer "tattooing", using microneedles employing a pH-responsive release-layer to rapidly implant biodegradable vaccine-loaded polymer films into the skin. (Note that this new approach should not be confused with prior studies of "DNA tattooing", where DNA solutions are literally applied to the skin using a commercial tattoo device[104,122,128]– a completely different method.) Multilayer tattooing simultaneously addresses several issues in DNA vaccine delivery: implanted multilayers deliver DNA with transfection agents, promoting transfection *in situ*; molecular adjuvants are co-delivered to amplify the immune response; and we have shown that the multilayer structure allows the kinetics of vaccine release to be tailored over days to weeks. Combined, these features enabled multilayer tattooing to elicit immune responses in mice far exceeding naked DNA injections. These responses were also comparable to *in vivo* electroporation, an approach currently viewed as a gold standard for experimental DNA vaccine potency but which requires special equipment, elicits pain and discomfort in recipients,[129,130] and is unlikely to be feasible in widespread prophylactic vaccination. Notably, vaccines have been shown to vary widely in potency based on the duration of exposure to antigen and adjuvant combinations.[104-107] Our studies suggest that the continuous release of polyplexes from implanted multilayers may be critical to the enhanced immunogenicity of multilayer tattooing, as bolus injection of free polyplexes formed from the same components elicited very weak immune responses. Finally, we have shown that formulation of DNA vaccines as multilayer coatings on microneedles provides the opportunity for long term maintenance of DNA bioactivity in a dried state without refrigeration, addressing cost and availability limitations imposed by the cold-chain in the global distribution and storage of vaccines. We focused here on DNA vaccination due to the relevance of needle-free vaccines for global health and the need for enhanced DNA vaccination strategies. However, the well-known adaptability of multilayers for incorporation and controlled release of diverse therapeutics[60-63,88,90,99] suggests this approach should be applicable to diverse drug delivery applications. Further, the pH-sensitive release-layer strategy employed here is a generalizable approach to create selectively-released multilayer films. While the true potential of any vaccination strategy can only be established in human clinical trials, the data shown here suggest that multilayer tattooing is a promising approach to enhance the efficacy of DNA vaccines, a platform technology with the potential to be applied universally in vaccine development.

4. RELEASABLE LAYER-BY-LAYER ASSEMBLY OF STABILIZED LIPID NANOCAPSULES ON MICRONEEDLES FOR ENHANCED TRANSCUTANEOUS VACCINE DELIVERY

4.1. Introduction

In Chapter 2 we focused on the development of an approach for vaccine and therapeutic encapsulation into multilayer films for delivery from microneedles. Chapter 3 expanded upon this concept to design an improved strategy for nucleic acid vaccine delivery. Here, in Chapter 4 we explore further the second theme illustrated in Chapter 2, the loading and delivery of particulate vaccines from multilayer films for improved transcutaneous vaccination.

The generation of polyelectrolyte multilayers (PEMs) through the iterative and sequential adsorption of complimentary materials is an attractive approach for nanoscale assembly of functional systems capable of controlled encapsulation and delivery of diverse therapeutics. The inherent adaptability of multilayer processing, as well as its biocompatibility, scalability, and simplicity make it an ideal strategy for the creation of conformal coatings on complex surfaces (reviewed in [112,131]). Recently, multilayers have been optimized for the encapsulation of lipid vesicles, with the aim of increasing the drug loading capacity of multilayer films, allowing for biological cargos to be entrapped in films in native aqueous conditions, and providing triggered materials release through programmed vesicle disruption.[78,132-138] A key issue for incorporation of liposomal carriers in multilayer films is the need for stabilization of vesicles against rupture during the assembly process or drying of the resulting films. Previous approaches have relied on vesicle stabilization strategies such as *in situ* silica polymerization[132,133] or polyelectrolyte adsorption on the vesicle surface prior to multilayer assembly.[78,134,135,137,138] Without such stabilizing measures, layer-by-layer (LbL) deposition results in spontaneous vesicle disruption into lipid bilayers on the target substrate.

We recently reported a new approach for lipid vesicle stabilization, where covalent crosslinks are introduced between adjacent phospholipid bilayers in the walls of multilamellar vesicles to create robust lipid nanocapsules.[139,140] These interbilayer-crosslinked multilamellar vesicles (ICMVs) encapsulate protein cargos within their interior and exhibit enhanced serum stability in extracellular conditions, but can be readily degraded upon cellular internalization.[139] Vaccination with ICMVs elicited potent cellular and humoral immune responses against the model antigen ovalbumin (OVA), and enhanced long-term humoral responses to a recombinant malaria antigen following subcutaneous injection.[139,140] Given their enhanced stability and unique potency in the context of protein vaccine delivery, we hypothesized that LbL deposition of ICMVs would provide an interesting opportunity for the design of ICMV-containing multilayer delivery systems for subunit vaccination.

In parallel studies, we and others have recently demonstrated the utility of microneedle arrays for the safe, rapid, and convenient delivery of drugs through the pain-free disruption of the stratum corneum to access the immune-competent epidermal and dermal tissue.[115,125,141] Microneedles have particularly shown promise in vaccine delivery.[115,126,142] Microneedle application is known

to improve safety, eliminate pain upon treatment, and reduce the generation of hazardous medical waste associated with needle-based delivery.[11,13,143] Further, creation of conformal surface coatings on microneedle arrays has proven to be an effective method for therapeutic formulation and delivery into the skin *via* rapid, topical microneedle application.[115,144] We therefore set out to design a PEM system for the stable encapsulation and release of ICMVs for transcutaneous delivery into the skin *via* microneedle insertion. We envisioned several potential advantages for such an approach including *(i)* improved dry state storage through PEM-embedding of ICMVs, *(ii)* controlled encapsulation and release of ICMVs from degradable PEMs implanted in the skin, *(iii)* delivery of ICMVs to an inherently immunogenic tissue for enhanced immunity through microneedle application, and *(iv)* convenient and self-contained combination of vaccine and administration device for rapid, safe, and painless vaccine delivery that could potentially be self-administered in minutes.

Here we report studies intended to test these hypotheses, focusing on the generation of a PEM system capable of stable ICMV encapsulation and release for protein immunization. We first show the ability of degradable PEMs to stably incorporate ICMV particles, both on flat silicon substrates as well as poly(lactide-*co*-glycolide) (PLGA) microneedles, controlling film thickness and ICMV dosage, and verifying that incorporated ICMVs are intact within dried multilayer films. We then demonstrate the ability for PEM-coated microneedles to transfer their ICMV-loaded films into the cutaneous tissue upon brief application to the skin of mice. Following film degradation and ICMV dispersion in the epidermal tissue, ICMVs were found to be taken up by resident antigen presenting cells (APCs) within the skin, which were activated *in situ* by adjuvants delivered by the particles. Finally, we show that transcutaneous vaccination with ICMVs embedded in microneedle-based multilayers significantly enhanced humoral immune responses to a protein antigen, compared to mice vaccinated with either conventional intradermal bolus injection of antigen or microneedle-mediated delivery of soluble protein antigen. Together, these results suggest the potential of microneedle-based multilayers for the effective transcutaneous delivery of functional nanoscale vesicles. In this work, we have improved protein subunit vaccination by taking advantage of the immunogenicity of ICMVs delivered to the skin, a site known for high frequency of epidermal and dermal APCs; however, this work describing vesicle deposition on multilayer-coated microneedles can be readily adapted as a modular, general strategy for non-invasive drug delivery to the skin.

4.2. Materials and Methods

4.2.1. Materials

Poly-1 (16 kDa) was synthesized according to previous literature.[69] Alexa Fluor 647-conjugated ovalbumin, and 1,1'-dilinoleyl-3,3,3',3'-tetramethylindocarbocyanine (DiI) were purchased from Invitrogen (Eugene, OR). PLGA (50:50, IV 1.9 dL/g) was purchased from Lakeshore Biomaterials (Birmingham, AL). DOPC (1,2-Dioleoyl-*sn*-Glycero-3-Phosphocholine) and MPB (1,2-dioleoyl-*sn*-glycero-3-phosphoethanolamine-N-[4-(p-maleimidophenyl) butyramide) were purchased from Avanti Polar Lipids (Alabaster, AL). MPLA was purchased from Sigma Aldrich

(St. Louis, MO). Poly I:C was obtained from Invivogen (San Diego, CA). Chromatographically purified ovalbumin, purchased from Worthington (Lakewood, NJ), was processed through Detoxi-Gels (Pierce, Rockford, IL) to remove any residual endotoxin.

4.2.2. *PLGA Microneedle Fabrication*

PDMS molds (Sylgard 184, Dow Corning) were fabricated by laser ablation using a Clark-MXR CPA-2010 micromachining system (VaxDesign Inc.). PLGA pellets (IV 0.35 dL/g) were melted over the molds under vacuum (-25 in. Hg) at 140°C for 40 min, and then cooled to -20°C before separating the cast PLGA microneedles from the PDMS mold. Microneedles were characterized by SEM using a JEOL 6700F FEG-SEM.

4.2.3. *ICMV Synthesis*

Synthesis of ICMVs was performed as described previously.[139,140] Briefly, dried films of 1.26 μmol of lipids (DOPC:MPB at 1:1 mol ratio) and 2.9 μg of MPLA were rehydrated in 20 mM bis-tris propane at pH 7.0 with 325 μg ovalbumin for 1 hr with vortexing every 10 min, and sonicated in alternating power cycles of 6 watts and 3 watts in 30s intervals for 5 min on ice (Misonix Microson XL probe tip sonicator, Farmingdale, NY). DTT and Ca^{2+} were then sequentially added at final concentrations of 3 mM and 40 mM, respectively, and incubated for 1 hr at 37°C to form ICMVs. The particles were recovered by centrifugation, washed twice, resuspended in PBS at pH 5.0, and stored at 4°C until usage. In some experiments, ICMVs were prepared including a lipophilic tracer, DiI, at 0.2 molar % concentration, and 325 μg of Alexa Fluor 647-conjugated OVA was used to hydrate the lipid films.

4.2.4. *Polymer Multilayer Film Preparation*

All LbL films were assembled using a Carl Ziess HMS DS50 slide stainer. Films were constructed on Si wafers and PLGA microneedle arrays. To build (PS/SPS) base layers, substrates were dipped alternatively into PS (2 mg/mL, PBS, Sigma-Aldrich) and SPS (5 mM, PBS, Sigma-Aldrich) solutions for 10 min, separated by two sequential 1 min rinses in PBS. (Poly-1/ICMV) and (Poly-1/MLV) multilayers were deposited similarly, alternating 5 min dips in Poly-1 (2 mg/mL, PBS) and ICMV/MLV solutions (1 mg/mL, PBS) separated by two sequential 30 sec rinsing steps in PBS. (Poly-1/OVA) multilayers were deposited by alternating 10 min dips in Poly-1 (2 mg/mL, 0.2M sodium acetate) and OVA solutions (0.1 mg/mL, 0.2M sodium acetate) separated by two sequential 1 min rinsing steps in deionized water. All solutions were adjusted to pH 5.0 and filtered (0.2μm, except ICMV/MLV and OVA) prior to dipping.

4.2.5. *Multilayer Film Characterization*

Film thickness on Si wafers was characterized using a Veeco Dektak (Plainview, NY) surface profilometer and a Veeco Dimension 3100 AFM. Film growth and morphology on PLGA microneedles was characterized by SEM using a JEOL 6700F FEG-SEM and CLSM using a Carl Zeiss LSM 510. Data analysis was performed using Image J[95] and Graphpad Prism (La Jolla, CA). Film loading was determined for fluorescent cargos using a SpectraMax 250

spectrophotometer (Molecular Devices, Sunnyvale, CA) following elution of films in PBS, pH 7.4, 2M NaCl for 24 hours.

4.2.6. Characterization of Film Delivery In Vivo

ICMV or soluble OVA delivery was measured *in vivo* following application of coated microneedles to the skin of mice. Animals were cared for in the USDA-inspected MIT Animal Facility under federal, state, local, and NIH guidelines for animal care. Microneedle application experiments were performed on anesthetized 6-10-week-old female C57BL/6 (Jackson Laboratories) and C57Bl/6-MHC II-GFP transgenic mice (a gift from Prof. Hidde Ploegh, MIT) at the dorsal ear or flank skin. Skin was rinsed briefly with PBS and dried before application of microneedle arrays by gentle pressure. Following application, mice were euthanized at subsequent time points and the application site was dissected. Excised skin was stained with trypan blue before imaging for needle penetration. In separate experiments treated skin and applied microneedle arrays were imaged by confocal microscopy to assess transcutaneous delivery of encapsulated ICMVs or soluble OVA. MHC II-GFP$^+$ cell number and morphology were analyzed by CLSM in dissected tissue following microneedle treatment. Image analysis was performed using NIH Image J software.[95]

4.2.7. Vaccinations and Characterization of Humoral Immune Responses

Groups of 6-10-wk old female C57Bl/6 mice were immunized on days 0, 28, and 56 with 1 μg OVA, 0.03 μg MPLA, and 10 μg polyI:C either in suspension or microneedle formulations. Microneedle coating compositions were chosen so that the dose of antigen/MPLA delivered into the skin matched the injected cases: MN coatings were dissolved in sodium chloride buffer and the amount of antigen present was assessed using a spectrofluorimeter for as-prepared and post-skin-application microneedles; the delivered dose was determined as the difference between these two values. For intradermal administration, immunogens in 15 μL PBS were injected intradermally in the dorsal auricular skin. Transcutaneous administration of microneedles was performed as described above, following brief rinsing with sterile PBS at the dorsal ear skin. For multilayers containing OVA/MPLA-loaded ICMVs, polyI:C was administered in 5μl PBS to the surface of the skin prior to treatment and left in place during the duration of microneedle application. For multilayers containing soluble OVA, polyI:C and MPLA were similarly administered to the skin prior to microneedle treatment. Microneedles were secured in place for 5 minutes for both ICMV- and soluble OVA-containing multilayer coating variations. Sera obtained from immunized mice at various time points were analyzed for IgG, IgG_1, and IgG_{2c} antibodies by ELISA using OVA-coated plates. Anti-OVA IgG titers were defined as the lowest serum dilution at which the ELISA OD reading was ≥ 0.5.

4.2.8. Statistical Analysis

Data sets were analyzed using one- or two-way analysis of variance (ANOVA), followed by Tukey's HSD test for multiple comparisons with Prism 5.0 (GraphPad Software, San Diego,

CA). p-values less than 0.05 were considered statistically significant. All values are reported as mean ± s.e.m.

4.3. Results and Discussion

4.3.1. ICMV Encapsulation into Degradable Multilayers

In Chapter 2 we demonstrated that microneedles coated with PLGA nanoparticle-loaded PEMs could be used for rapid implantation of particle-loaded films in skin.[115] PLGA particles are attractive for small-molecule drug delivery but have limitations for delivery of biologics such as vaccines, due to the low doses of proteins that can be encapsulated and the potential for antigen denaturation during processing. We hypothesized that the deposition of an ICMV-containing multilayer coating on the surface of microneedles would provide a solution to these issues and enable a simple, self-contained, and effective method for recombinant protein vaccine storage and delivery to the skin, an attractive tissue target due to its dense matrix of resident innate immune cells (**Figure 4-1**).[24,145,146] To fabricate an erodible PEM system capable of encapsulating and delivering intact nanoscale vesicles we selected Poly-1 (**Supplementary Figure S4-1**) a biocompatible, hydrolytically degradable polymer from a class of polyelectrolytes known as poly(β-amino esters) (PBAEs), to serve as a complimentary degradable partner for ICMV encapsulation in multilayers. Poly-1 has been extensively studied in a variety of contexts and has been proven effective in generating erodible multilayer films containing many diverse cargos for controlled drug release.[7,65,69,71,115,117,144] We selected ICMVs to serve as a stable poly-anionic vesicular partner for Poly-1 in multilayer deposition, taking advantage of their colloidal stability and potency as vaccine delivery vehicles.[139,140] In this context, ICMVs could serve as a modular delivery vehicle for antigen and adjuvant incorporated either in the aqueous vesicle core or the hydrophobic lipid capsule walls of ICMVs, and the covalent inter-bilayer maleimide crosslinks would provide stability for multilayer encapsulation (**Figure 4-1a**). We hypothesized that (Poly-1/ICMV) multilayers would be deposited into the skin through brief topical microneedle application (**Figure4- 1b**), where hydrolytic degradation of Poly-1 over time would lead to ICMV release (**Figure 4-1c**) into the surrounding tissue, followed by uptake into local APCs (**Figure 4-1d**) that would initiate adaptive immunity.

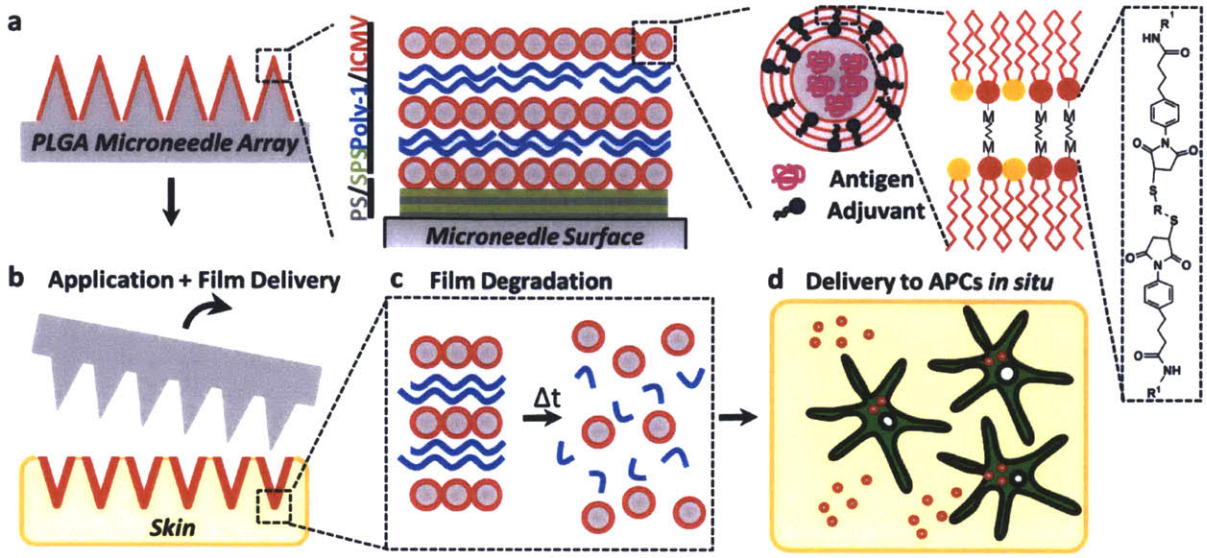

Figure 4-1. Schematic illustration of ICMV multilayer deposition and delivery

(a) *Schematic illustration of (Poly-1/ICMV) multilayers deposited onto PLGA microneedle surfaces. ICMV lipid nanocapsules are prepared with inter-bilayer covalent crosslinks between maleimide head groups (M) of adjacent phospholipid lamellae in the walls of multi-lamellar vesicles. (Poly-1/ICMV) PEMs were constructed on microneedles after (PS/SPS) base layer deposition.* ***(b)*** *Microneedles transfer (Poly-1/ICMV) coatings into the skin as cutaneous depots at microneedle insertion points.* ***(c)*** *Hydrolytic degradation of Poly-1 leads to PEM disintegration and ICMV release into the surrounding tissue. (d) ICMV delivery to skin-resident APCs provides coincident antigen exposure and immunostimulation, leading to initiation of adaptive immunity.*

Negatively-charged ICMVs encapsulating fluorescent ovalbumin (OVA) and composed of DOPC and maleimide-lipid MPB (**Supplementary Figure S4-1)** in a 1:1 mole ratio (diam. 240 ± 10 nm, 0.19 ± 0.05 polydispersity index, zeta potential -41 ± 1.0 mV, incorporating 0.1 wt% DiI as a fluorescent tracer in the vesicle walls) were prepared as previously described.[139,140] To determine whether ICMVs could be stably embedded into degradable multilayer films, we first synthesized model LbL films on atomically-flat silicon substrates. First, 20 bilayers of protamine sulfate (PS) and sulfonated poly(styrene) (SPS) were deposited to form a base layer of uniform surface charge.[101,115] Through subsequent LbL steps, we attempted to construct ICMV-encapsulating multilayers through sequential immersion in aqueous Poly-1 and ICMV suspensions of varying concentrations. As shown in **Figure 4-2a**, when LbL assembly was performed using ICMVs at 0.5 mg/ml in phosphate buffered saline (PBS) at pH 5.0, we observed insignificant and irregular film growth, with film thickness remaining steady after 15 deposition cycles at ~400 nm as measured by profilometry. However, using a more concentrated 1 mg/ml ICMV dispersion, we observed a regular linear increase in measured film thickness (~50

nm/bilayer) with each deposition cycle up to 35 rounds of LbL deposition, resulting in films more than 1.5 μm thick (**Figure 4-2a**). For comparison with the crosslink-stabilized ICMVs, we also synthesized non-crosslinked multilamellar vesicles (MLVs) *via* the same process used to prepare ICMVs, leaving out the final interbilayer crosslinking step. In contrast to ICMVs, MLVs (diam. 270 ± 17 nm, 0.23 ± 0.014 polydispersity index, zeta potential -33.6 ± 0.9 mV) displayed inconsistent and irregular film growth plateauing at ~500 nm after 15 bilayers (**Figure 4-2a**). This result is consistent with previous evidence showing ineffective LbL growth of phospholipid vesicles without sufficient stabilization to prevent spontaneous disruption upon adsorption.[147,148] Spectroscopic measurement of fluorescent signal obtained after (Poly-1/ICMV) film disruption in NaCl for 24 hours indicated a loading of ~5 μg OVA/cm^2 and ~15 μg lipids/cm^2 for multilayers containing 35 bilayers (~1.6 μm in thickness), consistent with the known OVA loading density of intact ICMVs;[139] this loading is within the effective dose range needed for ICMVs to generate potent immune responses *in vivo* when administered by traditional routes.[139,140] Further, previous studies have demonstrated enhanced potency of transcutaneously-administered vaccines, suggesting that additional dose sparing might be possible in this context.[19-21]

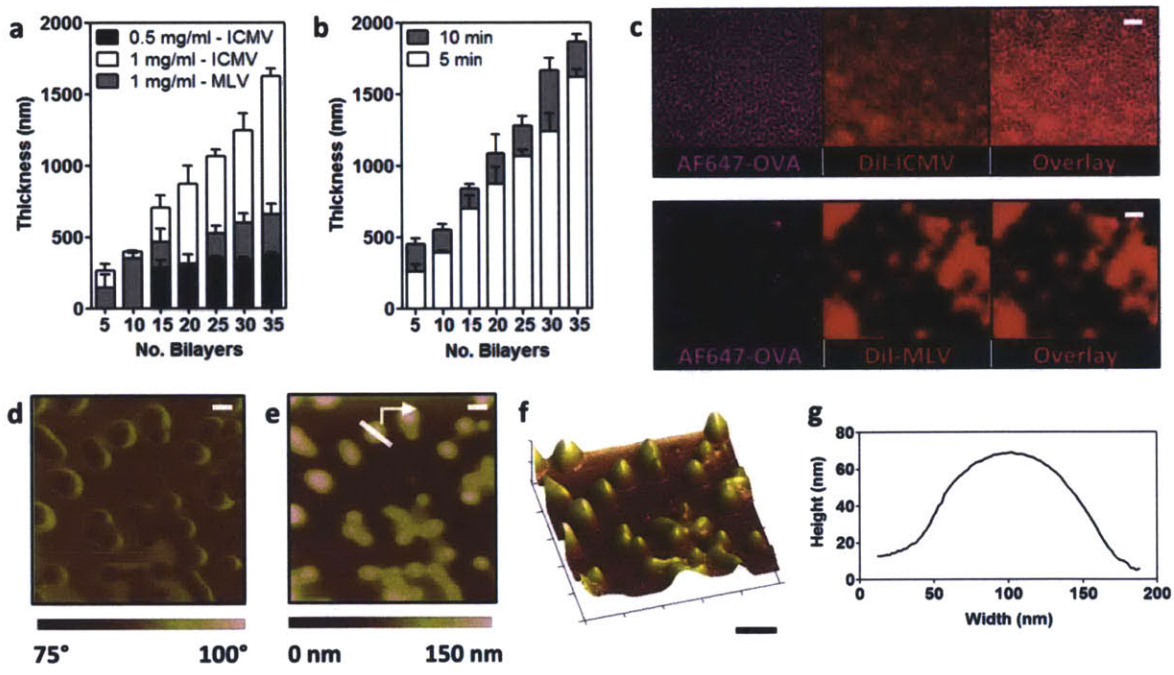

Figure 4-2. ICMV multilayer film deposition and characterization

Shown are (poly-1/lipid) film thicknesses determined by profilometry for deposited ICMVs or MLVs varying ***(a)*** *concentration and* ***(b)*** *deposition time (n = 12).* ***(c)*** *CLSM image of* $(PS/SPS)_{20}(Poly\text{-}1/ICMV)_{20}$ *or* $(PS/SPS)_{20}(Poly\text{-}1/MLV)_{20}$ *multilayers deposited on silicon (scale bar ~ 20μm). ICMVs and MLVs contained AF647-OVA (pink) and were labeled with DiI (red).* ***(d-g)*** *AFM imaging of a dried* $(Poly\text{-}1/ICMV)_5(PS/SPS)_{20}$ *multilayers built on silicon (scale bar 100 nm). Shown are phase* ***(d)****, height* ***(e)****, and 3-D rendered AFM height micrograph data* ***(f)*** *for*

*a (Poly-1/ICMV)$_5$(PS/SPS)$_{20}$ multilayer (scale bar 100 nm). **(g)** Height trace data (trace shown in panel (e) for a single embedded ICMV in a (Poly-1/ICMV)$_5$(PS/SPS)$_{20}$ multilayer.*

Given the success of film growth at these initial conditions, we then measured the effect of deposition time on the growth of (Poly-1/ICMV) containing films, and observed no significant increase in film growth per bilayer when the duration for Poly-1 and ICMV adsorption was increased from 5 to 10 minutes (**Figure 4-2b**). We thus concluded that 5 minutes was a sufficient time period to achieve ICMV adsorption and reversal of surface charge for successful LbL adsorption. To confirm that ICMVs were stably incorporated into Poly-1 films, we performed confocal laser scanning microscopy (CLSM) on (Poly-1/ICMV) multilayers constructed using ICMVs labeled with DiI in the lipid phase of the particles and encapsulating fluorescent AF647-OVA. CLSM imaging showed the presence of overlaid punctate fluorescent signals indicating colocalization of AF647-OVA and DiI in submicron spherical particles, suggesting the incorporation of intact, OVA-loaded ICMVs into Poly-1 multilayers (**Figure 4-2c**). This punctate fluorescent signal was not observed in films constructed using MLVs formed in the absence of interbilayer crosslinks, and only low levels of OVA fluorescence were detected in such films, providing evidence for the importance of the stabilizing inter-bilayer crosslinks of ICMVs for preventing vesicle disruption during LbL processing (**Figure 4-2c**). In addition, large contiguous patches of the DiI lipid tracer were observed in films prepared with non-crosslinked MLVs, suggesting fusion among vesicles occurring in this case (**Figure 4-2c**). To obtain further confirmation of intact ICMV incorporation into multilayers, we performed atomic force microscopy (AFM) to investigate the surface of (Poly-1/ICMV) films on silicon. Consistent with previous studies showing intact vesicle incorporation,[78,132,133,137,138] we observed individual spherical structures 100-300 nm in diameter in height and phase AFM images, suggesting that multilayer-embedded ICMVs were intact and unchanged following LbL deposition (**Figure 4-2d-e**). This was readily apparent upon 3-D rendering of AFM height data (**Figure 4-2f**) and in analysis of height traces (**Figure 4-2g**), suggesting individual ICMVs embedded within the (Poly-1/ICMV) multilayers. The exposed dimensions of particles at the top of films measured in this way showed diameters of ~100-300 nm and heights of ~50-75 nm, consistent with the previously measured average bilayer thickness and suggesting some deformation and burial of the particles in underlying Poly-1 layers, as observed in prior studies of vesicles incorporated in multilayers.[78,135] Additional AFM measurement of dry films stored at room temperature for 7 days revealed similar punctate patterns with no significant change in dimension, indicating the potential for multilayer encapsulated ICMVs to maintain their structure upon dry-state storage (**Supplementary Figure S4-2**), an attractive feature for potential vaccine delivery systems in the developing world.

4.3.2. *Multilayer Deposition and Delivery from PLGA Microneedles*

Given the ability of Poly-1 multilayers to encapsulate intact ICMVs, we next sought to use this approach for ICMV delivery and release into the skin. In Chapters 2 and 3 we reported the

successful generation of multilayer films on the surface of microneedle arrays for transcutaneous delivery *in vivo*.[115,144] We hypothesized that a similar approach could allow for ICMV-loaded multilayer delivery, and given the demonstrated potency of ICMVs for generating adaptive immunity,[139,140] we anticipated that ICMV delivery to the APC-rich epidermis might provide enhanced dose sparing immunogenicity. To test whether ICMV-loaded multilayers could be deposited as surface coatings on microneedles, we first fabricated PLGA microneedles using poly(dimethyl siloxane) (PDMS) molding as previously described, yielding arrays of conical microneedles each ~650 μm in height and 250 μm in diameter at the base. Then, following (PS/SPS) base-layer deposition on these microneedles, we performed LbL assembly using fluorescently-labeled DiI-ICMVs encapsulating AF647-OVA as before. CLSM on the resulting multilayer-coated microneedles revealed consistent and uniform fluorescent signal localized to the surface of each microneedle, indicating effective multilayer deposition as observed for flat silicon substrates (**Figure 4-3a**). Using confocal z-scanning, we then performed quantitative analysis of the total fluorescent signal on individual microneedles following deposition of 10, 20, or 30 bilayers. This analysis demonstrated a similar linear growth profile for both DiI-labeled ICMVs and the encapsulated AF647-OVA cargo, consistent with the thickness increase measured with profilometry on silicon (**Figure 4-3b**). In addition to confirming the similar growth of silicon- and microneedle-based films, these results provide additional evidence for intact ICMV incorporation on microneedle surfaces, consistent with our previous demonstration of nanoparticle encapsulation on microneedle arrays through spray LbL deposition.[115] Finally, we imaged the resulting multilayer-coated microneedles using scanning electron microscopy (SEM) and observed the presence of consistent surface coatings uniformly covering the entire microneedle array surface (**Figure 4-3c**).

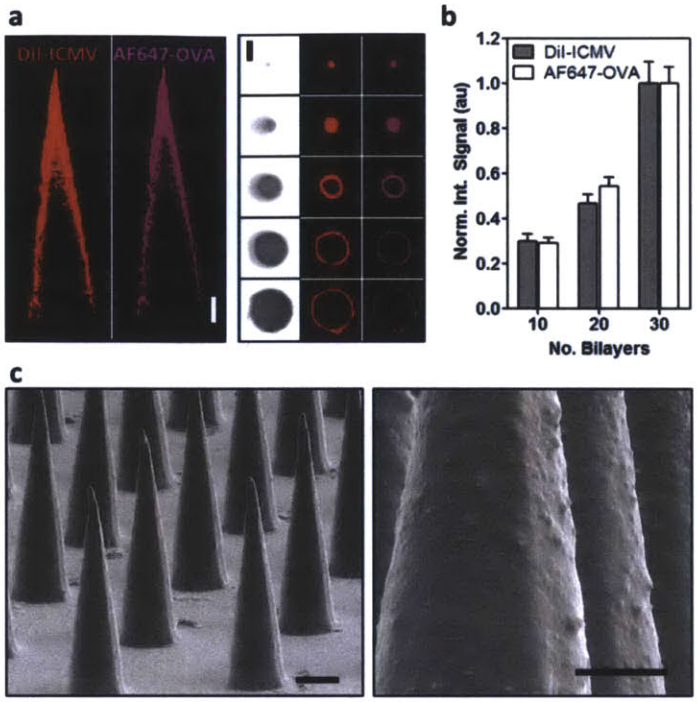

Figure 4-3. ICMV multilayer deposition on PLGA microneedles

(a) *Representative confocal images of PLGA microneedles coated with* $(PS/SPS)_{20}(Poly\text{-}1/ICMV)_{35}$ *films (left, transverse optical sections; right, lateral sections; 100 μm interval; scale bar 100 μm; Red, DiI-ICMVs; Pink, AF647-OVA).* ***(b)*** *Quantification of DiI-ICMV and AF647-OVA incorporation into* $(PS/SPS)_{20}(Poly\text{-}1/ICMV)_n$ *films on microneedles. Analysis was performed using Image J measurement of total fluorescent signal intensity in confocal z-stacks collected along the length of microneedles, normalized to the total intensity obtained for 30 bilayer films (results shown are averaged from n = 15 individual microneedles per condition).* ***(c)*** *SEM micrographs of* $(PS/SPS)_{20}(Poly\text{-}1/ICMV)_{35}$ *multilayer-coated PLGA microneedles (scale bars: left 200 μm, right 50 μm).*

We next tested whether microneedle-based multilayers encapsulating ICMVs were delivered into skin following microneedle application *in vivo*. We have previously shown that microneedles similar to those used here are effective in providing consistent disruption of the stratum corneum and insertion into the outer layers of the skin following brief topical application to the skin of mice.[115] We confirmed this result using trypan blue staining of treated skin and observed uniform staining patterns indicating microneedle insertion as before (data not shown). To test for transcutaneous delivery, multilayer-coated microneedles carrying AF647-OVA-loaded, DiI-labeled ICMVs were applied to the dorsal ear or flank skin of C57Bl/6 mice. We then performed quantitative CLSM image analysis to determine the relative loss of fluorescent signal from individual microneedles following application. Microneedles applied for only 5 minutes showed significant losses of both DiI and AF647-OVA fluorescent signal over the entire microneedle

surface, with ~80% reduction in fluorescent intensity observed on the microneedle surfaces (**Figure 4-4a-c**). Fluorescent signal reduction was equivalent for both the lipophilic tracer and protein cargo, suggesting delivery of intact multilayer-embedded ICMVs. These results are consistent with our previous demonstration of polymer nanoparticle-loaded multilayer delivery, in which we observed that, unlike multilayers composed only of polymeric materials, PEMs containing embedded particles were rapidly transferred to the skin after brief application of microneedle arrays.[115] This difference in the kinetics of multilayer transfer may reflect a decreased degree of interpenetrating molecular entanglements between complementary polymer and nanoparticle pairs, compared to multilayers composed of complementary polymers alone. The microneedles themselves make up 45% of the total coated surface area on the microneedle array, meaning that with 80% delivery of the coated material, overall ~36% of the vaccine components coated on the microneedles are estimated to be delivered into the skin. Approaches to increase this fraction can be readily envisioned by using a hydrophobic base to prevent wetting of the backing and/or employing strategies to carry out LbL deposition only on the microneedle tips.[49,144]

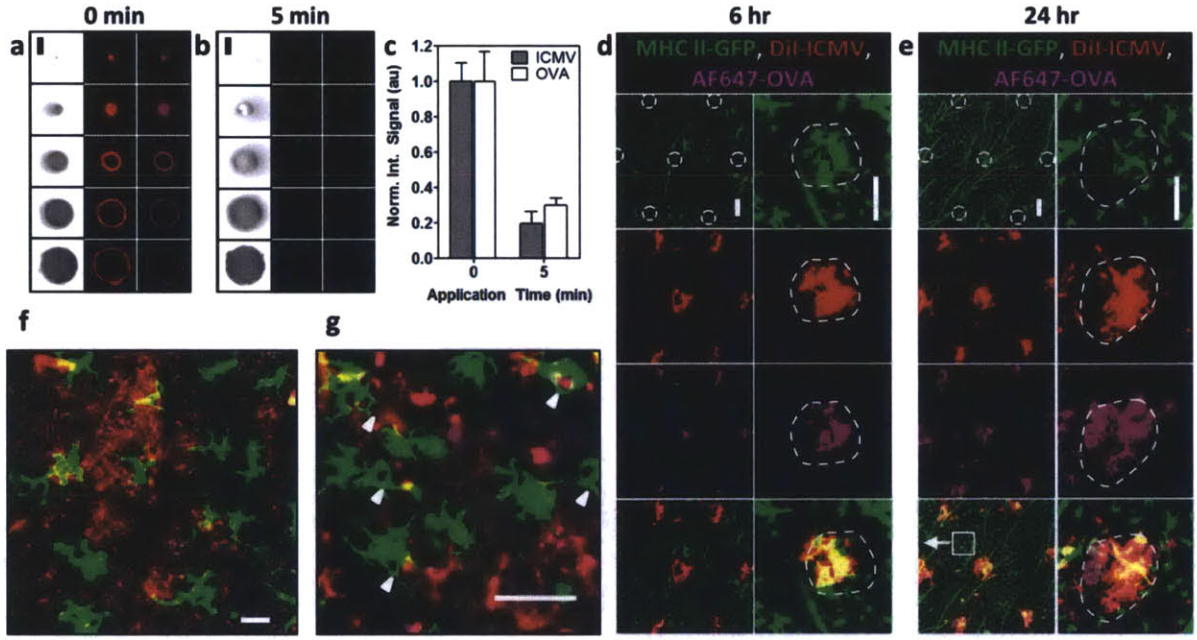

Figure 4-4. ICMV multilayer delivery following microneedle treatment *in vivo*

(a-c) *Representative confocal images of PLGA microneedles coated with* $(PS/SPS)_{20}(Poly\text{-}1/ICMV)_{35}$ *films before application* ***(a)*** *and after a 5 minute application to murine skin in vivo* ***(b)*** *(lateral sections, 100 μm z-interval; scale bar 100 μm; Red, DiI-ICMVs; Pink, AF647-OVA).* ***(c)*** *Quantitation of confocal fluorescence intensities (n = 15) showing loss of DiI-ICMV and AF647-OVA films from coated microneedles upon application to skin.* ***(d-g)*** *Representative confocal images of mouse skin treated for 5 minutes with* $(Poly\text{-}1/ICMV)_{35}(PS/SPS)_{20}$ *multilayer-coated PLGA microneedles after 6 hr* ***(d)*** *or 24 hr* ***(e)*** *showing ICMV delivery at microneedle insertion*

sites (outlined). Shown is fluorescent signal from (top to bottom) MHC II-GFP (green), DiI-ICMVs (red), AF647-OVA (pink), and overlay (yellow) at low (left) and high (right) magnification (scale bars 100 μm). ***(f)*** *High magnification CLSM image (field location highlighted by box in panel* ***(e)****) showing colocalization of ICMVs and OVA with APCs in the skin (scale bar - 20μm).* ***(g)*** *High magnification CLSM image showing APC phagocytosis of ICMVs with OVA after 24 hr (scale bar 20 μm).*

We next examined microneedle-treated skin to observe deposition of ICMV-loaded multilayers into the tissue. ICMVs were prepared with AF647-OVA loaded in the aqueous core as a model protein antigen. As adjuvants to provide local inflammatory cues necessary to drive the immune response, we embedded the Toll like receptor (TLR)-4 agonist monophosphoryl lipid A (MPLA) in the ICMV capsule walls, and further applied aqueous solutions of the TLR-3 agonist polyI:C (a double-stranded RNA mimic of viral RNA) directly to the skin just prior to microneedle application. To observe ICMV delivery in relation to target antigen presenting cell (APC) populations in the skin, we applied microneedles to the skin of MHC II-GFP mice. These animals express all major histocompatibility class II (MHC II) molecules as a fusion with green fluorescent protein (GFP), allowing MHC II^+ APCs in the viable epidermis/dermis to be observed through CLSM imaging in auricular or flank skin.[96] Microneedles were applied to ear skin for 5 min, which was then dissected 6 or 24 hr later for CLSM imaging. After 6 hr, we observed AF647-OVA and DiI fluorescence in clusters around microneedle insertion sites; these signals were colocalized in the same *z*-plane as epidermal APCs expressing MHC II-GFP and extended several hundred microns below the skin surface (**Figure 4-4d and Supplementary Figure S4-3**). In skin collected 24 hours following treatment, we observed similar fluorescent signal colocalization (**Figure 4-4e**) at microneedle insertion sites. However, after 24 hours, low and high magnification CLSM imaging revealed the emergence of punctate fluorescent signal dispersed throughout the tissue, similar to that observed for multilayer-embedded ICMVs, suggesting multilayer disintegration and release/diffusion of ICMVs *in situ* (**Figure 4-4e-f**). This finding is consistent with the known degradation kinetics of Poly-1 multilayers, which undergo complete breakdown within 24 hours.[75,115] Dispersed particles were consistently localized within the viable epidermal layers as evidenced by colocalization within the same z-plane as MHC II-GFP^+ APCs (likely Langerhans cells). Further imaging indicated direct interaction between epidermal APCs and ICMVs within the treated skin, as GFP^+ cells were observed with internal fluorescent signal from both AF647-OVA and DiI (**Figure 4-4f**). In some cases, MHC II-GFP^+ APCs were observed with membrane extensions around punctate fluorescent particles, suggesting that ICMVs released from implanted multilayers were actively being phagocytosed by resident immune cells in the skin (**Figure 4-4g**).

4.3.3. *Recruitment and Maturation of Cutaneous Antigen Presenting Cells*

The presence of TLR-3 and TLR-4 molecular adjuvants triggered striking changes in the APC populations present in the skin of mice with implanted ICMV multilayers (**Figure 4-5**). To

determine the effect of co-delivery of ICMVs with MPLA and polyI:C, mice were treated with either uncoated microneedles, or microneedle arrays delivering ICMVs with or without MPLA and polyI:C. A representative series of CLSM images from the 6 and 24 hour timepoints following treatment were analyzed using Image J software particle analysis algorithms[95] to determine various phenotypically significant parameters including total cell number per field, individual cell area and perimeter, and individual cell MHC II-GFP mean fluorescent intensity (MFI). From representative CLSM fields (**Figure 4-5a-b**), as well as the dependent quantitative analysis, we observed a dramatic increase in MHC II^+ cells present in the skin tissue between 6 and 24 hours for mice treated with polyI:C and microneedles coated with ICMVs encapsulating OVA with MPLA, compared to microneedles alone or MN coated with only ICMVs (**Figure 4-5c**). This recruitment of antigen presenting cells to the MN application site contrasts with recent studies using microneedle arrays composed of shorter (100 μm in length) silicon needles (either bare or coated with antigens and saponin adjuvants), where a slight decrease in the density of MHC II^+ cells was observed by 24 hr, suggesting activation and migration of dendritic cells toward lymphatics following patch application.[149,150] However, APC accumulation is consistent with the normal physiological response to inflammation following vaccination, as local chemokine release from stimulated keratinocytes and innate immune cells triggers both resident cell division and homing of blood-borne APCs to the inflamed tissue microenvironment.[24,145,146] Notably, prior studies using adjuvants such as the TLR agonist imiquimod[151] or cytokines such as GM-CSF or FLT-3L[152,153] have shown similar infiltration of dendritic cells to skin vaccination sites (including in human trials), which correlates with greater frequencies of antigen-carrying APCs arriving at draining lymph nodes. Such dramatic APC recruitment to the application site was not observed for bare microneedles, suggesting that the response observed in this study vs. the silicon microneedle studies cited above are not simply due to greater wounding of the skin by the larger microneedles used here.

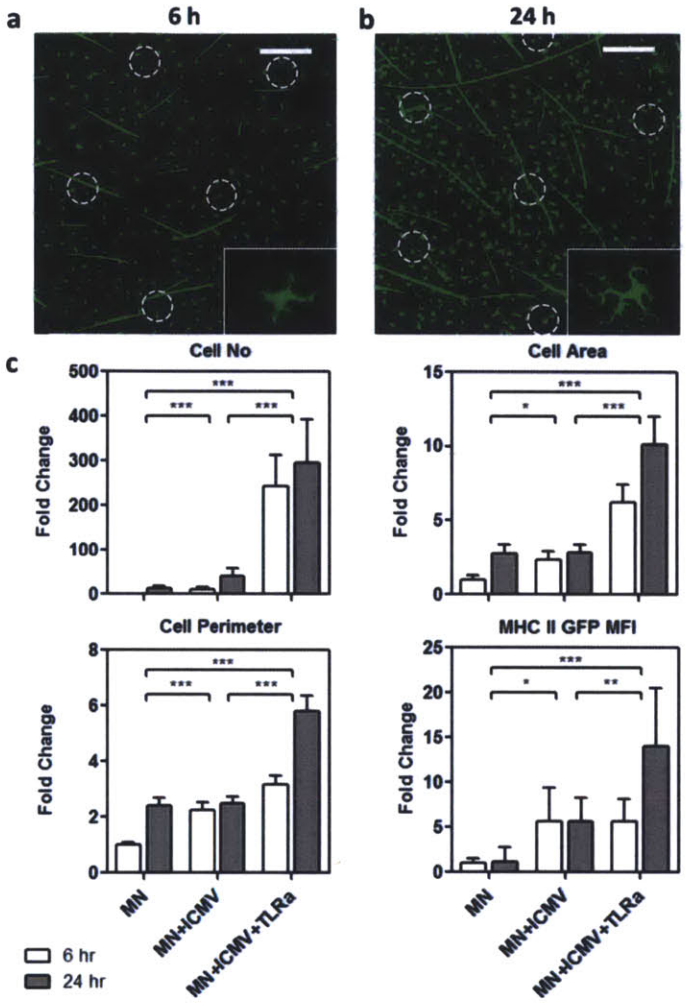

Figure 4-5. Cutaneous antigen presenting cell recruitment and maturation

Representative CLSM images of MHC II-GFP$^+$ cells in skin dissected 6 ***(a)*** *or 24 hours* ***(b)*** *after $(PS/SPS)_{20}(Poly\text{-}1/ICMV)_{35}$–coated microneedle treatment for 5 minutes (insertion points outlined); ICMVs were loaded with MPLA and polyI:C was added to the skin directly before treatment (scale bar 200 μm).* ***(c)*** *Results of quantitative CLSM image analysis to determine total cell number per field, individual cell area and perimeter, and MHC II-GFP MFI, expressed as fold change relative to uncoated microneedle treated mice. Mice were either treated with uncoated microneedles (MN), or microneedles coated with $(PS/SPS)_{20}(Poly\text{-}1/ICMV)_{35}$ multilayers with or without added MPLA and polyI:C (MN+ICMV and MN+ICMV+TLRa, respectively). Data was analyzed for significance using two-way ANOVA (* - $p<0.05$, ** - $p<0.01$, *** - $p<0.001$).*

In addition, TLR agonists trigger activation of APCs, which is accompanied by morphological changes and upregulation of MHC expression,[154-156] which we also saw reflected in skin treated with ICMVs with MPLA and polyI:C. Here individual GFP^+ APCs were observed to take on an extended dendritic morphology (**Figure 4-5a, b**) and increase in area (~3x), perimeter (~2x), and mean MHC II-GFP fluorescence intensity (~10x, **Figure 4-5c**) as compared to bare microneedle or ICMV-only treatments. Together these parameters are indicative of a shift towards an activated phenotype in APCs, as stimulated DCs increase cellular processes to more effectively capture antigen and increase expression of MHC II for effective communication with naive lymphocytes in the generation of adaptive immunity. Thus, we have observed the effective delivery of ICMV-containing multilayers from microneedle arrays into treated skin, the subsequent disintegration of multilayer depots releasing ICMVs, which are dispersed throughout the skin for uptake by resident APCs, ultimately resulting in coincident antigen delivery and activation and maturation of the resident APC population.

4.3.4. Microneedle Delivery of ICMVs for Enhanced Transcutaneous Vaccination

Finally, we tested whether transcutaneous administration of microneedle-based multilayers encapsulating ICMVs could elicit immune responses against an antigen incorporated within ICMVs. Groups of C57Bl/6 mice were immunized on day zero and given booster immunizations after 4 weeks and 8 weeks with 1 μg OVA (model antigen), 0.03 μg MPLA, and 10 μg polyI:C. For each immunization, mice received transcutaneous administration of microneedles delivering Poly-1 multilayers encapsulating either ICMVs (containing OVA and MPLA, OVA-ICMV-MN) or equivalent doses of soluble OVA (OVA-MN, **Figure 4-6a**). In both cases microneedle multilayer delivery was performed in the presence of soluble polyI:C (and MPLA in the case of OVA multilayers) applied to the skin surface before treatment. Multilayers loaded with soluble OVA were constructed based upon previously reported methods adapted for microneedle deposition.[117] Characterization of OVA-multilayer loading and delivery *in vivo* demonstrated effective OVA loading into microneedle-based multilayers, and efficient transcutaneous delivery upon microneedle application (**Supplementary Figure S4-4**). To further delineate the efficacy of microneedle-based transcutaneous vaccination from conventional bolus injection of immunogens, we also vaccinated control groups of mice by intradermal injection of ICMVs (containing OVA and MPLA, OVA-ICMV-ID) with polyI:C or soluble formulations delivering the same doses of antigen and adjuvants as in the microneedle treated groups (OVA-ID, **Figure 4-6a**). All groups received the same total dose of OVA, MPLA, and polyI:C. Notably, following the first booster immunization all groups responded with increased OVA-specific serum IgG titers, and the total IgG titer of ICMV vaccines were identical for injected vs. microneedle formulations by day 56 **(Figure 4-6b)**. However, only mice immunized with microneedle delivery of ICMV-carrying multilayers responded to the second boost at day 56, with serum IgG titers showing an additional >10-fold increase for this group, while the other immunization regimens elicited stable or declining titers at subsequent timepoints. The need for multiple vaccinations to achieve this high titer is offset by the potential for enhanced protection by such a substantial increase in strength of the humoral response and the self-administrable nature of

microneedle patch vaccines. We further analyzed sera obtained on day ~110 post-immunization to determine the isotypes of antibodies generated by transcutaneous vs. intradermal administration of either soluble or ICMV vaccine formulations. Vaccination with free OVA protein either *via* microneedles or intradermal injection resulted in Th2-biased IgG_1 responses without any detectable level of Th1-associated IgG_{2c} antibodies (**Figure 4-6c, d**). In contrast, ICMVs administered by traditional syringe intradermally or delivered by multilayer-coated microneedles elicited a more balanced Th1/Th2 response with both IgG_1 and IgG_{2c} titers, with transcutaneous delivery of ICMV-carrying microneedles achieving 10-fold higher IgG_{2c} titers than "free" ICMV injection **(Figure 4-6c,d)**. This is of interest since IgG_2 antibody isotypes have been implicated in enhanced protection in both infectious disease and cancer vaccines.[157-159] Thus, these results suggest that microneedle-based multilayers encapsulating ICMVs are a promising platform for delivery of vaccine antigen and adjuvant to skin-resident APCs *via* a non-invasive, needle-free route for promotion of long-lived, high-titer humoral immune responses.

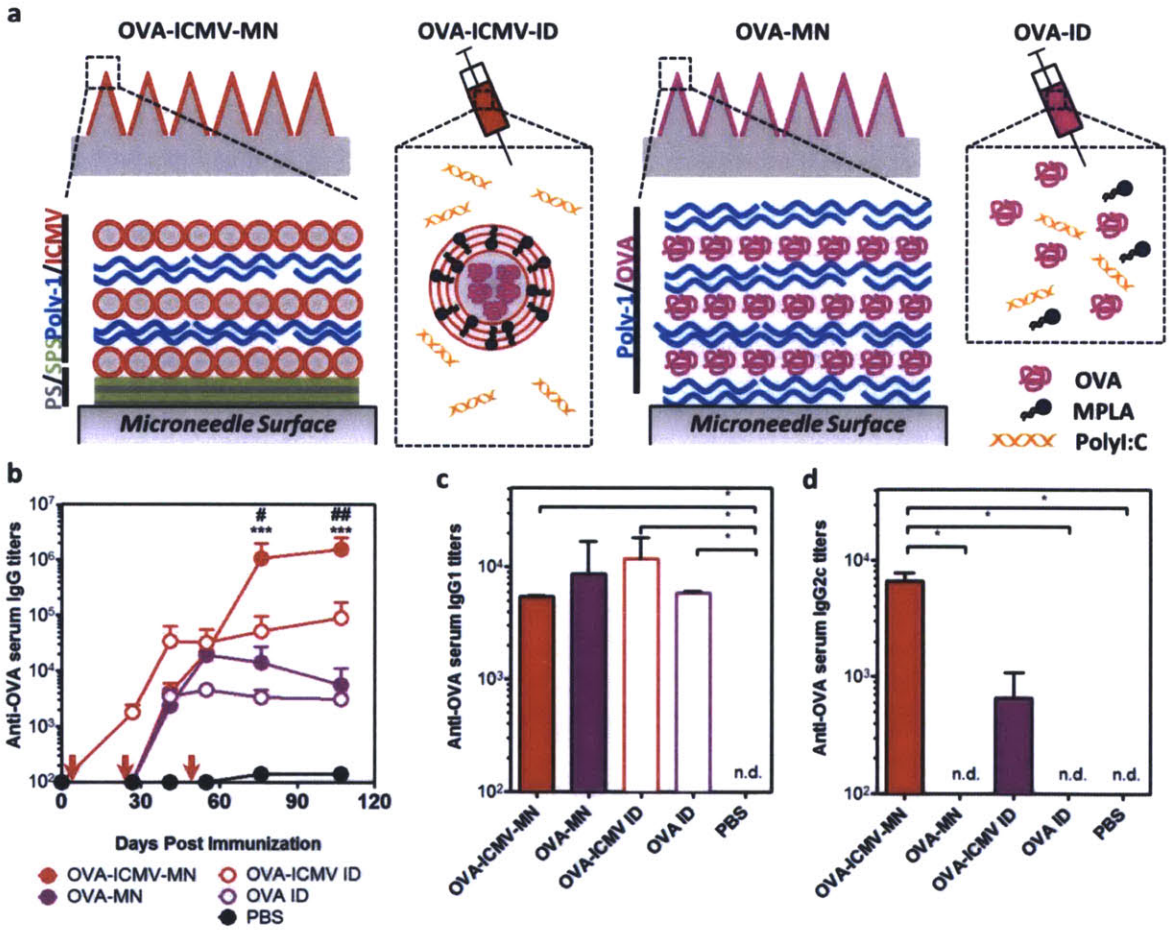

Figure 4-6. Microneedle subunit vaccination

(a) *Schematic representation of vaccine treatments tested.* ***(b)*** *Anti-OVA serum IgG titers were measured over time with immunizations on days 0, 28, and 56 with OVA-ICMVs or soluble*

antigen administered via either microneedle-based multilayers or intradermal bolus injection at dorsal auricular skin. ***(c, d)*** *Quantification of anti-OVA IgG_1* ***(c)*** *and IgG_{2c}* ***(d)*** *subtypes in sera at day 107. #, $p < 0.05$ and ##, $p < 0.01$, compared to OVA-ICMV ID, and ***, $p < 0.001$, compared to OVA-MN or OVA ID, as analyzed by two-way ANOVA, followed by Tukey's HSD. *, $p < 0.05$, as analyzed by one-way ANOVA, followed by Tukey's HSD.*

4.4. Conclusions

In summary, we have shown the successful incorporation of intact multilamellar phospholipid vesicles into erodible multilayer films through the use of an inter-bilayer molecular crosslinking stabilization strategy. We have further demonstrated the potential utility of such functional multilayer coatings constructed on microneedle arrays for rapid transfer of particle-carrying multilayers into microneedle-treated skin, and for the subsequent release of vesicle cargos through multilayer degradation *in situ*. Thus, this platform may ultimately serve as a potent platform for protein vaccination providing enhanced immunogenicity, simple and safe administration, and the potential for dry-state storage. These advantages provide the opportunity for more effective and less costly vaccine storage and distribution to the developing world, as multilayer stabilized formulations could be stored easily without refrigeration until rehydration upon microneedle insertion into the target tissue. Though we employed an LbL dipping process in multilayer fabrication for these lab-scale studies for convenience, note that commercial scale processes could readily employ spray deposition to eliminate loss of precious vaccine materials during fabrication.[81] The combination of multilayer deposition with microneedle application for transcutaneous delivery also addresses the need for a safe, potent, and non-invasive alternative to hypodermic needle-based administration. The simplicity of microneedle application also provides the prospect of rapid self-administration potentially streamlining mass vaccination and eliminating the need for healthcare worker training.[20,22,23] In addition, the ability of ICMVs and multilayers to incorporate diverse drug compounds and biologics makes this approach of broader interest for enhanced transcutaneous delivery of therapeutics.

5. Composite Dissolving Microneedles for Coordinated Control of Antigen and Adjuvant Delivery Kinetics in Transcutaneous Vaccination

5.1. Introduction

Chapters 2-4 present the design and preclinical testing of several strategies involving multilayer formulation of vaccine coatings for microneedle delivery. In Chapters 5-6 we introduce a new approach for microneedle vaccine design utilizing composite dissolving microneedle structures to allow for rapid administration, and flexible control over vaccine formulation and sustained release *in vivo*.

Recently, microneedle arrays have been employed as an enabling technology for safe and convenient transcutaneous delivery of diverse bioactive materials, including high molecular weight hydrophilic biologics, through pain-free mechanical disruption of the stratum corneum. For such barrier-disruption systems, rapid delivery of therapeutics into the skin by a brief application of the microneedle array is desirable, to minimize the potential risk of infection. This strategy has been demonstrated by various approaches, such as the use of microneedles that rapidly dissolve on entry into skin with release of encapsulated materials over minutes to hours.[57,142,160-168] However, while rapid drug release allows a brief microneedle application time, bolus drug delivery by microneedles, like bolus injections, can lead to rapid clearance of administered drugs and a need for large drug doses in order for released drug to remain at therapeutic doses (locally and/or systemically) for a sufficient temporal window to have a beneficial effect. Sustained or kinetically-controlled drug release is more desirable than bolus delivery for many therapeutics and is essential to fulfill the full potential of transcutaneous delivery for sustaining drug levels within a therapeutic window over time. Previous strategies for obtaining controlled drug release with microneedle systems employed intradermal injection from hollow microneedles,[169] or delivery from coatings on microneedle surfaces.[115,170] Alternatively, long term delivery has been achieved through encapsulation of drugs directly into biodegradable microneedles intended to remain in the skin for hours or days.[171,172] In each of these approaches, the microneedles must remain embedded in the skin, which raises the potential for infection in the setting of long-term/continuous drug delivery over days or weeks. To overcome this limitation, several strategies have been developed, including the use of microneedles to generate physical openings in the epidermis for topically-applied controlled-release particle suspensions to diffuse into the skin,[173] rapid delivery of drug-loaded polymer particles into the skin using dissolving microneedles,[174] or fabrication of solid PLGA microneedles which rapidly fracture into implanted fragments upon skin insertion due to swelling of embedded hydrogel beads.[175] The success of these approaches represents a strong proof of principle for the potential utility of microneedle platforms providing either rapid delivery or sustained release of therapeutics to the skin.

Vaccines have been shown to vary widely in potency based on the duration and kinetic profile of exposure to antigen and adjuvant combinations.[105,106,176-179] Recently, we demonstrated that intra-

lymph node injection of vaccines composed of soluble protein mixed with sustained-release adjuvant-loaded polymer particles could dramatically enhance the immune response to a model protein antigen.[106] However, intranodal injection is a more complex procedure than traditional vaccine administration, and is best suited to vaccines against cancer or more specialized settings such as allergy treatment.[180,181] Here, we sought to determine whether control over antigen/adjuvant exposure kinetics could also enhance immune responses elicited by microneedle vaccines applicable to widespread prophylactic vaccination. We developed two parallel approaches for fabrication of composite dissolving microneedles combining a rapid release phase and sustained release phase for independently controlling the kinetics of antigen and adjuvant exposure during transcutaneous vaccination. These composite arrays were composed of poly(acrylic acid) (PAA) and poly(lactide-*co*-glycolide) (PLGA) in either a microparticle form or a bulk implant contained in the microneedle tip and intended for implantation within the skin upon application. PAA forms a glassy hard solid in bulk (E ~ 4 GPa[182]) but also dissolves rapidly in water. Exploiting this duality, we employed bulk solid PAA as a supportive matrix or pedestal as well as the base of the microneedle array itself. When inserted into skin, near-instantaneous dissolution of the PAA on hydration by interstitial fluid in skin provided a mechanism for rapid needle-tip disintegration or release and implantation in the cutaneous tissue. This approach enables delivery of diverse cargos that are hydrophilic or hydrophobic including small molecules or macromolecular drugs, either through encapsulation into PLGA particles or the PAA matrix. The selection of PLGA molecular weight or co-polymer ratio provides flexibility for tuning the kinetics of sustained cargo release and PAA encapsulation provides the additional ability for bolus delivery upon dissolution *in vivo*. These composite microneedle designs provide the ability for rapid administration leading to cutaneous implantation of controlled release depots for either bolus or sustained combinatorial release of therapeutics for various potential applications including vaccine delivery, as demonstrated here.

5.2. Materials and Methods

5.2.1. PLGA Microparticle Synthesis

Polyvinyl alcohol (PVA)-stabilized PLGA microparticles were prepared by a single/double emulsion/solvent evaporation approach. Briefly, 80 mg PLGA (50:50 lactide:glycolide ratio, IV 0.35 dL/g, Lakeshore Biomaterials or Resomer RG 755 S, IV 0.70 dL/g) was dissolved in 5 ml dichloromethane. The PLGA solution was then added to 40 ml 0.5% PVA (MW 150,000 Da, MP Biomedicals) while homogenizing at 12,000rpm using a T-25 Digital Homogenizer (IKA). Homogenization was performed for 3 minutes following PLGA addition, and solvent was subsequently removed by stirring overnight. For fluorescently labeled particles 160 μg 1,1'-dilinoleyl-3,3,3',3'-tetramethylindocarbocyanine (DiI) or 1,1'-Dioctadecyl-3,3,3',3'-tetramethylindodicarbocyanine (DiD, Invitrogen) were codissolved with PLGA. For poly(I:C) loaded particles, 3mg Cy3-labeled poly(I:C) (Invivogen, labeled using Mirus LabelIT, according to the manufacturer's instructions) was dissolved in distilled water and added to the polymer-containing organic phase while sonicating at 12W with a Microson XL probe tip (Microson). After sonication for 30 s the resulting emulsion was added to the PVA solution and homogenized

as before. The resulting particles were collected by centrifugation, washed, and resuspended in distilled water before lyophilization and storage under desiccation at 4°C until use. Particle size and zeta potential was determined using a BIC 90+ light scattering instrument (Brookhaven Instruments Corp).

5.2.2. *Composite Microneedle Fabrication*

Microneedles encapsulating free PLGA microparticles or bulk PLGA implants were fabricated from PDMS molds (Sylgard 184, Dow Corning) machined using laser ablation (Clark-MXR, CPA-2010 micromachining system) to create patterns of micron-scale surface-cavities. First, PLGA microparticles were deposited into PDMS molds through addition of aqueous particle suspensions to the mold surface. Following PLGA microparticle addition (0.2-3.0 mg/array), molds were centrifuged for 20 minutes at rcf ~450 to compact particles into mold cavities. Following removal of residual material from the mold surface, molds were dried at 25°C. For microneedles encapsulating free microparticles, addition of 35% poly(acrylic acid) (PAA, 250kDa) to the mold surface was followed by centrifugation (20 minutes, rcf ~450) and drying at 25°C (48 hours on the benchtop, followed by 2-14 days under desiccation), before removal. Microneedles encapsulating multiple distinct particle populations were fabricated similarly through addition of mixed particle suspensions. For microneedles encapsulating bulk PLGA implants, PDMS molds encapsulating free microparticles were heated under vacuum (-25 in. Hg) at 145°C for 40 minutes, and then cooled at -20°C before addition of 35% PAA, centrifugation, and drying as previously described. For microneedles encapsulating layered PLGA implants, sequential microparticle deposition, drying, and melting was performed as previously described. All microneedles were stored under desiccation at 25°C until use. Microneedle arrays were characterized by scanning electron microscopy (SEM) using a JEOL 6700F FEG-SEM and confocal microscopy using a Zeiss LSM 510.

5.2.3. *Characterization of Microparticle and Implant Delivery*

Microparticle and bulk implant release was characterized *in vitro* through brief (<30 sec) exposure of fabricated arrays to PBS. Microparticles and bulk implants were then collected through centrifugation and washed in PBS before application of aqueous suspensions to glass coverslips. After drying, microparticles and implants were imaged by confocal microscopy. Similar delivery was measured *in vivo* following array application to the skin of mice. Animals were cared for in the USDA-inspected MIT Animal Facility under federal, state, local, and NIH guidelines for animal care. Microneedle application experiments were performed on anesthetized C57BL/6 mice (Jackson Laboratories) at the flank or dorsal ear skin. Skin was rinsed briefly with PBS and dried before application of microneedle arrays by gentle pressure. Following application mice were euthanized at subsequent time points and the application site and draining lymph nodes were dissected. Excised skin was stained with trypan blue before imaging for needle penetration. In separate experiments treated skin and applied microneedle arrays were imaged by confocal microscopy to assess transcutaneous delivery of encapsulated microparticles and bulk implants. In some cases, treated skin was excised and fixed in 3.7%

formaldehyde for 18 hours, then incubated in 30% sucrose/PBS for 2 hours before embedding in Optimal Cutting Temperature (OCT) medium (Tissue-Tek) for histological sectioning on a cryotome. Lymph nodes were similarly embedded in OCT and sectioned. Histological sections were then imaged using confocal microscopy.

5.2.4. In Vivo Imaging

Live whole animal imaging was performed using a Xenogen IVIS Spectrum (Caliper Life Sciences) on anesthetized mice. Fluorescence data was processed using region of interest (ROI) analysis with background subtraction and internal control ROI comparison to untreated skin using the Living Image 4.0 software package (Caliper).

5.2.5. Immunizations

All animal studies were approved by the MIT IUCAC and animals were cared for in the USDA-inspected MIT Animal Facility under federal, state, local, and NIH guidelines for animal care. Groups of 4 C57Bl/6 mice were immunized on days 0 and 35 with 15 μg ovalbumin and 50 ng poly(I:C) by intramuscular injection (15 μl in the quadriceps) intradermal injection (15 μl in the dorsal caudal ear skin) or by microneedle array (5 min application). Frequencies of OVA-specific $CD8^+$ T-cells and their phenotypes elicited by immunization were determined by flow cytometry analysis of peripheral blood mononuclear cells at selected time points following staining with DAPI (to discriminate live/dead cells), anti-CD8α, anti-CD44, anti-CD62L (BD Biosciences), and phycoerythrin-conjugated SIINFEKL/H-$2K^b$ peptide-MHC tetramers (Beckman Coulter). To assess the functionality of primed $CD8^+$ T-cells peripheral blood mononuclear cells were stimulated ex vivo with 10ug/ml OVA-peptide SIINFEKL for 6 h with Brefeldin-A (Invitrogen), fixed, permeabilized, stained with anti-IFNγ, anti-TNFα, and anti-CD8α (BD Biosciences), and analyzed by flow cytometry. Anti-Ovalbumin IgG titers, defined as the dilution of sera at which 450 nm OD reading was 0.25, were determined by ELISA analysis of sera from immunized mice. Animals were cared for following NIH, state, and local guidelines.

5.3. Results and Discussion

5.3.1. Fabrication of PLGA-Microparticle-PAA Composite Microneedle Arrays

To create microneedle arrays capable of rapid simultaneous delivery of both soluble and PLGA-encapsulated cargos, we developed two parallel microneedle approaches intended to deposit either (1) PLGA microparticles or (2) solid PLGA implants into the superficial layers of the skin upon the aqueous dissolution of a supportive PAA matrix or pedestal. We hypothesized that such a platform would provide rapid administration through brief microneedle application while enabling combined bolus and long-term dosing of cargos released from cutaneously-implanted PAA and PLGA depots, respectively. To fabricate the polymer composite microneedle structures needed to achieve these design goals, we employed a molding technique using polydimethylsiloxane (PDMS) molds. PDMS blocks were patterned with microscale cavities across their surface by laser micromachining, yielding a negative mold. In this strategy, cavity

shape and the resulting microneedle geometry are easily controllable through variation of the laser micro-ablation process.[115] We selected molds containing conical cavities, approximately 700 μm in height and 250 μm in width at the base. Microneedles of this size and shape have been shown to effectively penetrate the murine stratum corneum for cutaneous materials delivery[115] and are also appropriate for delivery in humans. To begin the microneedle fabrication process, PLGA microparticles (1580 ± 95 nm in diameter, -26 ± 2 mV zeta potential) formed through double-emulsion-solvent-evaporation were applied to the surface of the mold in aqueous suspension and compacted into the mold cavities through centrifugation (**Figure 5-1**, step 1). Excess microparticles were then removed from the PDMS surface and the microparticle-loaded mold was allowed to dry (**Figure 5-1,** step 2a). To form dissolving microneedles carrying dispersible PLGA microparticles, we next added a concentrated aqueous solution of PAA (35 wt%) to the mold surface and infiltrated the PAA solution into the packed PLGA particle bed *via* centrifugation (**Figure 5-1**, step 3a). The loaded molds were then dried at 25°C for 48 hr before desiccation under vacuum to obtain solid PLGA-PAA microparticle matrices. The dry composite microneedles were finally removed from the PDMS mold for characterization or stored under vacuum at 25°C until use (**Figure 5-1**, step 4a).

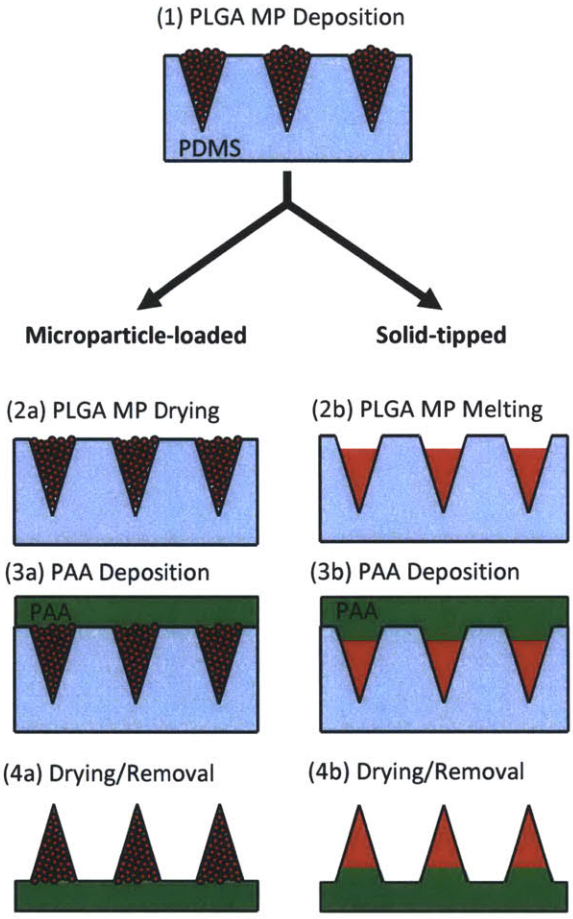

Figure 5-1. Composite microneedle fabrication scheme

Schematic view of composite microparticle and bulk PLGA tip microneedle array fabrication. PDMS molds were first filled with PLGA microparticles through centrifugation ***(1)****. PLGA microparticles were then either dried in mold cavities* ***(2a)*** *or fused at high temperature to create a solid tip* ***(2b)****. Concentrated aq. PAA solution was then centrifuged onto the filled molds to create a supportive matrix* ***(3a)*** *or pedestal* ***(3b)*** *for rapid dissolution in vivo. After drying microneedles were removed from PDMS molds* ***(4a, 4b)****.*

To characterize the internal structure of microneedles created in this way, we performed the described fabrication steps using PLGA microparticles loaded with distinct lipophilic fluorescent tracers to serve as a model drug cargos: either 1,1'-dilinoleyl-3,3,3',3'-tetramethylindocarbocyanine (DiI) or 1,1-dinoleyl-3,3,3',3'-tetramethylindoc dicarbocyanine (DiD). Localization of the PAA matrix within the microneedle array was tracked through encapsulation of Alexafluor-488 (AF488) as a hydrophilic fluorescent tracer in the PAA matrix. The AF488 dye also served as a model for potential hydrophilic therapeutic compounds that could be encapsulated for bolus cutaneous delivery upon dissolution of the PAA matrix *in vivo*. Confocal imaging of microneedles fabricated using DiD-loaded PLGA microparticles together

with AF488-loaded PAA showed uniform microneedle formation with DiD fluorescence localized in the microneedle tip, and AF488 fluorescence throughout the needle length (**Figure 5-2a**). This indicates the successful deposition of PLGA microparticles to the microneedle tip, and the effective formation of an encapsulating, supportive PAA matrix surrounding the microparticles and forming the base of the microneedle array itself. Further, confocal analysis demonstrated the flexibility of this approach through the similar successful fabrication of microneedles bearing multiple microparticle populations encapsulating either DiD or DiI in two different microparticle populations comprised of PLGA with high vs. low molecular weight (to obtain two distinct kinetics of drug release, **Supplementary Figure S5-1a**). SEM imaging demonstrated the fidelity of the final composite microneedles to the mold cavity architecture (**Figure 5-2b**). Additional imaging of the internal structure of needles intentionally broken after fabrication also confirmed the confocal imaging results, showing the presence of nodules of discrete PLGA microparticles surrounded by PAA matrix (**Figure 5-2c**).

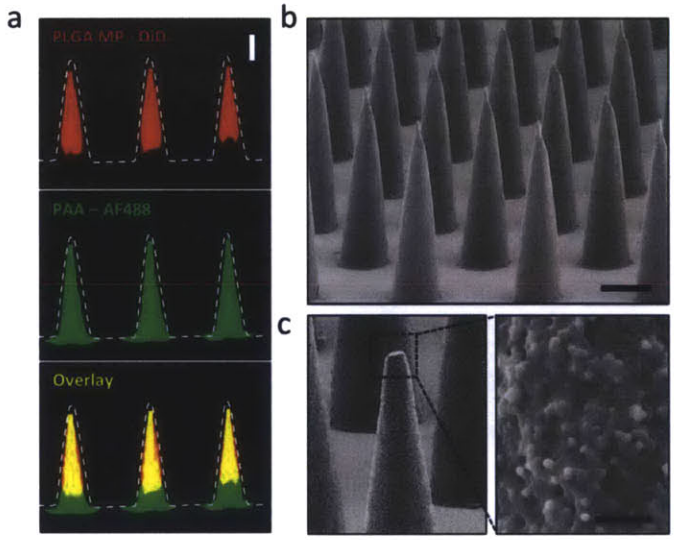

Figure 5-2. Fabrication of PLGA-microparticle-PAA composite microneedle arrays

(a) *Confocal micrographs of PLGA-PAA composite microneedles fabricated to encapsulate DiD-loaded PLGA microparticles (MP) (right, scale bar 200 μm). SEM micrographs of* ***(b)*** *resulting microparticle-encapsulating microneedle array (scale bar 200 μm) and* ***(c)*** *high magnification image of the composite needle interior of a fractured microneedle (scale bar 10 μm).*

5.3.2. *Fabrication of Solid PLGA-PAA Composite Microneedle Arrays*

A similar fabrication approach was developed for the generation of microneedles capable of implanting solid PLGA tips directly into skin. As previously described, PLGA microparticles were first deposited into the cavities of a PDMS mold (**Figure 5-1**, step 1). After drying, the microparticle-loaded PDMS molds were incubated at 140°C for 40 minutes under vacuum to fuse the embedded PLGA particles. The molds were then allowed to cool, solidifying the PLGA

into solid cones at the tips of each mold cavity (**Figure 5-1**, step 2b). As before, concentrated PAA was then added and infiltrated into the PDMS molds through centrifugation, before drying and finally removal of the completed arrays (**Figure 5-1**, steps 3b and 4b). Confocal imaging of DiD-loaded PLGA together with AF488-loaded PAA showed the internal composite structure of the resulting microneedle arrays. In this case fluorescent signal from encapsulated DiD-loaded PLGA was localized to the tip of the microneedles, while AF488-PAA was only seen forming the base of the microneedle array (**Figure 5-3a**), consistent with the melted microparticles forming a continuous PLGA matrix in the microneedle tip, supported by a PAA pedestal at the microneedle base. Fabrication in which two distinct PLGA microparticle populations were sequentially added and melted in sequence yielded a layered microneedle structure in which the DiD-loaded PLGA added first formed the needle tip, while the remainder of the needle was composed of the second DiI-loaded PLGA layer, and finally the AF488-loaded PAA pedestal (**Supplementary Figure S5-1b**). Fine control over the size of the PLGA "warheads" (and therefore of encapsulated drug cargos) was readily achieved through simple variation of the mass of PLGA microparticles added to the mold: Confocal imaging analysis of microneedles fabricated using varying amounts of PLGA microparticles showed the formation of PLGA tips of increasing height and correspondingly shorter PAA pedestals as the mass of added PLGA particles was increased (**Figure 5-3b, c**). Control over PLGA tip size and PAA pedestal height is potentially an important parameter not only for controlling cargo dosage, but also for efficiency of delivery upon insertion to the skin.

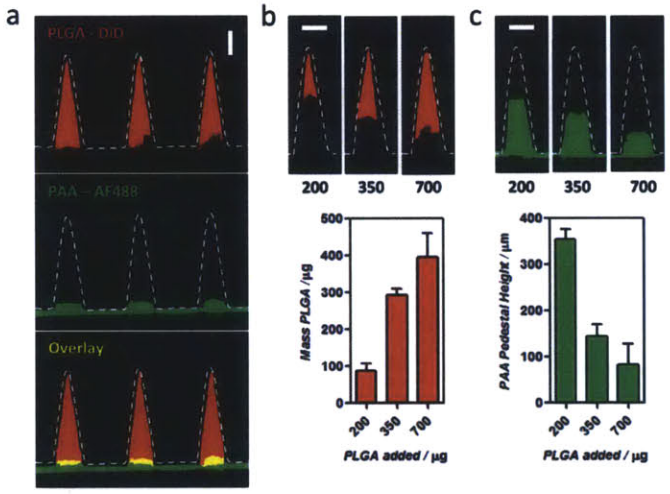

Figure 5-3. Fabrication of solid PLGA-PAA composite microneedle arrays

(a) *Confocal micrographs of PLGA-PAA composite microneedles fabricated with a PAA base and DiD-loaded solid PLGA tip (scale bar 200 µm). Confocal micrographs of microneedles fabricated with varying amounts of DiD-loaded PLGA microparticles as indicated giving a range of PLGA tip sizes* ***(b)*** *and PAA pedestal heights* ***(c)****.*

5.3.3. *In Vitro Testing of Composite Microneedle Delivery*

To test our hypothesis that PLGA-PAA composite microneedles should be able to rapidly release either PLGA microparticles or solid PLGA tips upon exposure to interstitial fluids in the skin, we exposed composite microneedles to phosphate buffered saline (PBS) *in vitro* for short periods of time to observe the kinetics of PAA dissolution. When PAA microneedles encapsulating DiD-loaded PLGA particles were submerged in PBS, PAA dissolution was nearly instantaneous. After 5 seconds, the remaining microneedle array backing was recovered and the released microparticles were collected through centrifugation of the PBS solution for confocal imaging. The recovered particles were identical to those initially used for microneedle fabrication with no particle aggregation observed (**Figure 5-4a**). PAA microneedles encapsulating DiD-loaded bulk PLGA tip implants were similarly exposed to PBS and exhibited equally rapid separation from the residual PAA base after only 5 seconds. After centrifugation for collection, confocal imaging of the released PLGA tips showed retention of overall tip morphology (**Figure 5-4b**). Together these results suggested that the composite PLGA-PAA microneedle designs we had fabricated should be capable of rapidly depositing their PLGA payload upon dissolution of the supportive PAA matrix or pedestal in skin interstitial fluids.

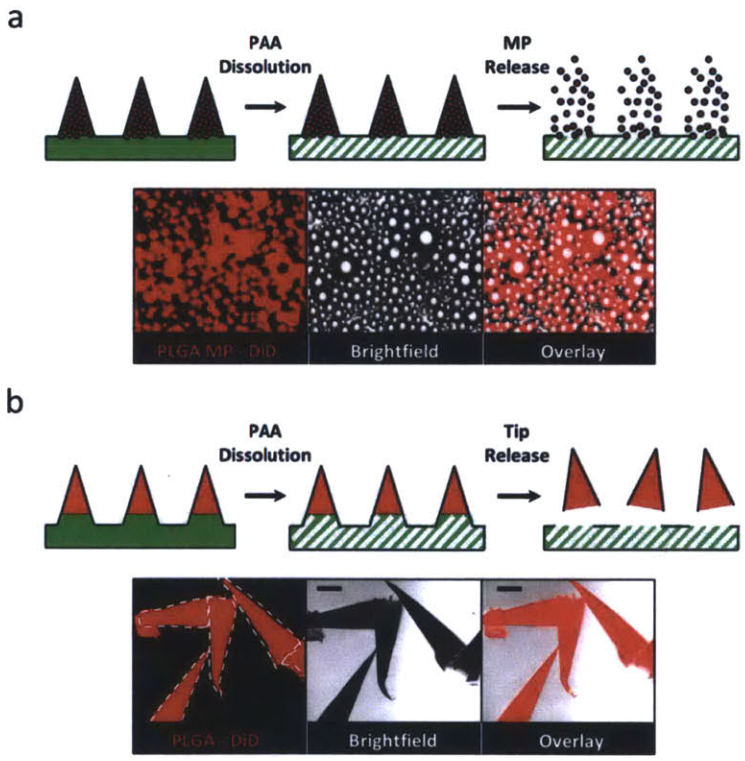

Figure 5-4. *In vitro* microneedle disintegration

(a) *Schematic of PAA/microparticle composite microneedle dissolution and confocal micrograph of DiD-loaded PLGA microparticles recovered following 5 sec exposure of composite microneedles to PBS solution (scale bar 10μm).* ***(b)*** *Schematic of PLGA solid tip microneedle*

dissolution and confocal micrograph of DiD-loaded PLGA microneedle tips recovered following 5 sec exposure of solid tip microneedles to PBS (scale bar – 200μm).

5.3.4. *In Vivo Testing of Composite Microneedle Delivery*

Given the rapid *in vitro* release of both PLGA particles and solid PLGA tips from PLGA-PAA microneedles, we next sought to test the delivery capabilities of these composite designs *in vivo*. We hypothesized that composite microneedles encapsulating PLGA particles should have sufficient strength to penetrate the skin upon application (**Figure 5-5a**, step 1) before exposure to fluid in the cutaneous tissue would cause rapid dissolution of the PAA supportive matrix (**Figure 5-5a**, step 2). This would then lead to disintegration of the microneedle itself, releasing and implanting the encapsulated microparticles into the epidermis (**Figure 5-5a**, step 3). Then, after the residual microneedle backing was removed, implanted microparticles would remain as cutaneous depots for hydrolytic degradation and sustained release of their encapsulated cargos *in situ* (**Figure 5-5a**, step 4). We first tested AF488-PAA microneedles encapsulating DiD-loaded PLGA microparticles. To determine the efficiency and timescale of PAA dissolution and PLGA microparticle release, we applied microneedles to the dorsal ear skin of anesthetized C57Bl/6 mice. Following application to the skin, we performed confocal imaging on the post-application microneedle arrays to observe residual microneedle morphologies. Similar to the *in vitro* results, microneedle application to murine skin *in vivo* for 5 minutes was sufficient to produce nearly complete loss of both DiD-PLGA signal and AF488-PAA signal in the microneedle shaft, indicating rapid dissolution and disintegration of the composite microneedle matrix (**Figure 5-5b**). We stained the skin surface over the microneedle application site with trypan blue to visualize areas of stratum corneum disruption, and found uniform and consistent penetration of the composite microneedle arrays to the viable epidermis (**Figure 5-5c**). Confocal imaging analysis of dissected skin samples immediately following microneedle application indicated the presence of cutaneous microparticle depots at the sites of microneedle penetration, with colocalization of fluorescent signal from DiD-loaded PLGA microparticles and AF488 from the dissolved PAA matrix (**Figure 5-5d**). Using 3-dimensional rendering of confocal z-stacks, these depots were observed to extend 300-400μm below the skin surface, consistent with the proposed paradigm for intact microneedle insertion, followed by PAA dissolution and microneedle disintegration, leaving depots of implanted material following removal of the microneedle backing (**Figure 5-5e**). Notably, we did not observe any short- or long-term local toxicity due to PAA exposure on the skin of treated animals, despite the relatively large chain length of the polymers used. This is likely due to the small amount of PAA (>150ug) introduced into the skin tissue through microneedle application, as well as the known low toxicity of PAA in commercial topical indications such as in detergents, cosmetics, or pharmaceutical use.[183]

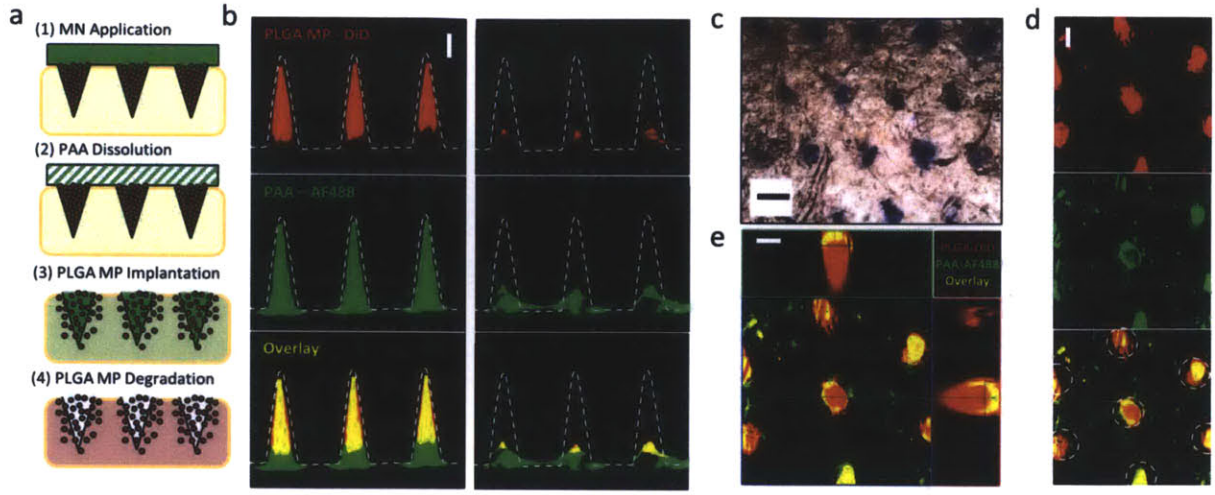

Figure 5-5. PLGA-microparticle-PAA composite microneedle insertion and delivery *in vivo*

(a) *Microneedle delivery scheme: (1) Microneedle (MN) arrays are applied briefly to penetrate skin. (2) Cutaneous microneedle penetration exposes needles to interstitial fluid resulting in rapid dissolution of the supportive PAA matrix and microneedle disintegration. (3) Following microneedle base removal, microparticles are left behind at penetration sites where soluble PAA-encapsulated cargoes are rapidly delivered to the surrounding tissue. (4) Microparticle deposition into the skin establishes a depot for sustained delivery of PLGA encapsulated cargoes over time.* ***(b)*** *Confocal micrographs of DiD-microparticle-loaded microneedles before application (left) and following a 5 minute application to murine skin (right, scale bar 200 μm).* ***(c)*** *Optical micrograph of microneedle-treated skin showing penetration sites stained using trypan blue (scale bar 500 μm).* ***(d)*** *Confocal micrograph of treated skin, showing deposition of DiD-loaded PLGA microparticles together with soluble AF488-loaded PAA at needle penetration sites directly following microneedle application for 5 minutes (scale bar 100 μm, penetration sites outlined).* ***(e)*** *Reconstructed confocal x-y/x-z/y-z images depicting the microneedle application site showing deposition of microparticle-cargos within the cutaneous tissue (scale bar 100 μm).*

We hypothesized a similar mechanism for delivery in the case of composite microneedles bearing bulk PLGA tips. As before, we theorized that intact composite needles would effectively insert into the outer layers of the skin before dissolution of the PAA pedestal by interstitial fluid, causing release and implantation of the PLGA tip for degradation and release of encapsulated cargos over time (**Supplementary Figure S5-2a**). Using AF488-PAA microneedles bearing DiD-loaded solid PLGA tips, we performed a similar set of tests to assay composite microneedle performance *in vivo*. As in the case of microparticle-loaded microneedles, application of composite microneedles bearing bulk PLGA tip implants for only 5 minutes to murine skin gave complete loss of DiD-PLGA signal as well as AF488-PAA signal from the patch backing, indicating PAA dissolution and needle tip separation (**Supplementary Figure S5-2b**). Trypan

blue staining also confirmed that bulk PLGA tipped microneedles were able to penetrate skin consistently (**Supplementary Figure S5-2c**) following application for 5 minutes. Finally, confocal imaging of dissected skin following microneedle array application showed implantation of the PLGA microneedle tips following removal of the residual microneedle array base (**Supplementary Figure S5-2d**). As in the case of microparticle delivery, these bulk PLGA implants were observed 300-400μm below the skin surface at the sites of microneedle penetration, together with fluorescent signal from the dissolved PAA pedestal (**Supplementary Figure S5-2e**).

5.3.5. *Formation and Retention of Cutaneous Particle Depots for Sustained Cargo Release*

We next sought to determine the fate of soluble PAA-loaded cargo and microparticle-loaded model drugs following deposition into the skin by composite microneedle application. As previously described, microneedles encapsulating DiD-loaded PLGA microparticles in an AF488-loaded PAA microneedle matrix were applied to the flank skin of C57Bl/6 mice for 5 minutes. Following treatment, individual animals were euthanized at various time points, and after dissection of the treatment site, confocal imaging and histological sectioning were performed to detect the presence of microparticle depots in the skin. Histological sectioning of tissue collected 24 hours after treatment showed distinct cutaneous depots of microparticles extending several hundred microns below the skin surface, colocalizing with signal from PAA-encapsulated AF488 (**Figure 5-6a**). Similarly, confocal imaging of treated skin 24 hours after administration indicated the retention of cutaneous microparticle deposits at the sites of microneedle insertion (**Figure 5-6b**). Consistent with the histological evidence, optical sectioning analysis of confocal data indicated the colocalization of DiD-labeled particle depots extending 300-400 μm beneath the skin surface. High magnification imaging of the depot site showed individual particles dispersed within the cutaneous tissue (**Figure 5-6b**). To determine whether the microneedle-implanted particles persist in the skin, we performed similar analyses of treated skin 10 days after microneedle administration. DiD-loaded microparticles were still found several hundred microns deep within the skin at this timepoint by histology (**Figure 5-6c**). However, tissue sections collected after 10 days consistently showed the loss of AF488 signal within the tissue at the sites of microneedle insertion, indicating the clearance of soluble PAA-loaded cargo over this time period.

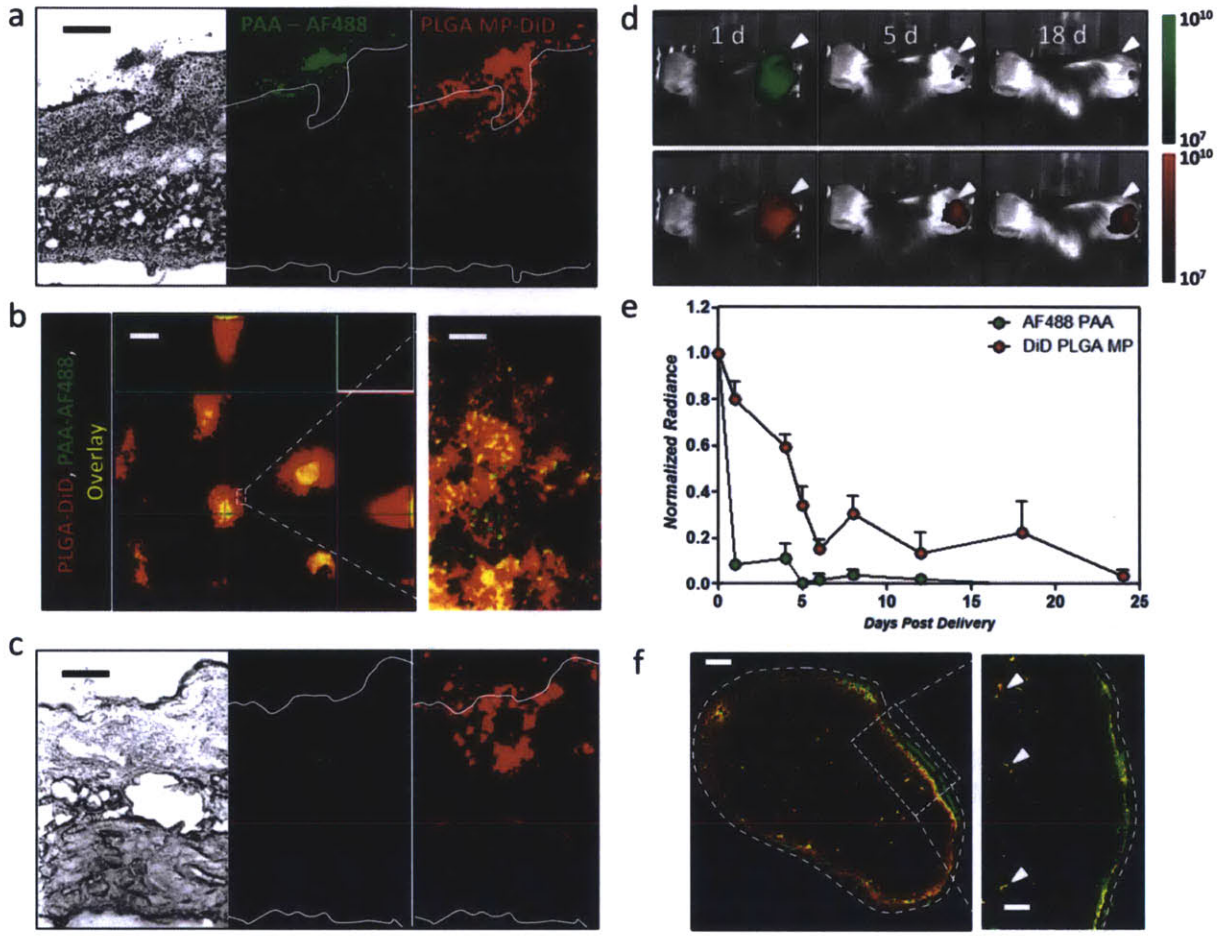

Figure 5-6. Cutaneous depot formation, controlled release, and systemic delivery

Composite DiD-loaded PLGA microparticle/AF488-loaded PAA microneedles were applied to the flank or dorsal ear skin of C57Bl/6 mice for 5 min, followed by histological, confocal microscope, and whole-animal fluorescence analysis at 1-18 days post treatment. ***(a)*** *Histological section of treated skin 24 hours following microneedle array application. Microparticles are shown implanted together with AF488-loaded PAA at a single microneedle penetration site (scale bar 200μm).* ***(b)*** *Parallel x-y/x-z/y-z confocal reconstruction of the treatment site at 24 hours post application shows DiD-loaded microparticle depots persisting at the penetration sites (left, scale bar 100 μm). High magnification imaging at a single penetration site shows microparticle dispersion within the cutaneous tissue (right, scale bar 20 μm).* ***(c)*** *Histological section of skin 10 days following microneedle application (scale bar 200 μm).* ***(d)*** *Whole animal fluorescence imaging of mice 1, 5, and 18 days after microneedle array application. Fluorescence signal from released AF488 and DiD-PLGA microparticles is shown.* ***(e)*** *Quantification of relative AF488 and DiD whole-animal fluorescence signal detected at microneedle application sites.* ***(f)*** *Histological section of the draining inguinal lymph node 10 days after microneedle application showing persistence of DiD PLGA-loaded cargos in the*

subcapsular sinus (left, scale bar 100 μm), as well as cell-trafficked PLGA particles in the cortical regions (arrows in inset at right, scale bar 10 μm).

Given the ability of composite microneedles to implant cutaneous microparticle deposits that were retained at the treatment site for long periods of time, we hypothesized that these microneedles might serve as an effective platform for sustained delivery of PLGA-loaded drugs, while also providing an opportunity to rapidly deliver bolus doses of additional cargos encapsulated in the PAA matrix. To determine the time course for cargo delivery following microneedle application, we performed composite microneedle treatments on the dorsal ear skin of C57Bl/6 mice as before, to deliver DiD-loaded PLGA microparticles together with PAA-loaded AF488. Tissue retention and clearance of these fluorescent model drug cargos was then monitored using whole animal fluorescent imaging. Results of this analysis showed that PAA-loaded AF488 was rapidly cleared from the site of application within 1 day, while DiD-fluorescent signal was retained within the ear skin for greater than 20 days following delivery (**Figure 5-6d, e**). These results are consistent with the previous confocal and histological analyses already discussed, and together support the hypothesized mechanism of microneedle insertion, followed by PAA dissolution, and needle disintegration to form long-lived cutaneous PLGA particle depots for sustained release over time. Similar whole animal imaging results obtained following delivery of bulk PLGA implants suggest an equivalent mechanism for composite microneedles of this variation (**Supplementary Figure S5-3**).

Nanoparticles and microparticles deposited in skin are known to be phagocytosed over time and transported to draining lymph nodes by antigen presenting cells[184-186]. This transport process could affect the biodistribution of particle-released drugs and is an important factor in particle-based vaccines. To assess transit of particles from microneedle insertion sites to draining lymph nodes over time, confocal imaging of histologically sectioned draining lymph nodes was performed to detect the presence of microneedle-delivered cargos 10 days after treatment. These analyses clearly showed the presence of both AF488 (our model water-soluble PAA-encapsulated drug) and microparticle-loaded DiD within the subcapsular sinus of sectioned lymph nodes, suggesting these materials were able to drain through the lymphatics following release at the cutaneous depot site (**Figure 5-6f**). Further, intact microparticles were observed by high magnification imaging within the cortical regions of the lymph nodes, indicating trafficking of particles by cells from the implantation site. No fluorescent signal was observed in lymph nodes from untreated animals (data not shown). Together these results support the idea that cutaneously-delivered soluble materials as well as microparticles themselves are trafficked to draining lymph nodes.

5.3.6. *Composite Microneedle Subunit Vaccine Delivery*

As a final test of the ability of composite microneedles to provide effective therapeutic delivery *in vivo,* we fabricated arrays for the transcutaneous delivery of a subunit vaccine formulation. We synthesized PLGA microparticles encapsulating Cy3-labeled poly(I:C) (Cy3-poly(I:C)), a

synthetic double stranded RNA mimic of viral RNA, as a molecular adjuvant.[187] Microneedles composed of poly(I:C)-loaded PLGA particles and fluorescently-labeled ovalbumin (AF647-OVA, model antigen) embedded in a supporting PAA matrix were fabricated following the approach of **Figure 5-1**. Characterization of the resulting microneedles using confocal imaging showed restriction of the Cy3-poly(I:C) microparticles in the microneedle tips, with fluorescent signal from AF647-OVA throughout the microneedle length (**Figure 5-7a**). Upon application of these vaccine-loaded composite microneedles to the dorsal ear skin of mice, we observed successful deposition of both antigen and adjuvant at the application site using whole-animal fluorescence imaging (**Figure 5-7b**), consistent with our previous results using model drug cargos.

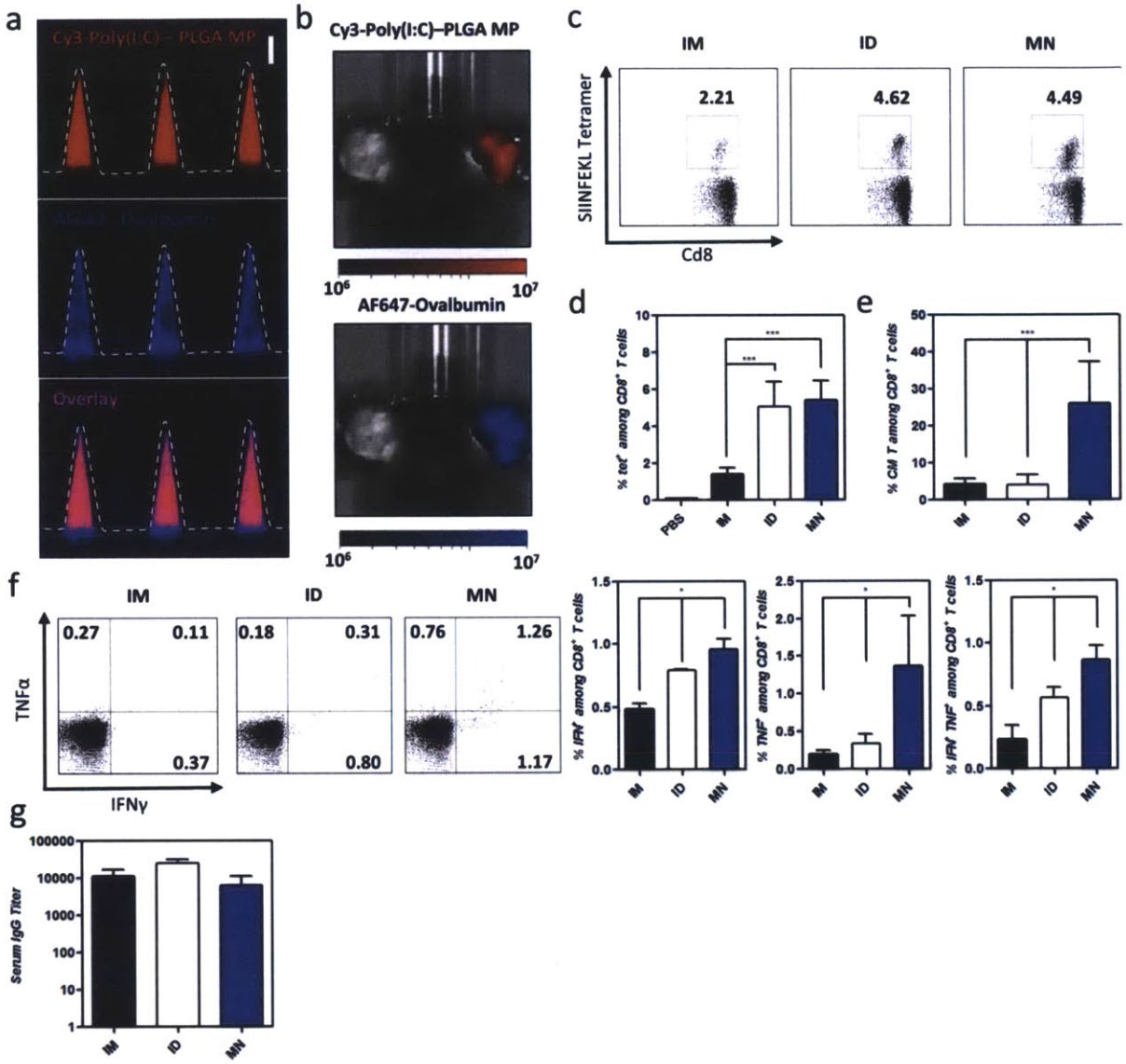

Figure 5-7. Composite microneedle subunit immunogenicity

(a, b) *Composite microneedles were fabricated, comprised of Cy3-labeled poly(I:C)-loaded PLGA microparticles surrounded by PAA with entrapped AF647-ovalbumin.* ***(a)*** *Confocal micrographs of composite microneedles (right, scale bar 200 μm).* ***(b)*** *Whole animal fluorescence imaging of mice treated with microneedles after 1 day.* ***(c-f)*** *Groups of C57Bl/6 mice (n = 4) were vaccinated with 15 μg ovalbumin and 50 ng poly(I:C) intramuscularly (IM), intradermally in the dorsal ear skin (ID), or administered transcutaneously to the ear via microneedles (MN), with the poly(I:C) entrapped in PLGA microparticles and ovalbumin entrapped in the PAA phase. Mice were primed on day 0 and boosted on day 35 with identical formulations.* ***(c)*** *Frequency of SIINFEKL-specific T cells in peripheral blood assessed by flow cytometry analysis of peptide-MHC tetramer$^+$ CD8$^+$ T cells. Shown are representative*

*cytometry plots from individual mice and mean tetramer$^+$ frequencies from day 49. **(d)** Analysis of T-cell effector/central memory phenotypes in peripheral blood by CD44/CD62L staining on tetramer$^+$ cells from peripheral blood. Shown are mean percentages of tetramer$^+$CD44$^+$CD62L$^+$ among CD8$^+$ T cells at day 63. **(e)** Frequency of tetramer$^+$ CD8$^+$ T cells in peripheral blood producing IFN-γ and TNF-α following SIINFEKL restimulation assessed by flow cytometry. Shown are representative cytometry plots from individual mice and mean cytokine$^+$ frequencies for day 56. **(f)** Enzyme-linked-immunosorbent assay analysis of total ovalbumin-specific IgG in sera at day 63.*

To test the efficacy of these dissolving composite microneedles for vaccination compared to traditional vaccine administration, mice were immunized on day 0 and boosted on day 35 with 15 μg ovalbumin and 50 ng PLGA-encapsulated poly(I:C) administered either intramuscularly (IM) in the quadriceps, intradermally (ID) in the dorsal ear skin, or by microneedle application (MN) for 5 minutes, also at the dorsal ear site. We then monitored the induction of OVA-specific cellular immunity through the detection of OVA-reactive CD8$^+$ T cells using flow cytometry. Two weeks following the first immunization we observed expansion of antigen-specific CD8$^+$ T cells to ~2% of the total CD8$^+$ population in all treatment groups, suggesting that microneedle delivery provided similar initial immunogenicity compared with traditional parenteral immunization strategies (**Supplementary Figure S5-4a**). Upon contraction of the antigen-specific T cell population two weeks later, we measured the frequency of antigen-specific CD44$^+$CD62L$^+$ cells, central memory T cells that have been correlated with long-lived effective protection against re-exposure to pathogens.[188] On day 28, we observed that microneedle immunization generated central memory cells much more efficiently than animals receiving either intramuscular or intradermal vaccination, with greater than 30% of OVA-specific memory T-cells expressing CD44 and CD62L (**Supplementary Figure S5-4b**). These trends were similarly observed after the booster immunization, with antigen-specific T-cells reaching ~5% of the total CD8$^+$ population in mice receiving ID or MN dosing (**Figure 5-7c, d**). Similar to the pre-boost response, elevated frequencies of central memory CD8$^+$ T cells were observed in microneedle vaccinated mice after contraction of the response on day 63, compared to both control IM and ID injected vaccine groups (**Figure 5-7e**). We also evaluated the functional capacity of the vaccine-elicited T-cell response through detection of cytokine production following re-stimulation of peripheral blood mononuclear cells with SIINFEKL peptide (the immunodominant peptide from OVA in C57Bl/6 mice). These analyses indicated enhanced cytokine production by T-cells elicited by microneedle vaccination for antigen-dependent production of both IFN-γ and TNF-α, key cytokines for combating viral infection (**Figure 5-7f**). Furthermore, microneedle delivery generated a higher frequency of multi-functional CD8$^+$ T cells able to secrete both IFN-γ and TNF-α upon peptide stimulation. Together these results indicate the ability of microneedle immunization with slow-released adjuvant to elicit phenotypically and functionally superior cellular immunity compared to traditional vaccine administration. Finally, we measured the level of ovalbumin-specific IgG in

the sera of immunized animals to compare the capacity for generating humoral immunity. Here we observed the presence of similarly high levels of anti-ovalbumin IgG in all immunized animals on day 63, suggesting that composite microneedle delivery can also generate antibody responses comparable to traditional immunization strategies (**Figure 5-7g**). Notably, the microneedles used in these vaccination studies were fabricated and stored dry at 25°C for between 4 and 8 weeks before administration for both the prime and boost immunizations, indicating the potential for long-term maintenance of vaccine potency without the need for cold storage, a pressing need for the effective distribution of vaccines to remote areas of the developing world. Taken as a whole, these results demonstrate the strength of our approach for rapid transcutaneous multi-component delivery using composite PLGA-PAA microneedles.

5.4. Conclusions

Here we have demonstrated an approach for modular cargo encapsulation into composite dissolving microneedles for rapid delivery of PLGA microparticles or solid tips to form long-lived cutaneous depots promoting controlled and sustained release over several weeks. The combination of PLGA-formulated drug with a rapidly water-soluble PAA supporting matrix (in the case of microparticles) or pedestal (in the case of solid PLGA tips) provides the combined ability to rapidly and simply deliver the PLGA payload upon application to skin for only 5 minutes and to maintain drug release from implanted PLGA depots long after removal of the microneedle backing. Additionally, this composite microneedle architecture provides substantial flexibility in loading of single or multiple diverse cargos either into PLGA through standard double emulsion particle synthesis, or into the supporting PAA matrix through simple co-dissolution during fabrication. The composite structure also allows for simple tuning of extended cargo release kinetics through selection of PLGA copolymer ratio and molecular weight or bolus delivery upon needle disintegration through encapsulation in the PAA matrix. We have demonstrated the utility of these microneedle designs for the systemic dispersion of drugs released upon skin insertion or upon release from implanted PLGA over time. Finally, we have shown the successful application of this materials platform for encapsulation and delivery of a protein vaccine formulation generating potent humoral and cellular immunity matching or exceeding that resulting from traditional needle-based vaccine administration, even after storage for several weeks at room temperature. Together these results suggest that PLGA-PAA composite microneedles are an effective platform for straightforward and robust transcutaneous drug and vaccine delivery. Aside from applications in vaccination, the flexibility and modularity of this approach suggests its potential to serve as a platform for generalized therapeutics delivery providing both rapid and convenient administration as well as the potential for controlled and sustained systemic delivery.

6. Implantable Silk Composite Microneedles for Programmable Vaccine Release Kinetics and Enhanced Immunogenicity in Transcutaneous Immunization

6.1. Introduction

Chapter 5 introduced an alternative approach for transcutaneous vaccination using composite dissolvable microneedles to rapidly administer vaccines and control the coordinated release of antigen and adjuvant over days to weeks for enhanced immunogenicity in soluble protein vaccines. Here, in Chapter 6, we expand upon this theme to provide additional practical advantages and more robust controlled release capacities using silk hydrogel matrices to safely load and release high densities of fragile bio-active vaccine components *in vivo*.

Immunological studies have begun to reveal the importance of antigen and adjuvant delivery kinetics in the developing immune response, both within the context of vaccination and natural responses to infection.[106,189-191] For example, the magnitude, functionality, and phenotype of elicited $CD8^+$ T cell responses following vaccination have been correlated with the kinetic profile of both antigen and inflammatory signals *in vivo*. These findings are correlated with known differences in the natural immunity generated against transient or persistent pathogens, indicating specific mechanisms of immunity that may be exploited through engineered vaccine kinetics to yield greater vaccine efficacy.

In Chapter 5 we began to explore the ability of microneedle delivery systems to control vaccine kinetics. Microneedle patches composed of a single monolithic polymer phase require that patches remain on the skin for prolonged time periods to achieve extended drug release. Conversely, our previous composite microneedle structures, based on solid biodegradable poly(lactide-*co*-glycolide) (PLGA) polymer tips supported on a water-soluble poly(acrylic acid) (PAA) base rapidly disintegrate upon skin application, implanting the solid polymer tips into the skin following a brief ~5 min application.[192] The implanted polymer tips can subsequently provide sustained release of encapsulated cargos over a tunable period of days to weeks. In these previous studies, vaccination utilizing PLGA/PAA composite microneedles implanting persistent polymer depots for slow cutaneous release of adjuvant following bolus antigen delivery yielded improved proliferation, stronger antigen-dependent cytokine secretion, and altered memory phenotypes in assays of $CD8^+$ T cell immunity.[192] Here we have expanded upon this concept through the design of a microneedle system based on silk protein, thereby creating implantable hydrogel microneedle matrices for efficient vaccine loading and highly tailorable vaccine release kinetics *in vivo*. Unlike PLGA, loading of biomolecules in silk protein matrices is a simple one-step process and silk has previously been used as a safe and effective material for high-density loading of sensitive bio-molecules into non-immunogenic hydrogels under mild aqueous processing conditions, which subsequently release entrapped cargo for extended periods of time.[193,194] Recent work has demonstrated the ability of dried silk hydrogels to form dense microneedle structures capable of inserting into murine skin *ex vivo*.[172,195] The additional capacity for effective stabilization of vaccines and drugs in silk at room temperature offers an

attractive opportunity to formulate vaccines which could avoid the cold chain, thus making vaccines more inexpensive and readily available.[196]

Here we sought to combine the advantages of this composite microneedle design with the beneficial properties of silk as a controlled release matrix for entrapped proteins, and explored the ability of silk/PAA composite microneedles to regulate the kinetics of vaccine delivery in skin with the goal of mimicking patterns of antigen and inflammatory signal exposure during natural infections. Composite microneedles were loaded with a subunit vaccine comprised of a model protein antigen and the molecular adjuvant polyI:C, a synthetic double-stranded RNA compound that stimulates immune responses through the danger sensors Toll-like receptor-3 (TLR-3) and melanoma-differentiation associated protein 5 (MDA5).[187] Vaccine loaded into the PAA phase of the microneedles provided a rapid initial bolus of vaccine release, followed by a slow/sustained release of additional antigen/adjuvant from the implanted silk depots. We observed dramatic variations in the strength of antigen-specific T cell responses dependent upon the temporal patterns of bolus and extended vaccine delivery programmed through materials engineering of the silk-composite structure. This approach allowed for the generation of antigen-specific T cell responses following a single prime microneedle vaccination that were equivalent to those measured following a prime-boost parenteral immunization routine, suggesting the utility of this strategy for streamlined prime-only vaccine delivery. Combined with the recently demonstrated room temperature stability of vaccines embedded in silk,[196] this controlled-release microneedle platform has the potential to combine three important features of next-generation vaccines for use in the developing world: *(i)* needle-free delivery, *(ii)* inexpensive long-term room temperature storage without the need for a 'cold chain', and *(iii)* effective single-dose immunization providing potent immunological memory. Additionally, we have confirmed through these studies the potential for engineering optimal immune responses through programmed vaccine release kinetics, an important finding supporting the future use of advanced drug delivery approaches in the progression of vaccine research.

6.2. Materials and Methods

6.2.1. Silk Fibroin Solution Preparation

Cocoons of *Bombyx mori* silkworm silk were purchased from Aurora Silk (Portland, OR). All other chemicals were purchased from Sigma-Aldrich (St. Louis, MO) and used as received. Silk fibroin was prepared from cocoons as previously described.[197] Briefly, cocoons were boiled for 40 min in a solution of 0.02 M sodium carbonate and then rinsed thoroughly with deionized water to extract the glue-like sericin protein. After drying, the extracted silk was dissolved in 9 M lithium bromide solution at 60°C for 4 hours, and subsequently the salt was removed by dialysis against deionized water using a Slide-a-Lyzer dialysis cassette (Pierce, Rockford, IL) for 48 hours, changing the water regularly at least six times. The resulting solution was centrifuged twice at 4°C for 20 min to remove impurities and the aggregates that formed during dialysis. The supernatant was stored at 4°C and filtered through a 450 nm syringe filter prior to use. The final

concentration of silk fibroin solution was determined by weighing the residual solid of a known volume of solution after drying.

6.2.2. *Fabrication of Silk/PAA Microneedle Arrays*

PDMS microneedle molds (Sylgard 184, Dow-Corning, Midland, MI) were prepared using a Clark-MXR-CPA-2010 laser micromachining instrument (VaxDesign Inc., Orlando, FL). Soluble ovalbumin (OVA, Worthington, Lakewood, NJ) and polyI:C (Invivogen, San Diego, CA) were combined with aqueous silk solutions (8% w/v) to give the desired immunogen concentration (generally ~5 mg/ml OVA, 0.5 mg/ml polyI:C). PDMS molds were then treated with O_2 plasma before addition of silk-vaccine formulations to the mold surface by pipette. Molds were centrifuged for 30 minutes at rcf $\approx$ 450 and excess silk-vaccine solution was removed from the mold surface for potential reuse. Molds containing silk-vaccine were then dried at 25°C for 12 hours and treated with 9:1 (v/v) methanol for 5 minutes or left untreated. Polyacrylic acid (PAA, 250 kDa, 35%) was then added to soluble OVA and polyI:C at the desired concentrations (generally ~1 mg/ml OVA, ~0.1 mg/ml polyI:C) and mixed well. PAA pedestals were then formed through addition of 35% PAA to the mold surface, followed by centrifugation (30 min, rcf $\approx$ 450) and drying at 25°C (48 h on the benchtop, followed by 2–14 days under desiccation), before removal. All microneedles were stored under desiccation at 25°C until use. Microneedle arrays were characterized by optical and confocal microscopy using a Leica DMXR and a Zeiss LSM 510 respectively.

6.2.3. *In vitro Vaccine Release*

Silk implant release was characterized *in vitro* through brief (< 30 s) exposure of fabricated arrays to deionized water. Implants were then collected through centrifugation and washed before application of aqueous suspensions to glass coverslips. After drying, implants were imaged by SEM using a JEOL 6700F FEG-SEM.

To differentiate the release kinetics of OVA loaded in PAA or silk and to evaluate the effect of methanol treatment on release profiles, *in vitro* OVA release experiments were performed by immersing silk/PAA composite microneedles in PBS buffer at pH 7.4 and 37±0.5°C. Dried silk tips in PDMS were fabricated as described above with or without treatment in 9:1 (v/v) methanol:water solution for 5 min prior to PAA addition. Three experimental groups (n = 4 for each group) were designed: AlexaFluor 555 labeled ovalbumin (AF555-OVA) loaded in PAA, AlexaFluor 647 labeled ovalbumin (AF647-OVA) loaded in non-treated silk tips, AF647-OVA loaded in methanol-treated silk tips. For AF555-OVA release from the PAA portion of composite microneedles, 1 ml aliquots were removed from 10 ml volume of release bath at predetermined time points and replaced with 1ml of fresh pre-warmed PBS. For AF647-OVA release from the untreated or methanol-treated silk portion, microneedles were transferred between 0.5 ml aliquots of fresh pre-warmed PBS at pre-set time points. The concentration of AF555-OVA and AF647-OVA in each of the release samples was quantified by fluorescence spectroscopy (M200 Pro, Tecan, Mannedorf, Switzerland). At each time point, samples were loaded in triplicate and the averaged reading was taken for further quantification.

6.2.4. *In vivo Microneedle Application and Vaccine Release*

All animal studies were approved by the MIT IUCAC and animals were cared for in the USDA-inspected MIT Animal Facility under federal, state, local, and NIH guidelines for animal care. Microneedle application experiments were performed on anesthetized C57BL/6 mice (Jackson Laboratories, Bar Harbor, ME) at the flank or dorsal ear skin. Skin was rinsed briefly with PBS and dried before application of microneedle arrays by gentle pressure. Following application mice were euthanized at subsequent time points and the application site was dissected. Treated skin and applied microneedle arrays were imaged by confocal microscopy to assess transcutaneous delivery of silk implants. In some cases, treated skin was excised and fixed in 3.7% formaldehyde for 18 h, then incubated in 30% sucrose/PBS for 2 h before embedding in optimal cutting temperature (OCT) medium (Tissue-Tek) for histological sectioning on a cryotome. Histological sections were then imaged using confocal microscopy. Live whole animal imaging was performed using a Xenogen IVIS Spectrum (Caliper Life Sciences, Hopkinton, MA) on anesthetized mice. For luminescent imaging of myeloperoxidase (MPO)-dependent oxidative burst, luminol sodium salt (Santa Cruz Biotech, Santa Cruz, CA) was administered i.p. (250 mg kg^{-1}) before imaging. Fluorescence/luminescence data was processed using region of interest (ROI) analysis with background subtraction and internal control ROI comparison to untreated skin using the Living Image 4.0 software package (Caliper).

6.2.5. *Immunizations*

C57Bl/6 mice (5/group) were immunized on day 0 with 9 μg ovalbumin and 150 ng polyI:C by intradermal (i.d.) injection (15 μL in the dorsal caudal ear skin) or by microneedle array (5 min application). Microneedles contained ~98% of the total vaccine dose in the PAA fraction, with the remaining 2% in the silk implant. Silk implants were either left untreated or cross-linked with methanol as previously described to give differential vaccine release kinetics. In some cases microneedles were fabricated to contain vaccine in only silk implants, or otherwise in only the PAA pedestal. Animals vaccinated by i.d. injection received an identical boost on day 28. Mice were then mock challenged on day 77 with 10 μg pCl-neo-sOVA (pOVA, Addgene, Cambridge, MA) encoding soluble OVA, by intramuscular (i.m.) injection (25 μl, split between both quadriceps).

6.2.6. *In vivo Murine Immunogenicity*

Frequencies of OVA-specific $CD8^+$ T-cells and their phenotypes elicited by immunization were determined by flow cytometry analysis of peripheral blood mononuclear cells at selected time points following staining with DAPI (to discriminate live/dead cells), anti-CD8α , anti-CD44, anti-CD62L, anti-KLRG1 (BD Biosciences, San Jose, CA), and phycoerythrin-conjugated SIINFEKL/H-$2K^b$ peptide-MHC tetramers (Beckman Coulter, Indianapolis, IN). To assess the functionality of primed $CD8^+$ T-cells peripheral blood mononuclear cells were stimulated *ex vivo* with 10 μg/ mL OVA-peptide SIINFEKL for 6 h with Brefeldin-A (Invitrogen, San Diego, CA), fixed, permeabilized, stained with anti-IFNγ, anti-TNFα , and anti-CD8α (BD Biosciences), and analyzed by flow cytometry. Anti-ovalbumin or anti-silk IgG, IgG_1, IgG_{2C}, and IgM titers,

defined as the dilution of sera at which 450 nm OD reading was 0.25, were determined by ELISA analysis of sera from immunized mice. To measure avidity index, ELISA was performed after 10 minute exposure of bound serum to 6M urea, to strip weakly bound immunoglobulins.[198] IgG avidity index was calculated as the ratio of measured titer without urea treatment to titer measured with urea treatment.

6.3. Results and Discussion

6.3.1. Fabrication of Silk-PAA Composite Microneedles

In Chapter 5 we reported a strategy for the fabrication of composite microneedles based on PAA and PLGA for microneedle-mediated implantation of solid PLGA microtips or microspheres *in vivo*.[192] Here we adapted this approach to create microneedles bearing a solid silk tip, supported by a PAA pedestal intended to rapidly dissolve in cutaneous tissue fluids following needle insertion, releasing silk tips for retention in the skin following microneedle patch removal. To fabricate these structures we first generated PDMS molds bearing square pyramidal micro-scale cavities across their surface using laser ablation as previously described (**Figure 6-1a, step 1**).[115] We then surface treated the molds with O_2 plasma to generate a hydrophilic surface and facilitate infiltration of the mold cavities by the silk-vaccine solution. Silk fibroin protein was co-dissolved in aqueous solution with ovalbumin protein (OVA, a model antigen) and the TLR-3 agonist polyI:C, a potent double-stranded RNA adjuvant for stimulating anti-viral immune responses. This solution was added to plasma-treated molds and infiltration of the mold cavities was further completed through centrifugation (**Figure 6-1a, step 2**). After removing excess silk-vaccine solution, silk-filled molds were allowed to dry at room temperature for 12 hr to produce hardened silk hydrogel tips within the PDMS molds (**Figure 6-1a, step 3**).[172,195] Silk protein is known to undergo physical cross-linking upon exposure to methanol, and this results in prolonged cargo release from rehydrated silk hydrogels.[197] Here, we exposed solidified silk tips to methanol by pipetting solvent onto the mold surface, to introduce physical crosslinking and retard release of encapsulated vaccine from silk tip implants following implantation *in vivo* (**Figure 6-1a, step 3**). Following methanol treatment, we added vaccine-loaded aqueous PAA solutions carrying co-dissolved OVA and polyI:C to the mold surface and again performed centrifugation to compact the PAA into the mold cavities forming complete PAA pedestal structures (**Figure 6-1a, step 4**). Microneedles were then dried in the mold at room temperature for several days and placed under vacuum to complete the drying process before removal and storage under vacuum at 25°C (**Figure 6-1a, step 5**). This process reliably produced arrays of composite pyramidal microneedles 550μm in height bearing a tip-pedestal structure where vaccine-containing silk hydrogel tips were supported by vaccine-loaded PAA pedestals (**Figure 6-1b**). This structure was readily visible by optical microscopy imaging of microneedles fabricated with Alexafluor 647-labeled OVA (AF647-OVA) and Alexafluor 555-labeled OVA (AF555-OVA) loaded within the silk tip and PAA pedestal, respectively (**Figure 6-1b**). We further confirmed this needle microstructure using confocal microscopy to detect the localization of the vaccine cargo within the tip or pedestal of the resulting microneedles. This analysis revealed AF647-OVA restricted to the silk tip of each microneedle with AF555-OVA signal

observed only in the PAA pedestal (**Figure 6-1c**). Given our previous results with similar PLGA/PAA systems, we expected that this composite structure should allow for effective cutaneous insertion of the hardened composite microneedles, where exposure to interstitial fluids would rapidly dissolve the PAA pedestals releasing the silk tips, which would remain implanted in the skin following removal of the array backing.[192]

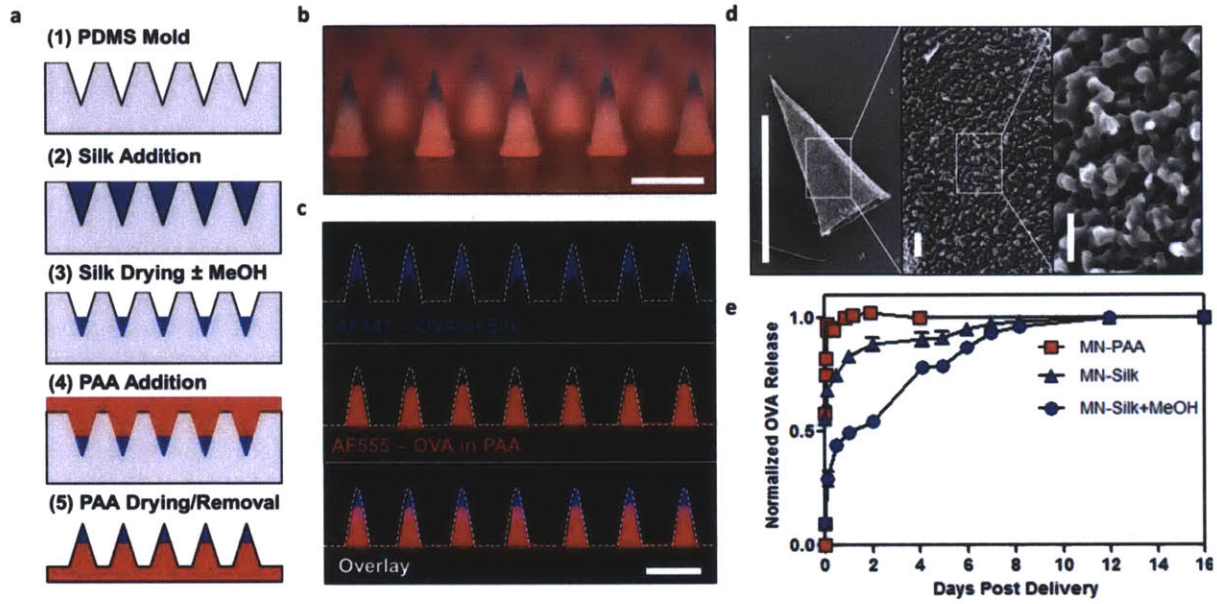

Figure 6-1. Fabrication and *in vitro* characterization of silk/PAA composite microneedles.

(a) *Schematic of microneedle fabrication: (1) PDMS molds were fabricated using laser ablation, (2) silk-vaccine formulations were added to plasma treated molds and infiltrated into mold cavities by centrifugation, (3) silk was dried in mold cavities forming hardened tips and left untreated or exposed to MeOH, (4) vaccine-loaded PAA was added to the mold and infiltrated into mold cavities by centrifugation, and (5) arrays were dried before removal.* ***(b)*** *Optical micrograph of silk/PAA microneedle array encapsulating AF647-OVA (blue) in silk tips, and AF555-OVA (red) in PAA pedestals (scale bar - 500μm).* ***(c)*** *Confocal micrographs of composite microneedles showing AF647-OVA (blue) in silk tips and AF555-OVA (red) in PAA pedestals (scale bar - 500μm).* ***(d)*** *SEM micrographs of a separated silk tip following 30 seconds exposure of a composite array to deionized water. Micrographs show intact tip structure (left, scale bar - 500μm) and micro-porous silk hydrogel structure (center, scale bar - 20μm, and right, scale bar - 5μm).* ***(e)*** *Quantitative analysis of fluorescent OVA release from silk and PAA fractions of composite microneedles over time.*

6.3.2. In Vitro Characterization of Silk Tip Release and Vaccine Cargo Delivery

To test our expectation that composite silk/PAA microneedles would rapidly release silk tips upon exposure to tissue fluids *in vivo*, we exposed microneedle arrays to deionized water *in vitro* for short periods of time to observe PAA dissolution and silk tip release. Here we visually

observed rapid and complete separation of silk tips from PAA composite microneedle arrays after only 30 seconds immersion. We then collected the separated silk tips by centrifugation and imaged them using SEM to observe their structure. Collected tips maintained their pyramidal geometry with dimensions consistent with the molds used in their fabrication (**Figure 6-1d**). Further high magnification SEM imaging of released tips revealed a nano-porous network structure consistent with bundling of silk proteins to form a cross-linked hydrogel structure (**Figure 6-1d**).

To confirm the ability of composite silk/PAA microneedles to provide control over vaccine release profiles, we fabricated microneedle arrays containing AF647-OVA loaded in the silk needle tips or AF555-OVA in the PAA pedestals. Silk tips were either left untreated or treated with methanol as before to introduce additional cross-linking into the silk hydrogels. We then immersed each array in phosphate buffered saline pH 7.4 (PBS) at 37°C and collected fractions of the solution at subsequent time points to measure the release of encapsulated AF555-OVA and AF647-OVA by fluorescence spectroscopy. Consistent with expectations, AF555-OVA loaded into the PAA pedestal was rapidly dispensed from dissolving PAA pedestals, with complete release over the course of only 2 hours (**Figure 6-1e**). Conversely, AF555-OVA loaded into silk hydrogel tips was released more slowly with kinetics further modulated by methanol exposure during fabrication. For microneedles bearing untreated silk tips, AF647-OVA exhibited a burst release of ~70% over the course of 2 hours with sustained release of the remaining 30% over the next 5-6 days (**Figure 6-1e**). Delivery from methanol-treated silk was further delayed with only 25% burst release over 2 hours, and sustained near-linear release of the remaining 75% over the course of 8-12 days (**Figure 6-1e**). Thus, the combination of rapidly dissolving PAA or slow swelling of silk hydrogels permits the kinetics of vaccine release to be varied over a wide range spanning hours to more than a week.

6.3.3. *Composite Microneedles Rapidly Implant Silk Tips to Form Cutaneous Vaccine Depots In Vivo*

We previously demonstrated that composite PLGA/PAA microneedles penetrate murine skin, and prior work has also shown the ability of solid silk microneedles to effectively insert into murine skin.[172] To confirm the ability of composite silk/PAA microneedles to effectively penetrate skin, we fabricated silk/PAA microneedles encapsulating AF647-OVA and AF555-OVA in the silk and PAA microneedle phases, respectively, and applied these arrays to the skin of C57Bl/6 mice for 5 minutes. Confocal imaging of microneedle arrays before and after application revealed complete loss of both silk- and PAA-associated OVA fluorescent signal from the length of each microneedle following 5 min insertion in skin (**Figure 6-2a**). Confocal imaging on excised skin or skin histological sections where patches were applied revealed overlaid punctate fluorescent signal from AF647-OVA and AF555-OVA at individual sites of microneedle insertion indicating the effective delivery of both silk- and PAA-loaded materials upon microneedle penetration into the cutaneous space (**Figure 6-2b-c**). In these images microneedles were observed to insert several hundred microns below the skin surface in the epidermal space, consistent with previous demonstrations of microneedle delivery.[192,199,200]

Three-dimensional rendering of confocal z-stacks to visualize the depth of fluorescent OVA delivery showed fluorescent signals from AF647- and AF555-OVA from silk and PAA respectively, extending several hundred microns below the skin surface at sites of microneedle insertion (**Supplementary Figure S6-1**). Together these results confirm the ability of silk/PAA microneedles to effectively insert into murine skin, with rapid dissolution of the PAA pedestal upon exposure to skin fluids to leave behind vaccine-loaded silk hydrogels.

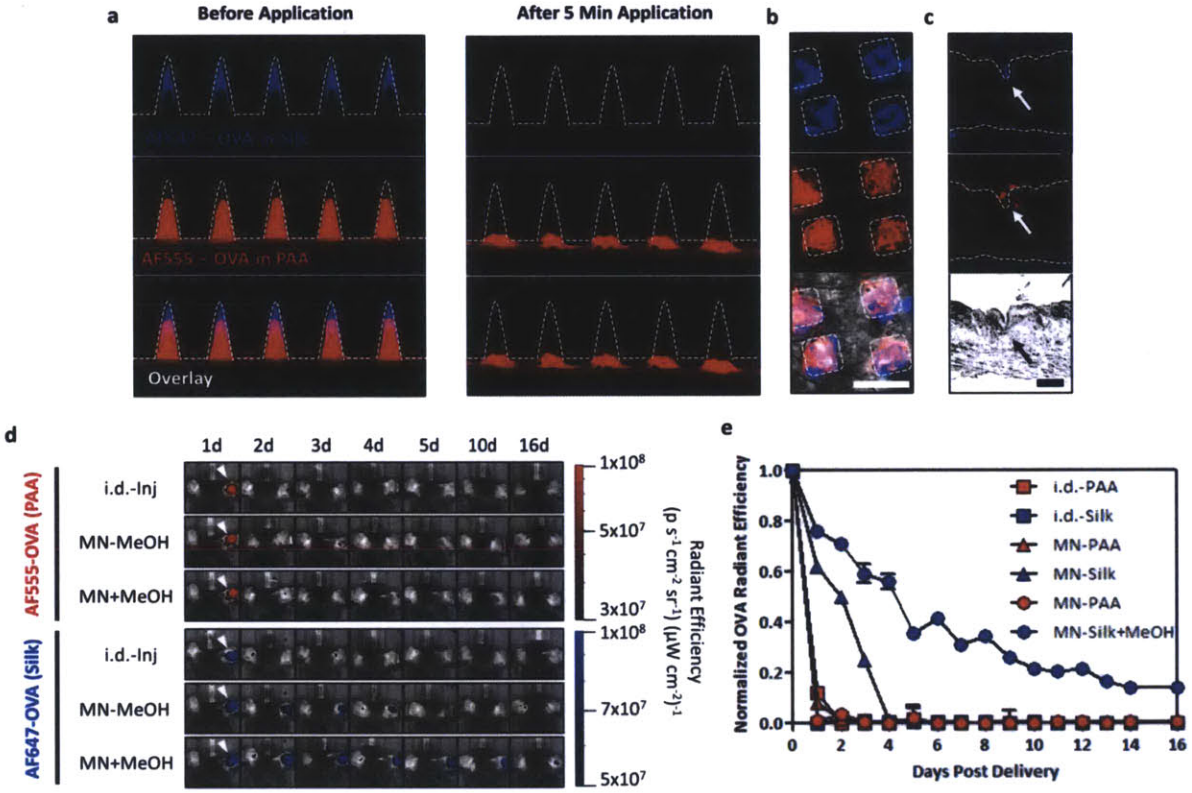

Figure 6-2. Composite microneedles deliver loaded vaccines to murine skin *in vivo*.

(a) *Confocal micrographs of composite microneedles showing AF647-OVA (blue) in silk tips and AF555-OVA (red) in PAA pedestals (scale bar - 500μm) before application (left) and following a 5 minutes application to murine auricular skin (right).* ***(b)*** *Confocal micrographs showing OVA delivery to murine skin following 5 minutes application of composite microneedles (AF647-OVA in silk tips – blue, andAF555-OVA in PAA pedestals – red, scale bar - 500μm).* ***(c)*** *Confocal micrograph of histologically sectioned skin treated for 5 minutes with composite microneedles (AF647-OVA in silk tips – blue, and AF555-OVA in PAA pedestals – red, scale bar - 100μm).* ***(d)*** *Whole animal fluorescent images of mice treated (arrows, right ear) with composite microneedles containing AF647-OVA (blue) in silk tips (±methanol treatment) and AF555-OVA (red) in PAA pedestals.* ***(e)*** *Quantitative analysis of total fluorescent OVA signal measured at the treatment site for mice receiving i.d. injection or microneedle delivery of AF647-OVA in silk tips (±methanol treatment) and AF555-OVA in PAA pedestals.*

6.3.4. *Cutaneous Silk Implants Control Vaccine Release Kinetics In Vivo*

We next tested whether microneedle-delivered vaccine release *in vivo* could be programmed during array fabrication. Similar to previous experiments, we fabricated microneedles containing AF647-OVA and AF555-OVA in the silk or PAA needle fraction respectively, and applied these to the auricular skin of anesthetized C57Bl/6 mice. For comparison to parenteral administration, we performed intradermal (i.d.) injection of dose-matched soluble fluorescent vaccine formulations in the dorsal ear skin. We then used whole-animal fluorescence imaging to monitor the persistence of the OVA fluorescent signal at the treatment site and determine the release characteristics of injected or microneedle-delivered vaccine *in vivo*. Fluorescence imaging revealed the rapid loss of AF555-OVA signal in all test groups indicating the clearance of soluble OVA from the treatment site within 24 hours of delivery either by i.d. injection, or from the PAA phase of composite microneedles (**Figure 6-2d-e**). Clearance of AF647-OVA was similarly rapid in the case of i.d. injection. Conversely, AF647-OVA encapsulated in silk-implants was retained at the treatment site for days to weeks following microneedle treatment, depending on whether methanol treatment was performed during fabrication to induce additional silk hydrogel cross-linking (**Figure 6-2d-e**). Animals treated with silk/PAA microneedles without methanol cross-linking showed nearly linear clearance of silk-loaded AF647-OVA over the course of 4 days following treatment. In the case of microneedles pretreated with methanol, AF647-OVA fluorescent signal was detectable at the treatment site for >16 days following array application (**Figure 6-2d-e**). Notably, these *in vivo* antigen release profiles showed roughly the same total duration for complete release as measured *in vitro,* but showed little or no burst release as observed *in vitro*. These results indicate the ability of microneedle-delivered silk tip implants to control the rate of vaccine release *in vivo* with a kinetic profile dependent on methanol treatment during fabrication.

6.3.5. *Microneedle Vaccine Release Kinetics Determine the Strength of Cellular Immunity*

Many natural infections are characterized by an initially abundant microbe burden lasting a few days, which is predominantly eliminated by the initial immune response. However in many "acute" infections, this initial clearance of microbes is followed by a delayed clearance of residual low levels of the pathogen that persist for a more prolonged period prior to complete eradication.[201-205] Thus the natural immune system is frequently exposed to a large pathogenic bolus of antigenic and inflammatory stimuli, followed by a prolonged low level exposure which can persist for days to months following acute infection. Given that such kinetic patterns in natural infection are often associated with profound T-cell responses and robust immune memory, we sought to determine whether tailoring vaccine exposure kinetics using silk/PAA microneedles to mimic this natural progression of infection would impact vaccine immunogenicity relative to bolus injection or bolus microneedle delivery. We vaccinated mice with 9 μg OVA and 150 ng polyI:C either by i.d. injection at the dorsal ear site (i.d. Inj.) or by microneedle administration as before. Microneedles were fabricated with the vaccine dose split (98% and 2%) between the PAA and silk fractions with or without methanol pretreatment (MN

PAA(98)/Silk(2) and MN PAA(98)/MeOH-Silk(2)); control microneedles were fabricated with either 98% of the vaccine dose in the PAA fraction (MN PAA(98)/Silk(0)) or 2% of the dose in the silk fraction (MN PAA(0)/Silk(2)). To monitor cellular immunity we measured OVA-specific $CD8^+$ T-cell proliferation in peripheral blood using SIINFEKL/H-$2K^b$ peptide-MHC tetramers (SIINFEKL is the immunodominant peptide epitope of OVA). This analysis revealed that i.d. injected vaccines elicited extremely weak antigen-specific $CD8^+$ T-cell responses, with minimal expansion of OVA-specific cells over 4 weeks following a single immunization (~1% of $CD8^+$ T cells, **Figure 6-3a-c**). Microneedles carrying a fraction of the vaccine dose solely in the PAA or solely in the silk phase induced stronger $CD8^+$ T-cell proliferation, reaching a few percent $tetramer^+$ $CD8^+$ T-cells by 14 days following immunization (**Figure 6-3b, c**). Interestingly, for the two microneedle groups containing a small fraction of the vaccine dose in the silk tips and the bulk of the vaccine in the PAA phase, the T-cell response was stronger than each of the prior groups (**Figure 6-3a-c**). Strikingly, methanol-crosslinked silk tip implants that provided a sustained low dose of the vaccine over 2 weeks after the initial bolus PAA release resulted in dramatic increases in the frequency of tet^+ $CD8^+$ T-cells compared to the other vaccination regimens (**Figure 6-3a-c**). Two weeks following microneedle patch application, SIINFEKL-specific $CD8^+$ T-cells expanded to 10-20% of all $CD8^+$ T cells in this group. To test the functionality of these expanded T-cells, we restimulated peripheral blood mononuclear cells (PBMCs) on day 14 *ex vivo* with SIINFEKL and assessed production of the inflammatory cytokines IFN-γ and TNF-α using intracellular staining. Flow cytometric analysis revealed high frequencies of antigen-specific functional cytokine-secreting $CD8^+$ T cells in the case of microneedle vaccination, while i.d. injection treated animals showed only background levels of activation, as expected from the previous tetramer-staining analysis (**Figure 6-3d-e**). Sustained low-level vaccine exposure from methanol cross-linked silk tip implants resulted in significantly higher frequencies of IFN-γ^+ and IFN-γ^+ TNF-α^+ multi-functional T-cells compared to the other vaccine groups (**Figure 6-3d-e and Supplementary Figure S6-2**). Notably, the single silk/PAA composite microneedle treatment was able to induce $CD8^+$ T cell responses of similar magnitude and cytokine secretion capacity as those observed after a prime + boost regimen administered by i.d. injection (**Supplementary Figure S6-3**). These significant increases in the magnitude of cellular immune responses suggest that both microneedle delivery and prolonged antigen/adjuvant delivery kinetics can substantially enhance the strength of the adaptive cellular immune response in transcutaneous vaccination.

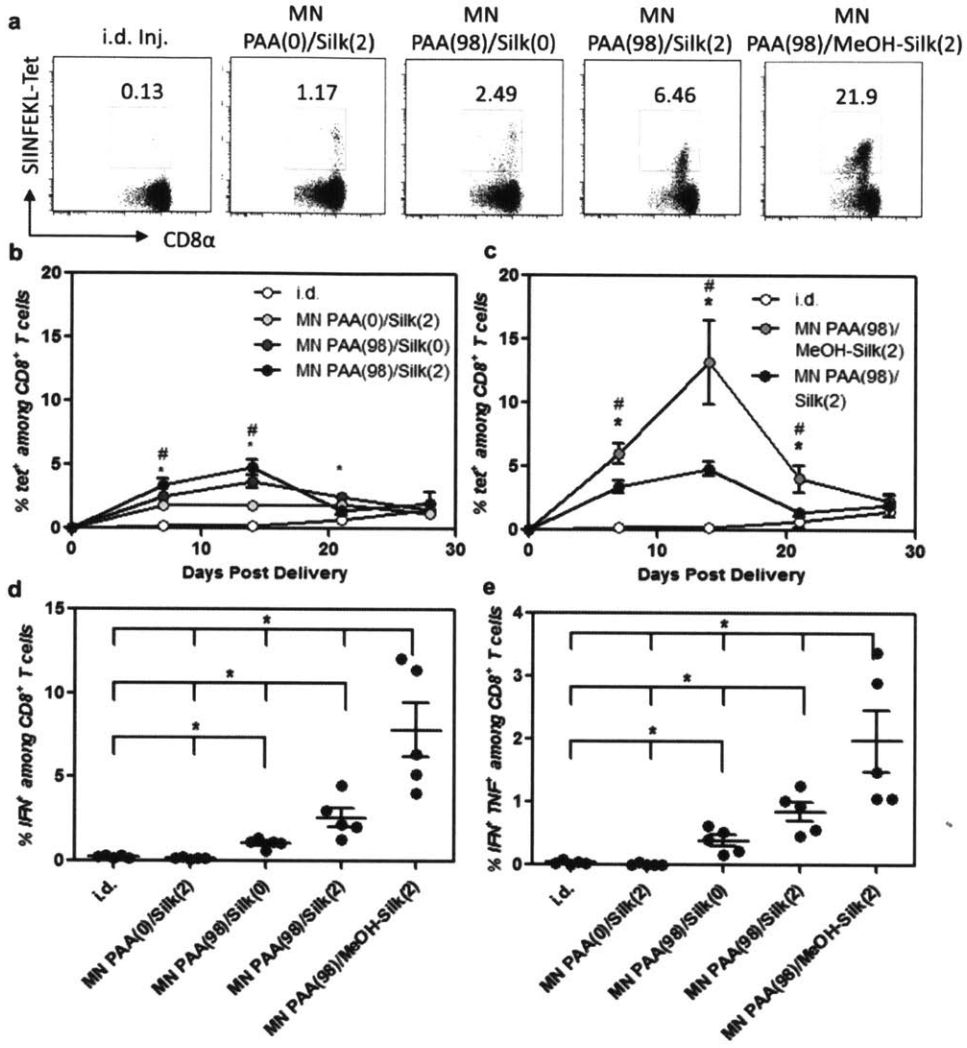

Figure 6-3. Prolonged vaccine release profile elicits increased proliferation of antigen-specific CD8$^+$ T cells.

Mice were vaccinated on day 0 either by i.d. injection, or microneedle treatment (±methanol to cross-link silk implants) to deliver 9 μg OVA and 150 ng polyI:C. Microneedles were fabricated with 98% of the total vaccine dose in the PAA fraction, with the remaining 2% in the silk implant (MN PAA(98)/Silk(2) and MN PAA(98)/MeOH-Silk(2)); control microneedles were fabricated with either 98% of the total vaccine dose in the PAA (MN PAA(98)/Silk(0)) or 2% of the total dose in the silk fraction (MN PAA(0)/Silk(2)). ***(a-c)*** *Flow cytometry analysis of antigen-specific CD8$^+$ T cell proliferation in peripheral blood. Shown is* ***(a)*** *representative cytometry plots from day 14, and* ***(b-c)*** *quantitative analysis of SIINFEKL-tetramer$^+$ CD8$^+$ T cell frequencies for 4 weeks following vaccination. (b, * $p<0.05$ for MN PAA(98)/Silk(0) versus MN PAA(0)/Silk(2), # $p<0.05$ for MN PAA(98)/Silk(0) and MN PAA(0)/Silk(2) versus i.d., c, * $p<0.05$ for MN PAA(98)/MeOH-Silk(2) versus MN PAA(98)/MeOH-Silk(2), # $p<0.05$ for MN PAA(98)/MeOH-*

Silk(2) and MN PAA(98)/Silk(2) versus i.d.). ***(d-e)*** *Flow cytometry analysis of inflammatory cytokine expression following ex vivo antigen stimulation. Shown is quantitative analysis of* $IFN\gamma^+$ *and* $IFN\gamma^+/TNF\alpha^+$ $CD8^+$ *T cells measured on day 14. (* $p<0.05$)*

Sustained antigen stimulus has been implicated in controlling memory cell phenotype and function.[190,191] Thus, we next compared the memory phenotype of $CD8^+$ T cells elicited by single silk/PAA microneedle treatment to prime-boost vaccination administered by i.d. injection, and observed a significant increase in the frequency of $CD44^+$ $CD62L^+$ central memory $CD8^+$ T cells on day 63 following microneedle vaccination compared to injection (**Figure 6-4a-b**). Central memory T cells have previously been correlated with effective immunological responses through more rapid recall upon re-exposure to pathogen, and are thought to be important for long term protection.[188] We also characterized the expression patterns of KLRG1, a marker which indicates effector T cell memory status upon long term exposure to pathogen or antigen. Cytometric analysis on day 70 showed that animals treated with a single microneedle vaccination generated similar frequencies of $KLRG1^+$ $CD8^+$ T cells in peripheral blood relative to mice given prime and boost vaccine injections (**Supplementary Figure S6-4**). Finally, we measured the strength of $CD8^+$ T cell expansion upon recall *in vivo* with injected OVA-expressing plasmid DNA (pOVA). Here we observed statistically identical expansion of SIINKEFL reactive, cytokine-secreting $CD8^+$ T cells 14 days following i.m. injection of pOVA in mice vaccinated with prime-only silk/PAA microneedles or prime-boost i.d. injection, suggesting that a single immunization by silk/PAA microneedle delivery can provide similar recall immunity compared to a prime-boost parenteral vaccine (**Figure 6-4c-e**).

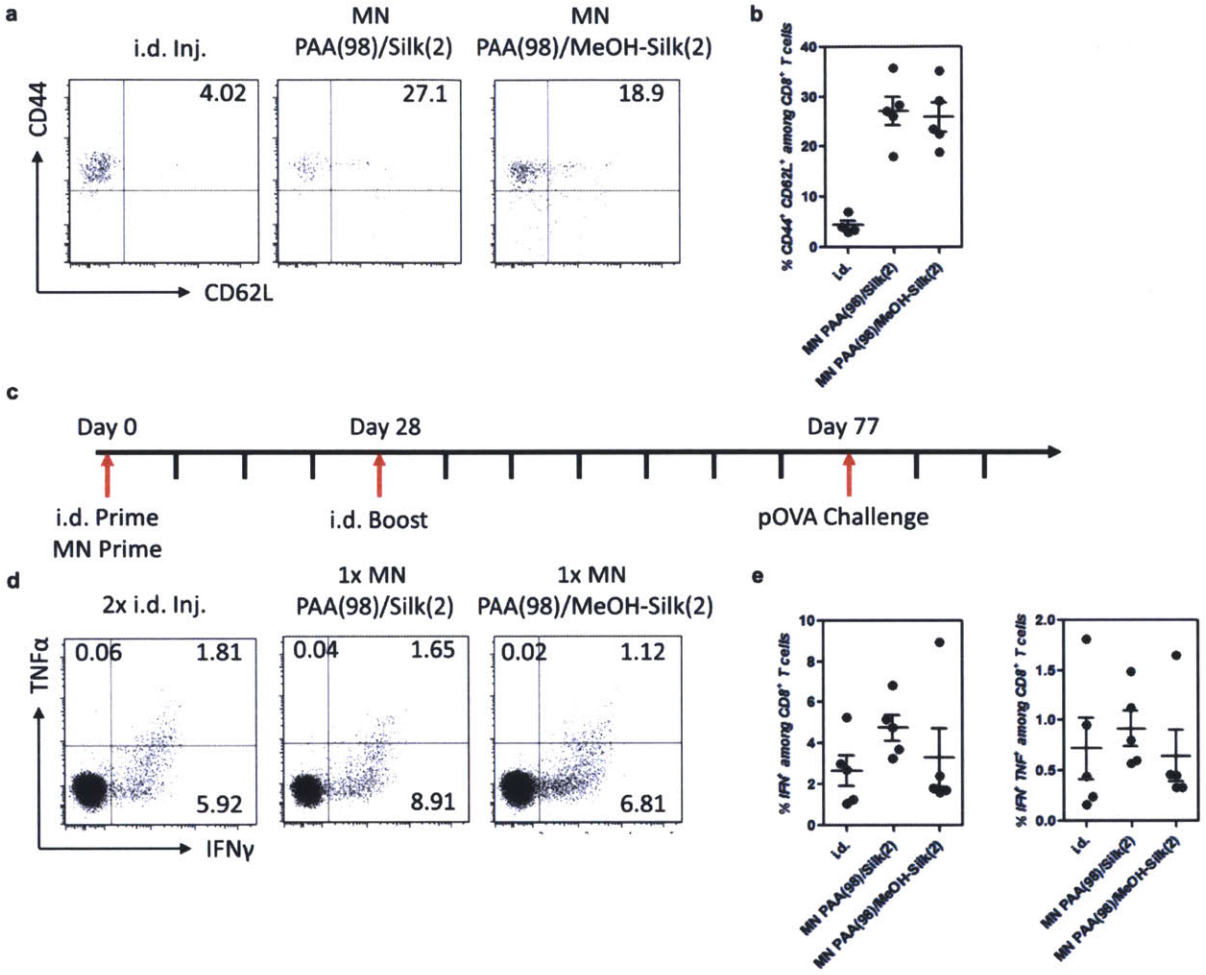

Figure 6-4. Microneedle vaccination gives enhanced memory CD8$^+$ T cell phenotype effector function.

Mice were vaccinated on day 0 either by i.d. injection, or microneedle treatment (±methanol to cross-link silk implants) to deliver 9 μg OVA and 150 ng polyI:C. Microneedles were fabricated with 98% of the total vaccine dose in the PAA fraction, with the remaining 2% in the silk implant (MN PAA(98)/Silk(2) and MN PAA(98)/MeOH-Silk(2)); control microneedles were fabricated with either 98% of the total vaccine dose in the PAA (MN PAA(98)/Silk(0)) or 2% of the total dose in the silk fraction (MN PAA(0)/Silk(2)). ***(a-b)*** *Flow cytometry analysis of antigen-specific CD8$^+$ T cell memory phenotype in peripheral blood. Shown are* ***(a)*** *representative cytometry and* ***(b)*** *quantitative analysis of CD44 and CD62L on SIINFEKL-tetramer$^+$ CD8$^+$ T cells for day 63 following vaccination.* ***(c)*** *Single microneedle vaccination gives equivalent recall immunity relative to prime-boost injection. Mice were then recalled by i.m. injection of 20μg pOVA on day 77.* ***(d-e)*** *Flow cytometry analysis of inflammatory cytokine expression following ex vivo antigen stimulation of PBMCs. Shown are* ***(d)*** *representative cytometry plots and* ***(e)***

quantitative analysis of IFNγ$^+$ and IFNγ$^+$/TNFα$^+$ CD8$^+$ T cells measured on day 91 (day 14 post recall).

6.3.6. *Microneedle Vaccination Gives More Potent and Balanced Humoral Immunity*

To evaluate the antibody response elicited by composite silk/PAA microneedles vaccines, we collected sera from immunized mice on day 21 following a single i.d. injection of vaccine, MN PAA(98)/Silk(2) vaccination, MN PAA(98)/MeOH-Silk(2), or MN PAA(98)/Silk(0) vaccination. ELISA measurements of serum titers of OVA-specific IgM, IgG, IgG_1, and IgG_{2C} showed a consistent increase in the serum titers of class-switched OVA-specific antibodies for microneedle-immunized animals. Microneedle vaccines induced significant increases in serum titers for anti-OVA IgG, IgG_1, and IgG_{2C}, while no difference was observed for IgM (**Figure 6-5a-d**). The effect on "Th1-like" IgG_{2C} antibody responses was particularly striking, as i.d. injection elicited no OVA-specific IgG_{2C} response, while both microneedle groups elicited readily detectable IgG_{2C} titers. These results suggest that microneedle delivery was able to elicit a more potent, Th1/Th2 balanced antibody repertoire compared to i.d. injection. Further, we analyzed avidity of the elicited IgG responses using urea exposure before ELISA detection to strip away weakly binding immunoglobulins.[198] This analysis demonstrated significantly improved IgG avidity for mice receiving microneedle vaccines as compared to i.d. injected vaccines, with uncross-linked silk microneedles eliciting the greatest increase in avidity (**Figure 6-5e**). Finally, to further confirm the low immunogenicity of silk protein used in these studies we measured the presence of silk-specific serum IgG by ELISA. In mice given i.d. injection or microneedle vaccines, no significant increase in anti-silk IgG was detected following vaccination relative to naïve levels (**Supplementary Figure S6-5**). Together, these results indicate that microneedle vaccines strongly augment the humoral response relative to traditional syringe injections whether vaccine is given by bolus or release kinetics are prolonged for a few days or a few weeks.

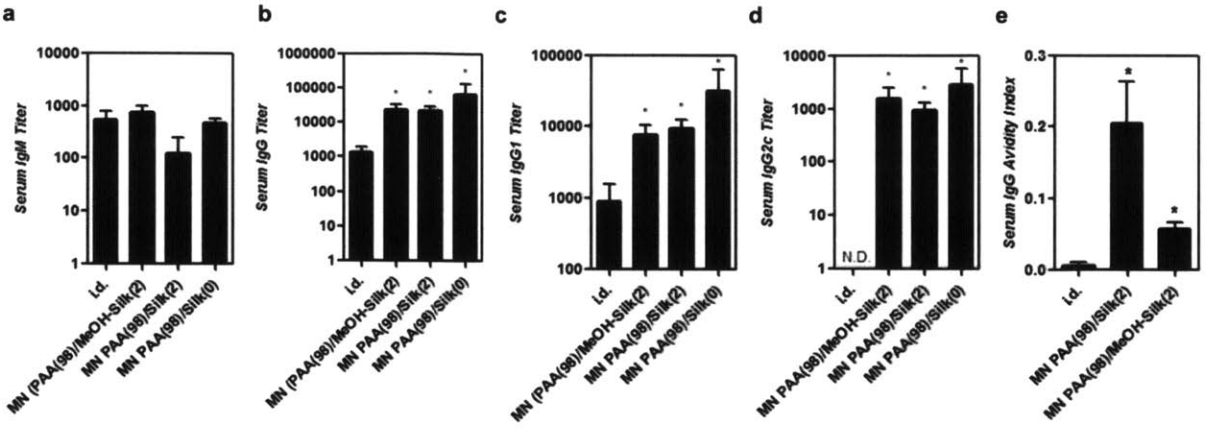

Figure 6-5. Delivery route determines the strength and isotype balance of humoral responses following parenteral i.d. or microneedle vaccination.

Shown are serum OVA-specific antibody titers and avidity indices measured on day 21. Serum OVA-specific antibody titers are shown for ***(a)*** *IgM,* ***(b)*** *IgG,* ***(c)*** *IgG_1, and* ***(d)*** *IgG_{2C}.* ***(e)*** *Avidity index for serum IgG , calculated as the ratio of titer measured without urea pretreatment of bound serum to titer with urea pretreatment. (*$p<0.05$ compared to i.d.)*

6.3.7. *Cutaneous Silk Implants Give Sustained Local Inflammatory Activation In Vivo*

Having shown the ability of composite silk/PAA microneedles to achieve prolonged vaccine release, we next sought to determine whether persistent local inflammation in the case of MN PAA(98)/MeOH-Silk(2) immunizations might be contributing to the enhanced cellular immunity observed for these microneedle vaccines. To this end, we used whole-animal luminescent imaging with the chemiluminescent probe luminol to longitudinally measure myeloperoxidase (MPO)-dependent oxidative flux in locally-recruited inflammatory cells as an indication of inflammatory activation at the treatment site.[109,206] This approach has previously been used to observe recruitment of activated immune cells such as neutrophils and serves as a general marker for local innate inflammatory responses. Groups of mice were immunized by i.d. injection of OVA mixed with polyI:C as before, or treated with microneedles loaded with OVA and the TLR-3 agonist polyI:C in both the silk (±MeOH) and PAA fractions. Luminescent imaging indicated that i.d. injection produced only low-level inflammation at the treatment site which resolved completely after 4 days (**Figure 6-6a-b**). Conversely, microneedle delivery with either untreated or methanol-treated silk/PAA microneedles showed a significant burst of inflammation for 3 days following treatment. After 4 days mice vaccinated with untreated silk showed only background levels of MPO-dependent chemiluminescence, while methanol treated silk microneedles gave significant luminescent signal above background on days 4, 5, and 11, suggesting persistent low level inflammatory activation in these mice, likely resulting from prolonged release of antigen/adjuvant from silk implants. However, no visible signs of excessive inflammation or tissue damage were observed in any of the mice in these treatment groups.

Further, i.d. injection of 5x excess silk doses produced signal similar to i.d. injection alone, confirming the non-inflammatory nature of purified silk proteins *in vivo* (data not shown, reviewed in [193]). Together with the previous *in vivo* OVA delivery results, this indicates the ability of silk/PAA microneedles to sustain both antigen exposure and inflammatory cues from days to weeks following treatment *in vivo*. This sustained low level of inflammation combined with continuous antigen delivery is likely a key factor in eliciting the potent $CD8^+$ T cell proliferation for microneedle vaccination, specifically cases where methanol cross-linked silk maintains release over several weeks.

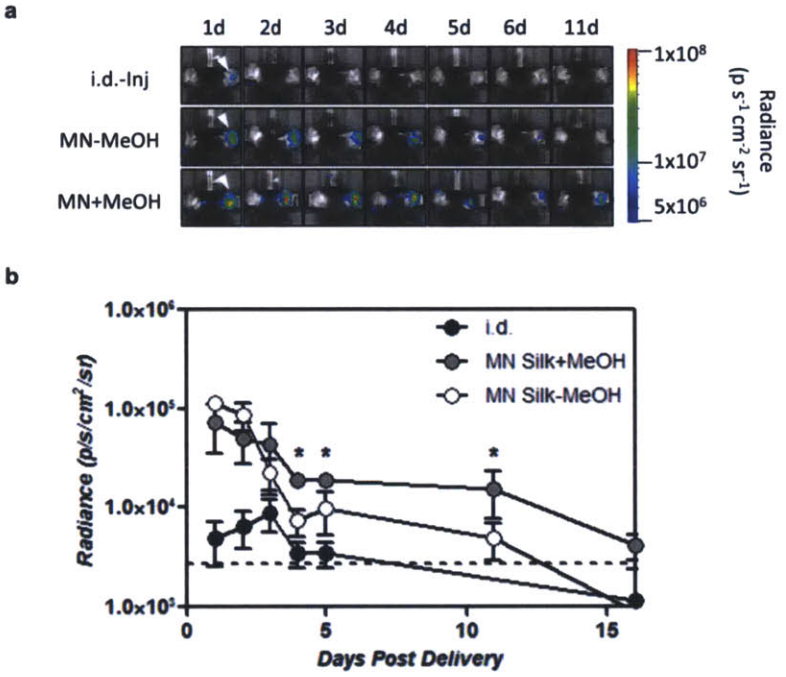

Figure 6-6. Composite microneedles prolong local inflammation.

(a) *Whole animal chemiluminescent images of mice treated (arrows, right ear) with composite microneedles containing OVA and polyI:C in silk tips (±methanol treatment) and PAA pedestals. Mice were imaged following luminol administration to visualize MPO-dependent oxidative flux in activated immune cells.* ***(b)*** *Quantitative analysis of total luminescent signal measured at the treatment site for mice receiving i.d. injection or microneedle delivery of OVA and polyI:C in silk tips (±methanol treatment) and PAA pedestals. (* $p<0.05$ compared to baseline)*

6.4. Conclusions

The development of materials strategies for microneedle fabrication has yielded impressive progress in the advancement of effective, safe, and convenient delivery of macromolecules for vaccination in the skin.[199,207,208] These efforts have sought to effectively balance the many critical features essential for the effective clinical deployment of microneedle patch delivery systems including *(i)* suitable mechanical properties, *(ii)* control over micron-scale needle

geometry and dimension, *(iii)* the ability to achieve rapid administration, *(iv)* effective encapsulation of sensitive biomolecules, and *(v)* avoidance of unwanted toxicity (reviewed in [209]). Here we have demonstrated the combination of these critical design parameters in the fabrication of silk/PAA composite microneedle arrays. These structured skin patches readily penetrate murine skin *in vivo*, provide rapid deposition of vaccine into the skin over several minutes, are able to encapsulate fragile protein or nucleic acid vaccine components in densely-loaded polymer matrices, and exhibited no toxicity *in vivo*. Further, composite silk/PAA microneedles provide enhanced flexibility in programming vaccine dosage and long-term delivery kinetics while retaining the ability to provide rapid and simple administration, a feature which we have shown to be critical for tuning the potency of immunity.

Previous studies of silk have shown effective loading of sensitive biomolecules including vaccines for storage at room temperature.[193,196,197,210] This is an attractive feature which could allow for inexpensive and broader global dissemination of vaccines to remote areas of the world. Here we confirmed the potential for silk to stabilize subunit vaccines during room temperature storage, as all silk/PAA microneedles used in these studies were stored at room temperature for >2 months prior to use. Further, as observed previously, our choice of PAA as a water soluble component in the encapsulation of vaccine during fabrication of silk/PAA microneedles allowed for similar room temperature storage without loss of *in vivo* immunogenicity.[192] Prior studies of silk microneedles have demonstrated effective methods for fabrication as well as consistent insertion into murine skin.[172,195] We have expanded upon these results here to demonstrate a new approach for silk microneedle fabrication to take advantage of the controlled release capacity for silk hydrogels while also improving the practicality and speed of microneedle application. These advances allowed us to perform comprehensive tests of silk microneedle immunogenicity *in vivo*, and to demonstrate the utility of silk as a material for effective loading, storage, and delivery of vaccines. Recently, a similar approach for controlling vaccine release from microneedles has been described for the dermal implantation of chitosan reservoirs from PLA pedestals.[211] These embeddable chitosan microneedles showed control over week-long protein release resulting in enhanced humoral immune responses indicating the potential of this approach for tuning immunity. Here we have demonstrated that the flexibility of silk fibroin to form tunable matrices with programmable release of antigen and adjuvant over days to weeks can provide additional control over elicited cellular and humoral immunity.

It is well established that microneedle delivery of vaccines to the skin can enhance immunity through targeted delivery of antigen and adjuvant to response-governing antigen presenting cells present at high density within the skin. The physical disruption of the epidermal/dermal tissues during microneedle delivery is thought to be an important factor in mediating this enhanced immunity through the recruitment and maturation of antigen presenting cells.[200,212] Further, vaccine delivery in the context of epidermal wounding resulting from microneedle treatment may contribute to a pro-inflammatory microenvironment during cutaneous vaccination as keratinocytes and other skin-resident cells are known to actively sense and respond to tissue damage as well as pathogen-associate molecular patterns such as TLR-agonists.[213] Thus the

success of microneedle delivery is likely in part founded in the natural mechanisms of the skin as a barrier to entry for sensing and responding to natural infections.

Here we have shown that microneedle vaccination can be further enhanced through the adoption of a similar approach for replicating the natural time course of many diseases in which acute infection provides initially high levels of antigen and adjuvant stimuli which then rapidly decrease through immunological mechanisms of pathogen clearance, leading to long-term low levels of persistent pathogenic stimulus.[201-205] In previous studies the presence of protein antigen or pathogen-derived genetic material has been observed for weeks to months in the local site of infection and in draining lymph nodes persisting after the relatively rapid clearance of infectious agent over the course of several days.[201,202,214,215] This pattern of sustained antigen exposure following primary clearance of infection has suggested a potential role for continued antigen/adjuvant stimulation in the development of primary effector and memory T cell responses, including effects on T cell migration/homing,[203] establishment of T cell memory phenotypes,[216] and maintenance of effective long-lived protective T cell responses.[217] Conversely, in some cases, chronic antigen presentation can lead to dysfunctional memory T cell responses including loss of effector or proliferative functions or poor long-term survival.[218] This dichotomous development of either enhanced or defective long-term protective response is thought to be determined in part by the relative magnitude of sustained antigen exposure with chronic high antigen load frequently leading to exhausted or anergic phenotypes, while low level exposure commonly results in maintenance of protective functions. Thus the ability to finely tune the level and persistence of antigenic or inflammatory cues following microneedle vaccination is likely critical for eliciting the desired effect on immunogenicity.

The silk/PAA composite microneedle system we have developed allows for vaccine delivery that can be tuned to replicate the timing and dosage features of natural infection through the combination of bolus vaccine release from rapidly soluble PAA, and extended release from vaccine-loaded silk depots implanted in the skin upon microneedle application. In our studies this ability to provide bolus vaccine exposure combined with additional multi-week low-level delivery was able to drastically improve the proliferative capacity of antigen-specific T cells, yielding increased levels of peripheral antigen-specific, functionally active effector $CD8^+$ T cells greatly exceeding those responses generated through injection. These results indicate the need for both bolus vaccine delivery and sustained release as individual bolus or sustained release vaccine components gave much weaker responses. Further, the ability to program the duration of extended release proved critical as multi-week exposure resulted in 2.8-fold increases in $CD8^+$ T cell responses over shorter multi-day release profiles. Notably, we observed that $CD8^+$ T cell responses to injected vaccines were only able to match single microneedle immunizations following multiple vaccine doses, suggesting that the combination of microneedle delivery with programmed vaccine release may eliminate the need for costly and less effective prime-boost vaccine regimens.

Microneedle vaccines have traditionally exploited the naturally endowed immune-functionality of the skin as a primary barrier to pathogen entry, however further improvements to skin vaccination can be realized through the design of delivery approaches which similarly mimic the natural time course of pathogen invasion, recognition, and response. Here we have demonstrated the potency of this approach by designing a microneedle delivery approach capable of mimicking the extended kinetic profile for antigen and adjuvant exposure following natural infection. Composite silk/PAA microneedles were able to rapidly disintegrate after insertion into the skin releasing vaccine bolus from dissolving PAA pedestals while simultaneously forming persistent cutaneous silk implants to mediate the sustained low-level delivery of vaccine over time. The flexibility of this approach for high-density loading and controllable release of biologically-sensitive vaccine components allowed for programmable vaccine delivery in the skin to generate potent cellular and humoral immunity superior to prime vaccination by hypodermic injection. Notably, these responses were elicited following months of microneedle storage at room temperature and gave equivalent immunity to those following prime-boost injection regimens. This ability for potent immunity following a single immunization, combined with the potential for long term room temperature storage, and safe needle-free administration make this strategy an attractive option for effective global vaccine distribution, and deployment.

7. IMMUNOGENIC DELIVERY OF ADENOVIRAL VECTORS IN NONHUMAN PRIMATES FROM SKIN PATCHES ENABLING DRY, REFRIGERATION FREE VACCINE STORAGE

7.1. Introduction

Where Chapters 1-6 focused on the design and initial preclinical testing of novel microneedle vaccination and delivery approaches, Chapter 7 focuses on more comprehensive preclinical testing of a simple and robust microneedle strategy for delivery of a clinically advanced viral vector vaccine in a late-stage primate preclinical model of HIV. Preclinical rodent models are useful for the development of new vaccination strategies but cannot accurately predict success in human clinical trials. Therefore, the studies presented here are meant to provide meaningful preclinical evidence of the potential of microneedle vaccination for translation to human clinical use.

Transcutaneous drug delivery from planar adhesive skin patches (which adhere to but do not disrupt the stratum corneum) has been very successful for the delivery of hydrophobic small-molecule drugs (reviewed in [219]) and has been shown to be effective for delivery of skin-permeable vaccine adjuvants in humans.[220-222] However, delivery of proteins and other macromolecular components into the skin requires a means to bypass the barrier posed by the stratum corneum. To this end, new technologies for cutaneous needle-free vaccination based on topical patches containing arrays of micron-scale solid projections ('microneedles') that can penetrate the superficial layers of the skin have shown promise for safe and effective vaccine delivery.[223] On application to the skin, patch microprojections penetrate the stratum corneum and enter the viable epidermis, enabling vaccines coated on or encapsulated within the microneedles to be dispersed into the local tissue. This technology may facilitate a new paradigm for vaccination which *(i)* eliminates the risk of blood-borne pathogen transmission or needle-stick injury, *(ii)* streamlines vaccine administration for large-scale immunization campaigns by minimally trained personnel or even self-administration, and *(iii)* employs dry, solid-state vaccine formulations that may reduce cold chain requirements for cost-effective vaccine storage and dissemination, particularly in the developing world.[87,209] Recent studies have demonstrated the ability of microneedles to effectively deliver vaccines as dried coatings on the surface of each projection (which dissolve rapidly upon insertion into the skin) or encapsulated within microneedles which themselves dissolve in the skin, eliciting protective immunity in mouse models of influenza,[125,142,224] hepatitis C,[93] and West Nile virus.[149] However, this approach has not yet been tested for efficacy in non-human primates, an important large-animal model that is thought to be more predictive of human immune responses to many vaccines than small animal models.[225-227]

Given the anatomical and immunological differences between mice or other small animal models and primates or humans[228] and the common failure of small-animal models to predict vaccine success in humans,[229] we set out to test the safety and immunogenicity of a prototypical microneedle patch vaccine delivering a clinically-relevant vaccine vector in Rhesus macaques.

We chose for these studies to focus on recombinant replication-incompetent adenoviral vectors, which have emerged as a potent vaccine platform in non-human primate models of HIV-1 infection.[230-234] In previous studies, adenovirus serotype 5 (Ad5), as well as less common serotypes unlikely to trigger pre-existing vector immunity such as Ad26 and Ad35 have yielded impressive immunogenicity in clinical and preclinical trials.[235-238] To this end, biodegradable microneedle patches composed of the polymer poly(L-lactic acid) (PLA, used in resorbable sutures and approved drug delivery formulations, reviewed in [239]) were coated with Ad5 vectors encapsulated in a sucrose sugar-glass matrix. Adenovirus-loaded microneedle patches (Ad-MN) allowed dry storage of Ad5 for several months at 25°C with no loss in bioactivity in mice. Similar to traditional syringe injections, Ad-MN delivery of adenovirus SIV vaccines elicited potent systemic cellular and humoral immunity in both mice and macaques, as well as strong immunity at mucosal sites typically serving as barriers to entry for SIV/HIV viral transmission. These results suggest that microneedle patch delivery can enable important practical benefits for vaccine deployment including solid-state stabilization of vaccine for enhanced long-term room temperature storage and needle-free administration while maintaining immunogenicity comparable to traditional needle-and-syringe liquid vaccines.

7.2. Materials and Methods

7.2.1. Adenovirus Vector Preparation

DNA for E1/E3-deleted adenovirus virus was transfected into Per55K cells as previously described.[240-242] After homologous recombination of linearized plasmids, recombinant virus particles were generated. Transfection lysate was plaque purified, screened for transgene expression, expanded, purified by Cesium-Chloride gradient centrifugation, and dialyzed in PBS containing 5% sucrose. Virus was stored at -80 °C until use.

7.2.2. PLA Microneedle Patch Fabrication

PDMS molds (Sylgard 184, Dow-Corning, Midland, MI) were prepared using a Clark-MXR-CPA-2010 laser micromachining instrument (VaxDesign Inc., Orlando, FL). PLA (IV 1.9 dL g^{-1}, Lakeshore Biomaterials) was melted over the molds under vacuum (-25 in. Hg, 200°C, 40 min), and then cooled to -20°C before removal.

7.2.3. Sucrose Microneedle Coating

Adenovirus stocks were thawed and suspended in 5% sucrose/0.01% Tween 20. Coating solution was pipetted onto the surface of 1 cm^2 PLA patches, dried under vacuum for 1 hour at 25°C, and stored at 25°C under desiccation until use. In some cases, AF555 (Invitrogen) was added to the coating solution to yield labeled coatings.

7.2.4. In Vivo Delivery

Mouse studies were approved by the MIT IUCAC and animals were cared for in the USDA-inspected MIT Animal Facility under federal, state, local, and NIH guidelines for animal care. For microneedle treatment, dorsal ear skin of anesthetized C57Bl/6 mice (Jackson Laboratories,

Bar Harbor, ME) was rinsed with PBS and dried before application of microneedle arrays by gentle pressure. Microneedles were imaged before and after application by optical microscopy (Leica DMXR). Delivery of AF555 into skin was measured using an IVIS Spectrum 200 (Caliper Lifesciences, Hopkinton, MA). Intradermal injections of control formulations were performed in the dorsal ear skin (15μl). For luminescent measurements of luciferase expression, mice were imaged following i.p. administration of D-luciferin (150mg kg^{-1}). Data was processed using region of interest (ROI) analysis (ROIs were set to include the entire ear site) with background subtraction and internal control ROI comparison to untreated skin using Living Image 4.0 software (Caliper).

7.2.5. Murine Vaccinations

Groups of 5 C57Bl/6 mice were immunized on day 0 with $1x10^8$ vp Ad5-SIV-gag by i.m. injection (100 μl, quadriceps), i.d. injection (15 μl, dorsal ear skin), or by microneedles (5 min application). Frequencies of gag-specific $CD8^+$ T-cells and their phenotypes were determined by flow cytometry analysis of PBMCs following staining with DAPI (live/dead), anti-CD8α, anti-CD44, anti-CD62L, and AL-11/H-$2K^b$-peptide-MHC tetramers. Similar analysis was performed on mononuclear cells isolated from spleen, vaginal tissue, lungs, and intestinal tissues collected following necropsy. Spleens and lungs were collected, meshed, and strained (70 μm) to obtain lymphocytes. Vaginal lymphocytes were isolated by digesting tissue in 100 MU/ml collagenase D (Roche, Branchburg, NJ) at 37°C for 30 min and straining (70 μm). To isolate intra-epithelial lymphocytes, small intestines were incubated with RPMI 1640 supplemented with 5 mM EDTA and 0.145 mg/ml dithiothreitol at 37°C; recovered lymphoyctes were isolated by spinning through a 67% Percoll layer. Cytokine expression in $CD8^+$ T-cells was measured by flow cytometry analysis of PBMCs following stimulation with AL11 peptide, treatment with brefeldin A, and staining with DAPI, anti-CD8α, anti-IFNγ, and anti-TNFα. Anti-gag IgG titers, defined as the dilution of sera or vaginal wash at which OD reading was 0.25, were determined by ELISA using SIV-mac251-coated plates (My Biosource, San Diego, CA) using HRP-conjugated anti-IgG (Jackson Immunoresearch, West Grove, PA).

7.2.6. Ex Vivo Macaque Skin Culture and Microneedle Testing

Macaque studies were approved by the Harvard Medical School IACUC. Outbred Rhesus monkeys were housed at the New England Primate Research Center (NEPRC). Fresh skin was obtained from the deltoid of euthanized Rhesus macaques, mounted on slides, and microneedles were applied by gentle pressure. To evaluate delivery of sucrose coatings, microneedles were coated with sucrose encapsulating green 100nm carboxylate-modified polystyrene nanoparticles (Invitrogen) in lieu of viral particles. Treated skin was stained using trypan blue, formaldehyde fixed, and embedded in paraffin or OCT compound for sectioning and hemotoxylin/eosin staining. Sections were imaged either using optical microscopy to detect microneedle insertion or confocal microscopy to observe fluorescent cargo delivery. To assay *ex vivo* transduction, $1x10^8$ Ad5-LUC vp were injected i.d. (15 μl) or delivered by microneedles (5 min application).

Skin was cultured as previously described[110] and imaged using an IVIS Spectrum after addition of 300 μg luciferin to the culture media.

7.2.7. *Rhesus Macaque Vaccinations*

All animals were housed at the NEPRC and maintained in accordance with the "Guide for the Care and Use of Laboratory Animals" of the Institute of Laboratory Animal Resources, NRC. The facility is AAALAC-accredited and all work was approved by Harvard Medical School's Standing Committee on Animals. Animals originated form the NEPRC specific-pathogen-free breeding colony but had been housed in conventional housing prior to this study. Prior to Ad-MN vaccination, animals were anesthetized with dexdomitor. Hair was removed from the upper arms and deltoid skin was washed with PBS-soaked gauze. Macaques were immunized on day 0 and day 84 with $4x10^9$ vp Ad5-SIV-gag and $7x10^9$ vp Ad5-SIV-env by microneedle array (5 min application, total dose split into 4 identical arrays per vector, applied on the left and right deltoid respectively). Microneedle patches were applied gently by hand and held in place manually for 5 minutes. Alternatively, a clamp device set to a similar clamping pressure as that obtained manually was used to secure the microneedles. Animals were allowed to recover from anesthesia and no side effects of the vaccination procedure were noted. For all procedures, macaques were sedated with ketamine (10-15 mg/kg IM, FortDodge) or telazol (5 mg/kg, FortDodge). Blood samples were obtained from the femoral vein using a 22 gauge needle attached to a vacutainer system. For colorectal biopsies, animals were sedated and biopsies of the rectal and distal colonic mucosa were obtained using a 1.9mm pinch biopsy forceps and placed into GIBCO RPMI media. Rectal mucosal secretions were collected using Weck-Cel sponges and extracted for assays as previously described.[230]

7.2.8. *Rhesus Macaque ELISPOT*

Gag- and Env-specific cellular immune responses in vaccinated animals were assessed by IFN-γ ELISPOT as described previously.[230,232] Overlapping 15-amino-acid peptide pools from both SIVmac239 Gag and Env were used to stimulate PBMCs. Following an 18-hr incubation at 37°C, plates were washed, incubated with 2 μg/ml biotinylated anti-human IFN-γ (BD Biosciences, San Diego, CA), washed again, and incubated with streptavidin-alkaline phosphatase (Southern Biotechnology Associates, Birmingham, AL). Plates were then developed with nitroblue tetrazolium-5-bromo-4-chloro-3-indolyl-phosphate chromogen (Pierce, Rockford, IL), stopped with water, dried, and analyzed (Cellular Technology Ltd., Cleveland, OH). Background levels were typically <15 SFC per 10^6 cells.

7.2.9. *Rhesus Macaque Intracellular Cytokine Staining*

The magnitude and phenotype of Gag-specific cellular immune responses in vaccinated rhesus monkeys were assessed by multi-parameter ICS assays as previously described.[230,232] PBMCs ($3x10^6$) were incubated for 6 h at 37°C with RPMI 1640 containing 10% FBS alone, the SIVmac239 Gag peptide pool (2 μg/ml), or 10 pg/ml phorbol myristate acetate and 1 μg/ml ionomycin (Sigma-Aldrich, St. Louis, MO). The cultures contained monensin (BD Biosciences,

San Diego, CA) and 1 μg/ml anti-CD49d (BD Biosciences). Cells were then stained with anti-CD3, anti-CD4, anti-CD8, anti-CD28, and anti-CD95, fixed, and permeabilized. Cells were then stained intra-cellularly with anti-IFN-γ, fixed, and analyzed with an LSR II (BD Biosciences) using FlowJo software (TreeStar, Ashland, OR). Approximately 500,000 to 1,000,000 events were collected per sample. Background levels were typically <0.02% of the levels of gated $CD8^+$ or $CD4^+$ T lymphocytes.

7.2.10. Rhesus Macaque ELISA

SIV Env-specific antibody titers in serum or rectal mucosal secretions from immunized monkeys were measured by ELISA as described previously.[230,232] Coated plates (100 μl/well of 1 μg/ml recombinant SIVmac251 gp120 - Immune Technology Corporation) were blocked before serum addition in serial dilutions. Plates were washed, incubated with peroxidase-conjugated, affinity-purified rabbit anti-human secondary antibody (Jackson Laboratories, Bar Harbor, ME), washed again, developed with tetramethylbenzidine (Kirkegaard & Perry Laboratories, Gaithersburg, MD), and analyzed with a Dynatech MR5000 ELISA plate reader.

7.2.11. Rhesus Macaque Neutralizing Antibody Assays

Serum neutralizing antibody responses were measured using a luciferase-based assay in TZM.bl cells as previously described.[243] A neutralization-sensitive SIVmac251 Env pseudovirus clone was utilized for these assays (SIVmac251.TCLA.15). Briefly, 3-fold serial dilutions of serum samples were performed in 10% D-MEM. Virus was added to each well and the plates were incubated for 1 hour at 37° C. TZM.bl cells were then added ($1x10^4$/well in 100 μl volume) in 10% D-MEM containing DEAE-Dextran (11 μg/ml, Sigma, St. Louis, MO). Assay controls included TZM.bl cells alone and TZM.bl cells with virus. Following 48 hr at 37° C, Bright-Glo luciferase reagent (Promega, Madison, WI) was added. Cells were allowed to lyse and cell lysate was measured using a Victor 3 luminometer (Perkin Elmer). The 50% inhibitory dose (ID_{50}) titer was calculated as the serum dilution that caused a 50% reduction in relative luminescence units (RLU) compared to the virus control wells after subtraction of cell control RLUs.

7.2.12. Statistical Analysis

Statistical analysis was performed with Graphpad Prism (La Jolla, California) using two-way analysis of variance or t-test. Values are reported as mean ± s.e.m.

7.3. Results and Discussion

7.3.1. Fabrication of Sucrose-coated Polymer Microneedles and Adenovirus Delivery in Murine Skin

Polymer microneedles composed of PLA and its copolymers with glycolic acid are known to have suitable mechanical properties for effective skin penetration,[50,115,200] and in previous chapters we have reported an approach for fabricating PLA microneedle patches through melt-molding of PLA polymer on PDMS molds under vacuum.[115,199] Using this process we fabricated skin patches 1 cm^2 in diam. bearing 78 conical PLA microprojections each 650 μm in height and

250 μm in diameter at the base. Prior work has suggested that solid state encapsulation of bioactive materials can provide improved stability against degradation at elevated temperature, and sugars such as sucrose and trehalose have been used successfully to form dried coatings on microneedle patches for skin delivery.[22,48,49,244-246] Based on these prior findings, adenovirus was coated by applying a 5% aqueous sucrose solution containing Ad5 vectors ($2.5x10^9 - 2.5x10^{11}$ vp/mL) and 0.01% Tween-20 surfactant to individual patches to cover the microneedles, and patches were dried at 25°C under vacuum (**Figure 7-1a**). This simple process yielded microneedles coated with a uniform conformal sugar-glass layer on the surface of each microprojection that retained the sharp tips of the original polymer array (**Figure 7-1b**). To confirm the ability of sucrose-coated microneedles to effectively deliver encapsulated cargos in the skin, we incorporated a fluorescent tracer (Alexafluor 555, AF555) into sucrose coatings and applied coated microneedles to the dorsal ear skin of C57Bl/6 mice. Imaging of coated microneedles before and after *in vivo* application showed significant loss of the sucrose coatings and loaded AF555 after a 5 min treatment, and also indicated some blunting or breaking of microneedle tips upon treatment (**Figure 7-1b**), however any PLA fragments remaining in the skin will harmlessly dissolve over time. Quantification of AF555 remaining on microneedles following treatment showed that ~25% or 60% of encapsulated AF555 was released following a 30 second or 5 min application to skin, respectively (data not shown). The same fraction of delivered dose was calculated from direct measurements of AF555 fluorescence in the treated skin measured by whole-animal IVIS imaging relative to a control i.d. injection of the total coated amount of AF555 (**Figure 7-1c-d**). To test bioactive delivery of Ad5, we encapsulated luciferase-expressing Ad5 vectors (Ad5-LUC) in sucrose coatings and applied these patches to the dorsal ear skin of mice or injected an equivalent dose of Ad5-LUC i.d. by syringe at the same site as before. Whole-animal bioluminescent imaging of the administration site revealed strong and persistent expression of the luciferase transgene peaking on day 2 and declining over the course of 30 days at the site of treatment in both injected and Ad5-MN treatment groups (**Figure 7-1e**). Quantitation of bioluminescence obtained from Ad-MN vs. i.d. injections suggested that ~12% of the coated dose is functionally delivered to cells in the tissue following a 5 min application of the microneedles. This value could almost certainly be increased by increasing the application time or by optimizing coating procedures to coat only the microneedle tips,[48,244] but we chose to focus on this simple formulation and rapid delivery regimen for these proof-of-concept studies.

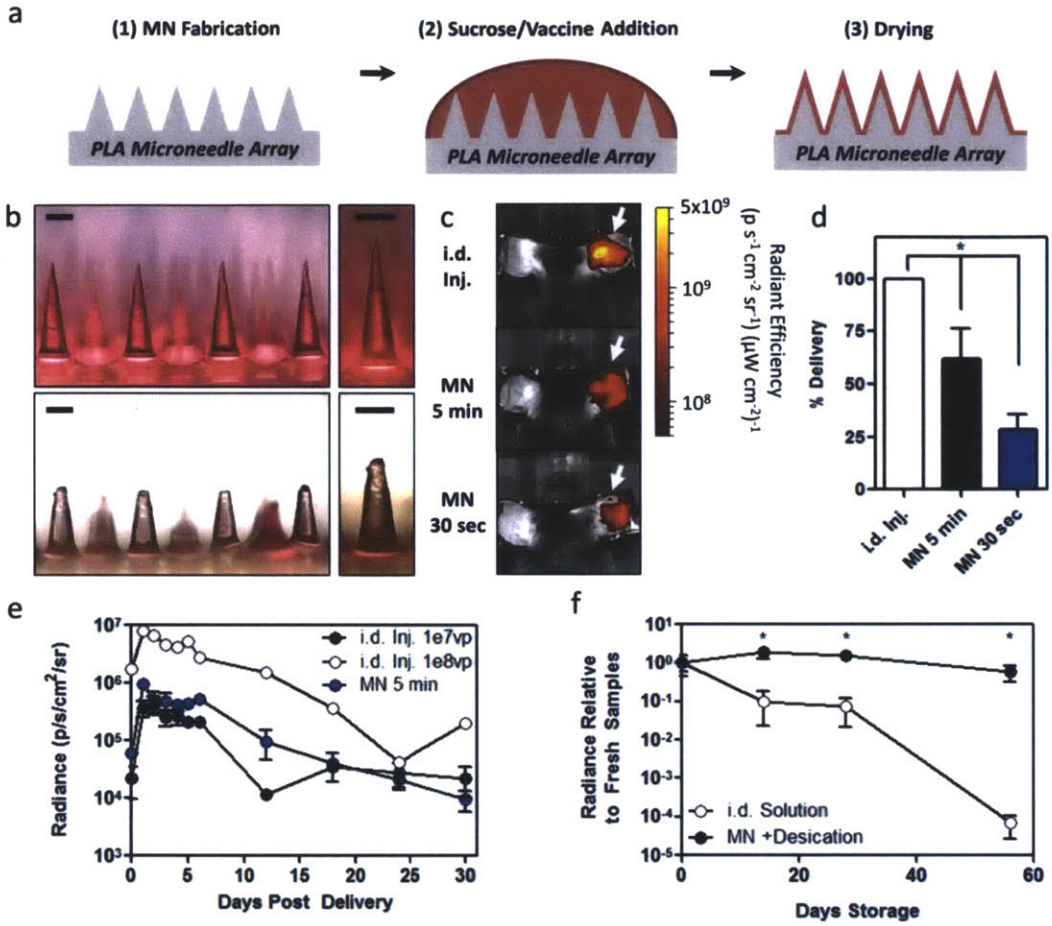

Figure 7-1. Fabrication, application, and storage of microneedle vaccines

*(**a**) Schematic of microneedle patch (MN) coating strategy in which PLA microneedle patches are fabricated by PDMS molding (1), followed by application of an aqueous sucrose coating formulation (2), and drying under vacuum to generate hardened vaccine coatings (3). **(b)** Optical micrographs of microneedles bearing AF555-loaded sucrose coatings before application (top) and following a 5 minute application to murine skin (bottom, scale bar 100 μm). **(c-d)** Analysis of sucrose coating delivery following microneedle patch application. **(c)** Representative whole-animal fluorescence images of mice directly following treatment with either i.d. injection of AF555 or application of microneedles bearing AF555-loaded sucrose coatings for 5 minutes or 30 seconds. **(d)** Quantitative analysis of total AF555 delivery by IVIS fluorescence imaging of treated skin. **(e)** Quantitative analysis of total bioluminescent signal measured over time following treatment of mice with either i.d. injection or microneedle delivery ($1x10^8$ total coated vp) of Ad5-LUC. **(f)** Quantitative analysis of day 2 bioluminescent signal collected from mice treated with either i.d. injection or microneedle delivery of Ad5-LUC. Aqueous Ad5-LUC suspensions and sucrose coated microneedle patches were stored at 25°C for 0-56 days before treatment, and bioluminescent signal was normalized to day 0 values.*

7.3.2. *Enhanced Room Temperature Vaccine Stability of Ad5 Vectors in Sucrose Matrix*

To determine the ability of sucrose coatings on microneedles to protect encapsulated Ad5 vectors during storage at room temperature, we fabricated microneedles with Ad5-LUC/sucrose coatings and stored them at 25°C for 2 weeks to 2 months under desiccation, then applied the dry patches to murine auricular skin. For comparison we performed i.d. injections of aqueous coating solutions stored at 25°C for the same periods of time. Comparison of total measured bioluminescent signal in mice 2 days after treatment revealed that Ad5-LUC stored in solution rapidly lost ~90% of its initial activity over 14 days as expected,[247] while Ad5-LUC encapsulated on sucrose-coated patches showed no significant loss of activity over 56 days at 25°C (**Figure 7-1f**). This prolonged dry state stability without refrigeration may be valuable for improving availability and reducing vaccination costs in the developing world.

7.3.3. *Ad-MN Immunization Shows Immunogenicity Comparable to Syringe Injection in Mice*

Previous studies have demonstrated that Ad5 vectors are able to elicit potent cellular and humoral immunity in mice following parenteral injection.[248,249] These vectors elicit systemic immunity in the peripheral blood and spleen, as well as strong disseminated mucosal immunity.[249] To confirm that the effective transfection observed with Ad-MN was accompanied by robust immune response induction, we compared the immunogenicity of Ad5 vectors encoding SIV-gag delivered by Ad-MN, i.d. injections at the same site as MN application, or standard intramuscular (i.m.) injections, dose-matching the fraction of bioactive delivered vector from 5 min-applied patches. Cellular immunity in peripheral blood mononuclear cells (PBMCs) was measured weekly using peptide-MHC tetramers detecting $CD8^+$ T-cells specific for the immunodominant gag peptide AL11 in the context of $I\text{-}A^b$ class I MHC.[248,249] Consistent with previous studies, i.m. administration primed strong expansion of antigen-specific $CD8^+$ cells, peaking on day 21 at ~20% of the total $CD8^+$ cell population, and slowly declining over the next 3 months; i.d. administration elicited a similar pattern of T-cell expansion, at slightly lower levels (**Figure 7-2a-b**). Ad-MN elicited statistically identical T-cell responses with a similar expansion and contraction profile, with peak responses intermediate between i.m. and. i.d. injections. We also measured the frequency of AL11-specific $CD8^+$ T cells in spleens collected on day 21 and similarly observed no statistical difference in the frequency of antigen-specific cells between groups given parenteral or microneedle-delivered vaccines (~10% of $CD8^+$ T cells, data not shown). Intracellular cytokine staining on *ex vivo* AL11-restimulated PBMCs revealed similar levels of IFN-γ– and TNF-α-producing cells in all 3 immunization groups (**Figure 7-2c-d**). Interestingly, flow cytometry analysis of homing/memory marker expression by AL11-specific T-cells on day 42 revealed an enhanced generation of antigen-specific $CD44^+CD62L^+$ lymph node-homing $CD8^+$ T cells in microneedle-treated animals relative to those receiving traditional i.m. injection (**Figure 7-2e-f**).

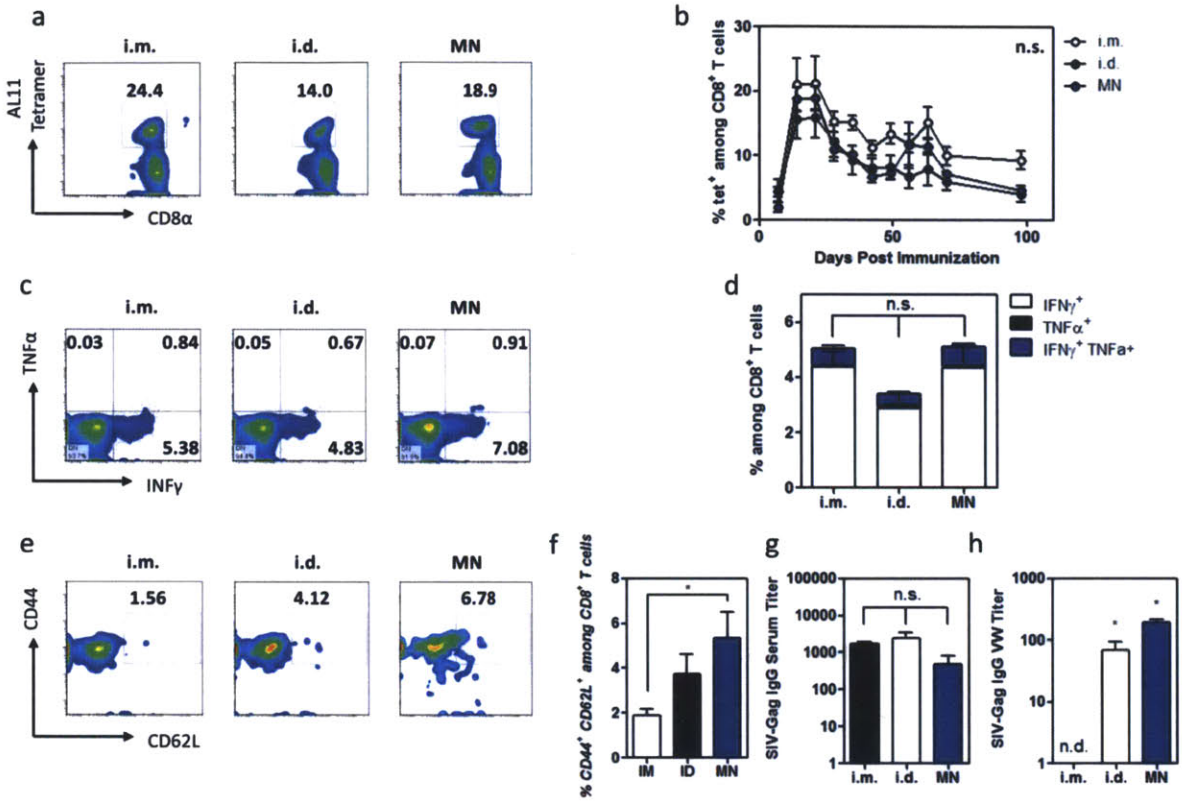

Figure 7-2. Microneedle patch vaccination gives potent immunogenicity in mice similar to parenteral immunization

C57Bl/6 mice (n = 5/group) were immunized with $1x10^8$ vp Ad5-SIV-gag on day 0 intramuscularly (100 µl, in the quadriceps), intradermally (15 µl, in the dorsal ear skin), or by 5 minute application of coated microneedles to the dorsal ear skin. ***(a-b)*** *Frequency of gag-specific $CD8^+$ T-cells in peripheral blood assessed by flow cytometry analysis of AL11 $tetramer^+$ $CD8^+$ T-cells. Shown are* ***(a)*** *representative cytometry plots from individual mice on day 14 and* ***(b)*** *mean±s.e.m. $tetramer^+$ values from day 7-91.* ***(c-d)*** *Intracellular cytokine secretion assessed in peripheral blood upon ex vivo restimulation with AL11 peptide on day 35. Shown is representative* ***(c)*** *flow cytometry analysis of IFN-γ/TNF-α-producing $CD8^+$ T-cells and* ***(d)*** *mean±s.e.m. $cytokine^+$ values.* ***(e-f)*** *Analysis of T-cell effector/central memory phenotypes in peripheral blood by CD44/CD62L expression of $tetramer^+$ cells from peripheral blood. Shown are* ***(e)*** *representative cytometry plots from individual mice at day 49 and* ***(f)*** *mean±s.e.m. percentages of $tetramer^+CD44^+CD62L^+$ among $CD8^+$ T cells at day 49.* ***(g-h)*** *Enzyme-linked-immunosorbent assay analysis of total gag-specific IgG in sera* ***(g)*** *and vaginal wash* ***(h)*** *at day 42. Data represent the mean±s.e.m., *, $p< 0.005$, analyzed by two-way ANOVA.*

Parenteral administration of Ad5 vectors has been reported to induce strong $CD8^+$ proliferation in mucosal tissues in mice, a potentially attractive feature for generating protective responses

against mucosal exposure in the case of sexual transmission of HIV.[248,249] To determine the relative ability of microneedle vaccination to stimulate mucosal cellular immunity, mice were vaccinated by skin patches or by i.m. or i.d. injection and mucosal tissues were harvested 21 days later. AL11 tetramer staining analysis indicated strong mucosal responses across all treatment groups (**Supplemental Figure S7-1**). Equivalent frequencies of AL11-specific $CD8^+$ T cells were elicited by Ad-MN or i.m. or i.d. injections in the lungs (~30% $AL11^+$), vaginal tissues (~25% $AL11^+$), and gut intraepithelial compartments (~10% $AL11^+$).

Finally, to compare humoral immunity stimulated by the skin patch vaccine vs. syringe injection, we measured gag-specific serum IgG titers, and found that microneedle delivery produced statistically equivalent levels of systemic anti-gag IgG compared to either i.m. or i.d. vaccination (**Figure 7-2g**). We also measured levels of gag-specific IgG in vaginal wash collected on day 42 and observed elevated antibody levels in mice receiving i.d. injection or microneedle treatment relative to i.m. administration (**Figure 7-2h**). These results suggest that microneedle patch vaccination can produce equivalent systemic antigen-specific antibody responses compared with i.m. or i.d. treatment, and elicits enhanced mucosal antibody titers relative to parenteral i.m. vaccination.

7.3.4. Insertion and Adenovirus Delivery in Primate Skin

Although mouse models provide an effective context for the development of new vaccination approaches, skin physiology and immunity in mice has many differences from humans.[223] To evaluate the feasibility of coated microneedle vaccines in a model closer to humans, we set out to evaluate the immunogenicity of Ad-MN vaccines in Rhesus macaques, an accepted preclinical model for HIV and many other infectious diseases.[93,125,142,149,224] We first tested whether microneedles provide similar delivery in macaque skin compared to our previous results in mice. Patches were applied manually to the shaved deltoid skin of recently euthanized macaques and secured in place for 5 min. Treated skin was then excised and stained with trypan blue to visualize areas of microneedle insertion. Optical microscopic imaging of skin treated before dissection revealed consistent patterns of microneedle penetration (**Figure 7-3a**). Histological analysis of patch-treated skin showed uniform sites of microneedle insertion accessing the superficial epidermis while leaving the underlying dermal tissues undisturbed (**Figure 7-3b-c**). To determine the pattern of vaccine deposition, we treated macaque skin with patches coated with sucrose carrying 100 nm fluorescent carboxylated polystyrene nanoparticles as a surrogate for viral particles. Confocal imaging of treated skin revealed the consistent presence of punctate fluorescent signal from particles at sites of microneedle insertion, suggesting successful penetration of microneedles and dissolution-mediated delivery of sucrose-loaded cargos following a 5 minute application period (**Figure 7-3d**). Further, histological sections of treated skin showed permeation of nanoparticles several hundred microns into the surrounding epidermis at sites of microneedle penetration (**Figure 7-3e**). To assess the local bioactivity of Ad5 vectors delivered into macaque skin, we applied Ad-MN delivering $1x10^8$ vp Ad5-LUC to freshly explanted macaque skin *ex vivo*. Following treatment, skin samples were cultured *in*

vitro and expression of luciferase was measured using whole-tissue bioluminescent imaging. Here we observed strong luciferase expression for several days following treatment for both microneedle-treated skin and skin treated by i.d. injection of a dose-matched aqueous solution of the patch coating formulation (**Figure 7-3f-g**). In both treatment groups, statistically equivalent levels of luciferase expression were measured for multiple days following treatment, with peak expression observed on day 2 after administration (**Figure 7-3g**). Altogether, these results suggested effective epidermal delivery from sucrose-coated polymer microneedles in the skin of Rhesus macaques.

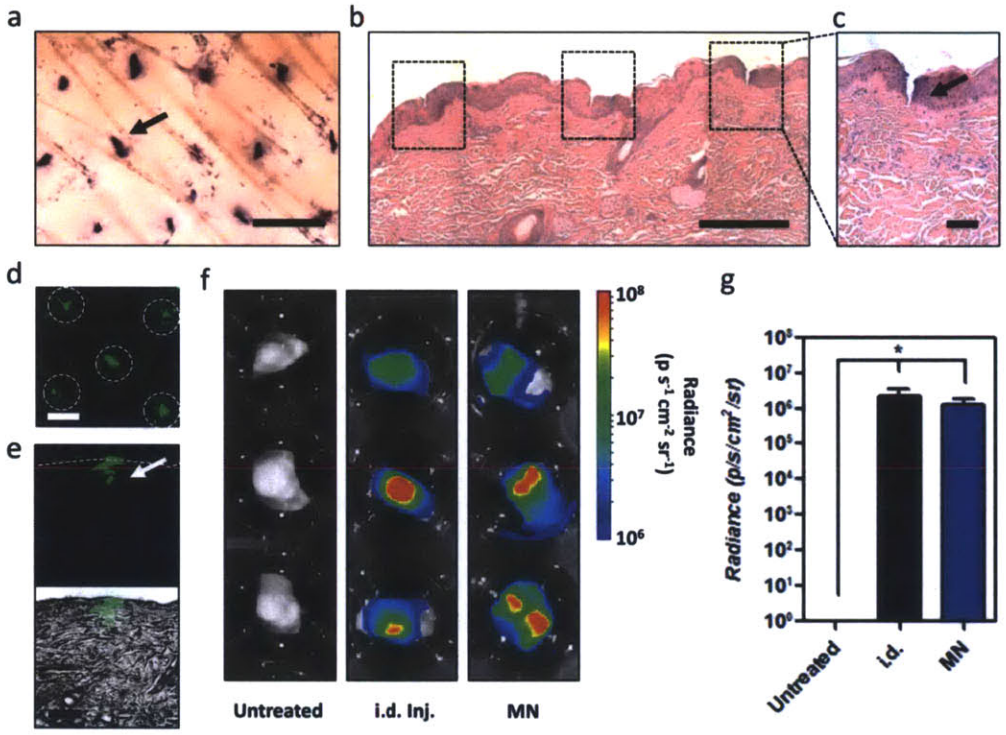

Figure 7-3. Microneedles penetrate primate skin to deliver vaccine coatings

(a) *Optical micrographs of macaque deltoid skin stained with trypan blue to reveal epidermal penetration following PLA microneedle patch application (one example penetration site indicated by arrow; scale bar, 500 μm).* ***(b-c)*** *Histological sections of microneedle-treated macaque skin showing epidermal disruption at microneedle insertion sites (scale bars:* ***b,*** *500 μm;* ***c,*** *200 μm with insertion site denoted by arrow).* ***(d)*** *Representative confocal micrograph of microneedle-treated deltoid skin showing delivery of 100nm carboxylate modified polystyrene nanoparticles (green) from sucrose coatings at microneedle insertion sites (circled).* ***(e)*** *Histological section of similarly treated macaque skin showing epidermal delivery of 100nm carboxylate modified polystyrene nanoparticles (green) from sucrose coatings at microneedle insertion site (arrow); scale bar 200 μm.* ***(f-g)*** *Analysis of Ad5-LUC delivery to macaque skin ex vivo.* ***(f)*** *Representative whole-tissue bioluminescent images of macaque deltoid skin treated with*

$1x10^8$ vp Ad5-LUC by i.d. injection or microneedle patch delivery ($1x10^9$ total coated vp). ***(g)*** *Quantitative analysis of total bioluminescent signal measured on day 2 following delivery.*

7.3.5. *Peripheral and Mucosal Immunogenicity of Ad-MN in Primates*

To evaluate the functional immunogenicity of adenovirus delivery from microneedles, we formulated patches coated with sucrose-encapsulated Ad5 vectors encoding SIV gag or env. We then applied four patches for each vector (total delivered dose $4x10^9$ vp Ad5-SIV-gag and $7x10^9$ vp Ad5-SIV-env) to the shaved deltoid skin of anesthetized macaques ($n = 4$) for 5 min to deliver the vaccines; animals were boosted by the same patch administration regimen at 12 weeks. No adverse reactions were noted at the application sites in any animals and visible redness resolved after only 30 minutes. As shown in **Figure 7-4a**, microneedle delivery of Ad vectors elicited robust ELISPOT responses against gag and env peptide pools, with gag responses maintained at high levels for at least 16 weeks. T-cell responses to env epitopes were initially weaker but were clearly boosted following the Ad-MN vaccination at week 12 (**Figure 7-4b**). Intracellular cytokine staining on restimulated T-cells from blood or colorectal biopsy samples at week 16 showed readily detectable $CD8^+$ and $CD4^+$ T-cells, suggesting the induction of both systemic and mucosal immune responses by the microneedle vaccines (**Figure 7-4c**). Analysis of env-specific antibody titers in serum over time showed the induction of gp120-specific humoral responses following priming which was further increased by more than a log following boosting (**Figure 74d**). Anti-env IgG was also detected in rectal mucosal secretions at week 16 (**Figure 7-4e**). By 4 weeks post prime, skin patch vaccines had induced high neutralizing antibody titers against a neutralization sensitive clone of SIVmac251 virus (**Figure 7-4f**). Thus, microneedle delivery of adenovirus vectors induces strong cellular and humoral immunity in line with results expected from traditional needle and syringe intramuscular vaccination, and promotes both systemic and mucosal immune responses.

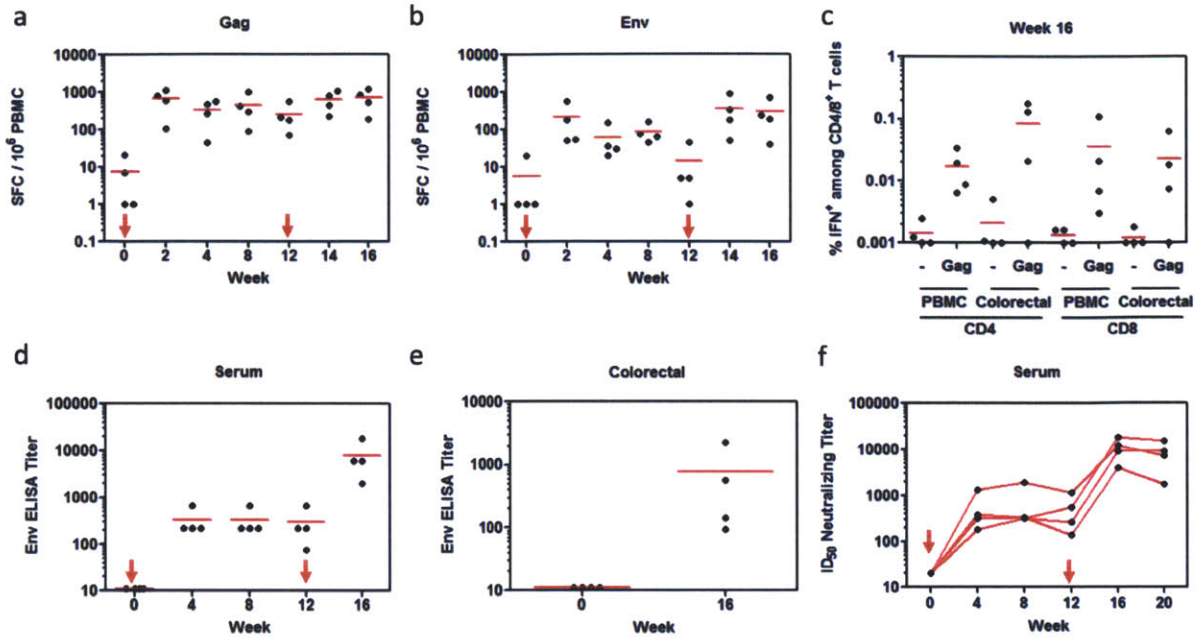

Figure 7-4. Microneedle patch vaccination is immunogenic in Rhesus macaques

Four macaques were immunized with $4x10^9$ Ad5-SIV-gag vp and $7x10^9$ vp Ad5-SIV-env vp by microneedle patch application for 5 min at week 0 and week 12. ***(a-b)*** *ELISPOT analysis of peripheral blood mononuclear cell secretion of IFNγ following ex vivo restimulation with representative overlapping peptide epitopes for SIV-gag and SIV-env. Shown are IFNγ spot forming cells (SFC) per $1x10^6$ PBMCs for each timepoint following stimulation with* ***(a)*** *SIV-gag or* ***(b)*** *SIV-env pooled peptides.* ***(c)*** *Week 16 flow cytometric analysis of IFNγ$^+$ cells isolated from peripheral blood or colorectal biopsy following ex vivo stimulation with media or SIV-gag peptide. Shown are responses for CD8$^+$ and CD4$^+$ T cells.* ***(d-e)*** *Anti-SIV-env antibody titers in serum and colorectal mucosal secretions. Shown are* ***(d)*** *anti-env serum IgG titers as measured at each timepoint and* ***(e)*** *anti-env IgG titers measured in colorectal secretions at week 16.* ***(f)*** *Serum neutralizing antibody titer analysis for SIVmac251 homologous virus. Shown are ID_{50} neutralizing titers at each timepoint following vaccination.*

7.4. Conclusions

The goal of this study was to evaluate the potential for microneedle patch delivery of a prototypical non-replicating adenovirus vaccine to generate immunity in mice and non-human primates. Microneedle vaccination could provide many practical advantages over the use of traditional hypodermic needles in vaccine delivery, including improved safety, simplified administration, and the potential for non-refrigerated, dry-state storage.[250,251] Further, microneedles localize vaccine delivery to the skin, thereby targeting potent epidermal and dermal antigen-presenting cells, which in some small-animal models has led to enhanced immunogenicity compared to traditional parenteral immunization.[23,125,142,252,253] The potency and

protective efficacy of microneedle vaccines has been demonstrated in a variety of disease models in rodents.[93,142,149,199,254,255] However, to our knowledge the immunogenicity of microneedle vaccines in non-human primates, an important step in preclinical vaccine development for advancement to human clinical trials, has not been tested.

A great variety of solid microneedle designs have been tested for delivery of vaccines in rodent models, ranging from simple metal microprojections coated with dried vaccine to polymer microneedles that encapsulate vaccine and dissolve in the skin.[142,192,200] Here we developed and tested a prototypical system representative of the most common microneedle strategy in vaccine delivery, where vaccines are encapsulated in a protective dissolving matrix coated on solid microneedle arrays. We employed FDA-approved PLA as the microneedle base for low-cost, high-throughput (melt-molding) fabrication, and used sucrose as a protective coating matrix for the adenoviral vector, based on its known ability to stabilize diverse biologics in a dried state, including viruses.[247] This patch composition provided substantial stabilization of Ad5 vectors for extended storage without refrigeration, and showed robust immunogenicity equivalent to traditional syringe injections in mice.

In Rhesus macaques, Ad-MNs provided reproducible skin penetration and delivery of sucrose coatings into the epidermis following brief applications of only 5 minutes. Local gene expression in the skin of macaques following patch application was quantitatively indistinguishable from an intradermal syringe injection. Skin patch vaccination elicited robust $CD4^+$ and $CD8^+$ T-cell responses as measured by ELISPOT and intracellular cytokine staining in both blood and mucosal tissues. Sustained anti-env IgG responses were elicited in the serum and mucosal sites, and sera from immunized macaques neutralized autologous SIVmac251 virus. Supporting the robustness and reproducibility of microneedle vaccination, both T-cell and antibody responses were clearly increased following boosting at 12 weeks. These responses are all in line with expectations for the response to this adenovirus vector from prior studies in our laboratory using traditional intramuscular injections of similar vector doses. Overall, these results demonstrate the potential for microneedle delivery to effectively deliver adenovirus vectors in non-human primates, an important step in establishing this technology as an attractive alternative to traditional syringe administration. Together with the many known practical advantages of microneedles, the results shown here indicate the significant promise of microneedle patch vaccination to improve immunization, particularly in the developing world.

8. Conclusions and Future Work

8.1. Conclusions

Here we have shown the development and testing of several novel approaches for microneedle formulation of subunit vaccines to enable effective and non-invasive transcutaneous delivery. Our goal throughout these studies was to employ innovative materials engineering approaches to the design of vaccination platforms capable of combining the numerous practical advantages of transcutaneous delivery, with systems capable of modular and tunable control over multicomponent vaccine formulation, delivery, and contextual presentation to the immune response. Although prior work has explored the use of microneedles for effective transcutaneous vaccination, much of this work has focused on the simple adaptation of existing parenteral vaccine formulations for delivery by microneedle array. Conversely, the results reported here have demonstrated the potential of microneedle delivery to enable several forms of recombinant subunit vaccination, including the delivery of defined antigenic and adjuvanting nucleic acids, proteins, and viral vectors. Furthermore, we have demonstrated the significant potential of advanced materials science concepts for control over vaccine loading, delivery, and release for enhancing immunity, thus providing a platform supporting the rational design of vaccines combining immunogenic cues to optimize immunity.

LbL directed assembly has previously been shown to be a robust and controllable approach for biological therapeutics formulation, enabling complex programming of multicomponent loading and release, and providing the potential for the design of responsive behaviors through selection of polymeric constituents. Given the need for more potent subunit vaccination strategies driven by the limitations of conventional killed/attenuated pathogen approaches for safely addressing emerging diseases such as HIV, we were motivated to explore the use of LbL for the rational and complex formulation and delivery of genetic vaccines. The adaptation of this strategy to enable controlled vaccine formulation into microneedle surface coatings allowed for tunable antigen-encoding nucleic acid encapsulation together with hydrolytic cationic polymers capable of mediating both controlled pDNA release, and *in situ* polyplex formation. LbL assembly also proved to be a modular approach allowing for defined incorporation of nucleic acid adjuvants together with antigenic pDNA, thus providing a coating capable of delivering a complete subunit vaccine. Finally, LbL assembly was able to interface with a pH-responsive polymer to allow for rapid film implantation upon microneedle application. Testing of this approach in mice using a model HIV antigen, showed promising induction of both cellular $CD8^+$ T cell and systemic humoral immunity comparable to electroporation, one of the most promising current clinical strategies for pDNA delivery in humans. Further, *ex vivo* LbL microneedle treatment of viable non-human primate skin showed >100x increased expression of a model protein compared to injection, an important result indicating the promise of microneedle delivery for effective translation to large animals and humans.

Given the inherent adaptability of LbL assembly we next explored the potential of this approach for incorporation and delivery of lipid nanocapsules from LbL-assembled microneedle surface

coatings. The ICMV delivery system has previously been shown to potently induce systemic CD8+ T cell responses following parenteral vaccination. Therefore we were motivated to test the potential of this platform for triggering similar immunity following non-invasive cutaneous immunization. Although, previous studies have introduced the concept of incorporating lipid particles into LbL-assemblies, these have largely been limited by the instability of native lipid particles exhibited during the adsorption process. ICMVs provide a unique opportunity to overcome this challenge by leveraging their enhanced physical stability endowed by inter-bilayer molecular crosslinks within the lipid lamellae. These studies proved the utility of this approach, which generated controllable ICMV-loaded microneedle coatings capable of rapidly dispersing into treated skin and effectively delivering immunogenic cargos to recruited APCs. These results also indicated a promising role for microneedle delivery of defined molecular adjuvants in recruiting cutaneous APCs and driving their concomitant uptake of vaccine and maturation for effective interaction with scanning naïve lymphocytes. Finally, transcutaneous delivery of LbL formulated ICMVs resulted in a more potent and diversified functional antibody response compared to parenteral administration, or microneedle delivery of soluble vaccine components, suggesting a synergistic combination of ICMV-mediated cellular delivery following microneedle-enabled transfer into the skin.

Control over the persistence of antigenic or inflammatory stimulus within the context of infection or vaccination is emerging as a deterministic variable in the shaping of effector and memory adaptive immune responses. To explore this concept in combination with the practical and immunological advantages of transcutaneous delivery we designed and constructed several parallel microneedle approaches able to mediate rapid implantation of controlled release matrices for programming vaccine persistence. These strategies were based upon the use of composite responsive structures which rapidly deliver bolus or controlled release vaccine formulations through dissolution mediated disintegration within the skin. Although previous studies have explored the use of rapidly dissolving microneedles, these studies were the first to combine rapid needle dissolution with the delivery of long-lived vaccine depots. The results of these studies, either using persistent PLGA or silk protein matrices in combination with dissolvable PAA, demonstrated the ability to program vaccine delivery and release over time depending on the combination of materials used for microneedle fabrication. This ability proved critical for tuning the duration and magnitude of subunit vaccine exposure *in vivo* and optimization of these features resulted in greatly enhanced cellular and humoral immunity. Furthermore, these approaches demonstrated a promising potential for enabling simple and cost effective room temperature storage, an important advance for improving vaccine economics and availability.

Finally, to complement our various studies for the development of sophisticated materials approaches to microneedle vaccine formulation, we were motivated to explore the potential for microneedle delivery to enable safe, reliable, and effective delivery of an advanced recombinant viral vector vaccine to elicit immunity in both preclinical mouse and nonhuman primate models of HIV. Although many reports have indicated the promise of microneedle vaccination in small animal models, no previous study has robustly characterized the potential for microneedle

delivery to induce immunity in large animal models thought to be more predictive of success in human clinical testing. In this work, we also developed a new approach for biologics encapsulation into sugar-glass coatings on the surface of polymer microneedle arrays through simple co-suspension of vaccine with sugar followed by liquid application and drying on the surface of the microneedle array. In these studies we demonstrated the effective loading, stable storage, and delivery of replication incompetent Ad5 viral vectors giving robust transgene expression in the treated tissues resulting in potent cellular and humoral immunity against SIV-gag in mice comparable to that elicited by parenteral injection. We then translated this approach for the treatment of Rhesus macaques, and observed strong, boostable, systemic and mucosal cellular responses against SIV-gag and SIV-env. Further, we detected potent and boostable serum antibody responses targeting SIV-env, which correlated with the development of similar responses within mucosal tissues at sites sensitive to sexual viral transmission. Together these results indicate the potential for microneedles to provide a viable alternative to parenteral injection of a clinically advanced recombinant vaccine platform in primates and potentially humans.

To conclude, we have successfully demonstrated several parallel approaches for the formulation and delivery of recombinant subunit vaccines for transcutaneous delivery using microneedle skin patches. These strategies represent a portfolio of materials platforms suggesting the promise of microneedle delivery technology to enable safer, more cost-effective, and more potent non-invasive vaccination based on a variety of next-generation recombinant vaccine technologies including pDNA, RNA, proteins, synthetic particles, and viral vectors. Further the flexibility and modularity of these approaches should support the increased success of such emerging vaccine technologies by facilitating greater control and rational design of vaccines to enhance immunological response.

8.2. Future Work

8.2.1. LbL Coated Microneedle Vaccine Delivery

Based on our studies so far, microneedle delivery of LbL-formulated pDNA vaccines can induce potent cellular and humoral antigen-specific immunity comparable to the most promising clinical approaches for DNA delivery. Given the many attractive features of pDNA-based immunization, including ease of good manufacturing practice production, lack of anti-vector immunity, greater stability in storage, and the capability to promote both cellular and humoral immune responses, future work should focus on *(i)* elucidating the mechanisms leading to this improved performance, *(ii)* development of streamlined fabrication approaches with improved throughput, efficiency, and consistency, and *(iii)* validation studies in large animal models of disease to support potential clinical translation.

Our current results indicate that the improved immunogenicity achieved by multilayer tattooing is mediated by a combination of microneedle delivery and multilayer pDNA formulation, as injected naked pDNA or polyplexes give very little measureable immunity. In other studies, microneedle delivery of naked pDNA resulted in similarly weak immunogenicity at similar

doses. Future work should work towards a more detailed understanding of the enhancement mediated by the combination of cutaneous delivery and multilayer formulation. Potential areas of exploration include *(i)* testing of various multilayer architectures to determine the design rules governing multilayer elicited immunity, *(ii)* more comprehensive measurement of both local pDNA cellular delivery, and local immune cell recruitment/response, and *(iii)* extension of these studies to nonhuman primates to validate potential mechanisms in a context more similar to humans. Variables of interest for exploring multilayer architecture include hydrolytic versus non-degradable polymer constituents, degradation kinetics, co-delivery of adjuvants, and overall inflammatory capacity. Characterization of local delivery and innate/adaptive immunity might reasonably focus on first determining which local cell populations are transfected *in vivo*, the timescale for antigenic gene expression, and second, the detailed profile of innate cell recruitment, activation, maturation, and finally interaction with the naïve adaptive response. Although mouse models will serve as a valuable context for preliminary exploration of these questions, study in explanted primate tissues or live animals will likely be critical given the known differences between murine and primate transfection mechanisms.

Further development of the LbL coating process for microneedles should also be a priority for future study. These efforts should focus on improving throughput, efficiency, and reliability in support of larger preclinical studies. These goals might be addressed through the development of an automated LbL process employing liquid handling robots to enable LbL in small volumes to increase efficiency. An ideal process will improve the efficient use of vaccine materials by facilitating reuse, and decreasing the total volume/concentration needed during adsorption. One potential option is shown in **Figure 8-1**, in which liquid handling robots manipulate small liquid volumes applied only to the surface of each array. This approach should decrease the total volume needed per array from ~750μl per 30 bilayers to ~75μl per 30 bilayers. Given, the preapproval of relevant robotic handling equipment by the FDA for good manufacturing practice, adoption of this approach would also allow for simple translation to production at scale in the event of clinical translation.

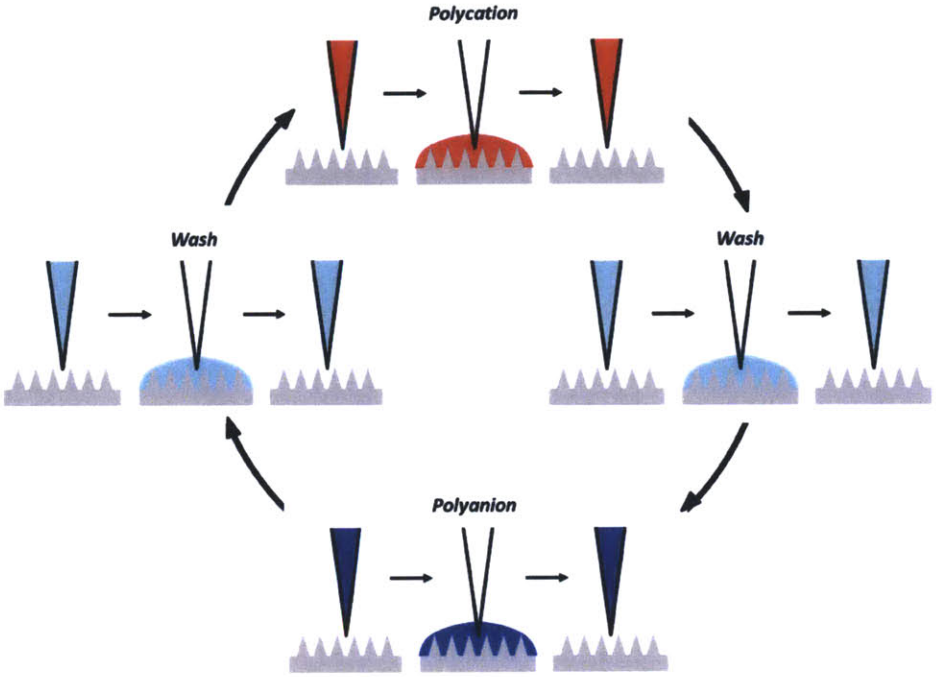

Figure 8-1. High throughput liquid handling assisted LbL

Schematic showing a potential approach for high throughput LbL using liquid handling robots to pipette coating solutions in small volumes onto only the surface of individual microneedle arrays.

Finally, although our current work suggests that microneedle tattooing promotes enhanced expression of pDNA in primate skin, antigen expression is only one of many variable determining immunogenicity. Therefore, future work must provide additional validation of efficacy in primates in order to be considered a viable platform for use in humans.

8.2.2. Sucrose Coated Microneedle Vaccine Delivery

Encapsulating vaccines in sucrose has proven to be a simple and flexible process enabling successful preclinical vaccine testing in both mice and primates. Further, sugar-glasses are known to improve the stability of sensitive biological molecules and vaccines stored at room temperature, a valuable feature for future vaccine deployment in remote areas of the world. Future work in this area should focus on *(i)* the further optimization of the microneedle coating process, and *(ii)* testing for effective vaccination with more advanced viral vector serotypes currently being developed for clinical trials.

Although microneedle coatings encapsulating recombinant viral vectors gave effective immunity in both mice and primates, there is significant room for improvement in the efficiency of vaccine delivery. For example, approaches enabling the coating of microneedles only should improve delivery efficiency by eliminating wasted material coated onto the base of the array.

Given the success of microneedle delivery of Ad5-SIV-gag and Ad5-SIV-env, future work should begin to explore the delivery of more advanced clinical grade vectors engineered to avoid pre-existing vector immunity, and to express mosaic antigens enabling global vaccination to address many sub-clades of HIV isolates prevalent in various regions. This work should enable more comprehensive testing of protective immunity following microneedle vaccination in primate models of S(H)IV challenge. Additionally, larger scale primate tests should aim to directly compare microneedle immunization with dose-matched parenteral treatments to establish potential differences resulting from microneedle delivery. Ultimately these studies should provide pivotal preclinical results to determine whether microneedle vaccination would be a valuable clinical candidate for testing in humans.

9. Appendix A: Supplementary Figures

9.1. *Nano-layered Microneedles for Transcutaneous Delivery of Polymer Nanoparticles and Plasmid DNA*

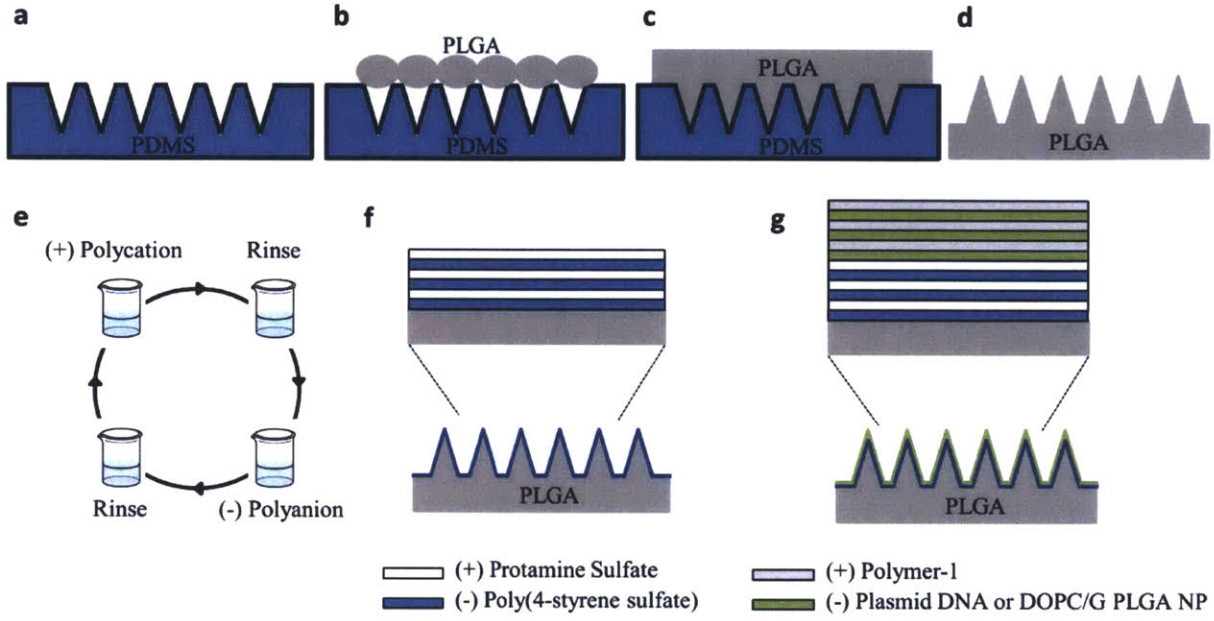

Supplementary Figure S2-1. Schematic of PLGA microneedle fabrication process.

(a) PDMS slabs were machined using laser ablation to create micron scale cavities before (b) application of PLGA to the surface of the mold. (c) PLGA was then melted under vacuum and cooled before (d) removal from the PDMS mold. (e) Schematic showing the LbL directed-assembly process of iterative deposition of oppositely charged polymers through immersion. (f) Initial multilayers were deposited using alternating immersion of PLGA microneedle arrays in solutions of polycationic protamine sulfate and polyanionic poly(4-styrene sulfate). (g) Additional multilayers were then deposited through alternating deposition of polycationic polymer-1 and polyanionic plasmid DNA or PLGA NP to give pDNA or PLGA NP coated arrays respectively. Microneedle arrays coated with both pDNA and PLGA NP were constructed in a similar way first depositing (PS/SPS) base layers, followed by (poly-1/pDNA) multilayers and finally (poly-1/PLGA NP) multilayers.

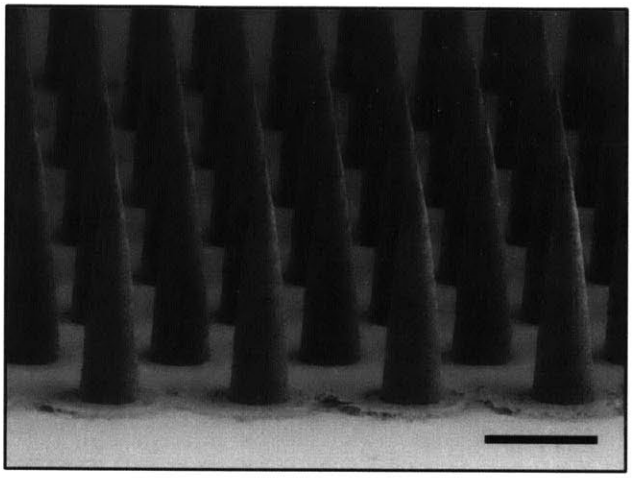

Supplementary Figure S2-2. SEM micrograph of PLGA microneedle array

SEM micrograph of uncoated PLGA microneedle arrays of conical geometry (scale - 500μm).

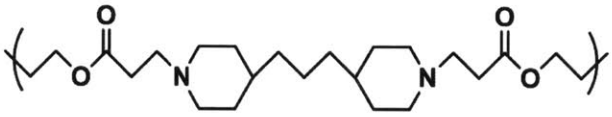

Supplementary Figure S2-3. Chemical structure of Poly-1

Chemical structure of poly-1 used in this study (molecular weight ~8,000 - 10,000 g/mol).

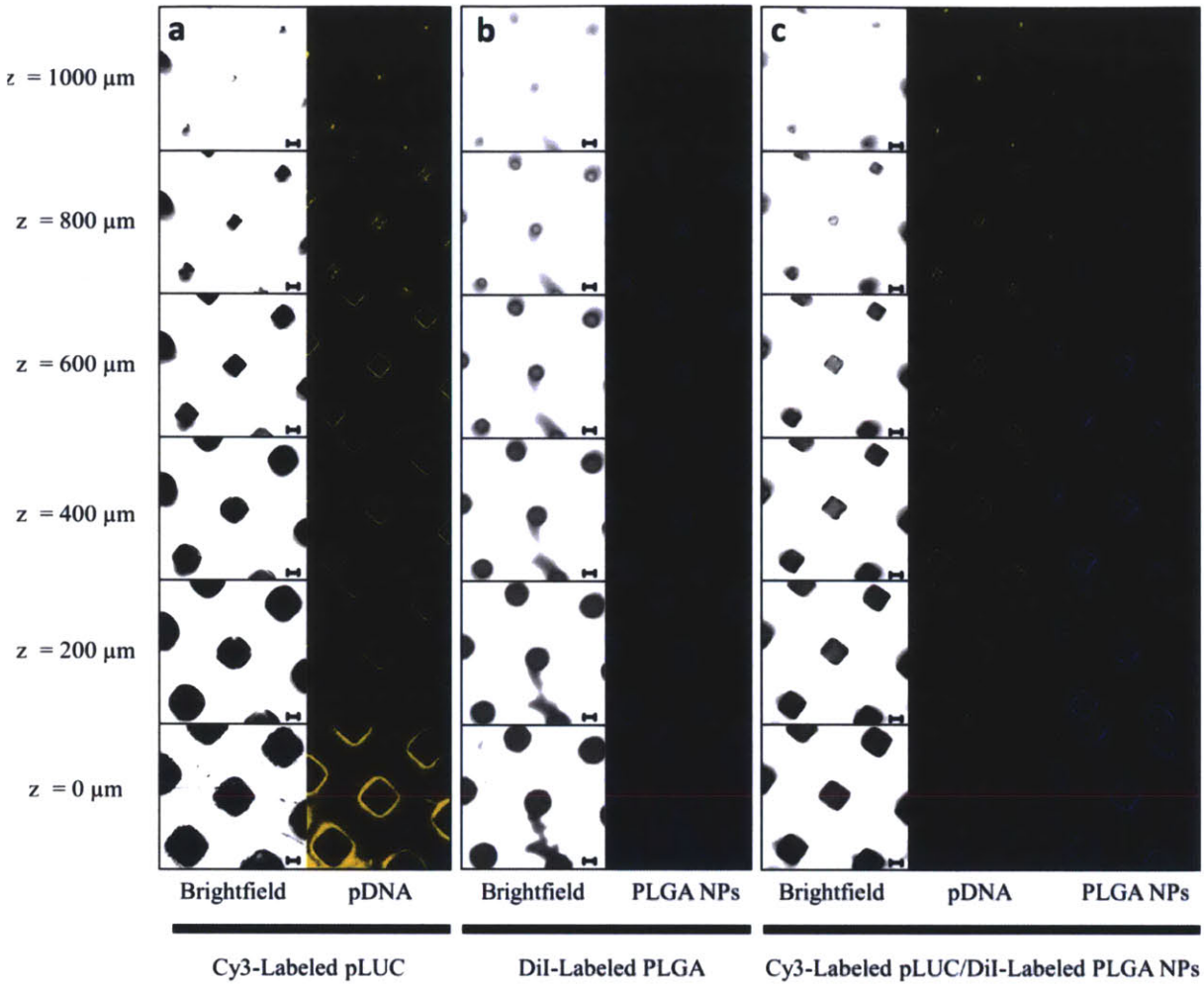

Supplementary Figure S2-4. Multilayer deposition on PLGA microneedles

(a) *Representative CLSM z-stacks of a* $(PS/SPS)_{20}$*-(Poly-1/Cy3-pLUC)*$_{24}$ *coated microneedle array and* ***(b)*** *a* $(PS/SPS)_{20}$*-(Poly-1/DiI-PLGA NP)*$_4$ *coated microneedle array.* ***(c)*** *CLSM z-stack of dual coated microneedle array* $(PS/SPS)_{20}$*-(Poly-1/Cy3-pLUC)*$_{24}$*-(Poly-1/DiD-PLGA NP)*$_4$ *(scale bar – 100 µm).*

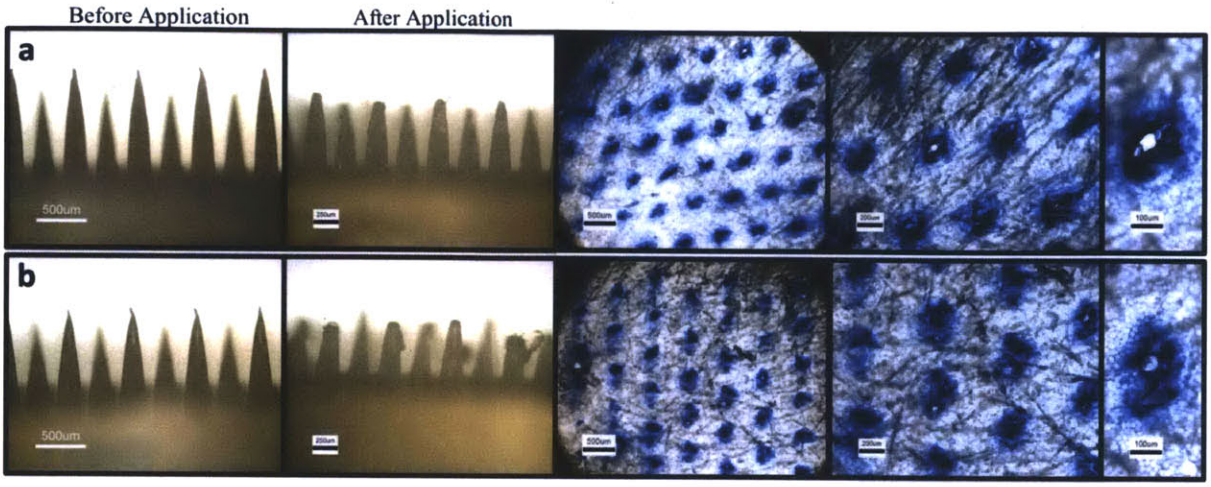

Supplementary Figure S2-5. *In vivo* murine skin penetration with PLGA microneedles

In vivo skin penetration results for microneedle arrays with ***(a)*** *pyramidal geometry and* ***(b)*** *conical geometry (left-optical micrographs of microneedle arrays before and after application, right -trypan blue staining of microneedle penetration patterns).*

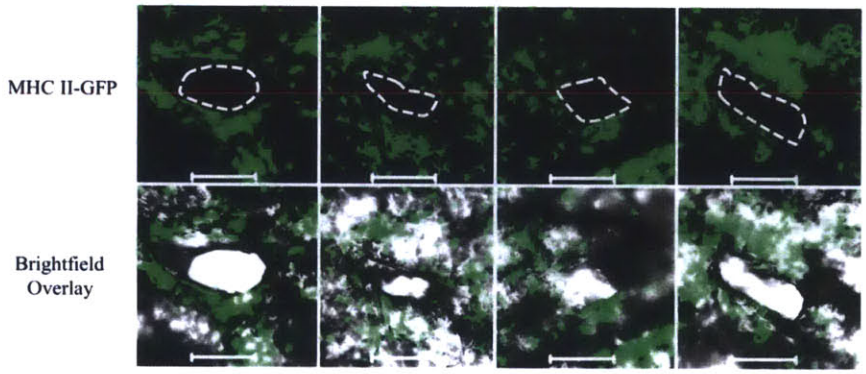

Supplementary Figure S2-6. *In vivo* murine skin penetration

In vivo skin penetration results for microneedle application to MHC II-GFP mice. CLSM images showing microneedle penetration colocalized with Langerhans DCs in the epidermis (scale bar – 100μm).

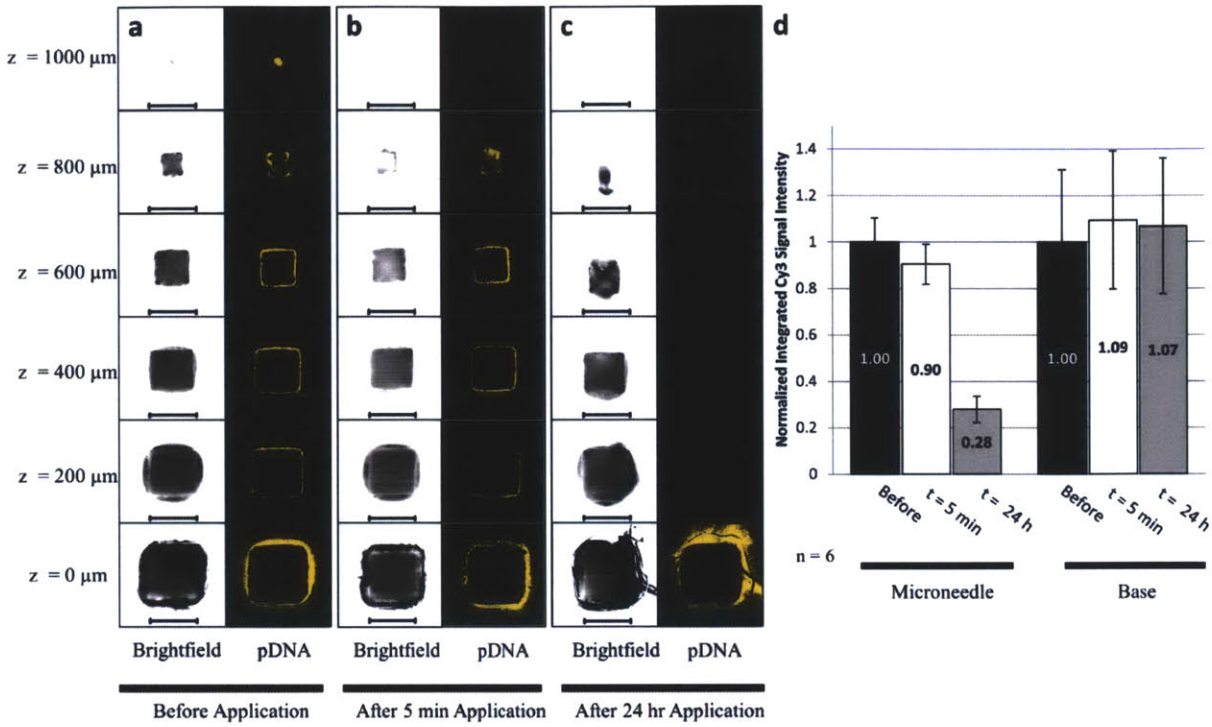

Supplementary Figure S2-7. *In vivo* delivery of microneedle-based pDNA multilayers

Representative CLSM z-stacks of a $(PS/SPS)_{20}$-$(Poly\text{-}1/Cy3\text{-}pLUC)_{24}$ coated microneedle array ***(a)*** *before application,* ***(b)*** *after a 5 minute application, and* ***(c)*** *after a 24 hour application in vivo.* ***(d)*** *Quantification (n = 6) of relative integrated Cy3 signal on both the microneedle surface and the base of the array before and after application.*

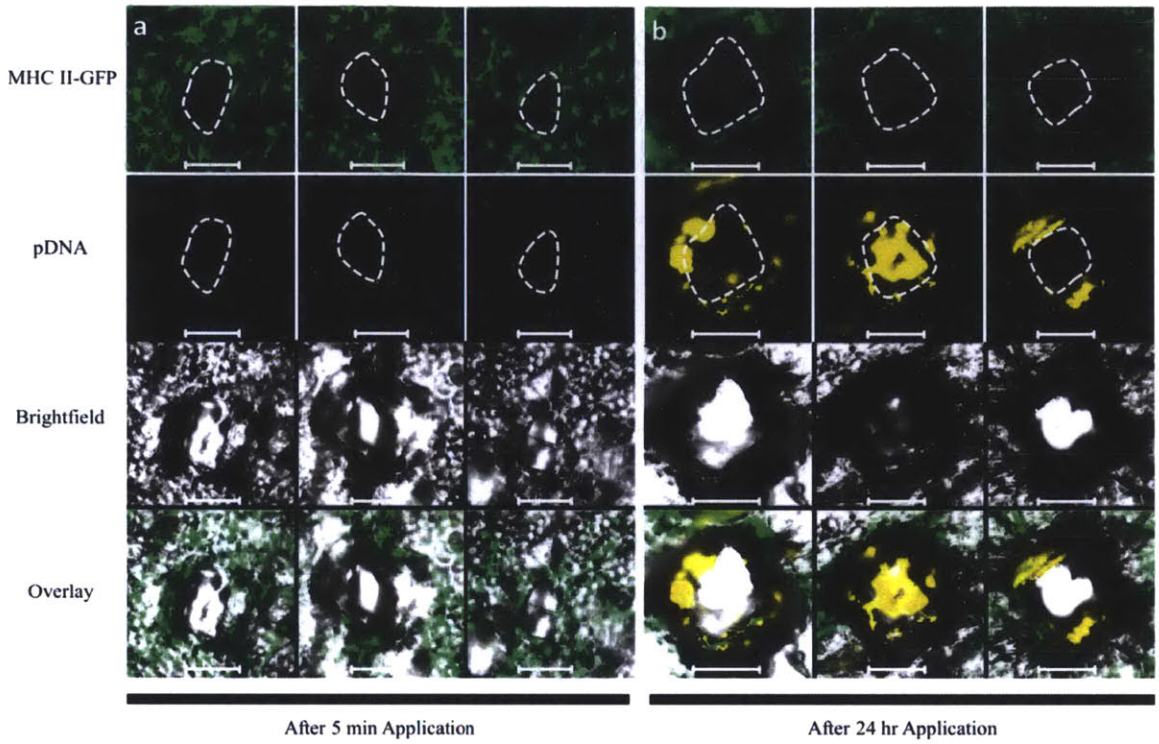

Supplementary Figure S2-8. *In vivo* delivery of pDNA multilayers from coated microneedles

In vivo delivery of Cy3-pLUC to ear skin of MHC II-GFP mice. CLSM images of MHC II-GFP ear skin following application of a $(PS/SPS)_{20}$-$(Poly\text{-}1/Cy3\text{-}pLUC)_{24}$ coated microneedle array for ***(a)*** *5 minutes and* ***(b)*** *24 hours (scale bar – 200μm).*

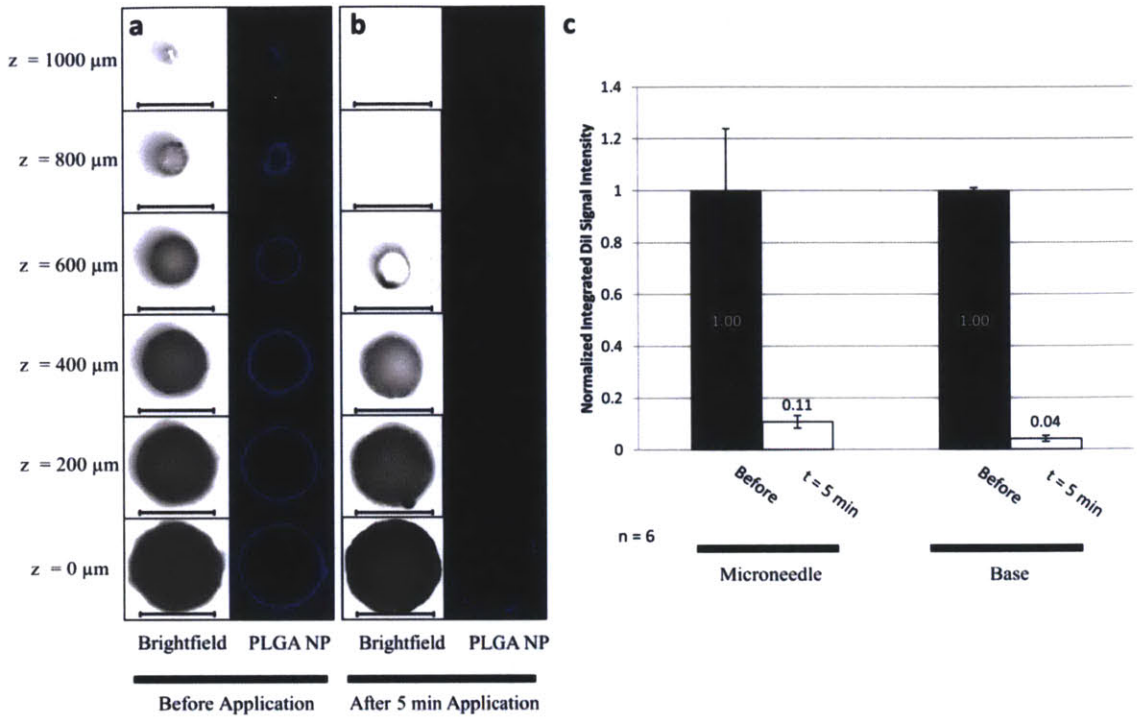

Supplementary Figure S2-9. *In vivo* delivery of microneedle-based polymer nanoparticle multilayers

Representative CLSM z-stacks of a $(PS/SPS)_{20}$-(Poly-1/DiI-PLGA NP)$_4$ coated microneedle array ***(a)*** *before application, and* ***(b)*** *after a 5 minute application.* ***(c)*** *Quantification (n = 6) of relative integrated DiI signal on both the microneedle surface and the base of the array before and after application.*

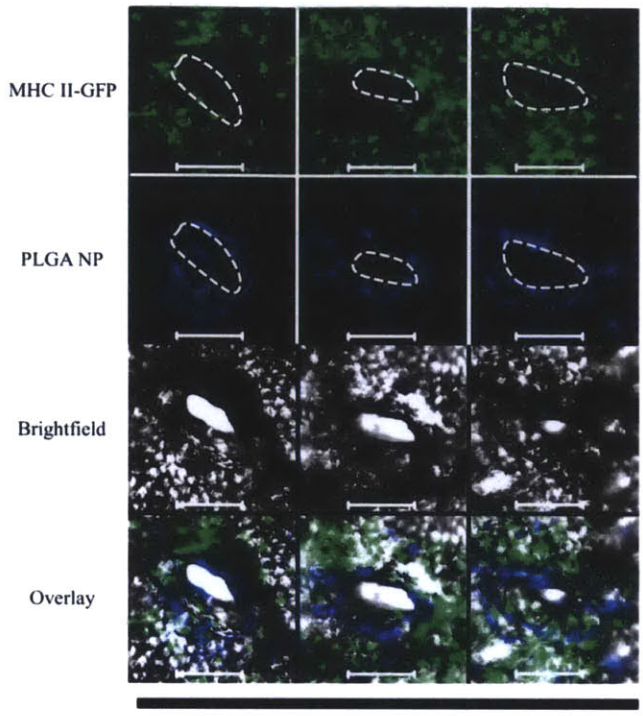

Supplementary Figure S2-10. *In vivo* delivery of polymer nanoparticle multilayers from coated microneedles

In vivo delivery of DiI-PLGA NP to ear skin of MHC II-GFP mice. CLSM images of MHC II-GFP ear skin following $(PS/SPS)_{20}$-(Poly-1/DiI-PLGA NP)$_4$ coated microneedle array application for 5 minutes indicates effective transfer of PEM films and delivery of PLGA NP to epidermal LCs (scale bar 100 μm).

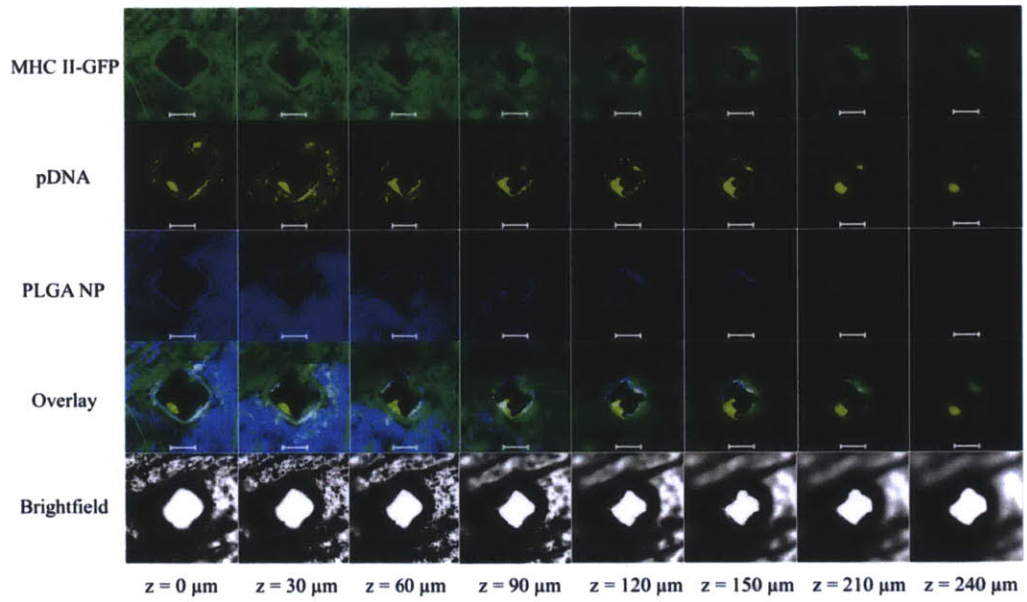

Supplementary Figure S2-11. *In vivo* delivery of pDNA and polymer nanoparticles multilayers from dual coated microneedles

In vivo co-delivery of Cy3-pLUC and DiD-PLGA NP to ear skin of MHC II-GFP mice. CLSM z-stack images of MHC II-GFP ear skin following $(PS/SPS)_{20}$-$(Poly\text{-}1/Cy3\text{-}pLUC)_{24}$-$(Poly\text{-}1/DiD\text{-}PLGA\ NP)_4$ coated microneedle array application for 24 hours indicates effective transfer of PEM films and delivery of pLUC and PLGA NP to epidermal LCs (scale bar 100 µm).

9.2. *Polymer Multilayer Tattooing for Enhanced DNA Vaccination*

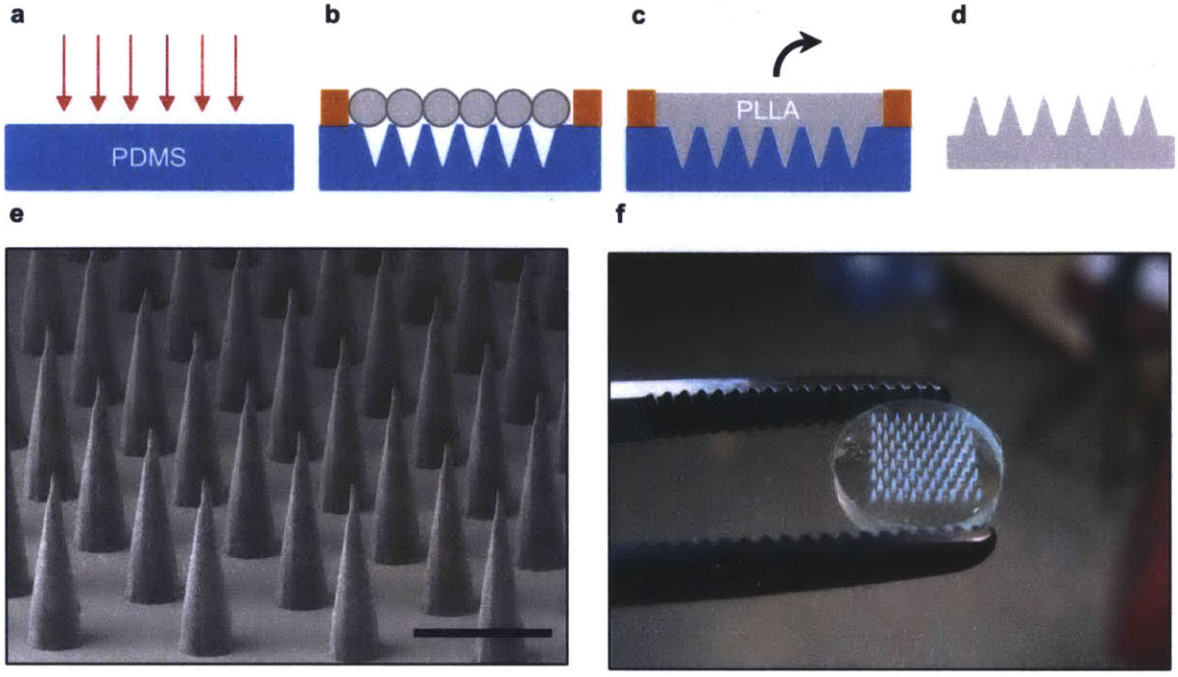

Supplementary Figure S3-1. PLLA microneedle fabrication

(a) *PDMS is laser ablated to form micron-scale cavities.* ***(b)*** *PLLA is added to the surface of the PDMS mold.* ***(c)*** *PLLA is melted under vacuum and then cooled before* ***(d)*** *removal of PLLA microneedle arrays.* ***(e)*** *SEM and* ***(f)*** *optical micrograph of PLLA microneedle arrays produced through PDMS melt-casting (scale bar - 500μm).*

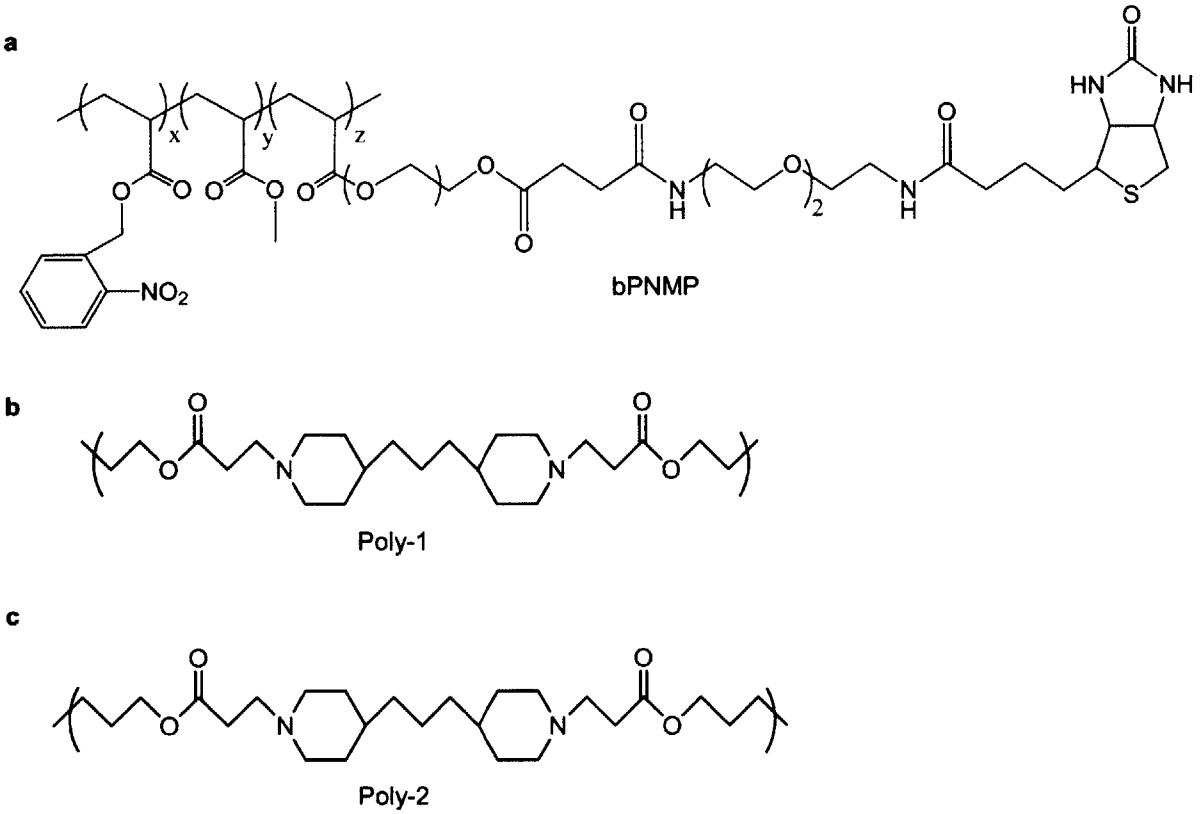

Supplementary Figure S3-2. Chemical structure of PNMP and PBAEs

(a) *Structure of biotinylated-PNMP (bPNMP, MW~17,000 Da, x:y:z – 31:59:10) in which a pendant biotin is conjugated to the free hydroxyl terminus of the PEG-methacrylate monomer unit.* ***(b)*** *Chemical structure of poly-1 (MW~15,000 Da) and* ***(c)*** *poly-2 (MW~21,000 Da) used in this study.*

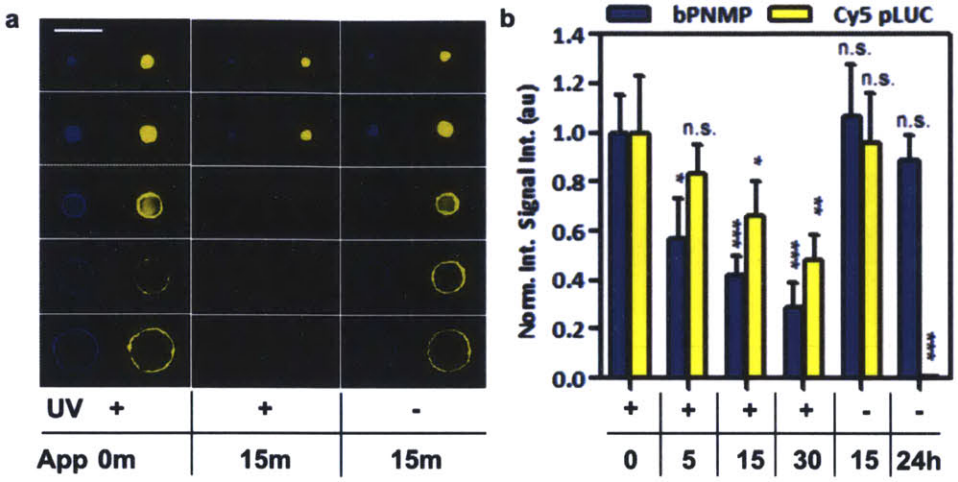

Supplementary Figure S3-3. *In vitro* release of polymer multilayers from coated microneedles

(a) *Representative confocal images of a (SAv488-bPNMP)(PS/SPS)$_{20}$(poly-1/Cy5-pLUC)$_{35}$-coated PLLA microneedle prepared with UV treatment of the PNMP release layer, before immersion in pH 7.4 PBS (left; lateral sections - 100μm interval; scale 200μm; blue - Sav488-bPNMP; yellow - Cy5-pLUC) and after 15 min in PBS (middle); this is compared to an identical multilayer-coated needle immersed in PBS for 15 min, where the PNMP release layer was not primed with UV prior to multilayer assembly (right).* ***(b)*** *Quantitation of confocal imaging (n = 15 microneedles) showing UV-dependent loss of SAv488-bPNMP and Cy5-pLUC signal following PBS exposure.*

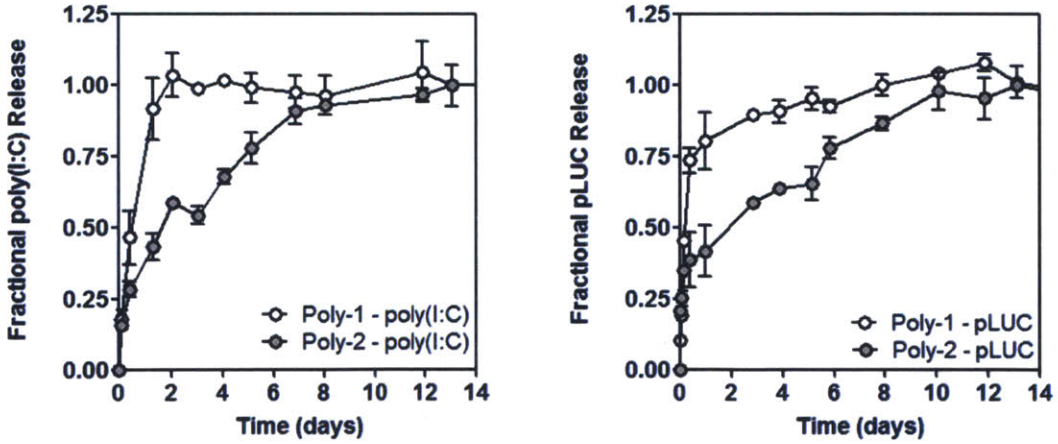

Supplementary Figure S3-4. *In vitro* release of pDNA and RNA from polymer multilayers

In vitro release of pLUC and poly(I:C) from (PS/SPS)$_{20}$(PBAE/pLUC)$_{35}$ and (PS/SPS)$_{20}$(PBAE/poly(I:C))$_{35}$ films on silicon.

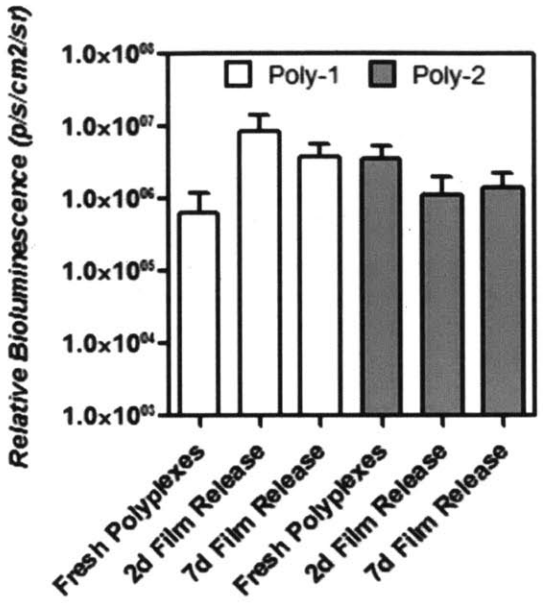

Supplementary Figure S3-5. Bioactivity of multilayer released pDNA *in vivo*

$(PS/SPS)_{20}(PBAE/pLUC)_{25}$ films were constructed using either poly-1 or poly-2 as the PBAE component. Films were then incubated in PBS at 37°C for 7 days and release fractions were collected after 2 or 7 days. Release fractions were normalized for concentration and injected intradermally (1μg) in the auricular skin. Fresh PBAE/pLUC polyplexes were formed by mixing poly-1 and poly-2 with fresh pLUC and these were similarly injected for comparison with polyplexes released from degrading $(PS/SPS)_{20}(PBAE/pLUC)_{25}$ films.

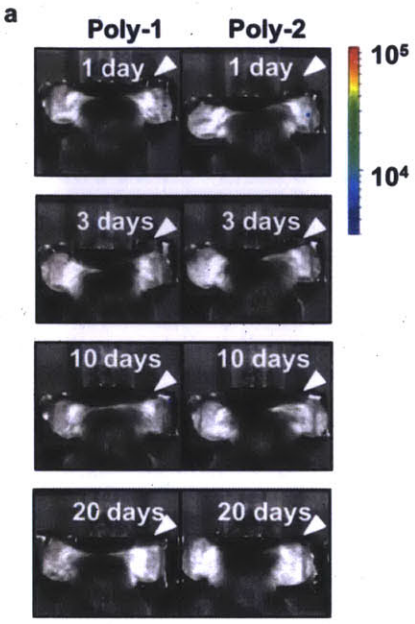

Supplementary Figure S3-6. Expression of pDNA following pDNA microneedle tattooing

Whole animal bioluminescence images of pLUC expression at application site 1, 3, 10, or 20 days following a 15 min application of (SAv488-bPNMP)((PS/SPS)$_{20}$(poly-1/pLUC)$_{35}$ coated microneedle array without UV pretreatment of the PNMP release layer. No bioluminescence signal was detected in the treated ears (marked by white arrows).

9.3. Releasable Layer-by-Layer Assembly of Stabilized Lipid Nanocapsules on Microneedles for Enhanced Transcutaneous Vaccine Delivery

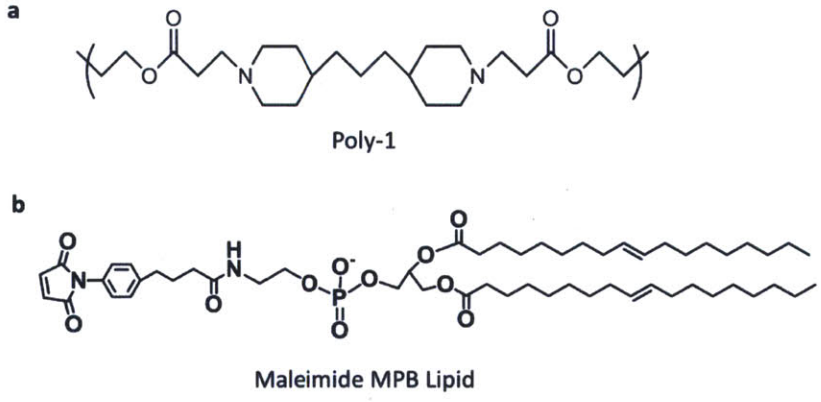

Supplementary Figure S4-1. Chemical structures of PBAE and MBP lipid

Chemical structures of ***(a)*** *poly(β-amino ester) poly-1 and* ***(b)*** *maleimide MBP lipid used in this study.*

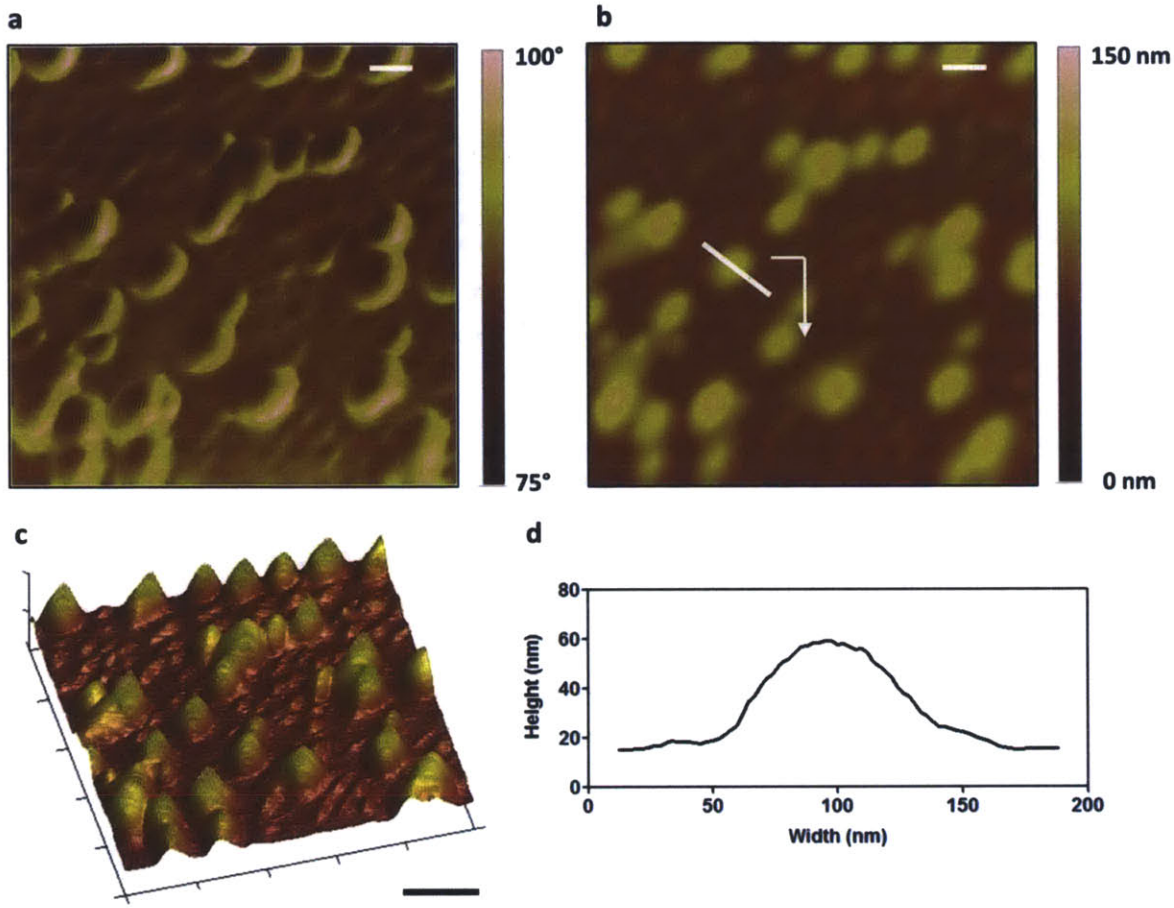

Supplementary Figure S4-2. AFM characterization of room temperature stored ICMV multilayers

AFM phase ***(a)*** *and height* ***(b)*** *micrographs of a* $(PS/SPS)_{20}(poly\text{-}1/ICMV)_5$ *multilayer built on silicon after 7 days at room temperature (scale bar 100nm).* ***(c)*** *3-D rendered AFM height micrograph data for a* $(PS/SPS)_{20}(poly\text{-}1/ICMV)_5$ *multilayer after storage for 7 days (scale bar 100nm).* ***(d)*** *Height trace data (trace shown in e) for a single embedded ICMV in a* $(PS/SPS)_{20}(poly\text{-}1/ICMV)_5$ *multilayer following room temperature storage.*

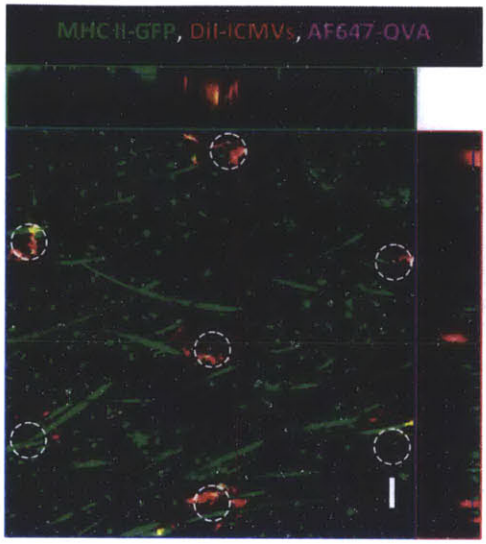

Supplementary Figure S4-3. *In vivo* microneedle delivery of ICMV multilayers

Representative confocal image of mouse skin treated for 5 minutes with $(PS/SPS)_{20}(poly\text{-}1/ICMV)_{35}$ multilayer-coated PLGA microneedles after 6 hours showing ICMV delivery at microneedle insertion sites (outlined) colocalized with APCs and in depots several hundred microns below the skin surface. Shown is fluorescent signal from MHC II-GFP (green), DiI-ICMVs (red), AF647-OVA (pink), and overlay (yellow) (scale bar 100μm).

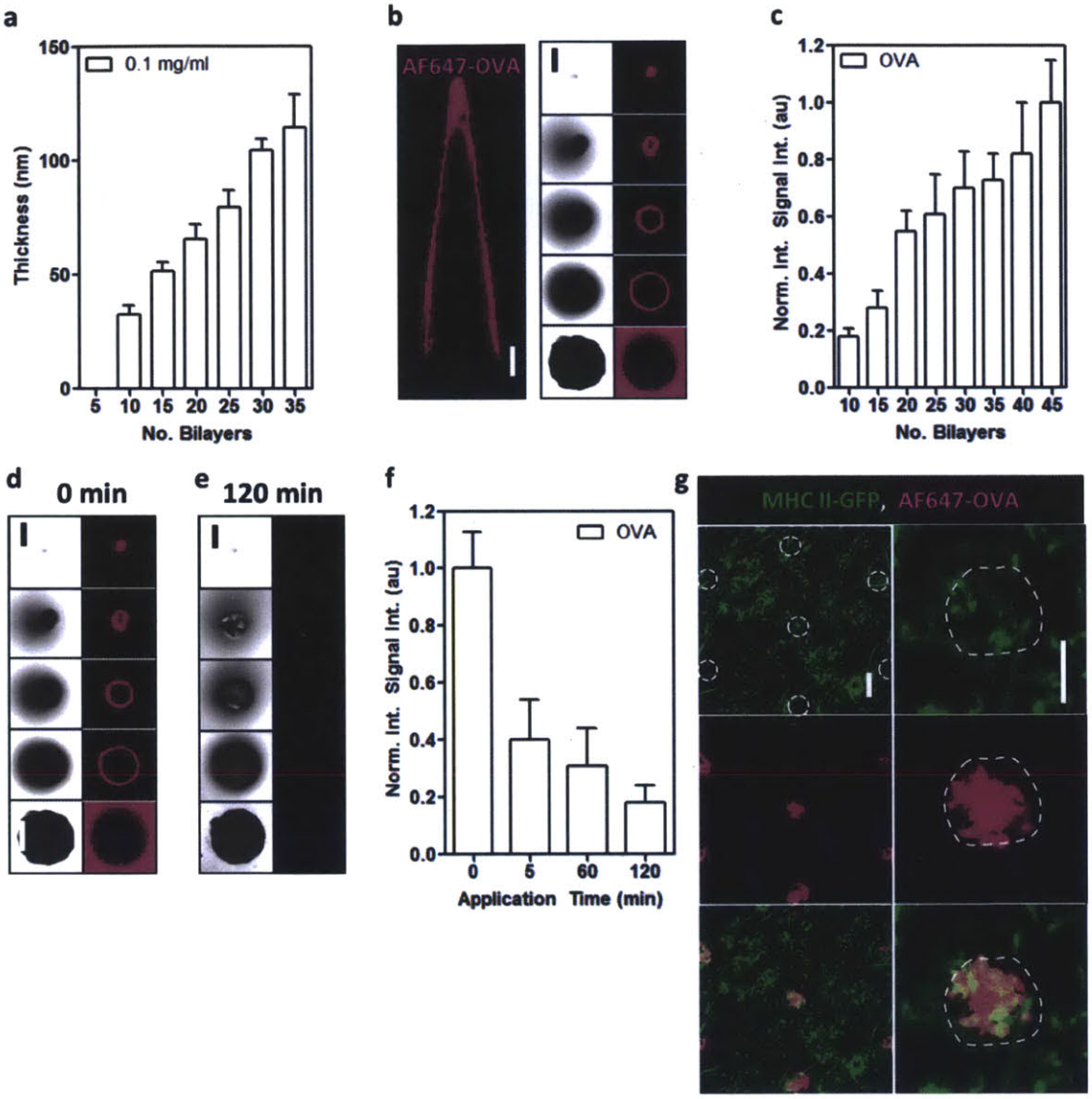

Supplementary Figure S4-4. Microneedle deposition and delivery of OVA multilayers

(a) *Growth curve for (poly-1/OVA)$_n$ multilayers on (PS/SPS)$_{20}$ on silicon, as assessed by surface profilometry.* ***(b)*** *Representative confocal images of PLGA microneedles coated with (PS/SPS)$_{20}$(poly-1/AF647-OVA)$_{45}$ films (left – transverse optical sections; right – lateral sections, 100μm interval; scale bar 100 μm; pink – AF647-OVA).* ***(c)*** *Quantification of AF647-OVA incorporation into (PS/SPS)$_{20}$(poly-1/AF647-OVA)$_n$ films on microneedles through confocal fluorescence intensity analysis (n = 15). Representative confocal images of PLGA microneedles coated with (PS/SPS)$_{20}$(poly-1/OVA)$_{45}$ films (lateral sections, 100μm interval; scale bar 100 μm; pink – AF647-OVA)* ***(d)*** *before application and* ***(e)*** *after a 120 minute application to murine skin in vivo.* ***(f)*** *Quantitation of confocal fluorescence intensities (n = 15) showing loss of AF647-OVA films from coated microneedles upon application to skin for 5, 60,*

or 120 minutes. Representative confocal images of mouse skin treated for 5 minutes with $(PS/SPS)_{20}(poly\text{-}1/OVA)_{45}$ multilayer-coated PLGA microneedles after ***(g)*** *6 hours showing ICMV delivery at microneedle insertion sites (outlined). Shown is fluorescent signal from (top to bottom) MHC II-GFP (green), AF647-OVA (pink), and overlay (scale bar 100μm).*

9.4. Composite Dissolving Microneedles for Coordinated Control of Antigen and Adjuvant Delivery Kinetics in Transcutaneous Vaccination

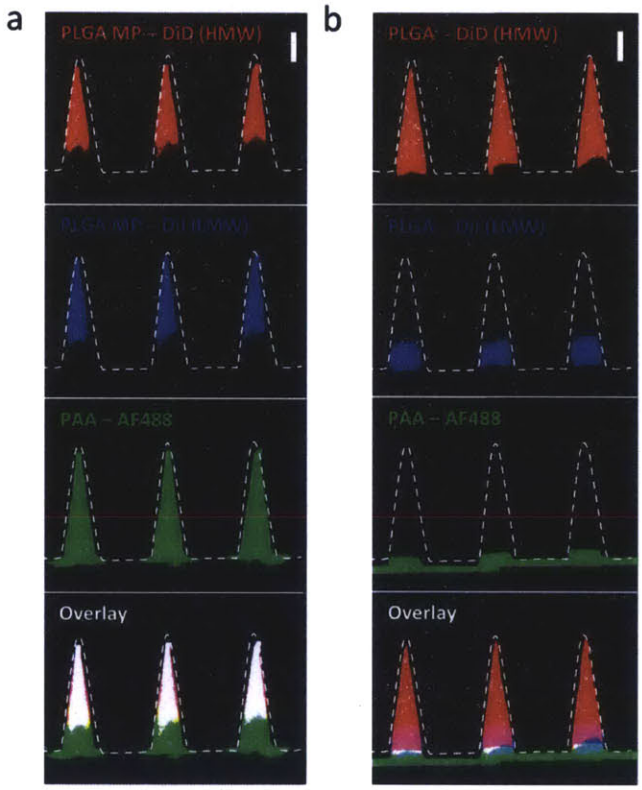

Supplementary Figure S5-1. Characterization of composite microneedles encapsulating multiple cargos

(a) *Confocal micrographs of PLGA-PAA composite microneedles fabricated to encapsulate both DiD- and DiI-loaded PLGA microparticles of high molecular weight (HWM) or low molecular weight (LWM) respectively (right, scale bar 200 μm)* ***(b)*** *Confocal micrographs of resulting PLGA-PAA composite microneedles fabricated to encapsulate a layered DiI/DiD-loaded PLGA tip implant (scale bar 200 μm). DiD and DiI were encapsulated in PLGA microparticles synthesized from PLGA with IV 0.35 (LMW) or 0.70 (HMW).*

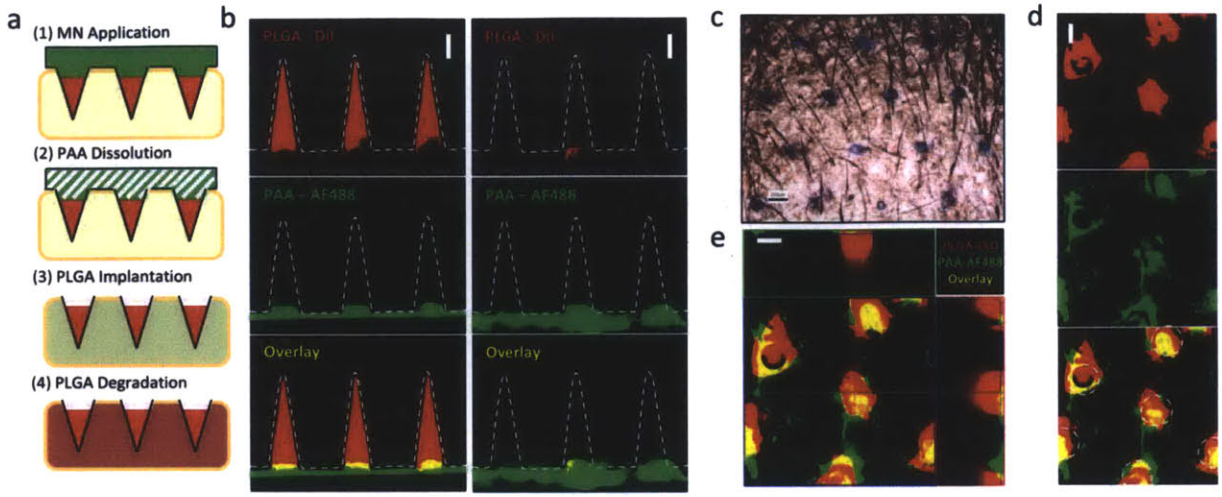

Supplementary Figure S5-2. *In vivo* delivery of solid PLGA-PAA composite microneedles

(a) *Microneedle delivery scheme: (1) Microneedle arrays are applied briefly to penetrate murine skin. (2) Cutaneous microneedle penetration exposes needles to interstitial fluid resulting in rapid dissolution of the supportive PAA pedestal. (3) Following microneedle base removal, released PLGA tips are left behind at penetration sites where soluble PAA-encapsulated cargoes are rapidly delivered to the surround tissue. (4) PLGA deposition into the skin establishes a depot for sustained delivery of encapsulated cargoes over time.* ***(b)*** *Confocal micrographs of solid DiD-loaded PLGA tip microneedles before application (left) and following a 5 minute application to murine skin (right, scale bar 200 μm).* ***(c)*** *Optical micrograph of microneedle treated skin showing penetration sites stained using trypan blue (scale bar 500 μm).* ***(d)*** *Confocal micrograph of treated skin, showing deposition of DiD-loaded PLGA tip implants together with soluble AF488-loaded PAA at needle penetration sites directly following microneedle application for 5 minutes (right, scale bar 100 μm, penetration sites outlined).* ***(e)*** *Reconstructed confocal z-stack depicting the microneedle application site showing deposition of PLGA-loaded cargoes within the cutaneous tissue (right, scale bar 100 μm).*

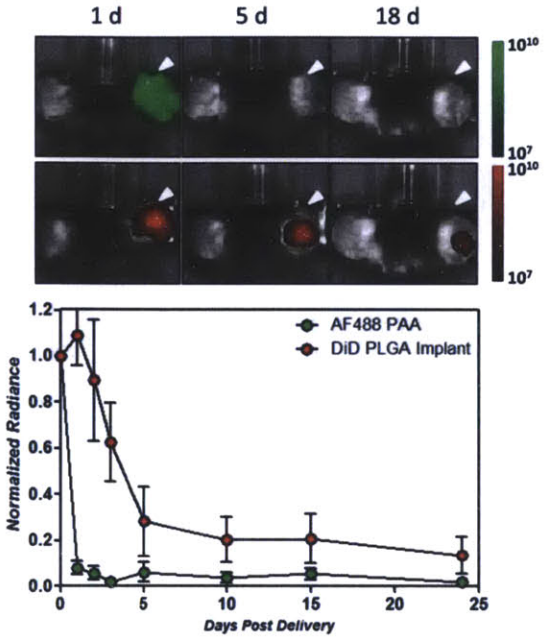

Supplementary Figure S5-3. ***In vivo*** **control over cargo release following solid PLGA-PAA microneedle treatment**

(a) *Whole animal fluorescence imaging of mice treated with DiD-loaded solid PLGA tip microneedles with AF488-loaded PAA pedestals after 1, 5, and 18 days. Fluorescence signal from AF488-PAA and DiD-PLGA implants is shown.* ***(b)*** *Quantification of relative fluorescent signal detected at microneedle application site for bulk implant delivery.*

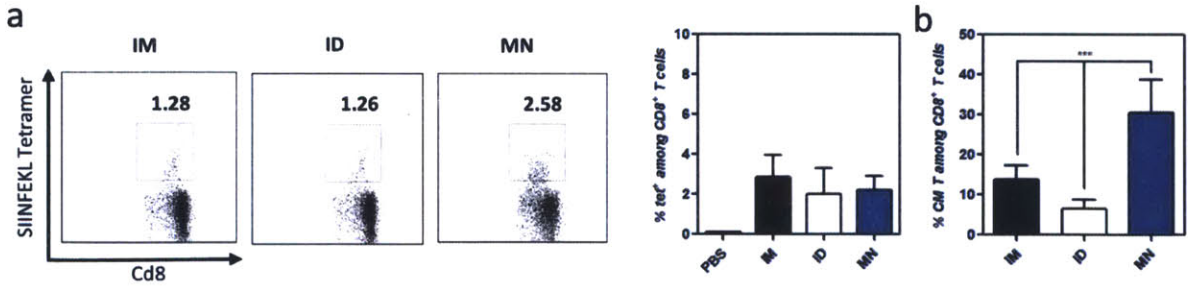

Supplementary Figure S5-4. ***In vivo*** **cellular immunogenicity for composite microneedle subunit vaccination**

(a) *Frequency of SIINFEKL-specific T cells in peripheral blood assessed by flow cytometry analysis of tetramer$^+$ CD8$^+$ T cells. Shown are representative cytometry plots from individual mice and mean tetramer$^+$ frequencies from day 14.* ***(b)*** *Analysis of T-cell effector/central memory phenotypes in peripheral blood by CD44/CD62L staining on tetramer$^+$ cells from peripheral blood. Shown are mean percentages of tetramer$^+$CD44$^+$CD62L$^+$ among CD8$^+$ T cells at day 28.*

9.5. *Implantable Silk Composite Microneedles for Programmable Vaccine Release Kinetics and Enhanced Immunogenicity in Transcutaneous Immunization*

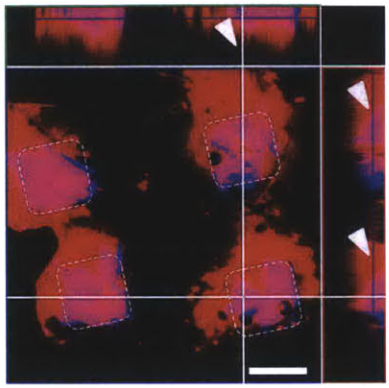

Supplementary Figure S6-1. Composite microneedles give effective cutaneous delivery.

Reconstructed confocal x-y/x-z/y-z image depicting the microneedle application site showing deposition of microparticle-cargos within the cutaneous tissue (AF647-OVA – blue, AF555-OVA – red, overlay – pink, scale bar 100 μ m).

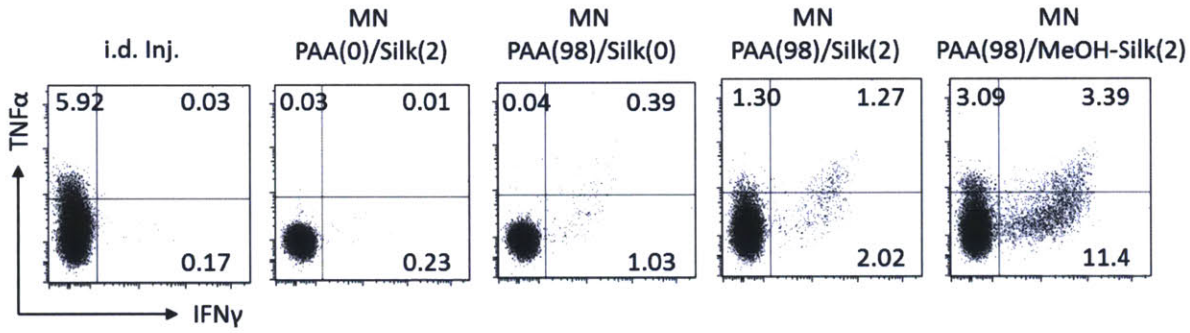

Supplementary Figure S6-2. Microneedle vaccination gives enhanced effector function.

Flow cytometry analysis of inflammatory cytokine expression following ex vivo antigen stimulation of PBMCs. Shown are representative cytometry plots of $IFN\gamma^+/TNF\alpha^+$ $CD8^+$ T cells measured on day 14.

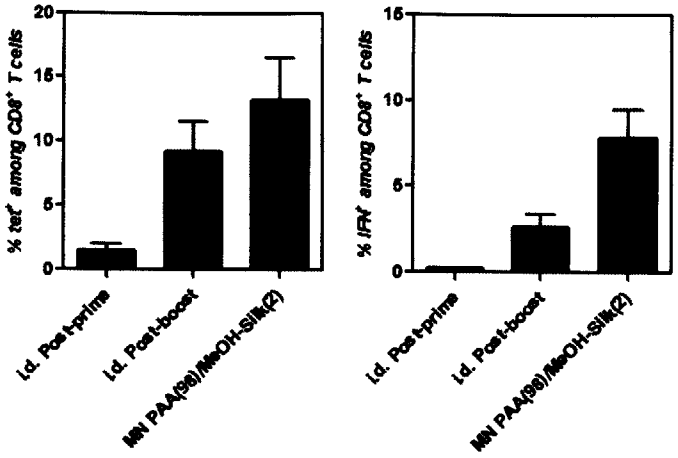

Supplementary Figure S6-3. Single microneedle vaccination gives comparable cellular immunity relative to prime-boost injection.

Mice were vaccinated on day 0 and 35 by i.d. injection, or on day 0 by microneedle treatment (+methanol to cross-link silk implants) to deliver 9 μg OVA and 150 ng polyI:C. . Microneedles were fabricated with 98% of the total vaccine dose in the PAA fraction, with the remaining 2% in the silk implant (MN PAA(98)/MeOH-Silk(2)). Flow cytometry analysis of antigen-specific $CD8^+$ T cell proliferation and cytokine secretion in peripheral blood. Shown is quantitative analysis of peak SIINFEKL-tetramer+ $CD8^+$ T cell frequencies for 14 days following either prime or boost immunization (left) and frequencies of $IFN\gamma^+$ among $CD8^+$ T cells on day 14 post prime/boost following in vitro restimulation with SIINFEKL (right).

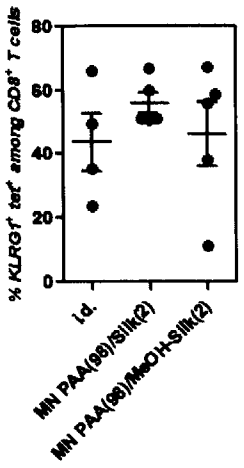

Supplementary Figure S6-4. Single microneedle vaccination gives prolonged antigen exposure.

Mice were vaccinated on day 0 and 35 by i.d. injection, or on day 0 by microneedle treatment (+methanol to cross-link silk implants) to deliver 9 μg OVA and 150 ng polyI:C. Microneedles were fabricated with 98% of the total vaccine dose in the PAA fraction, with the remaining 2% in the silk implant (MN PAA(98)/MeOH-Silk(2)). Flow cytometry analysis of antigen-specific $CD8^+$ T cell KLRG1 expression in peripheral blood. Shown is quantitative analysis of KLRG1 expression on SIINFEKL-tetramer$^+$ $CD8^+$ T cells for day 70 following vaccination.

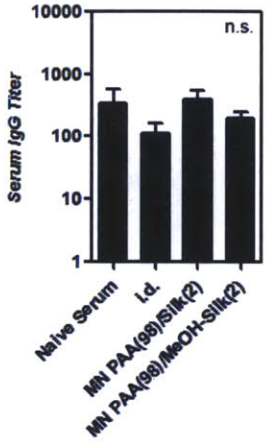

Supplementary Figure S6-5. Silk is non-immunogenic.

Mice were vaccinated on day 0 by i.d. injection or microneedle treatment (±methanol to cross-link silk implants) to deliver 9 μg OVA and 150 ng polyI:C. Microneedles were fabricated with 98% of the total vaccine dose in the PAA fraction, with the remaining 2% in the silk implant (MN PAA(98)/Silk(2) and MN PAA(98)/MeOH-Silk(2)). Shown are anti-Silk serum IgG levels for day 21 as measured by ELISA.

9.6. Immunogenic Delivery of Adenoviral Vectors in Nonhuman Primates from Skin Patches Enabling Dry, Refrigeration Free Vaccine Storage

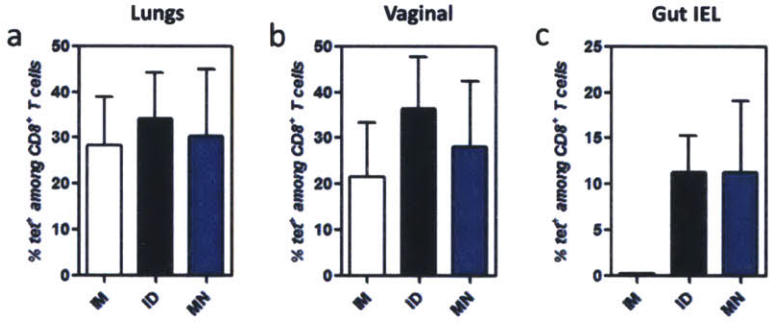

Supplementary Figure 7-1. Microneedles induce potent mucosal cellular immune responses in mice.

(a-c) *Frequencies of gag-specific CD8+ T-cells in mucosal tissues as assessed by flow cytometry analysis of tetramer$^+$ CD8$^+$ T-cells. Shown are mean±s.e.m. tetramer+ values from day 21 for* ***(a)*** *lungs* ***(b)*** *vaginal tissues, and* ***(c)*** *intraepithelial small intestinal tissues.*

10. REFERENCES

1 UNAIDS. Report on the global AIDS epidemic. (UNAIDS, 2008).

2 Letvin Norman, L. Progress and obstacles in the development of an AIDS vaccine. *Nat Rev Immunol* **6**, 930-939, (2006).

3 McMichael, A. J., Borrow, P., Tomaras, G. D., Goonetilleke, N. & Haynes, B. F. The immune response during acute HIV-1 infection: clues for vaccine development. *Nat. Rev. Immunol.* **10**, 11-23.

4 Kutzler, M. A. & Weiner, D. B. DNA vaccines: ready for prime time? *Nat. Rev. Genet.* **9**, 776-788, (2008).

5 Ulmer, J. B., Wahren, B. & Liu, M. A. Gene-based vaccines: Recent technical and clinical advances. *Trends Mol. Med.* **12**, 216-222, (2006).

6 Sumida, S. M. *et al.* Recruitment and expansion of dendritic cells in vivo potentiate the immunogenicity of plasmid DNA vaccines. *J. Clin. Invest.* **114**, 1334-1342, (2004).

7 Greenland, J. R. *et al.* Beta-Amino Ester Polymers Facilitate in Vivo DNA Transfection and Adjuvant Plasmid DNA Immunization. *Mol. Ther.* **12**, 164-170, (2005).

8 O'Hagan, D. T. & Singh, M. Microparticles as vaccine adjuvants and delivery systems. *Expert Rev. Vaccines* **2**, 269-283, (2003).

9 Chen, W. C. & Huang, L. Non-viral vector as vaccine carrier. *Adv. Genet.* **54**, 315-337, (2005).

10 Das, P. Revolutionary vaccine technology breaks the cold chain. *Lancet Infect Dis* **4**, 719, (2004).

11 Donatus, U., Bruce, G. & Robert, T. Model-Based Estimates of Risks of Disease Transmission and Economic Costs of Seven Injection Devices in Sub-Saharan Africa. *Bull World Health Organ* **80**, 859-870, (2002).

12 Weir, E. & Hatch, K. Preventing cold chain failure: vaccine storage and handling. *CMAJ* **171**, 1050, (2004).

13 Giudice, E. L. & Campbell, J. D. Needle-Free Vaccine Delivery. *Adv. Drug Delivery Rev.* **58**, 68-89, (2006).

14 A. Pruss-Ustun, E. R., Y. Hutin. in *WHO Environmental Burden of Disease Series, World Health Organization* (2003).

15 Dicko, M. *et al.* Safety of immunization injections in Africa: not simply a problem of logistics. *Bull World Health Organ* **78**, 163-169, (2000).

16 Miller, M. A. & Pisani, E. The cost of unsafe injections. *Bull World Health Organ* **77**, 808-811, (1999).

17 Simonsen, L., Kane, A., Lloyd, J., Zaffran, M. & Kane, M. Unsafe injections in the developing world and transmission of bloodborne pathogens: a review. *Bull World Health Organ* **77**, 789-800, (1999).

18 Ekwueme Donatus, U., Weniger Bruce, G. & Chen Robert, T. Model-based estimates of risks of disease transmission and economic costs of seven injection devices in sub-Saharan Africa. *Bull World Health Organ* **80**, 859-870, (2002).

19 Babiuk, S., Baca-Estrada, M., Babiuk, L. A., Ewen, C. & Foldvari, M. Cutaneous Vaccination: the Skin as an Immunologically Active Tissue and the Challenge of Antigen Delivery. *Journal of Controlled Release* **66**, 199-214, (2000).

20 Glenn, G. M. *et al.* Transcutaneous Immunization and Immunostimulant Strategies: Capitalizing on the Immunocompetence of the Skin. *Expert Rev. Vaccines* **2**, 253-267, (2003).

21 Warger, T., Schild, H. & Rechtsteiner, G. Initiation of Adaptive Immune Responses by Transcutaneous Immunization. *Immunol. Lett.* **109**, 13-20, (2007).

22 Quan, F.-S. *et al.* Stabilization of Influenza Vaccine Enhances Protection by Microneedle Delivery in the Mouse Skin. *PLoS One* **4**, e7152, (2009).

23 Kim, Y.-C. *et al.* Enhanced Memory Responses to Seasonal H1N1 Influenza Vaccination of the Skin with the Use of Vaccine-Coated Microneedles. *J Infect Dis* **201**, 190-198, (2010).

24 Nestle, F. O., Di Meglio, P., Qin, J.-Z. & Nickoloff, B. J. Skin Immune Sentinels in Health and Disease. *Nat. Rev. Immunol.* **9**, 679-691, (2009).

25 Lebre Maria, C. *et al.* Human keratinocytes express functional Toll-like receptor 3, 4, 5, and 9. *J Invest Dermatol* **127**, 331-341, (2007).

26 Kalali, B. N. *et al.* Double-Stranded RNA Induces an Antiviral Defense Status in Epidermal Keratinocytes through TLR3-, PKR-, and MDA5/RIG-I-Mediated Differential Signaling. *J. Immunol.* **181**, 2694-2704, (2008).

27 Albanesi, C., Scarponi, C., Giustizieri, M. L. & Girolomoni, G. Keratinocytes in inflammatory skin diseases. *Curr. Drug Targets: Inflammation Allergy* **4**, 329-334, (2005).

28 Miller, L. S. & Modlin, R. L. Human Keratinocyte Toll-like Receptors Promote Distinct Immune Responses. *J. Invest. Dermatol.* **127**, 262-263, (2007).

29 Klechevsky, E. *et al.* Functional specializations of human epidermal Langerhans cells and CD14+ dermal dendritic cells. *Immunity* **29**, 497-510, (2008).

30 Hunger, R. E. *et al.* Langerhans cells utilize CD1a and langerin to efficiently present nonpeptide antigens to T cells. *J. Clin. Invest.* **113**, 701-708, (2004).

31 Kissenpfennig, A. *et al.* Dynamics and function of langerhans cells in vivo: Dermal dendritic cells colonize lymph node areas distinct from slower migrating langerhans cells. *Immunity* **22**, 643-654, (2005).

32 Fukunaga, A., Khaskhely, N. M., Sreevidya, C. S., Byrne, S. N. & Ullrich, S. E. Dermal Dendritic Cells, and Not Langerhans Cells, Play an Essential Role in Inducing an Immune Response. *J. Immunol.* **180**, 3057-3064, (2008).

33 Guttman-Yassky, E. *et al.* Major differences in inflammatory dendritic cells and their products distinguish atopic dermatitis from psoriasis. *J. Allergy Clin. Immunol.* **119**, 1210-1217, (2007).

34 Lowes, M. A. *et al.* Increase in TNF-alpha and inducible nitric oxide synthase-expressing dendritic cells in psoriasis and reduction with efalizumab (anti-CD11a). *Proc. Natl. Acad. Sci. U. S. A.* **102**, 19057-19062, (2005).

35 Serbina, N. V., Salazar-Mather, T. P., Biron, C. A., Kuziel, W. A. & Pamer, E. G. TNF/iNOS-producing dendritic cells mediate innate immune defense against bacterial infection. *Immunity* **19**, 59-70, (2003).

36 Glenn, G. M. *et al.* Transcutaneous immunization and immunostimulant strategies: capitalizing on the immunocompetence of the skin. *Expert Rev. Vaccines FIELD Full Journal Title:Expert Review of Vaccines* **2**, 253-267, (2003).

37 Glenn, G. M., Scharton-Kersten, T., Vassell, R., Matyas, G. R. & Alving, C. R. Transcutaneous immunization with bacterial ADP-ribosylating exotoxins as antigens and adjuvants. *Infect. Immun.* **67**, 1100-1106, (1999).
38 Kotloff, K. L. *et al.* Safety and immunogenicity of oral inactivated whole-cell Helicobacter pylori vaccine with adjuvant among volunteers with or without subclinical infection. *Infect. Immun.* **69**, 3581-3590, (2001).
39 Watabe, S. *et al.* Protection against influenza virus challenge by topical application of influenza DNA vaccine. *Vaccine* **19**, 4434-4444, (2001).
40 Mkrtichyan, M. *et al.* Immunostimulant adjuvant patch enhances humoral and cellular immune responses to DNA immunization. *DNA Cell Biol.* **27**, 19-24, (2008).
41 Enioutina, E. Y., Visic, D. & Daynes, R. A. The induction of systemic and mucosal immune responses to antigen-adjuvant compositions administered into the skin: Alterations in the migratory properties of dendritic cells appears to be important for stimulating mucosal immunity. *Vaccine* **18**, 2753-2767, (2000).
42 Glenn, G. M. *et al.* Transcutaneous immunization with cholera toxin protects mice against lethal mucosal toxin challenge. *J Immunol* **161**, 3211-3214, (1998).
43 Gockel, C. M., Bao, S. & Beagley, K. W. Transcutaneous immunization induces mucosal and systemic immunity: a potent method for targeting immunity to the female reproductive tract. *Mol. Immunol.* **37**, 537-544, (2000).
44 Scharton-Kersten, T. *et al.* Transcutaneous immunization with bacterial ADP-ribosylating exotoxins, subunits, and unrelated adjuvants. *Infect. Immun.* **68**, 5306-5313, (2000).
45 El-Ghorr, A. A., Williams, R. M., Heap, C. & Norval, M. Transcutaneous immunisation with herpes simplex virus stimulates immunity in mice. *FEMS Immunol. Med. Microbiol.* **29**, 255-261, (2000).
46 Prausnitz, M. R. Microneedles for transdermal drug delivery. *Adv. Drug Delivery Rev.* **56**, 581-587, (2004).
47 Jiang, J. *et al.* Coated microneedles for drug delivery to the eye. *Invest Ophthalmol Vis Sci* **48**, 4038-4043, (2007).
48 Gill, H. S. & Prausnitz, M. R. Coated microneedles for transdermal delivery. *J. Controlled Release* **117**, 227-237, (2007).
49 Gill, H. S. & Prausnitz, M. R. Coating formulations for microneedles. *Pharm. Res.* **24**, 1369-1380, (2007).
50 Park, J.-H., Allen, M. G. & Prausnitz, M. R. Biodegradable polymer microneedles: Fabrication, mechanics and transdermal drug delivery. *J. Controlled Release* **104**, 51-66, (2005).
51 McAllister, D. V. *et al.* Microfabricated needles for transdermal delivery of macromolecules and nanoparticles: Fabrication methods and transport studies. *Proc. Natl. Acad. Sci. U. S. A.* **100**, 13755-13760, (2003).
52 Lin, W. *et al.* Transdermal delivery of antisense oligonucleotides with microprojection patch (Macroflux) technology. *Pharm. Res.* **18**, 1789-1793, (2001).
53 Wu, X.-M., Todo, H. & Sugibayashi, K. Enhancement of skin permeation of high molecular compounds by a combination of microneedle pretreatment and iontophoresis. *J. Controlled Release* **118**, 189-195, (2007).
54 Matriano, J. A. *et al.* Macroflux microprojection array patch technology: a new and efficient approach for intracutaneous immunization. *Pharm. Res.* **19**, 63-70, (2002).

55 Cormier, M. *et al.* Transdermal delivery of desmopressin using a coated microneedle array patch system. *J. Controlled Release* **97**, 503-511, (2004).
56 Lee, J. W., Park, J.-H. & Prausnitz, M. R. Dissolving microneedles for transdermal drug delivery. *Biomaterials* **29**, 2113-2124, (2008).
57 Sullivan, S. P., Murthy, N. & Prausnitz, M. R. Minimally invasive protein delivery with rapidly dissolving polymer microneedles. *Adv. Mater.* **20**, 933-938, (2008).
58 Miyano, T. *et al.* Sugar Micro Needles as Transdermic Drug Delivery System. *Biomed. Microdevices* 7, 185-188, (2005).
59 Sullivan Sean, P. *et al.* Dissolving polymer microneedle patches for influenza vaccination. *Nat Med* **16**, 915-920.
60 Kim, B.-S., Park, S. W. & Hammond, P. T. Hydrogen-Bonding Layer-by-Layer-Assembled Biodegradable Polymeric Micelles as Drug Delivery Vehicles from Surfaces. *ACS Nano* **2**, 386-392, (2008).
61 Lynn, D. M. Peeling back the layers: controlled erosion and triggered disassembly of multilayered polyelectrolyte thin films. *Adv. Mater.* **19**, 4118-4130, (2007).
62 Macdonald, M., Rodriguez, N. M., Smith, R. & Hammond, P. T. Release of a model protein from biodegradable self assembled films for surface delivery applications. *J. Controlled Release* **131**, 228-234, (2008).
63 Jessel, N. *et al.* Multiple and time-scheduled in situ DNA delivery mediated by beta-cyclodextrin embedded in a polyelectrolyte multilayer. *Proc. Natl. Acad. Sci. U. S. A.* **103**, 8618-8621, (2006).
64 Su, X., Kim, B.-S., Kim, S. R., Hammond, P. T. & Irvine, D. J. Layer-by-Layer-Assembled Multilayer Films for Transcutaneous Drug and Vaccine Delivery. *ACS Nano* **3**, 3719-3729, (2009).
65 Akinc, A., Anderson, D. G., Lynn, D. M. & Langer, R. Synthesis of Poly(Beta-Amino Ester)s Optimized for Highly Effective Gene Delivery. *Bioconjugate Chem.* **14**, 979-988, (2003).
66 Little, S. R. *et al.* Poly-Beta amino ester-containing microparticles enhance the activity of nonviral genetic vaccines. *Proc. Natl. Acad. Sci. U. S. A.* **101**, 9534-9539, (2004).
67 Jewell, C. M., Zhang, J., Fredin, N. J. & Lynn, D. M. Multilayered polyelectrolyte films promote the direct and localized delivery of DNA to cells. *J. Controlled Release* **106**, 214-223, (2005).
68 Wood, K. C., Chuang, H. F., Batten, R. D., Lynn, D. M. & Hammond, P. T. Controlling interlayer diffusion to achieve sustained, multiagent delivery from layer-by-layer thin films. *Proc. Natl. Acad. Sci. U. S. A.* **103**, 10207-10212, (2006).
69 Lynn, D. M. & Langer, R. Degradable Poly(Beta-amino esters): Synthesis, Characterization, and Self-Assembly with Plasmid DNA. *J. Am. Chem. Soc.* **122**, 10761-10768, (2000).
70 Jewell, C. M. *et al.* Release of Plasmid DNA from Intravascular Stents Coated with Ultrathin Multilayered Polyelectrolyte Films. *Biomacromolecules* 7, 2483-2491, (2006).
71 Jewell, C. M. & Lynn, D. M. Multilayered Polyelectrolyte Assemblies as Platforms for the Delivery of DNA and Other Nucleic Acid-Based Therapeutics. *Adv. Drug Delivery Rev.* **60**, 979-999, (2008).
72 Saltzman, W. M. & Olbricht, W. L. Building drug delivery into tissue engineering. *Nat. Rev. Drug Discovery* **1**, 177-186, (2002).

73 Hu, Y. *et al.* Surface mediated in situ differentiation of mesenchymal stem cells on gene-functionalized titanium films fabricated by layer-by-layer technique. *Biomaterials* **30**, 3626-3635, (2009).
74 Zhang, J. & Lynn, D. M. Ultrathin multilayered films assembled from "charge-shifting" cationic polymers: extended, long-term release of plasmid DNA from surfaces. *Adv. Mater.* **19**, 4218-4223, (2007).
75 Zhang, J., Chua, L. S. & Lynn, D. M. Multilayered Thin Films that Sustain the Release of Functional DNA under Physiological Conditions. *Langmuir* **20**, 8015-8021, (2004).
76 Zhang, J., Montanez, S. I., Jewell, C. M. & Lynn, D. M. Multilayered Films Fabricated from Plasmid DNA and a Side-Chain Functionalized Poly(Beta-amino Ester): Surface-Type Erosion and Sequential Release of Multiple Plasmid Constructs from Surfaces. *Langmuir* **23**, 11139-11146, (2007).
77 Qi, B., Tong, X. & Zhao, Y. Layer-by-Layer Assembly of Two Different Polymer Micelles with Polycation and Polyanion Coronas. *Macromolecules* **39**, 5714-5719, (2006).
78 Volodkin, D. *et al.* Composite Multilayered Biocompatible Polyelectrolyte Films with Intact Liposomes: Stability and Temperature Triggered Dye Release. *Soft Matter* **4**, 122-130, (2008).
79 Soike, T. *et al.* Engineering a Material Surface for Drug Delivery and Imaging using Layer-by-Layer Assembly of Functionalized Nanoparticles. *Adv. Mater.* **22**, 1392-1397.
80 Bershteyn, A. *et al.* Polymer-supported lipid shells, onions, and flowers. *Soft Matter* **4**, 1787-1791, (2008).
81 Krogman, K. C., Lowery, J. L., Zacharia, N. S., Rutledge, G. C. & Hammond, P. T. Spraying asymmetry into functional membranes layer-by-layer. *Nat. Mater.* **8**, 512-518, (2009).
82 Datta, S. K. *et al.* A Subset of Toll-Like Receptor Ligands Induces Cross-presentation by Bone Marrow-Derived Dendritic Cells. *J. Immunol.* **170**, 4102-4110, (2003).
83 Schwarz, K. *et al.* Role of Toll-like receptors in costimulating cytotoxic T cell responses. *Eur J Immunol* **33**, 1465-1470, (2003).
84 Bonifaz, L. C. *et al.* In vivo targeting of antigens to maturing dendritic cells via the DEC-205 receptor improves T cell vaccination. *J. Exp. Med.* **199**, 815-824, (2004).
85 Wille-Reece, U. *et al.* HIV gag protein conjugated to a Toll-like receptor 7/8 agonist improves the magnitude and quality of Th1 and CD8+ T cell responses in nonhuman primates. *Proc. Natl. Acad. Sci. U. S. A.* **102**, 15190-15194, (2005).
86 Kwissa, M. *et al.* Adjuvanting a DNA vaccine with a TLR9 ligand plus Flt3 ligand results in enhanced cellular immunity against the simian immunodeficiency virus. *J. Exp. Med.* **204**, 2733-2746, (2007).
87 Prausnitz, M. R. & Langer, R. Transdermal drug delivery. *Nat. Biotechnol.* **26**, 1261-1268, (2008).
88 Boudou, T., Crouzier, T., Ren, K., Blin, G. & Picart, C. Multiple Functionalities of Polyelectrolyte Multilayer Films: New Biomedical Applications. *Adv. Mater.* **22**, 441-467, (2010).
89 Cavalieri, F., Postma, A., Lee, L. & Caruso, F. Assembly and Functionalization of DNA-Polymer Microcapsules. *ACS Nano* **3**, 234-240, (2009).

90 Dimitrova, M. *et al.* Sustained delivery of siRNAs targeting viral infection by cell-degradable multilayered polyelectrolyte films. *Proc. Natl. Acad. Sci. U. S. A.* **105**, 16320-16325, (2008).
91 Pearton, M. *et al.* Gene Delivery to the Epidermal Cells of Human Skin Explants Using Microfabricated Microneedles and Hydrogel Formulations. *Pharm. Res.* **25**, 407-416, (2008).
92 Mikszta, J. A. *et al.* Improved genetic immunization via micromechanical disruption of skin-barrier function and targeted epidermal delivery. *Nat. Med.* **8**, 415-419, (2002).
93 Gill, H. S., Soederholm, J., Prausnitz, M. R. & Saellberg, M. Cutaneous vaccination using microneedles coated with hepatitis C DNA vaccine. *Gene Ther.*, 811-814, (2010).
94 Samuel, R. E. & Hammond, P. T. Protamine-based surface mediated gene transfer devices.
95 Abramoff, M. D., Magelhaes, P. J. & Ram, S. J. Image Processing with Image J. *Biophotonics International* **11**, 36-42, (2004).
96 Boes, M. *et al.* T-cell Engagement of Dendritic Cells Rapidly Rearranges MHC Class II Transport. *Nature* **418**, 983-988, (2002).
97 Haq, M. I. *et al.* Clinical administration of microneedles: skin puncture, pain and sensation. *Biomed Microdevices* **11**, 35-47, (2009).
98 Wood, K. C., Boedicker, J. Q., Lynn, D. M. & Hammond, P. T. Tunable Drug Release from Hydrolytically Degradable Layer-by-Layer Thin Films. *Langmuir* **21**, 1603-1609, (2005).
99 Kim, B.-S., Smith, R. C., Poon, Z. & Hammond, P. T. MAD (Multiagent Delivery) Nanolayer: Delivering Multiple Therapeutics from Hierarchically Assembled Surface Coatings. *Langmuir* **25**, 14086-14092, (2009).
100 Liang, J. F., Yang, V. C. & Vaynshteyn, Y. The minimal functional sequence of protamine. *Biochem. Biophys. Res. Commun.* **336**, 653-659, (2005).
101 Samuel, R. E. *et al.* Osteoconductive Protamine-Based Polyelectrolyte Multilayer Functionalized Surfaces. *Biomaterials* **32**, 7491-7502, (2011).
102 Rice, J., Ottensmeier, C. H. & Stevenson, F. K. DNA vaccines: precision tools for activating effective immunity against cancer. *Nat. Rev. Cancer* **8**, 108-120, (2008).
103 Sardesai, N. Y. & Weiner, D. B. Electroporation delivery of DNA vaccines: prospects for success. *Curr. Opin. Immunol.* **23**, 421-429, (2011).
104 Bins, A. D. *et al.* A rapid and potent DNA vaccination strategy defined by in vivo monitoring of antigen expression. *Nat. Med.* **11**, 899-904, (2005).
105 Johansen, P. *et al.* Antigen kinetics determines immune reactivity. *Proc. Natl. Acad. Sci. U. S. A.* **105**, 5189-5194, (2008).
106 Jewell, C. M., Bustamante, L. S. C. & Irvine, D. J. In situ engineering of the lymph node microenvironment via intranodal injection of adjuvant-releasing polymer particles. *Proc. Natl. Acad. Sci. U. S. A.* **108**, 15745-15750, (2011).
107 Prlic, M., Hernandez-Hoyos, G. & Bevan, M. J. Duration of the initial TCR stimulus controls the magnitude but not functionality of the CD8+ T cell response. *J. Exp. Med.* **203**, 2135-2143, (2006).
108 Doh, J. & Irvine, D. J. Photogenerated polyelectrolyte bilayers from an aqueous-processible photoresist for multicomponent protein patterning. *J. Am. Chem. Soc.* **126**, 9170-9171, (2004).

109 Gross, S. *et al.* Bioluminescence imaging of myeloperoxidase activity in vivo. *Nat. Med.* **15**, 455-461, (2009).
110 Stoitzner, P. *et al.* Migration of Langerhans cells and dermal dendritic cells in skin organ cultures: augmentation by TNF-α and IL-1β. *J. Leukocyte Biol.* **66**, 462-470, (1999).
111 Decher, G. Fuzzy nanoassemblies: toward layered polymeric multicomposites. *Science* **277**, 1232-1237, (1997).
112 Hammond, P. T. Engineering Materials Layer-by-Layer: Challenges and Opportunities in Multilayer Assembly. *AIChE J.* **57**, 2928-2940, (2011).
113 MacDonald, M. L. *et al.* Tissue integration of growth factor-eluting layer-by-layer polyelectrolyte multilayer coated implants. *Biomaterials* **32**, 1446-1453, (2011).
114 Shah, N. J. *et al.* Tunable dual growth factor delivery from polyelectrolyte multilayer films. *Biomaterials* **32**, 6183-6193, (2011).
115 DeMuth, P. C., Su, X., Samuel, R. E., Hammond, P. T. & Irvine, D. J. Nano-Layered Microneedles for Transcutaneous Delivery of Polymer Nanoparticles and Plasmid DNA. *Adv. Mater.* **22**, 4851-4856, (2010).
116 Katz, J. S., Doh, J. & Irvine, D. J. Composition-Tunable Properties of Amphiphilic Comb Copolymers Containing Protected Methacrylic Acid Groups for Multicomponent Protein Patterning. *Langmuir* **22**, 353-359, (2006).
117 Su, X., Kim, B.-S., Kim Sara, R., Hammond Paula, T. & Irvine Darrell, J. Layer-by-Layer-Assembled Multilayer Films for Transcutaneous Drug and Vaccine Delivery. *ACS Nano* **3**, 3719-3729, (2009).
118 Zhang, J., Fredin, N. J., Janz, J. F., Sun, B. & Lynn, D. M. Structure/property relationships in erodible multilayered films: influence of polycation structure on erosion profiles and the release of anionic polyelectrolytes. *Langmuir* **22**, 239-245, (2006).
119 Soria-Castro, I. *et al.* Cot/tpl2 (MAP3K8) Mediates Myeloperoxidase Activity and Hypernociception following Peripheral Inflammation. *J. Biol. Chem.* **285**, 33805-33815, (2010).
120 Bechler, S. L. & Lynn, D. M. Characterization of Degradable Polyelectrolyte Multilayers Fabricated Using DNA and a Fluorescently-Labeled Poly(β-amino ester): Shedding Light on the Role of the Cationic Polymer in Promoting Surface-Mediated Gene Delivery. *Biomacromolecules* **13**, 542-552, (2012).
121 Elnekave, M., Furmanov, K. & Hovav, A.-H. Intradermal naked plasmid DNA immunization: mechanisms of action. *Expert Rev. Vaccines* **10**, 1169-1182, (2011).
122 van Drunen Littel-van den Hurk, S. & Hannaman, D. Electroporation for DNA immunization: clinical application. *Expert Rev. Vaccines* **9**, 503-517, (2010).
123 Sallusto, F., Geginat, J. & Lanzavecchia, A. Central memory and effector memory T cell subsets: Function, generation, and maintenance. *Annu. Rev. Immunol.* **22**, 745-763, (2004).
124 Saade, F. & Petrovsky, N. Technologies for enhanced efficacy of DNA vaccines. *Expert Rev. Vaccines* **11**, 189-209, (2012).
125 Zhu, Q. *et al.* Immunization by Vaccine-Coated Microneedle Arrays Protects Against Lethal Influenza Virus Challenge. *Proc. Natl. Acad. Sci. U. S. A.* **106**, 7968-7973, (2009).
126 Chen, X. *et al.* Improved DNA Vaccination by Skin-Targeted Delivery Using Dry-Coated Densely-Packed Microprojection Arrays. *J. Controlled Release* **148**, 327-333, (2010).

127 Song, J.-M. *et al.* DNA Vaccination in the Skin Using Microneedles Improves Protection Against Influenza. *Mol. Ther.* **20**, 1472-1480.
128 Verstrepen, B. E. *et al.* Improved HIV-1 specific T-cell responses by short-interval DNA tattooing as compared to intramuscular immunization in non-human primates. *Vaccine* **26**, 3346-3351, (2008).
129 Denet, A.-R., Vanbever, R. & Preat, V. Skin electroporation for transdermal and topical delivery. *Adv. Drug Delivery Rev.* **56**, 659-674, (2004).
130 Wallace, M. *et al.* Tolerability of Two Sequential Electroporation Treatments Using MedPulser DNA Delivery System (DDS) in Healthy Adults. *Mol. Ther.* **17**, 922-928, (2009).
131 DeVilliers, M. M., Otto, D. P., Strydom, S. J. & Lvov, Y. M. Introduction to Nanocoatings Produced by Layer-by-Layer (LbL) Self-Assembly. *Adv. Drug Delivery Rev.* **63**, 701-715, (2011).
132 Katagiri, K., Hamasaki, R., Ariga, K. & Kikuchi, J.-i. Layered Paving of Vesicular Nanoparticles Formed with Cerasome as a Bioinspired Organic-Inorganic Hybrid. *J. Am. Chem. Soc.* **124**, 7892-7893, (2002).
133 Katagiri, K., Hamasaki, R., Ariga, K. & Kikuchi, J.-i. Layer-by-Layer Self-Assembling of Liposomal Nanohybrid "Cerasome" on Substrates. *Langmuir* **18**, 6709-6711, (2002).
134 Graf, N. *et al.* Electrochemically Driven delivery to Cells from Vesicles Embedded in Polyelectrolyte Multilayers. *Soft Matter* **8**, 3641-3648, (2012).
135 Michel, M. *et al.* Layer-by-Layer Self-Assembled Polyelectrolyte Multilayers with Embedded Liposomes: Immobilized Submicronic Reactors for Mineralization. *Langmuir* **22**, 2358-2364, (2006).
136 Michel, M. *et al.* Layer by Layer Self-Assembled Polyelectrolyte Multilayers with Embedded Phospholipid Vesicles Obtained by Spraying: Integrity of the Vesicles. *Langmuir* **21**, 7854-7859, (2005).
137 Michel, M., Vautier, D., Voegel, J.-C., Schaaf, P. & Ball, V. Layer by Layer Self-Assembled Polyelectrolyte Multilayers with Embedded Phospholipid Vesicles. *Langmuir* **20**, 4835-4839, (2004).
138 Volodkin, D. V., Schaaf, P., Mohwald, H., Voegel, J.-C. & Ball, V. Effective Embedding of Liposomes into Polyelectrolyte Multilayered Films: the Relative Importance of Lipid-Polyelectrolyte and Interpolyelectrolyte Interactions. *Soft Matter* **5**, 1394-1405, (2009).
139 Moon, J. J. *et al.* Interbilayer-Crosslinked Multilamellar Vesicles as Synthetic Vaccines for Potent Humoral and Cellular Immune Responses. *Nat. Mater.* **10**, 243-251, (2011).
140 Moon, J. J. *et al.* Enhancing Humoral Responses to a Malaria Antigen with Nanoparticle Vaccines that Expand Tfh Cells and Promote Germinal Center Induction. *Proc. Natl. Acad. Sci. U. S. A.* **109**, 1080-1085, (2012).
141 Wermeling, D. P. *et al.* Microneedles Permit Transdermal Delivery of a Skin-Impermeant Medication to Humans. *Proc. Natl. Acad. Sci. U. S. A.* **105**, 2058-2063, (2008).
142 Sullivan, S. P. *et al.* Dissolving Polymer Microneedle Patches for Influenza Vaccination. *Nat Med* **16**, 915-920, (2009).
143 Pruss-Ustun, A., Rapita, E. & Hutin, Y. Sharps injuries: global burden of disease from sharps injuries to health-care workers. *World Health Organization*, (2003).
144 Saurer, E. M., Flessner, R. M., Sullivan, S. P., Prausnitz, M. R. & Lynn, D. M. Layer-by-Layer Assembly of DNA- and Protein-Containing Films on Microneedles for Drug Delivery to the Skin. *Biomacromolecules* **11**, 3136-3143, (2010).

145 Kupper, T. S. & Fuhlbrigge, R. C. Immune Surveillance in the Skin: Mechanisms and Clinical Consequences. *Nat. Rev. Immunol.* **4**, 211-222, (2004).
146 Merad, M., Ginhoux, F. & Collin, M. Origin, Homeostasis and Function of Langerhans Cells and Other Langerin-Expressing Dendritic Cells. *Nat. Rev. Immunol.* **8**, 935-947, (2008).
147 Ichinose, I., Fujiyoshi, K., Mizuki, S., Lvov, Y. & Kunitake, T. Layer-by-Layer Assembly of Aqueous Bilayer Membranes on Charged Surfaces. *Chem. Lett.*, 257-258, (1996).
148 Zhang, L., Longo, M. L. & Stroeve, P. Mobile Phospholipid Bilayers Supported on a Polyion/Alkylthiol Layer Pair. *Langmuir* **16**, 5093-5099, (2000).
149 Prow, T. W. *et al.* Nanopatch-Targeted Skin Vaccination against West Nile Virus and Chikungunya Virus in Mice. *Small* **6**, 1776-1784, (2010).
150 Ruutu, M. P., Chen, X., Joshi, O., Kendall, M. A. & Frazer, I. H. Increasing mechanical stimulus induces migration of Langerhans cells and impairs the immune response to intracutaneously delivered antigen. *Exp. Dermatol.* **20**, 534-536, (2011).
151 Adams, S. *et al.* Immunization of Malignant Melanoma Patients with Full-Length NY-ESO-1 Protein Using TLR7 Agonist Imiquimod as Vaccine Adjuvant. *J. Immunol.* **181**, 776-784, (2008).
152 Mwangi, W. *et al.* DNA-encoded fetal liver tyrosine kinase 3 ligand and granulocyte macrophage-colony-stimulating factor increase dendritic cell recruitment to the inoculation site and enhance antigen-specific CD4+ T cell responses induced by DNA vaccination of outbred animals. *J. Immunol.* **169**, 3837-3846, (2002).
153 Soiffer, R. *et al.* Vaccination with irradiated autologous melanoma cells engineered to secrete human granulocyte-macrophage colony-stimulating factor generates potent antitumor immunity in patients with metastatic melanoma. *Proc. Natl. Acad. Sci. U. S. A.* **95**, 13141-13146, (1998).
154 Akira, S., Uematsu, S. & Takeuchi, O. Pathogen Recognition and Innate Immunity. *Cell* **124**, 783-801, (2006).
155 Gay, N. J., Gangloff, M. & Weber, A. N. R. Toll-Like Receptors as Molecular Switches. *Nat. Rev. Immunol.* **6**, 693-698, (2006).
156 Manicassamy, S. & Pulendran, B. Modulation of Adaptive Immunity with Toll-Like Receptors. *Semin. Immunol.* **21**, 185-193, (2009).
157 Aucan, C. *et al.* High Immunoglobulin G2 (IgG2) and Low IgG4 Levels are Associated with Human Resistance to Plasmodium Falciparum Malaria. *Infect. Immun.* **68**, 1252-1258, (2000).
158 Beenhouwer, D. O., Yoo, E. M., Lai, C.-W., Rocha, M. A. & Morrison, S. L. Human Immunoglobulin G2 (IgG2) and IgG4, but Not IgG1 or IgG3, Protect Mice Against Cryptococcus Neoformans Infection. *Infect. Immun.* **75**, 1424-1435, (2007).
159 Nimmerjahn, F. & Ravetch, J. V. Divergent Immunoglobulin G Subclass Activity Through Selective Fc Receptor Binding. *Science* **310**, 1510-1512, (2005).
160 Chu, L. Y., Choi, S.-O. & Prausnitz, M. R. Fabrication of dissolving polymer microneedles for controlled drug encapsulation and delivery: bubble and pedestal microneedle designs. *J. Pharm. Sci.* **99**, 4228-4238, (2010).
161 Fukushima, K. *et al.* Two-layered dissolving microneedles for percutaneous delivery of peptide/protein drugs in rats. *Pharm. Res.* **28**, 7-21, (2011).

162 Lee, J. W., Choi, S.-O., Felner, E. I. & Prausnitz, M. R. Dissolving Microneedle Patch for Transdermal Delivery of Human Growth Hormone. *Small* **7**, 531-539, (2011).
163 Lee, J. W., Park, J.-H. & Prausnitz, M. R. Dissolving microneedles for transdermal drug delivery. *Biomaterials* **29**, 2113-2124, (2008).
164 Lee, K., Lee, C. Y. & Jung, H. Dissolving microneedles for transdermal drug administration prepared by stepwise controlled drawing of maltose. *Biomaterials* **32**, 3134-3140, (2011).
165 Migalska, K. *et al.* Laser-Engineered Dissolving Microneedle Arrays for Transdermal Macromolecular Drug Delivery. *Pharm. Res.* **28**, 1919-1930, (2011).
166 Raphael, A. P. *et al.* Targeted, Needle-Free Vaccinations in Skin using Multilayered, Densely-Packed Dissolving Microprojection Arrays. *Small* **6**, 1785-1793, (2010).
167 Matsuo, K. *et al.* Transcutaneous immunization using a dissolving microneedle array protects against tetanus, diphtheria, malaria, and influenza. *J Control Release*, (2012).
168 Matsuo, K. *et al.* A low-invasive and effective transcutaneous immunization system using a novel dissolving microneedle array for soluble and particulate antigens. *J Control Release*, (2012).
169 Wang, P. M., Cornwell, M., Hill, J. & Prausnitz, M. R. Precise Microinjection into Skin Using Hollow Microneedles. *J. Invest. Dermatol.* **126**, 1080-1087, (2006).
170 Gill, H. S. & Prausnitz, M. R. Coated microneedles for transdermal delivery. *J. Controlled Release* **117**, 227-237, (2007).
171 Park, J.-H., Allen, M. G. & Prausnitz, M. R. Polymer microneedles for controlled-release drug delivery. *Pharm. Res.* **23**, 1008-1019, (2006).
172 Tsioris, K. *et al.* Fabrication of Silk Microneedles for Controlled-Release Drug Delivery. *Adv. Funct. Mater.* **22**, 330-335, (2012).
173 Zhang, W. *et al.* Combination of microneedles with PLGA nanoparticles as a potential strategy for topical drug delivery. *Curr. Nanosci.* **7**, 545-551, (2011).
174 Ke, C.-J. *et al.* Multidrug release based on microneedle arrays filled with pH-responsive PLGA hollow microspheres. *Biomaterials*, Ahead of Print.
175 Kim, M. Y., Jung, B. & Park, J.-H. Hydrogel swelling as a trigger to release biodegradable polymer microneedles in skin. *Biomaterials* **33**, 668-678, (2012).
176 Bins, A. D. *et al.* A rapid and potent DNA vaccination strategy defined by in vivo monitoring of antigen expression. *Nat. Med. (N. Y., NY, U. S.)* **11**, 899-904, (2005).
177 Smith, K. A. *et al.* Multivalent immunity targeting tumor-associated antigens by intra-lymph node DNA-prime, peptide-boost vaccination. *Cancer Gene Ther.* **18**, 63-76, (2011).
178 Smith, K. A. *et al.* Enhancing DNA vaccination by sequential injection of lymph nodes with plasmid vectors and peptides. *Vaccine* **27**, 2603-2615, (2009).
179 Wick, D. A., Martin, S. D., Nelson, B. H. & Webb, J. R. Profound CD8+ T cell immunity elicited by sequential daily immunization with exogenous antigen plus the TLR3 agonist poly(I:C). *Vaccine* **29**, 984-993, (2011).
180 Senti, G. *et al.* Intralymphatic allergen administration renders specific immunotherapy faster and safer: a randomized controlled trial. *Proc. Natl. Acad. Sci. U. S. A.* **105**, 17908-17912, (2008).
181 Weber, J. *et al.* Phase 1 Trial of Intranodal Injection of a Melan-A/MART-1 DNA Plasmid Vaccine in Patients With Stage IV Melanoma. *J. Immunother.* **31**, 215-223, (2008).

182 Fan, X.-D., Hsieh, Y.-L., Krochta, J. M. & Kurth, M. J. Study on molecular interaction behavior, and thermal and mechanical properties of polyacrylic acid and lactose blends. *J. Appl. Polym. Sci.* **82**, 1921-1927, (2001).

183 Final report on the safety assessment of Carbomers-934, -910, -934P, -940, -941, and -962. *J. Am. Coll. Toxicol.* **1**, 109-141, (1982).

184 Newman, K. D., Elamanchili, P., Kwon, G. S. & Samuel, J. Uptake of poly(D,L-lactic-co-glycolic acid) microspheres by antigen-presenting cells in vivo. *J. Biomed. Mater. Res.* **60**, 480-486, (2002).

185 Peyre, M., Fleck, R., Hockley, D., Gander, B. & Sesardic, D. In vivo uptake of an experimental microencapsulated diphtheria vaccine following subcutaneous immunization. *Vaccine* **22**, 2430-2437, (2004).

186 Randolph, G. J., Inaba, K., Robbiani, D. F., Steinman, R. M. & Muller, W. A. Differentiation of phagocytic monocytes into lymph node dendritic cells in vivo. *Immunity* **11**, 753-761, (1999).

187 Stahl-Hennig, C. *et al.* Synthetic double-stranded RNAs are adjuvants for the induction of T helper 1 and humoral immune responses to human papillomavirus in rhesus macaques. *PLoS Pathog.* **5**, e1000373, (2009).

188 Sallusto, F., Geginat, J. & Lanzavecchia, A. Central memory and effector memory T cell subsets: Function, generation, and maintenance. *Annu. Rev. Immunol.* **22**, 745-763, (2004).

189 Johansen, P. *et al.* Antigen kinetics determines immune reactivity. *Proc. Natl. Acad. Sci. U. S. A.* **105**, 5189-5194, (2008).

190 Bachmann, M. F. *et al.* Long-lived memory CD8+ T cells are programmed by prolonged antigen exposure and low levels of cellular activation. *Eur. J. Immunol.* **36**, 842-854, (2006).

191 Shaulov, A. & Murali-Krishna, K. CD8 T Cell Expansion and Memory Differentiation Are Facilitated by Simultaneous and Sustained Exposure to Antigenic and Inflammatory Milieu. *J. Immunol.* **180**, 1131-1138, (2008).

192 DeMuth, P. C., Garcia-Beltran, W. F., Ai-Ling, M. L., Hammond, P. T. & Irvine, D. J. Composite Dissolving Microneedles for Coordinated Control of Antigen and Adjuvant Delivery Kinetics in Transcutaneous Vaccination. *Adv. Funct. Mater.* **23**, 161-172, (2012).

193 Pritchard, E. M. & Kaplan, D. L. Silk fibroin biomaterials for controlled release drug delivery. *Expert Opin. Drug Delivery* **8**, 797-811, (2011).

194 Wenk, E., Merkle, H. P. & Meinel, L. Silk fibroin as a vehicle for drug delivery applications. *J. Controlled Release* **150**, 128-141, (2011).

195 You, X., Chang, J.-h., Ju, B.-K. & Pak, J. J. Rapidly dissolving fibroin microneedles for transdermal drug delivery. *Mater. Sci. Eng., C* **31**, 1632-1636, (2011).

196 Zhang, J. *et al.* Stabilization of vaccines and antibiotics in silk and eliminating the cold chain. *Proc. Natl. Acad. Sci. U. S. A.* **109**, 11981-11986, (2012).

197 Rockwood, D. N. *et al.* Materials fabrication from Bombyx mori silk fibroin. *Nat. Protoc.* **6**, 1612-1631, (2011).

198 Yue, Y., Xu, W., Hu, L., Jiang, Z. & Xiong, S. Enhanced resistance to coxsackievirus B3-induced myocarditis by intranasal co-immunization of lymphotactin gene encapsulated in chitosan particle. *Virology* **386**, 438-447, (2009).

199 DeMuth, P. C. *et al.* Polymer multilayer tattooing for enhanced DNA vaccination. *Nature Materials*, Ahead of print., (2013).
200 DeMuth, P. C., Moon, J. J., Suh, H., Hammond, P. T. & Irvine, D. J. Releasable Layer-by-Layer Assembly of Stabilized Lipid Nanocapsules on Microneedles for Enhanced Transcutaneous Vaccine Delivery. *ACS Nano* **6**, 8041-8051, (2012).
201 Lin, W.-H. W., Kouyos, R. D., Adams, R. J., Grenfell, B. T. & Griffin, D. E. Prolonged persistence of measles virus rna is characteristic of primary infection dynamics. *Proc. Natl. Acad. Sci. U. S. A.* **109**, 14989-14994, (2012).
202 Turner, D. L., Cauley, L. S., Khanna, K. M. & Lefrancois, L. Persistent antigen presentation after acute vesicular stomatitis virus infection. *J. Virol.* **81**, 2039-2046, (2007).
203 Zammit, D. J., Turner, D. L., Klonowski, K. D., Lefrancois, L. & Cauley, L. S. Residual antigen presentation after influenza virus infection affects CD8 T cell activation and migration. *Immunity* **24**, 439-449, (2006).
204 Kim, T. S., Hufford, M. M., Sun, J., Fu, Y.-X. & Braciale, T. J. Antigen persistence and the control of local T cell memory by migrant respiratory dendritic cells after acute virus infection. *J. Exp. Med.* **207**, 1161-1172, (2010).
205 Reetoo, K. N. *et al.* Quantitative analysis of viral RNA kinetics in coxsackievirus B3-induced murine myocarditis: biphasic pattern of clearance following acute infection, with persistence of residual viral RNA throughout and beyond the inflammatory phase of disease. *J. Gen. Virol.* **81**, 2755-2762, (2000).
206 Tseng, J.-C. & Kung, A. L. In Vivo Imaging of Inflammatory Phagocytes. *Chem. Biol.* **19**, 1199-1209, (2012).
207 Chen, X. *et al.* Site-Selectively Coated, Densely-Packed Microprojection Array Patches for Targeted Delivery of Vaccines to Skin. *Adv. Funct. Mater.* **21**, 464-473, (2011).
208 Koutsonanos, D. G. *et al.* Delivery of subunit influenza vaccine to skin with microneedles improves immunogenicity and long-lived protection. *Sci. Rep.* **2**, Ahead of print, (2012).
209 Kim, Y.-C., Park, J.-H. & Prausnitz, M. R. Microneedles for drug and vaccine delivery. *Adv. Drug Delivery Rev.* **64**, 1547-1568, (2012).
210 Numata, K. & Kaplan, D. L. Silk-based delivery systems of bioactive molecules. *Adv. Drug Delivery Rev.* **62**, 1497-1508, (2010).
211 Chen, M.-C., Huang, S.-F., Lai, K.-Y. & Ling, M.-H. Fully embeddable chitosan microneedles as a sustained release depot for intradermal vaccination. *Biomaterials*, Ahead of Print.
212 del Pilar Martin, M. *et al.* Local response to microneedle-based influenza immunization in the skin. *mBio* **3**, e00012-00012, (2012).
213 Nestle, F. O., Di, M. P., Qin, J.-Z. & Nickoloff, B. J. Skin immune sentinels in health and disease. *Nat. Rev. Immunol.* **9**, 679-691, (2009).
214 Lanford, R. E. *et al.* Acute hepatitis A virus infection is associated with a limited type I interferon response and persistence of intrahepatic viral RNA. *Proc. Natl. Acad. Sci. U. S. A.* **108**, 11223-11228, (2011).
215 Levine, B. *et al.* Antibody-mediated clearance of alphavirus infection from neurons. *Science* **254**, 856-860, (1991).
216 Woodland, D. L. & Kohlmeier, J. E. Migration, maintenance and recall of memory T cells in peripheral tissues. *Nat. Rev. Immunol.* **9**, 153-161, (2009).

217 Gray, D. A role for antigen in the maintenance of immunological memory. *Nat. Rev. Immunol.* **2**, 60-65, (2002).
218 Mueller, S. N. & Ahmed, R. High antigen levels are the cause of T cell exhaustion during chronic viral infection. *Proc. Natl. Acad. Sci. U. S. A.* **106**, 8623-8628, (2009).
219 Prausnitz, M. R., Mitragotri, S. & Langer, R. Current status and future potential of transdermal drug delivery. *Nat. Rev. Drug Discovery* **3**, 115-124, (2004).
220 Frech, S. A. *et al.* Improved immune responses to influenza vaccination in the elderly using an immunostimulant patch. *Vaccine* **23**, 946-950, (2005).
221 Frerichs, D. M. *et al.* Controlled, single-step, stratum corneum disruption as a pretreatment for immunization via a patch. *Vaccine* **26**, 2782-2787, (2008).
222 Glenn, G. M. *et al.* Transcutaneous immunization with heat-labile enterotoxin: development of a needle-free vaccine patch. *Expert Rev. Vaccines* **6**, 809-819, (2007).
223 Bal, S. M., Caussin, J., Pavel, S. & Bouwstra, J. A. In vivo assessment of safety of microneedle arrays in human skin. *Eur. J. Pharm. Sci.* **35**, 193-202, (2008).
224 Kim, Y.-C. *et al.* Enhanced memory responses to seasonal H1N1 influenza vaccination of the skin with the use of vaccine-coated microneedles. *J. Infect. Dis.* **201**, 190-198, (2009).
225 Carrion, R. & Patterson, J. L. Vaccines against viral hemorrhagic fevers: non-human primate models. *Hum. Vaccines* 7, 667-673, (2011).
226 Langhorne, J. *et al.* The relevance of non-human primate and rodent malaria models for humans. *Malar J* **10**, 23, (2011).
227 Morgan, C. *et al.* The use of nonhuman primate models in HIV vaccine development. *PLoS Med.* **5**, 1200-1204, (2008).
228 Godin, B. & Touitou, E. Transdermal skin delivery: Predictions for humans from in vivo, ex vivo and animal models. *Adv. Drug Delivery Rev.* **59**, 1152-1161, (2007).
229 Shedlock, D. J., Silvestri, G. & Weiner, D. B. Monkeying around with HIV vaccines: using rhesus macaques to define 'gatekeepers' for clinical trials. *Nat. Rev. Immunol.* **9**, 717-728, (2009).
230 Barouch, D. H. *et al.* Vaccine protection against acquisition of neutralization-resistant SIV challenges in rhesus monkeys. *Nature* **482**, 89-93, (2012).
231 Kaufman, D. R., Li, F., Cruz, A. N., Self, S. G. & Barouch, D. H. Focus and breadth of cellular immune responses elicited by a heterologous insert prime-boost vaccine regimen in rhesus monkeys. *Vaccine* **30**, 506-509, (2012).
232 Li, H. *et al.* Durable mucosal simian immunodeficiency virus-specific effector memory T lymphocyte responses elicited by recombinant adenovirus vectors in rhesus monkeys. *J. Virol.* **85**, 11007-11015, (2011).
233 Masek-Hammerman, K. *et al.* Mucosal trafficking of vector-specific CD4+ T lymphocytes following vaccination of rhesus monkeys with adenovirus serotype 5. *J. Virol.* **84**, 9810-9816, (2010).
234 Stephenson, K. E., Li, H., Walker, B. D., Michael, N. L. & Barouch, D. H. Gag-specific cellular immunity determines in vitro viral inhibition and in vivo virologic control following simian immunodeficiency virus challenges of vaccinated rhesus monkeys. *J. Virol.* **86**, 9583-9589, (2012).
235 Baden, L. R. *et al.* First-in-Human Evaluation of the Safety and Immunogenicity of a Recombinant Adenovirus Serotype 26 HIV-1 Env Vaccine (IPCAVD 001). *J. Infect. Dis.* **207**, 240-247, (2013).

236 Barouch, D. H. *et al.* Characterization of Humoral and Cellular Immune Responses Elicited by a Recombinant Adenovirus Serotype 26 HIV-1 Env Vaccine in Healthy Adults (IPCAVD 001). *J. Infect. Dis.* **207**, 248-256, (2013).
237 Lemckert, A. A. C. *et al.* Immunogenicity of heterologous prime-boost regimens involving recombinant adenovirus serotype 11 (Ad11) and Ad35 vaccine vectors in the presence of anti-Ad5 immunity. *J. Virol.* **79**, 9694-9701, (2005).
238 Nanda, A. *et al.* Immunogenicity of recombinant fiber-chimeric adenovirus serotype 35 vector-based vaccines in mice and rhesus monkeys. *J. Virol.* **79**, 14161-14168, (2005).
239 Middleton, J. C. & Tipton, A. J. Synthetic biodegradable polymers as orthopedic devices. *Biomaterials* **21**, 2335-2346, (2000).
240 Abbink, P. *et al.* Comparative seroprevalence and immunogenicity of six rare serotype recombinant adenovirus vaccine vectors from subgroups B and D. *J. Virol.* **81**, 4654-4663, (2007).
241 Holterman, L. *et al.* Novel replication-incompetent vector derived from adenovirus type 11 (Ad11) for vaccination and gene therapy: Low seroprevalence and non-cross-reactivity with Ad5. *J. Virol.* **78**, 13207-13215, (2004).
242 Vogels, R. *et al.* Replication-deficient human adenovirus type 35 vectors for gene transfer and vaccination: Efficient human cell infection and bypass of preexisting adenovirus immunity. *J. Virol.* **77**, 8263-8271, (2003).
243 Montefiori, D. C. Evaluating neutralizing antibodies against HIV, SIV, and SHIV in luciferase reporter gene assays. *Curr Protoc Immunol* **Chapter 12**, Unit 12.11, (2005).
244 Vrdoljak, A. *et al.* Coated microneedle arrays for transcutaneous delivery of live virus vaccines. *J. Controlled Release* **159**, 34-42, (2012).
245 Choi, H.-J. *et al.* Stability of influenza vaccine coated onto microneedles. *Biomaterials* **33**, 3756-3769, (2012).
246 Chen, X. *et al.* Dry-coated microprojection array patches for targeted delivery of immunotherapeutics to the skin. *J. Controlled Release* **139**, 212-220, (2009).
247 Alcock, R. *et al.* Long-term thermostabilization of live poxviral and adenoviral vaccine vectors at supraphysiological temperatures in carbohydrate glass. *Sci. Transl. Med.* **2**, 19ra12, (2010).
248 Kaufman, D. R., Bivas-Benita, M., Simmons, N. L., Miller, D. & Barouch, D. H. Route of adenovirus-based HIV-1 vaccine delivery impacts the phenotype and trafficking of vaccine-elicited CD8+ T lymphocytes. *J. Virol.* **84**, 5986-5996, (2010).
249 Kaufman, D. R. *et al.* Trafficking of Antigen-Specific CD8+ T Lymphocytes to Mucosal Surfaces following Intramuscular Vaccination. *J. Immunol.* **181**, 4188-4198, (2008).
250 Kersten, G. & Hirschberg, H. Needle-free vaccine delivery. *Expert Opin. Drug Delivery* **4**, 459-474, (2007).
251 Mitragotri, S. Immunization without needles. *Nat. Rev. Immunol.* **5**, 905-916, (2005).
252 Kim, Y.-C. *et al.* Increased immunogenicity of avian influenza DNA vaccine delivered to the skin using a microneedle patch. *Eur. J. Pharm. Biopharm.* **81**, 239-247, (2012).
253 Song, J.-M. *et al.* Microneedle delivery of H5N1 influenza virus-like particles to the skin induces long-lasting B- and T-cell responses in mice. *Clin. Vaccine Immunol.* **17**, 1381-1389, (2010).
254 Hiraishi, Y. *et al.* Bacillus Calmette-Guerin vaccination using a microneedle patch. *Vaccine* **29**, 2626-2636, (2011).

255 Zhou, Q. *et al.* Augmented humoral and cellular immune response of hepatitis B virus DNA vaccine by micro-needle vaccination using Flt3L as an adjuvant. *Vaccine* **28**, 1357-1362, (2010).